An Improved Model for One-Dimensional Polaronic Ferromagnetism: Poly-*meta*-phenylenefuchsone

Thesis by

Kraig Knute Anderson

In Partial Fulfillment of the Requirements

for the Degree of

Doctor of Philosophy

California Institute of Technology

Pasadena, California

1996

(Submitted February 20, 1996)

Acknowledgments

I've always thought an acknowledgments section rather dubious, as if our experiences in graduate school were a movie. Example: compare the dedication preceding any great work of literature, such as *Crime and Punishment*, with the credits to any *Police Academy* movie. Perhaps great works speak for themselves, while the projects of intellectual foot soldiers must be placed in context of their experiences to achieve their most sublime expression. That is, the people in our lives are far more important than the vanishingly small increment our theses add to the heap of science.

I'd like to thank my advisor, Dennis Dougherty, for providing me with an exciting environment to work in my graduate career. I appreciate and admire his intellectual breadth and depth, his encouragement, generosity, enthusiasm, and most of all, his patience.

Caltech has been a unique experience. I've met many people, who as friends and as colleagues have made these years memorable. In their approximate order of appearance in my graduate career, here are people who have made a difference: Jim Gerdy, Elaine Marzluff, Dave and Lisa Shultz, Josh Jacobs, Ed Stewart, Laura Mizoue, Pat Kearny, Alison McCurdy, Kevin Condroski, Milan Mrksich, Karen Shannon, Jonathan Forman, Susanne Lin, Terri Longin, Michael Murray, Neil Farrow, Sandro Mecozzi, Tracey Burr, Piotr Kaszynski, Jeff Clites, Scott Silverman, Seth Miller, Jennifer Ma, Justin Gallivan. Outside of Caltech, here are a few of the people who have helped me to keep my sanity: Ben Johnson, Becky Jones, Kari Stanway, Jason Delmont, Jeff Williamson, Jennifer Wahlsten, Eric Erslan, Peter Van Pelt. Of course, there's my parents, both adoptive & biological; my sister, Karen, and my brothers, Judd, Joel, and Jacob. If I've forgotten anyone, believe me, it's inadvertent—I gotta get this thing to the proofreader.

MAGNET, n. Something acted upon by magnetism.

MAGNETISM, n. Something acting upon a magnet.

The two definitions immediately foregoing are condensed from the works of one thousand eminent scientists, who have illuminated the subject with a great white light, to the inexpressible advancement of human knowledge.

Ambrose Bierce (1842-1914), "The Devil's Dictionary," 1911

God runs electromagnetics by wave theory on Monday, Wednesday, and Friday, and the Devil runs them by quantum theory on Tuesday, Thursday, and Saturday.

William H. Bragg, circa 1925

If we get involved in a nuclear war, would the electromagnetic pulses from exploding bombs damage my videotapes?

From a readers' Q and A column in TV GUIDE, 1985

Abstract

The design, reductive doping, and magnetic characterization of poly-*meta*-phenylenefuchsone, an improved model for one-dimensional polaronic ferromagnetism, are described. Previous work demonstrated that delocalized radical cations, when linked through appropriate topologies, can exhibit ferromagnetic, or high spin interactions between unpaired electron spins. Consideration of these examples led to the choice of the radical anion of 2,6-di-*tert*-butylfuchsone as a spin containing unit, due to its relative stability, solubility, spin density, and ease of generation. Electrochemical doping of its polymers is more convenient and effective than chemical doping, resulting in a substantial increase in magnetic properties relative to previous models. The magnetic results are aided by dilution of the doped polymer in a diamagnetic solid, which is interpreted as reducing intermolecular antiferromagnetic interactions. The significant results of this model system provide clear directions for future designs, including improving solubility, spin density, doping efficiency, and defect suppression.

A tetraphenoxyl analog to existing quintet tetraradical **A** was envisioned. The synthesis and oxidation of its precursor tetraphenol **I** are described, as well as a number of simpler analogs. No evidence of high spin interactions was observed. Instead, the X-ray crystal structure of the product indicates that the oxidized tetraphenol undergoes ring closure of its central cyclobutane ring to form a bicyclobutane, which rapidly rearranges to a ring opened butadiene. The novel feature of this known rearrangement in the current system is that it occurs readily, even under very mild conditions.

Table of Contents

Acknowledgments.....iii
Abstract.....v
List of Figures.....viii
List of Schemes.....x
List of Tables.....x
Chapter 1. Introduction and Overview.....1
Chapter 1 References.....11
Chapter 2. An Improved Model for One-Dimensional Polaronic Ferromagnetism: Electrochemically-Doped Poly-*meta*-phenylenefuchsone.....15
Introduction: The Polaronic Ferromagnet Paradigm.....16
Previous Work.....18
Goals of This Study.....21
Design Criteria.....21
Synthetic Strategy.....24
Doping Procedures.....25
Magnetic Characterization.....29
Results of Chemical Doping.....32
Results of Electrochemical Doping.....38
Discussion.....44
Doping Issues.....44
S values and Spin Concentration.....46
Balance of Ferromagnetic and Antiferromagnetic Interactions.....47
Future Directions.....51
Increasing Solubility.....51
Spin Density and Ferromagnetic Coupling Strength.....52
Increasing Spin Concentration.....56
Higher Magnetic Order, Increasing *S* Value.....57
Conclusions.....57
Experimental.....59
Electrochemical Doping Procedure.....60
Problems and Troubleshooting.....62
Magnetization Studies.....64
Synthetic Procedures.....66

Chapter 2 References 71
Chapter 3. Design, Synthesis, and Attempted Observation of a Tetraphenoxyl Tetraradical: Facile Rearrangement of a Substituted Bicyclobutane 75
Introduction 76
Target Structures and Synthetic Strategies 78
Results and Discussion 83
Conclusions 102
Experimental 103
Chapter 3 References 118
Chapter 4. Introduction to Ferromagnetic Coupling in Organic Systems: Theory, Design Strategies, and Magnetic Characterization 121
Introduction 122
Indistinguishability, the Pauli Principle and Electron Exchange 123
Spin Angular Momentum 127
Commutation Rules and Angular Momentum 128
The Quantum Mechanical Basis of Ferromagnetic Coupling 133
High Spin Organic Molecules 138
Spin Polarization 141
Topology Based Rules for Predicting Spin States 142
Magnetic Characterization 144
Chapter 4 References 157
Appendix A. Additional Polymer Models for One-Dimensional Polaronic Ferromagnetism 159
Appendix A References 167
Appendix B. Crystal Structure Data for Bisgalvinol **V** 168
X-ray Diffraction Study of Bisgalvinol **V** 170
Collection of X-ray Diffraction Data 170
Solution and Refinement of the Crystal Structure 170
Appendix B References 171
Appendix C. Additional Synthetic Procedures 185
Tetraphenol Analogs 186
Research Towards a Stable Analog of Non-Kekulé Benzene 193
Research Towards a TMM-Analog Ferromagnetic Coupling Unit 197
Appendix C References 200

Appendix D. Brillouin Function Fitting Implementation for KaleidaGraph 202
Appendix D References 203

List of Figures

1.1: Some Triplet Organic Biradicals 4
1.2: Two Rationally Designed High Spin Systems 4
1.3: Oxidation of Tetraphenol **I** Does Not Result in a Stable Tetraradical 5
1.4: Magnetism is a Bulk Property 7
1.5: Triplet *meta*-Xylylene 8
1.6: Schematic for One-Dimensional Ferromagnetic Coupling 8
1.7: Some Prior Models for Polaronic Ferromagnetism 8
1.8: Poly-*meta*-phenylenefuchsone as a Model For One-Dimensional Polaronic Ferromagnetism 9
2.1: Schematic for One-Dimensional Ferromagnetic Coupling 16
2.2: Three Ferromagnetic Organic Topologies 17
2.3: Polaron Generation in Poly-*para*-phenylene 17
2.4: Prior Models for Polaronic Ferromagnetism 19
2.5: Selected Spin Densities in 2,6-Di-*tert*-butylfuchsone Radical Anion 24
2.6: Sample #006 Sodium-Doped **PMPF** 31
2.7: Typical Noisy, High *S*, Low % Spins Data for Chemically Doped **PMPF** 34
2.8: Sonication Combined with Chemical Doping of **PMPF** 35
2.9: Sodium Naphthalide Doping of **PMPF** 36
2.10: Relative Effective Moment Plots for Chemically Doped **PMPF**. 37
2.11: *S* Value and Spin Concentration Scale Positively with Electrochemical Doping Level in **PMPF**. 40
2.12: Typical Saturation Plots for Electrochemically Doped Polymer. 41
2.13: Relative Effective Moment Plots 42
2.14: Stacked Relative Effective Moment Plots for **PMPF**. 43
2.15: Variation of *S* value Versus Spin Concentration 48
2.16: Polar Solubilizing Groups 52
2.17: Reducing Spin Dilution With **PMPF** Analogs 53

2.18: Coupling 1,3,5 Through Phenylene to Overcome Effects of Defect Formation 58
3.1: A Rationally Designed Quintet Tetraradical 76
3.2: Stable Phenoxyl Radicals 76
3.3: A Rationally Designed Room-Temperature Quintet? 76
3.4: Magnetooptical Switching in 2,4-Dimethylene-1,3-Cyclobutanediyl 77
3.5: Bicyclobutane Formation and Rearrangement 77
3.6: 15 line EPR Spectra for **III'** 84
3.7: 5 line EPR Spectra for **III->VI'** 85
3.8: 5 line EPR Spectra From Isolated **VI**. 88
3.9: 15 line EPR Spectra for **IV'**. 90
3.10: Representative 3 line EPR Spectra for **I'** and **II'** 92
3.11: Representative 3->5 line EPR Spectra for I2/Tetrabutylammonium Hydroxide Oxidations of **I** and **II**. 94
3.12: Representative 77 K Spectra. 95
3.13: 300MHz ^{1}H NMR Spectra of Bisgalvinol **V** 96
3.14: X-ray Structure of Bisgalvinol **V** 98
3.15: 5 line EPR Spectra of Bisgalvinol **V** 99
3.16: Photogeneration of RO• 101
3.17: Chloroformylation of BHT Anion 101
4.1: Triplet Ground State of Atomic Carbon 133
4.2: H_2 Has a Singlet Ground State For All **r** 133
4.3: 1,3-Cyclobutanediyl 138
4.4: Molecular Orbital Diagram of 1,3-Cyclobutanediyl 140
4.5: Spin Polarization in TMM 141
4.6: Spin Polarization in TMM 141
4.7: HMO Diagrams of Square Cyclobutadiene and TMM 142
4.8: The Star-Nonstar Rule Predicts Spin Ground States 143
4.9: A Bar Magnet in an External Magnetic Field 146
4.10: The Energy of a Magnetic Dipole is Scaled by Cos Q 146
4.11: Zeeman Splitting 147
4.12: Idealized Curie-Weiss Plots for Paramagnetic (top), Antiferromagnetic (middle), and Ferromagnetic Material (bottom) 149
4.13 Idealized Relative Effective Moment Plot 150

4.14: Theoretical Saturation Plots for Various *S* Values. 155
A.1: Representative Plots. Top: **PMP2P**, XS Na, Saturation Plot. Bottom: **PMP2P**, XS Na, Relative Effective Moment Plot....162
B.1: ORTEP Plot of Bisgalvinol **V** 169
C.1: Bisphenol Analogs of Tetraphenol **I** 186
C.2: Magnetooptical Switching in 2,4-Dimethylene-1,3-Cyclobutanediyl 193

List of Schemes

2.1: Synthesis of Poly-*meta*-phenylenefuchsone 22
2.2: Synthesis of 5-Tetradecylbenzene-1,3-bis-(1,3,2-benzodioxaborole) 26
2.3: Synthesis of Control Polymer Poly-*para*-fuchsone 26
2.4: Possible Synthetic Route to Poly-*para-meta*-fuchsone 54
2.5: Possible Route to Poly-*meta*-phenylenequinonemethide 55
3.1: Synthesis of Tetraphenol **I** 79
3.2: Synthesis of Bisphenol **II** 81
3.3: Synthesis of Bisphenol **III** 82
3.4: Synthesis of Phenol **IV** 82
3.5: Pathway to Galvinol **VI** 87
3.6: Oxidation of **IV** 89
3.7: A Possible Pathway to Bisgalvinol **V** 100
A.1: Model Polymers for Polaronic Ferromagnetism 161
C.1: Attempted Synthesis of **I** Analogs 187
C.2: Synthesis Towards Hexaphenyl-non-Kekulé Benzene 194
C.3: Synthesis of a Hindered Alkene 197

List of Tables

2.1: Representative *S* Values and Spin Concentrations (in Parentheses) From Previous Studies; Measured at 1.8 K. 19
2.2: Magnetic Characterization of Chemically Doped **PMPF** 33
2.3: Magnetic Characterization of Electrochemically Doped **PMPF** & **PPF** 39
A.1: *S* values & Spin Concentrations (Parentheses); Measured at 1.8 K 160
B.1: Experimental Data for the X-ray Diffraction Study 172

B.2: Atomic Coordinates ($X10^4$) and Equivalent Isotropic Displacement Coefficients ($Å^2$ $X10^4$) 173
B.3: Interatomic Distances (Å) with Esd's 174
B.4: Interatomic Angles (Deg.) with Esd's 175
B.5: Anisotropic Displacement Coefficients ($Å^2$ $X10^4$) 176
B.6: H-Atom Coordinates ($X10^4$) and Isotropic Displacement Coefficients ($Å^2$ $X10^4$) 177
B.7: Fractional Coordinates for All Atoms (Including Symmetry Equivalents) 178
B.8: Crystal Data. 182
B.9: Data Collection 183
B.10: Solution and Refinement 184

Chapter 1. Introduction and Overview

Magnetism has stirred human curiosity and contributed to our technology for thousands of years.[1,2] Despite the efforts by many of the great minds of classical science, no effective theory of spontaneous bulk magnetism was gained until the twentieth century and the advent of quantum mechanics. Furthermore, despite the explanatory power allowed by the concepts of electron spin and the Pauli exclusion principle, new experimental observations of exotic magnetic phenomena continue to challenge and develop the theory of magnetism.[3]

For several decades now, researchers have been investigating magnetic interactions in organic compounds.[4] In contrast, transition or rare earth metals are the sources of electron spin in all common magnetic materials. While important technologically, the traditional Edisonian trial and error approach to designing metal dependent magnetic materials is a crude tool for probing the development of macroscopic magnetic behavior from microscopic interactions between electron spins.[5] In comparison, the structural control and adaptability afforded by organic synthesis allows a stepwise, structure-function approach to understanding magnetism, beginning with simple two electron interactions in organic biradicals. Although organic materials may well have technologically important properties, such as transparency, solubility, or true magnetooptical switching, practical applications remain far in the future. Our primary motivation is the challenge of understanding magnetism and observing it in a completely new context.[6] The difficulty of this endeavor has long been appreciated; in 1928, Heisenberg concluded that bulk magnetic behavior would be impossible in light, nonmetallic elements.[7]

The fundamental magnetic interaction is the parallel coupling of two electron spins.[8,-10] This is not due to magnetic dipole-dipole interactions, but

rather to subtle consequences of the behavior of fermions, or particles with half integral quantum numbers. This behavior is concisely expressed by the Pauli exclusion principle, which says that no two electrons can have the same set of quantum numbers. Electrons which are spin parallel must then occupy different regions of space; in a simple two-electron system, the exclusion principle means that electron motion in the triplet state will be correlated so they remain apart. This coupling between the spin and space quantum numbers is a force called exchange, which has no classical counterpart. Although not due to Coulomb repulsions, it gives decreased Coulomb repulsions relative to the singlet state, leading to a triplet ground state. Chapter 4 provides a detailed introduction to spin behavior and magnetic coupling at the quantum mechanical level, strategies for designing organic compounds with interesting magnetic properties, and experimental behavior and magnetic characterization.

The first step in magnetic organic material research is to design systems where exchange dominates bonding interactions between unpaired electrons.[10] Early examples of organic biradicals with triplet ground states include Closs' biradical[11] and trimethylenemethane[12] (Figure 1.1). Initial research in this group extended Closs' biradical with a family of 1,3-substituted derivatives,[13] and developed a new class, the 1,3-substituted cyclobutanediyls.[14-17] Combination of two of these motifs, cyclobutanediyl and trimethylenemethane, led to two completely new biradicals, triplet 2,4-dimethylene-1,3-cyclobutanediyl, the non-Kekulé isomer of benzene,[18] and quintet tetraradical **A** (Figure 1.2).[19] Although these systems are magnetically stable, they are quite reactive chemically, requiring low temperatures and a rigid matrix to prevent decomposition. Chapter 3 describes the design and efforts to synthesize an analog of **A** (Figure 1.3) where the reactive methyl

Figure 1.1: Some Triplet Organic Biradicals

Closs' biradical

Trimethylenemethane

Substituted
1,3-cyclopentanediyls

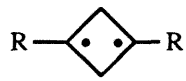

Substituted
1,3-cyclobutanediyls

Figure 1.2: Two Rationally Designed High-Spin Systems

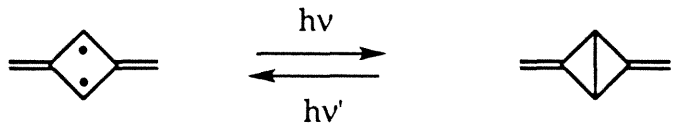

2,4-Dimethylene-1,3-cyclobutanediyl (and its closed shell isomer, 1,3-dimethylenebicyclobutane)

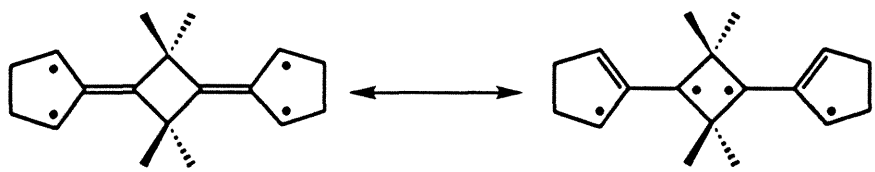

Quintet Tetraradical **A**

Figure 1.3: Oxidation of Tetraphenol I Does Not Result in a Stable Tetradical

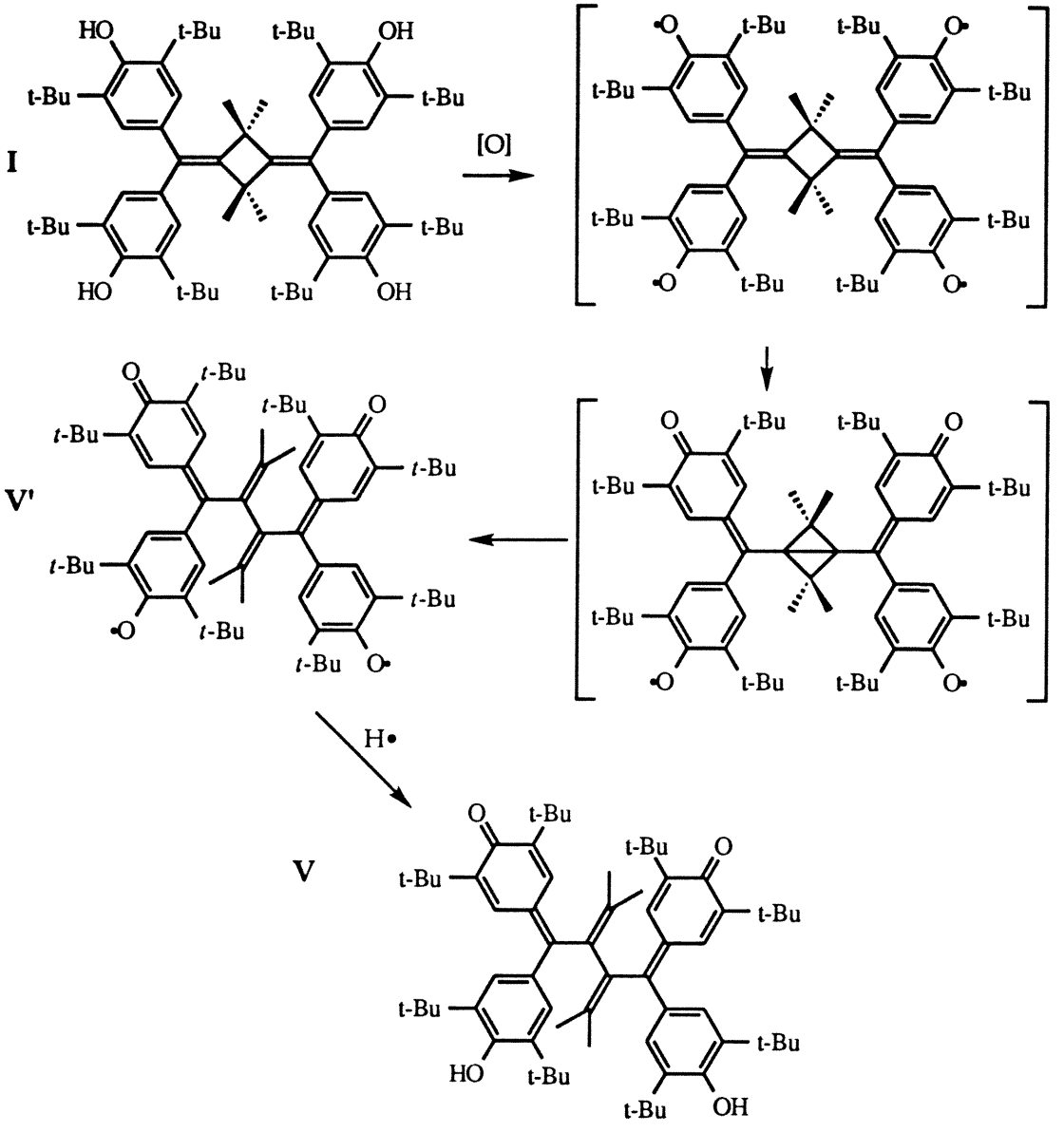

radical spin containing groups are replaced by hindered phenoxyl radicals. The tetraphenol precursor (I) to the target tetraradical was synthesized, as well as a number of related phenols. We anticipated that this tetraradical could undergo ring closure to a bicyclobutane structure and possibly function as a magnetooptical switch, akin to 2,4-dimethylene-1,3-cyclobutanediyl (Figure 1.2).[18] Unfortunately, no evidence of high spin was found in these phenoxyl systems, and the major product of oxidation of tetraphenol **I** was ring opened bisgalvinol **V**. This rearrangement is observed in unsubstituted and substituted bicyclobutane;[20,21] the novel feature of this system is that it proceeds under very mild conditions. This exemplifies a common theme in organic magnetic materials research; many potentially magnetic structures can be designed which can be difficult or impossible to achieve experimentally. Simple properties like solubility, stability, and ease of synthesis and characterization are just as important as magnetic coupling.

Spontaneous bulk magnetism requires more than simple two electron interactions.[3] Although we term the spin parallel electrons in a triplet biradical ferromagnetically coupled, there is no such thing as a ferromagnetic molecule. Magnetism is a bulk property which arises out of long range, cooperative interactions in three dimensions between individual moments (Figure 1.4). In an ideal paramagnet, moments throughout a material are randomly oriented, rapidly reorienting, and noninteracting. In a ferromagnet, these moments are coupled parallel in three dimensions, resulting in a net magnetic moment. In an antiferromagnet, moments are coupled antiparallel, resulting in no net moment, while in a ferrimagnet, antiparallel coupling of unequal moments results in a net magnetic moment. The required long range cooperative interactions can be divided into intermolecular and intramolecular components. Although

Figure 1.4: Magnetism is a Bulk Property

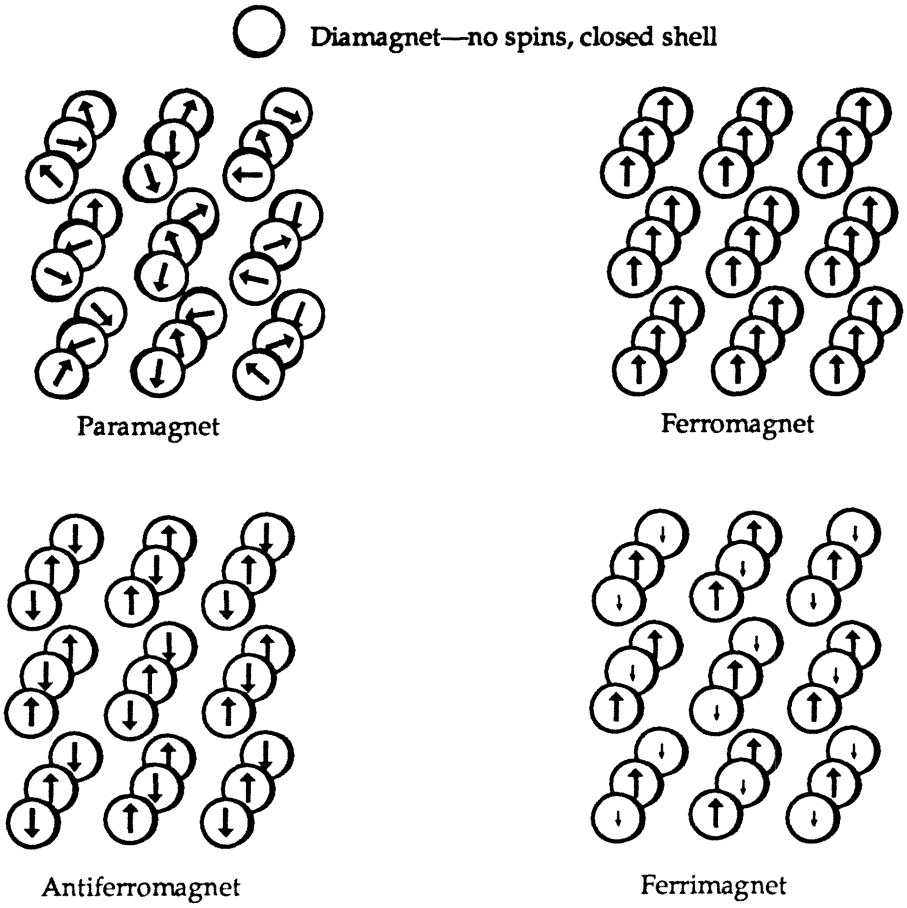

intermolecular interactions are certainly an important contributor to the behavior of many magnetic materials, they are generally weaker, antiferromagnetic, and far more difficult to control than intramolecular interactions. Therefore, our investigations of long range coupling in organic systems are of covalent, intramolecular ferromagnetic coupling.[6]

A theoretical study by Fukutome[22] suggested that segments of doped conducting polymer connected by proven magnetic topologies might serve as models for one-dimensional polaronic ferromagnetism. The doped spin containing segments, either radical cations or radical anions, are termed polarons. Pairwise coupling of such segments can be mediated by organic

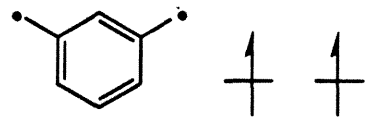

Figure 1.5 Triplet *meta*-Xylylene

units which have proven to induce high spin coupling regardless of substitution, such as *meta*-phenylene,[4,6,23,26] shown in *meta*-xylylene (Figure 1.5). This defines our approach to rational design of one-dimensional magnetic organic systems: spin containing units, made of charged, delocalized organic radicals, connected by units with a defined ferromagnetic topology, such as *meta*-phenylene (Figure 1.6).

Figure 1.6: Schematic for One-Dimensional Ferromagnetic Coupling

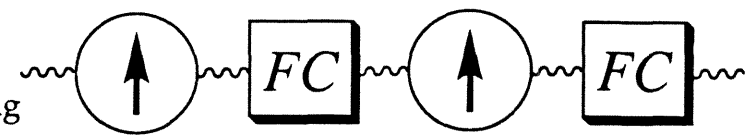

Previous research in the group constructed models of the one-dimensional polaronic ferromagnet by oxidatively doping alternating copolymers of *meta*-phenylene and groups such as octatetraene, thiophene and indoloindole (Figure 1.7).[24] While these results were encouraging, they did not demonstrate extensive, unmistakable ferromagnetic interactions. Almost exclusively, samples which demonstrated *S* values unambiguously

Figure 1.7: Some Prior Models for Polaronic Ferromagnetism

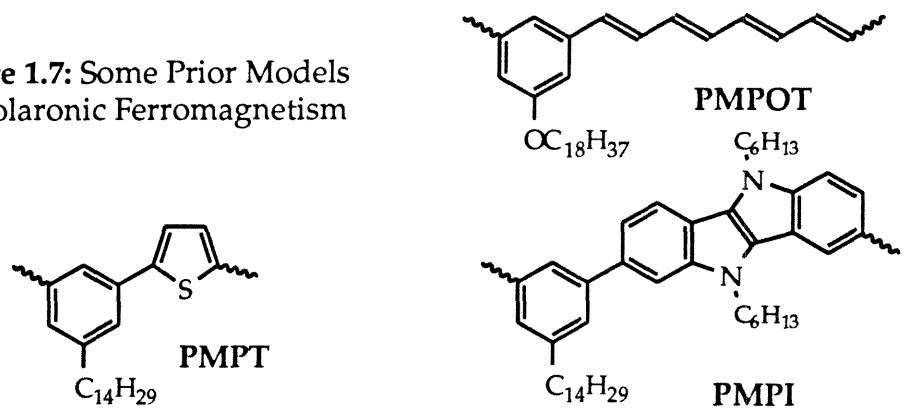

greater than $^{-1}/_{2}$ (S, in units of $^{-1}/_{2}$, indicates the average number of electrons coupled ferromagnetically, e.g., S=$^{-1}/_{2}$ is zero coupling, S=2 is 4 electrons coupled, etc.) had signal which corresponded to less than one percent of the maximum possible number of spin containing segments (such small moments could conceivably be due to paramagnetic impurities; only for **PMPOT** was a control experiment[24] using a *para* linked isomer performed, which showed the original signal was due solely to the *meta* polymer). Conversely, samples which contained a high percentage of spin versus theoretical displayed *S* values near $^{-1}/_{2}$, or essentially no evidence of ferromagnetic interactions. Factors which might contribute to this puzzling behavior include overpowering intermolecular antiferromagnetic interactions, crosslinking, bipolaron defects (spinless dications) due to overoxidation of the spin containing units, and weakened magnetic coupling resulting from minimal spin density. One additional problem in these studies was the difficulty of generating a large number of spins in a controlled, measurable fashion.

To address these issues, poly-*meta*-phenylenefuchsone, or **PMPF**, was designed (Figure 1.8). We desired a system that was more soluble, as this

Figure 1.8: Poly-*meta*-Phenylenefuchsone as a Model For One-Dimensional Polaronic Ferromagnetism

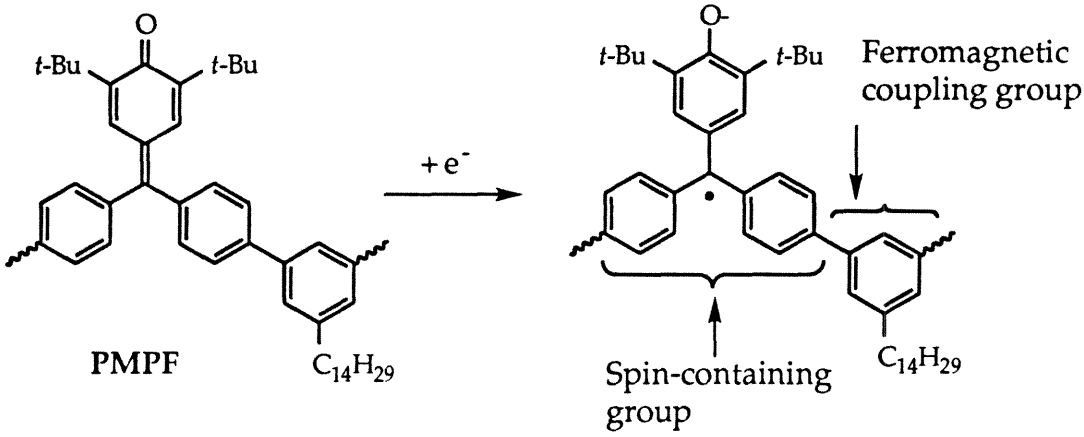

would allow the use of electrochemical doping, which would be more thorough, controlled, and homogeneous. Fuchsone was chosen as the precursor to the spin containing unit because electrochemical studies have shown its radical anion to be relatively easily generated, stable, and soluble.[25] Additionally, its second reduction potential is sufficiently removed that bipolaron (a spinless dianion, or defect) formation at the first reduction potential should be negligible.

Initial reductive doping with chemical dopants such as tetrakis(diethylamino)ethylene and sodium generated results which were qualitatively similar to the preceding cationic systems. Doping by electrochemical reduction was far more successful, both in controlling the extent of doping and in magnetic results. Originally, we worried about dilution of the magnetic signal of electrochemically doped **PMPF** because we were unable to separate the polymer and the supporting electrolyte (tetrabutylammonium perchlorate). Fortunately, dilution did not decrease the signal below our measurement limits, and furthermore, may actually have increased the chances of success by suppressing intermolecular antiferromagnetic interactions and crosslinking. Plots of relative effective moment versus temperature show a significant increase in ferromagnetic interactions beginning at about 40 K, consistent with that expected from scaling the coupling energy[19a] in *meta*-xylylene by the spin density in fuchsone radical anion. This suggests that redoping of some earlier systems[24] with dilution would generate improved results. Additionally, a clear, positive relationship was demonstrated between doping level, spin concentration, and extent of ferromagnetic coupling, culminating in an S value of 2.0 at a spin concentration of 60% of the theoretical maximum. This represents an increase of nearly two orders of magnitude in spin

concentration at this *S* value relative to previous research in the group.[24] Furthermore, a control study using a *para* linked polymer, poly-*para*-fuchsone proves that high-spin, ferromagnetic coupling in **PMPF** is due solely to a rationally designed *meta*-topology.

Although this is still far from our eventual goal of an organic ferromagnet, these results are significant and have provided inspiration for future work. Clearly, electrochemical doping is superior to chemical doping, even under the restrictions imposed by polymer solubility and polaron reactivity. A key factor here is solubility of the polymer in both undoped and doped states; solubility is not only important for synthesis and characterization, but also for doping. Dilution of paramagnetic species with weak intramolecular ferromagnetic coupling may be necessary to overcome intermolecular antiferromagnetic coupling. In summary, diluted, electrochemically doped poly-*meta*-phenylenefuchsone has validated the concept of one-dimensional polaronic ferromagnetism by exhibiting a substantial increase in spin concentration and ferromagnetic interactions over earlier work.[24]

Chapter 1 References

1. Mattis, D. C. *The Theory of Magnetism I;* 2nd ed.; Springer-Verlag: Berlin, 1981.

2. Carlin, R. L. *Magnetochemistry;* Springer-Verlag: New York, 1986.

3. Hurd, C. M. *Contemp. Phys.* **1982**, *23*, 469-493.

4. For reviews of the field see: (a) *Research Frontiers in Magnetochemistry;* O'Connor, C. J., Ed.; World Scientific Publishing Co.: Singapore, 1993. (b) *Magnetic Molecular Materials;* Gatteschi, D.; Kahn, O.; Miller, J. S.; Palacio, F., Ed.; Kluwer Academic Publishers: Dordrecht, The Netherlands, 1991. (c)

Ferromagnetic and High Spin Molecular Based Materials. Mol. Cryst. Liq. Cryst.; Miller, J. S.; Dougherty, D. A., Ed.; Gordon and Breach Science Publishers: USA, 1989; Vol. 176. (d) *Chemistry and Physics of Molecular Based Magnetic Materials. Mol. Cryst. Liq. Cryst.*; Iwamura, H.; Miller, J. S., Ed.; Gordon and Breach Publishers: USA, 1993; Vol. 232. (e) Rajca, A. *Chem. Rev.* **1994**, *94*, 871-893.

5. Most magnetic materials are extended structures such as network solids, rather than molecular solids, and thus are generally harder to synthesize, process, and characterize.

6. Dougherty, D. A. *Acc. Chem. Res.* **1991**, *23*, 88-94.

7. Heisenberg, W. *Z. Phys.* **1928**, *49*, 619-636.

8. Eisberg, R.; Resnick, R. *Quantum Physics*; 2nd ed., John Wiley and Sons: New York, 1985; pp 300-319.

9. Beveridge, D. L.; Pople, J. A. *Approximate Molecular Orbital Theory*; McGraw-Hill: New York, 1970; pp 1-56.

10. For reviews of the field see: (a) Dowd, P. *Acc. Chem. Res.* **1972**, *5*, 242-248. (b) Borden, W. T. *Diradicals*; John Wiley & Sons: New York, 1982, pp 321. (c) Salem, L.; Rowland, C. *Angew. Chem. Internat. Edit.* **1972**, *11*, 92-111. (d) Borden, W. T.; Davidson, E. R. *J. Am. Chem. Soc.* **1977**, *99*, 4587-4594. (e) Borden, W. T.; Davidson, E. R. *Acc. Chem. Res.* **1981**, *14*, 69-76.

11. (a) Buchwalter, S. L.; Closs, G. L. *J. Am. Chem. Soc.* **1975**, *97*, 3857-3858. (b) Buchwalter, S. L.; Closs, G. L. *J. Am. Chem. Soc.* **1979**, *101*, 4688-4694

12. (a) Baseman, R. J.; Pratt, D. W.; Chow, M.; Dowd, P. *J. Am. Chem. Soc.* **1976**, *98*, 5726-5727. (b) Dowd, P.; Chow, M. *J. Am. Chem. Soc.* **1977**, *99*, 6438-6440. (c) Dowd, P. *Acc. Chem. Res.* **1972**, *5*, 242-248. (d) Dowd, P.; Gold, A.; Sachdev, K. *J. Am. Chem. Soc.* **1968**, *90*, 2715-2716. (e) Dowd, P. *J. Am. Chem. Soc.* **1966**, *88*, 2587-2589. (f) Dowd, P.; Chow, M. *Tetrahedron* **1982**, *38*, 799-807.

13. Coms, F. D.; Dougherty, D. A. *Tetrahedron Lett.* **1988,** *29,* 3753-3756.

14. Sponsler, M. B.; Jain, R.; Coms, F. D.; Dougherty, D. A. *J. Am. Chem. Soc.* **1989,** *111,* 2240-2252.

15. Pranata, J.; Dougherty, D. A. *J. Phys. Org. Chem.* **1989,** *2,* 161-176.

16. Pranata, J.; Dougherty, D. A. *Synthetic Metals* **1987,** *22,* 171-178.

17. Jain, R.; Sponsler, M. B.; Coms, F. D.; Dougherty, D. A. *J. Am. Chem. Soc.,* **1988,** *110,* 1356-1366.

18. (a) Jain, R.; Snyder, G. J.; Dougherty, D. A. *J. Am. Chem. Soc.*. **1984,** *106,* 7294-7295. (b) Snyder, G. J.; Dougherty, D. A. *J. Am. Chem. Soc.* **1985,** *107,* 1774-1775. (c) Snyder, G. J.; Dougherty, D. A. *J. Am. Chem. Soc.* **1986,** *108,* 299-300. (d) Snyder, G. J.; Dougherty, D. A. *J. Am. Chem. Soc.* **1989,** *111,* 3942- 3954. (e) Snyder, G. J.; Dougherty, D. A. *J. Am. Chem. Soc.* **1989,** *111,* 3927- 3942.

19. (a) Jacobs, S. J.; Shultz, D. A.; Jain, R.; Novak, J.; Dougherty, D. A. *J. Am. Chem. Soc.* **1993,** *115,* 1744-1753. (b) Novak, J. A.; Jain, R.; Dougherty, D. A. *J. Am. Chem. Soc.,* **1989,** *111,* 7618-7619.

20. Wiberg, K. B. *Adv. Alicyclic Chem.* **1968,** *2,* 185-254.

21. (a) Freund, F.; Hünig, S. *J. Org. Chem.* **1987,** *52,* 2154-2161. (b) Horner, M.; Hünig, S. *J. Am. Chem. Soc.* **1977,** *99,* 6120-6122. (c) Horner, M.; Hünig, S. *J. Am. Chem. Soc.* **1977,** *99,* 6122-6124.

22. Fukutome, H.; Takahasi, I.; Ozaki, M. *Chem. Phys. Lett.* **1987,** *133,* 34-38.

23. (a) Itoh, K. *Pure & Appl. Chem.* **1978,** *50,* 1251-1259. (b) Yoshizawa, K.; Chano, A.; Ito, A.; Tanaka, K.; Yamabe, T.; Fujita, H.; Yamauchi, J. *Chem. Lett.* **1992,** 369-372. (c) Nakamura, N.; Inoue, K.; Iwamura, H. *Angew. Chem. Int. Ed. Engl.* **1993,** *32,* 872-874. (d) Wasserman, E.; Schueller, K.; Yager, W. A. *Chem. Phys. Lett.* **1968,** *2,* 259-260.

24. (a) Kaisaki, D. A.; Dougherty, D. A. *Tetrahedron Lett.* **1987,** *28,* 5263-5266. (b) Dougherty, D. A.; Kaisaki, D. A. *Mol. Cryst. Liq. Cryst.* **1990,** *183,* 71-79. (c)

Dougherty, D. A.; Grubbs, R. H.; Kaisaki, D. A.; Chang, W.; Jacobs, S. J.; Shultz, D. A.; Anderson, K. K.; Jain, R.; Ho, P. T.; Stewart, E. G. In *Magnetic Molecular Materials*; D. Gatteschi, O. Kahn, J. S. Miller and F. Palacio, Ed.; Kluwer Academic Publishers: The Netherlands, 1991; pp 105-120. (d) Kaisaki, D. A.; Chang, W.; Dougherty, D. A. *J. Am. Chem. Soc.* **1991**, *113*, 2764-2766. (e) Murray, M. M.; Kaszynski, P.; Kaisaki, D. A.; Chang, W.; Dougherty, D. A. *J. Am. Chem. Soc.* **1994**, *116*, 8152-8161.

25. (a) Prokof'ev, A. I.; Solodovnikov, S. P.; Rasuleva, D. Kh.; Volod'kin, A. A.; Ershov, V. V. *Izv. Akad. Nauk. SSSR, Ser. Khim.* **1970**, *7*, 1656-1658. (b) Merete, F. N.; Spriggs, S.; Utley, J. H. P.; Gao, Y. *J. Chem. Soc., Chem. Commun.* **1994**, *11*, 1395-1397. (c) Goulart, M. O. F.; Utley, J. H. P. *J. Org. Chem.* **1988**, *53*, 2520-2525.

26. Kato, S.; Morokuma, K.; Feller, D.; Davidson, E. R.; Borden, W. T. *J. Am. Chem. Soc.* **1983**, *105*, 1791-1795.

Chapter 2. An Improved Model for One-Dimensional Polaronic Ferromagnetism: Electrochemically-Doped Poly-*meta*-phenylenefuchsone

Introduction: The Polaronic Ferromagnet Paradigm

The realization of organic materials with interesting magnetic properties depends on inducing cooperative magnetic interactions between individual magnetic moments. The required cooperativity can be divided into intermolecular and intramolecular components; because intermolecular interactions are generally weaker, antiferromagnetic, and far more difficult to control, our research has been directed towards covalent, intramolecular interactions.[1]

The simplest model one might use to study long-range intramolecular interactions is a linear polymer, nominally a one-dimensional system. This can be broken down into two basic elements (Figure 2.1), individual magnetic moments and the intervening segments which induce pairwise cooperative

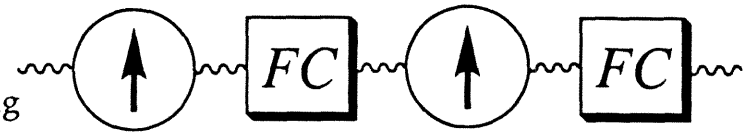

Figure 2.1: Schematic for One-Dimensional Ferromagnetic Coupling

interactions between them. Because our ultimate goal is the production of an organic ferromagnet, we wish to induce ferromagnetic, or spin parallel, coupling of the individual spin containing groups; an *anti*ferromagnet would couple individual moments antiparallel, resulting in no net moment, while a *ferri*magnet would employ antiferromagnetic coupling between unequal moments to generate a net moment.[2]

The topological requirements for ensuring high spin interactions in organic systems have been demonstrated by extensive work in small-molecule biradicals.[3] Three ferromagnetic coupling units which have been proven in small molecule systems are *meta*-phenylene (shown in *meta*-xylylene),[4] 1,1-ethylene (shown in trimethylenemethane),[5] and in substituted

Figure 2.2: Three Ferromagnetic Organic Topologies

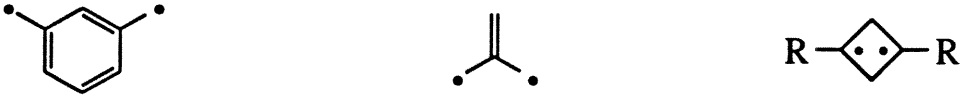

meta-Xylylene Trimethylenemethane 1,3-Cyclobutanediyl

1,3-cyclobutanediyls (Figure 2.2).[6] We consider these to be robust ferromagnetic coupling units because a variety of substituted analogs with these topologies are triplet ground states; the most robust and best studied of these is *meta*-phenylene, with a triplet ground state by about 10 kcal/mol.[4]

In organic systems the smallest possible spin containing groups are charged or uncharged monoradicals. Although the three examples above are magnetically stable, the methyl radicals which contain the magnetic moments are only chemically stable at low temperature in a solid matrix. Results from conducting polymer work show that delocalized radical cations or radical anions, also known as polarons, can be readily generated and are relatively chemically stable at room temperature[7] (technically, the radical ions in our polymers are not polarons since they are not in an infinite chain, but we find the term useful). Polarons can be generated by oxidation or reduction of a conjugated π system. For example, oxidative doping of poly-*para*-phenylene creates cationic polarons (Figure 2.3).

Figure 2.3: Polaron Generation in Poly-*para*-phenylene

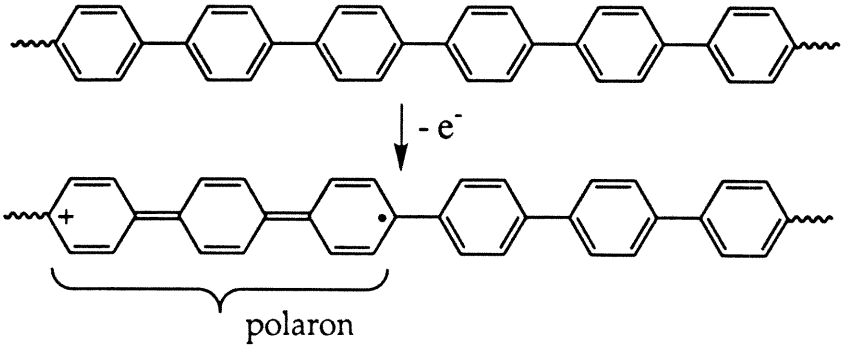

Combination of these two subunits defines our approach to rational design of one-dimensional magnetic organic systems: spin containing units, made of charged, delocalized organic radicals, connected by units with a defined ferromagnetic topology, such as *meta*-phenylene. Early theoretical work by Fukutome[8] coined the term "polaronic ferromagnet," and so we call these systems one-dimensional models for polaronic ferromagnetism.

Previous Work

This group has explored the viability of polymer models for one-dimensional polaronic ferromagnetism using several systems.[1] So far, these have made use of *meta*-phenylene as a ferromagnetic coupling unit and a variety of oxidatively-doped spin containing units. The very first study concerned poly-*meta*-phenyleneocatatetraene, or **PMPOT** (Figure 2.4). Later studies employed thiophene, thiophene-vinylene, indoloindole, and indoloindole-vinylene groups as precursors to spin containing units. Wittig chemistry was used to create the vinylene-containing polymers, while direct aryl-aryl couplings were performed by palladium-catalyzed Suzuki chemistry. Doping was accomplished by heterogeneous oxidation with gaseous arsenic pentafluoride or iodine, or homogenous oxidation in solution using iodine. Magnetic measurements were performed on neat oxidized polymer from which all solvent and unreacted dopant had been removed by drying under vacuum or in a glovebox. Despite the incorporation of long alkyl or ether chains on the *meta*-phenylene, which increased the solubility of the undoped polymers, doped samples could not be re-dissolved.

The results from these studies were both encouraging and troubling (Table 2.1).[1e] Almost exclusively, samples which had S values unambiguously greater than 0.5 (i.e., ≥ 1.0) had spin concentration of one percent or less of the theoretical maximum value. Such a small signal could

Figure 2.4: Prior Models for Polaronic Ferromagnetism

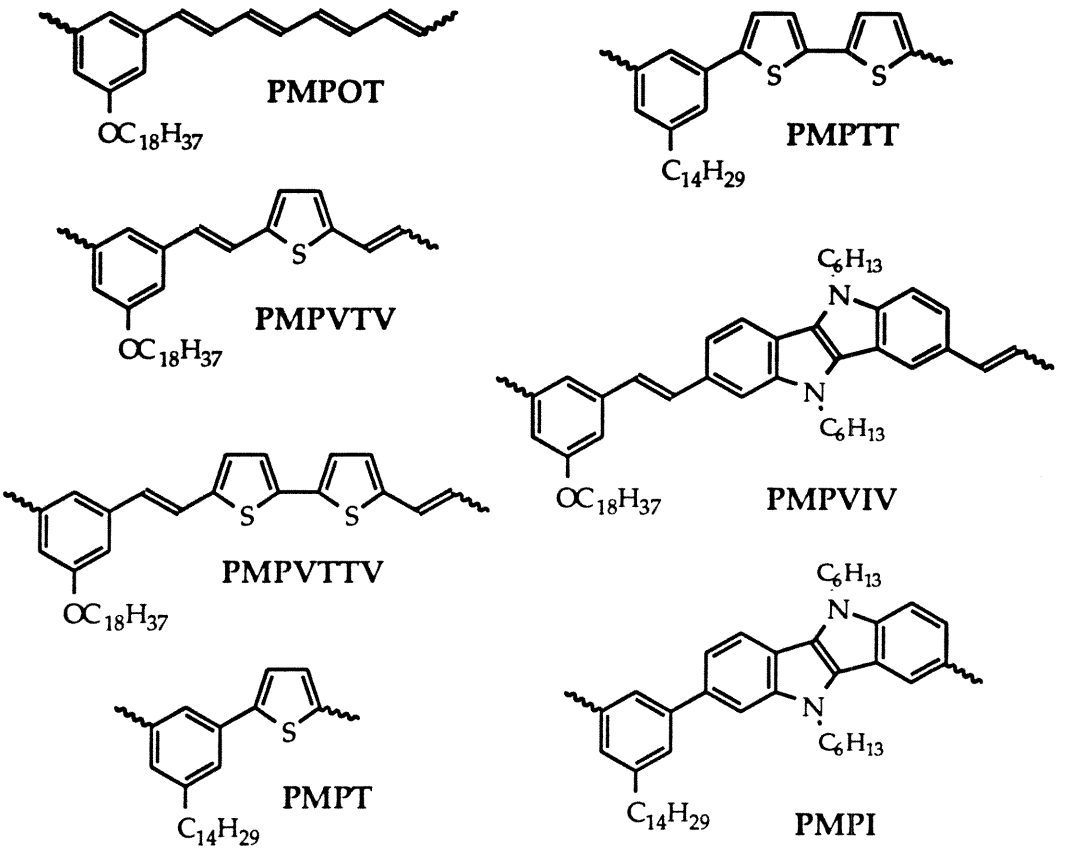

Table 2.1: Representative *S* Values and Spin Concentrations (in Parentheses) From Previous Studies; Measured at 1.8 K.[1]

Polymer	Iodine	AsF5: Light	Heavy
PMPOT	1.4 (0.6)	2.2 (0.5)	0.5 (3.6)
PMPTVT	1.4 (0.8)	2.1 (0.2)	0.5 (2.6)
PMPVTTV	0.5 (2.2)	0.6 (1.3)	0.6 (5.5)
PMPT	no moment	0.6 (0.6)	0.6 (6.5)
PMPTT	1.0 (1.0)	0.6 (8.8)	0.7 (18.1)
PMPVIV	0.6 (17)		
PMPI	0.8 (32)		

be due to paramagnetic impurities; only for PMPOT was a control experiment using a *para* linked isomer performed, which showed the original signal was due solely to the *meta* polymer. Conversely, samples with spin concentrations greater than one percent displayed *S* values of 1.0 or less. For samples with such low moments, it would be imprudent to regard an *S* value slightly greater than 0.5 as unambiguous proof of ferromagnetic coupling.

The first case, generally involving light oxidation suggests that spin distribution was highly inhomogeneous.[7] Since the degree of polymerization for these polymers ranges from 15 to 30, one percent spin concentration means less than one unpaired electron per polymer chain on average. One possible interpretation is that isolated islands of highly doped polymer were created where spins were coupled ferromagnetically.

The second case, generally involving heavier doping, indicated the presence of a large number of isolated single spins. The lack of significant coupling could be due to any number of factors, including overpowering intermolecular antiferromagnetic interactions, degradation of the coupling units by over-oxidation or crosslinking, bipolaron defects (spinless dications) due to over-oxidation of the spin containing units, weakened magnetic coupling resulting from minimal spin density in these delocalized radicals, and extensive twisting of the backbone leading to disruption of magnetic coupling.

One problem demonstrated by both cases is the simple difficulty of cleanly generating a large number of polarons. Unlike conducting polymers, where a modest amount of polaron formation may lead to significant changes in conductivity,[7] magnetic systems, especially one-dimensional models, depend critically on polaron concentration; every undoped site is a defect which interrupts magnetic coupling.

Goals of This Study

The goals of the present study are to substantiate and extend the validity of the one-dimensional polaronic ferromagnet by addressing these issues. The counterintuitive observation of an inverse relationship between *S* value and spin concentration might be eliminated if solubility were increased. This would likely allow more thorough, controlled, homogeneous doping, resulting in fewer non-magnetic defects, and would also allow the doped polymer to be diluted in some diamagnetic material, which could reduce intermolecular antiferromagnetic interactions, crosslinking, and even twisting of the polymer backbone. Choice of the spin containing group will embody a delicate balance of competing factors. Polaron generation must be facile yet bipolaron generation should be difficult; and, the doped unit must be relatively chemically stable, but must also possess significant spin density at connecting points or ferromagnetic coupling will suffer. A *para* linked control polymer should be examined to prove that any ferromagnetic interactions observed are solely due to the designed *meta* topology of the target polymer. Finally, it is desirable to obtain some quantitative measure of doping level to distinguish under-doping from over-doping as the cause of low performance.

Design Criteria

The ferromagnetic coupling unit chosen for this study is *meta*-phenylene, with a tetradecyl chain attached for solubility. The precursor to the spin containing unit, 2,6-di-*tert*-butylfuchsone, possesses a number of attractive features. We term the resulting target polymer poly-*meta*-phenylenefuchsone, or **PMPF** (Scheme 2.1). Electrochemical studies have shown that the radical anion of 2,6-di-*tert*-butylfuchsone is relatively stable in solution and easily generated, while the second reduction potential is

Scheme 2.1: Synthesis of Poly-*meta*-phenylenefuchsone

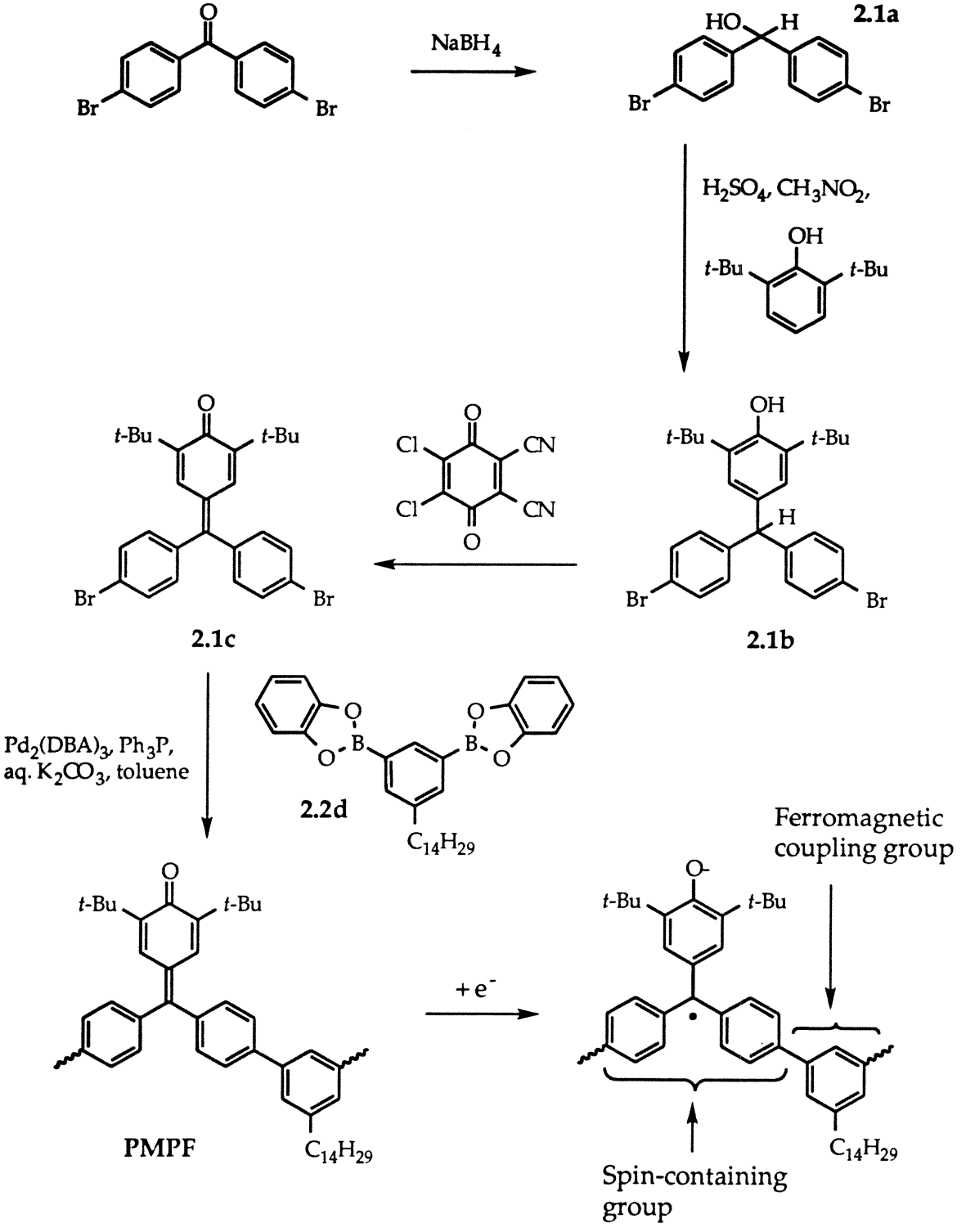

sufficiently removed (ca. 400 mV) so the amount of dianion (i.e., bipolaron defect) formation at the first reduction potential is negligible.[9] The steric bulk of the phenyl rings limits reaction at the central carbon and that of the *tert*-butyl groups help protect the oxygen. Additionally, the bulky *tert*-butyls may help to weaken intermolecular antiferromagnetic interactions by preventing close packing of adjacent phenoxy rings, but might also reduce the solubility of the doped and undoped polymers. Solubility can be improved by using an appropriate organic counter-ion such as tetrabutylammonium, which we have demonstrated for other di-*tert*-butylphenolate anions.[10] Also, it has been our observation, and seems generally known, that organic radical anions can be more soluble and less reactive than radical cations.[11]

Are there reasons besides solubility and chemical stability to prefer radical anions for models of polaronic ferromagnetism? A qualitative argument can be made that, all other things being equal, the ferromagnetic coupling of radical anions through an appropriate π topology could be stronger than for radical cations. The triplet state of a biradical experiences reduced Coulomb repulsions relative to the singlet because the Pauli exclusion principle correlates the motion of spin-parallel electrons so they remain apart.[12] In otherwise identical systems, a cationic singlet should experience fewer Coulomb repulsions than an anionic singlet. The cationic system, containing four fewer electrons, is by definition more open; the unpaired electrons simply have more space to avoid each other. Also, the unpaired electrons, bound tightly by the positive charge, should be localized apart from each other. The unpaired electrons in the more crowded, delocalized, anionic system interact more, so the anionic singlet has comparatively greater Coulomb repulsions; consequently, correlated electron motion in the triplet affords correspondingly greater stabilization, leading to a

larger singlet-triplet gap than in the cationic system. This argument is admittedly non-rigorous and could be disproved by a careful theoretical study, but it is sufficient justification to proceed with the present investigation.

Effective magnetic coupling will depend on the presence of sufficient spin density where the spin containing unit is connected to the ferromagnetic coupling unit.[13] Spin densities for the radical anion of 2,6-di-*tert*-butylfuchsone, derived from EPR data and calculated from Huckel considerations (Figure 2.5), are 0.094 and 0.0660 for the *para* positions on the unsubstituted phenyl rings.[9a,b] Given that the singlet-triplet gap in *meta*-xylylene is about 10 kcal/mol,[4] scaling[13] this interaction by the square of the

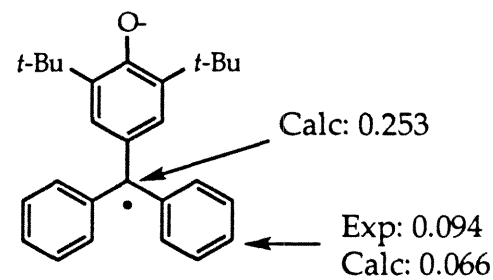

Figure 2.5: Selected Spin Densities in 2,6-Di-*tert*-butylfuchsone Radical Anion (from reference 9a,b)

preceding spin densities gives roughly 40 to 90 cal/mol for the target polymer. The corresponding temperature range for the onset of intramolecular ferromagnetic coupling is then 20 to 45 K, easily within the range of our measurement capability.

Synthetic Strategy

Synthesis of **PMPF** was accomplished by a palladium-catalyzed Suzuki coupling of bis-boronic ester **2.2d** with dibromo-di-*tert*-butylfuchsone **2.1c** (Scheme 2.1), similar to prior work in this group.[1e] Significant modifications include the use of smaller amounts (0.3 mole-percent) of a different palladium catalyst, tris(dibenzylidene)dipalladium.[14] The reaction gave **PMPF** in quantitative yield, with MW ca 4620 and degree of polymerization 7.

Polymer length seems to be limited by solubility, as reaction progress slows when product begins to precipitate.

Dibromofuchsone **2.1c** was prepared[15] from 4,4'-dibromobenzophenone by sodium borohydride reduction to **2.1a**, acid catalyzed condensation with 2,6-di-*tert*-butylphenol in nitromethane (attempts in acetic acid gave the acetate of **2.1a** as the major product) to triarylmethane **2.1b**, and oxidation to dibromofuchsone **2.1c** using 2,3-dichloro-5,6-dicyano-benzoquinone.

Synthesis of bis-boronic ester **2.2d**, precursor to the ferromagnetic coupling unit, was accomplished in 48% yield (Scheme 2.2) as has been reported previously.[1e] Briefly, *para*-dodecylaniline was reacted with bromine to form the 2,6-dibromo-4-tetradecylaniline (**2.2a**). The amino group was removed with *tert*-butyl nitrite. The resulting dibromide (**2.2b**) was then converted to the bis(trimethylsilyl) derivative (**2.2c**) by refluxing with magnesium and trimethylsilyl chloride. Subsequent treatment with boron tribromide followed by catechol gave bis-boronic ester **2.2d**.

For the control experiment, poly-*para*-fuchsone, **PPF**, (Scheme 2.4), a polymer with an antiferromagnetic, *para* topology, was generously provided by Seth Miller.[16] Synthesis was accomplished by a zinc-catalyzed homocoupling of 2,6-di-*tert*-butyl-4',4''-dichlorofuchsone.

Doping Procedures

All doping was carried out in a dry, oxygen-free, nitrogen-filled glovebox. Only non-magnetic glass, ceramic, Teflon, or Delrin utensils were used. These were carefully cleaned of trace metal before every experiment by soaking in dilute acid, then washing in succession with neutralizing buffer, a solution of sodium ethylenediaminetetraacetate, and distilled water. Solvents were removed under vacuum.

Scheme 2.2: Synthesis of 5-tetradecylbenzene-1,3-bis-(1,3,2-benzodioxaborole)

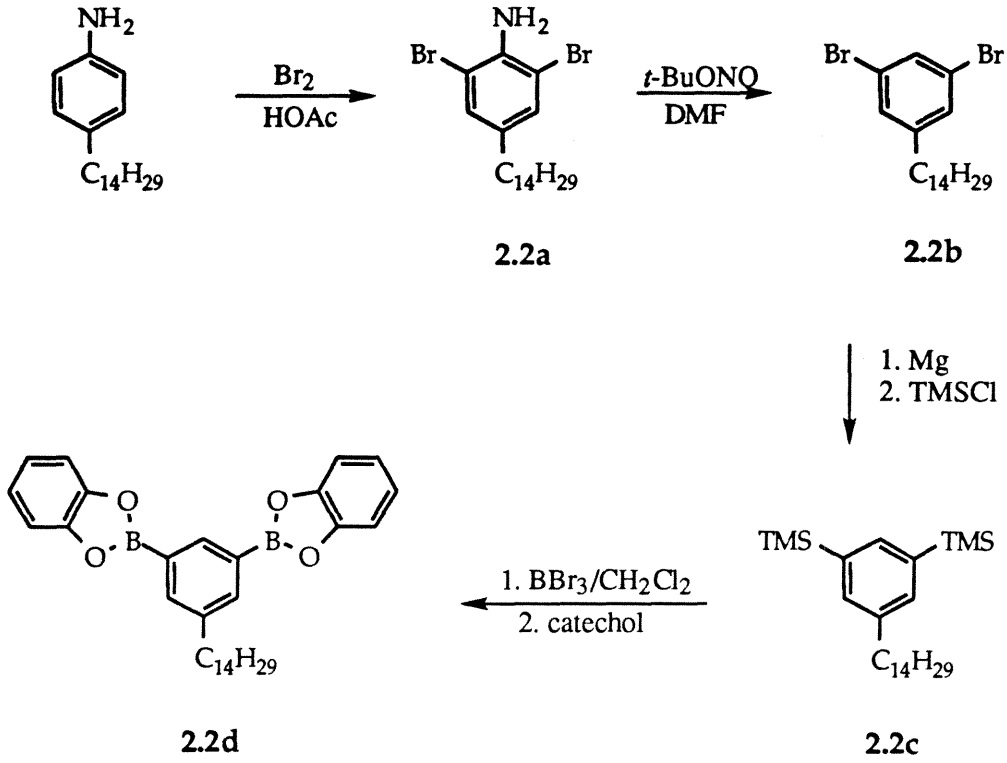

Scheme 2.3: Synthesis of Control Polymer **PPF**

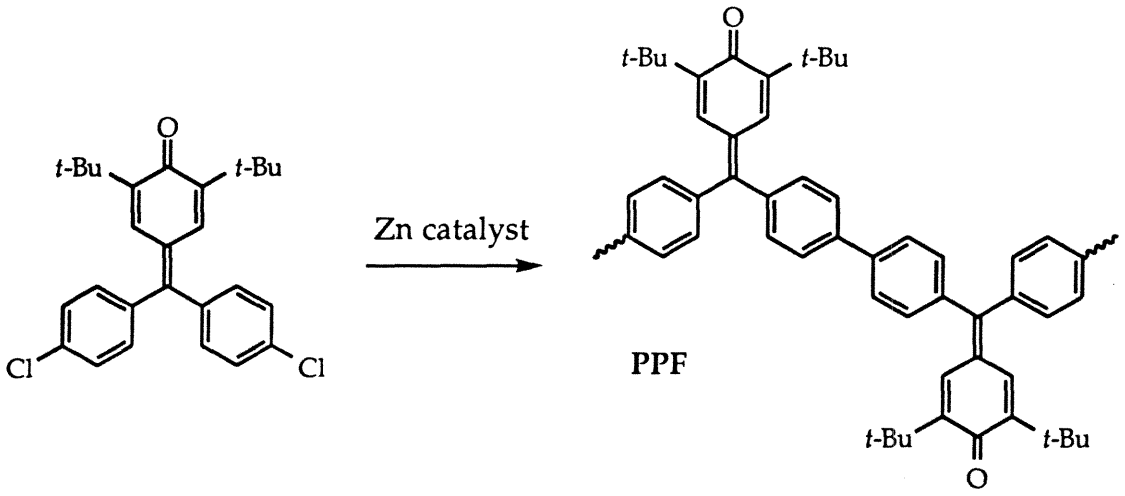

Chemical reduction[9a,b] was performed by stirring a concentrated solution of the polymer in THF with distilled tetrakis(dimethylamino)-ethylene, high-purity sodium, or sodium naphthalide. Stirring for at least 30 minutes with an equivalent or more of either sodium or tetrakis (dimethylamino)ethylene alone changed the solution's color from bright orange to brownish orange. When doping with sodium, no length of stirring resulted in significant dissolution of the solid metal. Treatment for prolonged periods with a high-power sonicator did not result in noticeable further dissolution. When doping with sodium naphthalide, the color of the reagent obscured any color change which might have occurred in the substrate. Removal of solvent from this mixture deposited a large amount of metallic sodium, although it had previously all been in solution.

Electrochemical reduction[9] was performed using working and counter electrodes made of high-purity platinum gauze, and a reference electrode made of high-purity silver wire plated with silver chloride. These were also carefully decontaminated before each experiment as described above. The cell's counter and working cells were separated by a fine glass frit. Electrolyses were performed in a solution (0.3 M) of high-purity tetrabutylammonium perchlorate in THF. Before adding polymer, the electrolyte solution was pre-electrolyzed at -1.75 V for about 20-40 min, until background current had dropped under 50 μA; background current then measured at the first reduction potential (-1.25 V) was less than 20 μA. An amount of polymer sufficient to make the concentration of the polymer's repeat unit between 1 to 4 mM was dissolved. The reference potential was applied starting at -1.0 V, stepping to more negative potential slowly to maintain the current ≤ 3 mA, but never below a potential of -1.40 V. The reduction was stopped when the desired amount of charge had been passed. After only a few seconds of

reduction at ~ 3 mA, the bright orange solution turned darker than any of the attempts at chemical reduction. Between 0.2 and 0.6 F/mol, solutions using **PMPF** were intensely black-green, almost opaque, with the color visible initially at the meniscus and later only by holding a microcapillary of the solution up to a bright light. After 0.8 F/mol, the color had become a deep, dark purple. For control polymer **PPF**, behavior was similar except the final color was not purple but an almost fluorescent green.

In electrolyses where the amount of charge passed exceeded 1.0 F/mol, the current did not drop to the pre electrolysis background but leveled off at about 400 μA. In such prolonged experiments, the electrolyte solution in the counter cell had been significantly oxidized, turning dark brown, and often became an opaque, viscous gel. Replacing this with fresh electrolyte and allowing the system to stand for an hour decreased the current somewhat, but still not to the pre electrolysis background.

Prolonged reduction also resulted in apparent corrosion of the silver chloride film on the surface of the reference electrode. We worried that this might be raising the background current, shifting the reference potential, and through dissolved metal ions, possibly even contributing contaminating magnetic moments. Replacement with a fresh electrode, however, did not bring any significant change in current or potential. Also, despite identical behavior during the electrolysis of control polymer **PPF**, no evidence of spurious magnetic moments was found. Thus, the only apparent consequence was the occasional necessity of re-plating the reference electrode.

After reduction, the solvent was removed by vacuum, leaving a dark black-green (**PPF**) or black-purple (**PMPF**) solid which was a mixture of the doped polymer and tetrabutylammonium perchlorate. The **PMPF** mixture could be redissolved in CH_3CN, and both could be redissolved in THF. These

solids were loaded into sample tubes and subjected to magnetic analysis without delay.

Magnetic Characterization[12,17]

As a finite, linear model for polaronic ferromagnetism, doped **PMPF** is not expected to display spontaneous bulk magnetic behavior.[1] Ideally, fully doped chains of **PMPF** would behave as isolated paramagnets, with seven unpaired electrons coupled ferromagnetically, since each repeat unit is designed to contain one unpaired electron and the polymer is on average a 7-mer. In practice, less than ideal behavior is expected because of intermolecular antiferromagnetic interactions (only lessened by dilution), doping variation, and defect formation.

The information to be obtained consists of the average number of electrons coupled ferromagnetically in individual moments (the *S* value), the number of individual spins generated versus the theoretical maximum (the spin concentration), and information regarding the balance of ferromagnetic and antiferromagnetic interactions. The *S* value can be determined by observing the resultant magnetization M upon varying an applied magnetic field H at constant temperature. At low temperatures, increasing field will begin to overcome the thermal randomization of each moment's orientation; at sufficiently low temperature and high field, all the moments in a paramagnetic material will be aligned with the field, or saturated. The value of *S* determines how quickly a given sample will reach M_{sat}, the limiting value of the magnetization at saturation. Fitting experimental magnetization versus field data to the Brillouin function allows the determination of *S* and of M_{sat}. The spin concentration can be calculated from M_{sat} and the mass of the sample. Further information may be obtained from magnetization observed versus temperature at constant field: a rise in relative effective

magnetic moment indicates increasing ferromagnetic interactions, while a decrease indicates antiferromagnetic interactions.

Caution should be used when attempting to interpret the results of Brillouin modeling.[1e,18] The derived numbers describe bulk, average properties of a doped polymer containing a distribution of moment sizes in varying local environments. For example, not every moment in a sample with $S = 2.0$ contains exactly four ferromagnetically coupled electrons. If this were the case, the experimental data would fit exactly to the Brillouin function, which never happens. Additionally, while mathematically good fits can still be made to such data, the variance in the fit is relatively insensitive to moderate changes in S or M_{sat}. For these reasons it is difficult to come up with meaningful error estimates for S and M_{sat}, and consequently spin concentration. What is important for such numbers is not the actual values but the general trends observed. A single sample with $S = 0.9$ would not constitute unambiguous proof of net ferromagnetic coupling but is useful as part of a series of experiments at different doping levels.

The raw magnetization data contain diamagnetic contributions from the polymer sample and our sample holder, which is a two-piece Delrin (a non-magnetic polyethylene oxide polymer) rod possessing a small sample cavity in its center.[18] Since the SQUID measures the difference in magnetic properties, the solid Delrin preceding and following the less dense sample through the measurement coils results in an apparent positive diamagnetic susceptibility, which considerably simplifies Brillouin analysis.

Because the paramagnetic moments we are investigating are small, this diamagnetic correction can be significant. Figure 2.6A shows magnetization data with and without the correction, demonstrating how the diamagnetic

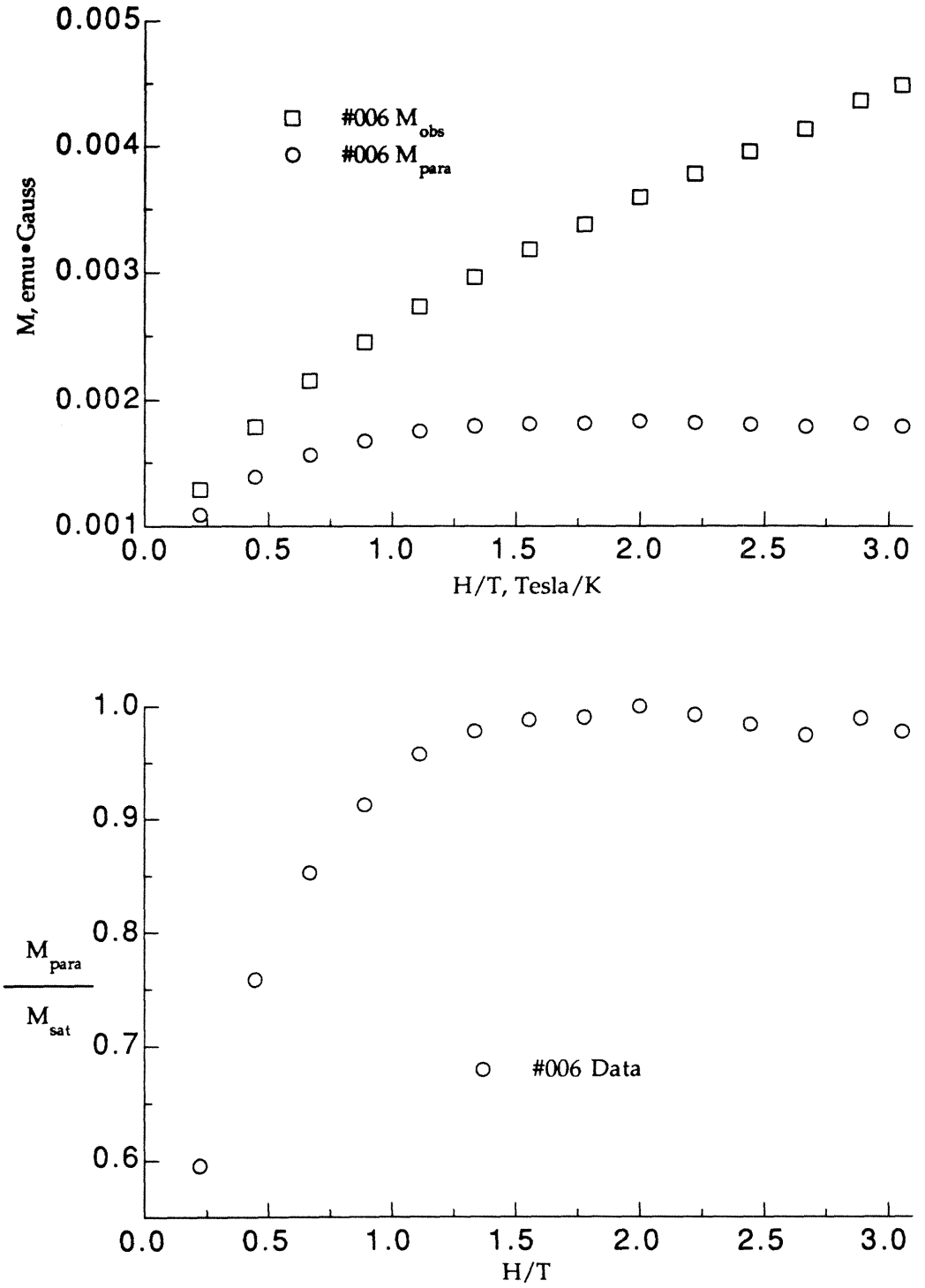

Figure 2.6: Sample #006 Sodium-Doped **PMPF**. **A.** (top) Raw magnetization data before (M_{obs}) and after (M_{para}) correction for diamagnetic contributions. **B.** (bottom) M_{para} data normalized to M_{sat}.

contribution can dominate the signal of a typical small-moment sample. The correction simply involves subtracting a straight line, of slope determined by the diamagnetic susceptibility. This line is obtained as part of the original Brillouin fit. All subsequent plots will show the paramagnetic moment M_{para} normalized to M_{sat} (Figure 2.6B).

Results of Chemical Doping

Chemical doping produced results (Table 2.2) that parallel earlier work in this group.[1e] Doping with sodium or tetrakis(diethylamino)ethylene alone produced samples with extremely low spin concentrations (less than 1%) and high S values, ranging from 2.6 to 7.1; typical plots are shown in Figure 2.7. In general, the high S/low spin concentration M versus H/T plots are noisy and fit poorly to the Brillouin function. Sonication did not help sodium doping but did provide a slightly higher spin concentration (2.3%) but lower S value (2.3) for tetrakis(dimethylamino)ethylene doping (Figure 2.8). Use of an equivalent of sodium naphthalide increased the spin concentration dramatically (19%) but S decreased to 1.2 (Figure 2.9B). One experiment using an equivalent of sodium, a catalytic amount of naphthalene, and sonication again gave an extremely low spin concentration (0.20%) and an S value of 2.6 (Figure 2.9A).

The relative effective moment versus temperature data were unexceptional, typified by that observed for a sodium-doped **PMPF** sample (Figure 2.10A). Virtually all such plots showed this inverted U shape, mirroring previous work in the group. The exception was for sodium-naphthalide doped **PMPF**, which contained a small hump centered around 20 K (Figure 2.10B).

Table 2.2: Magnetic Characterization of Chemically Doped **PMPF**

Sample #	Doping conditions	*S* value	Spin%
006	**PMPF** & Na	6.1	0.61
007	**PMPF** & Na	7.1	0.62
010	**PMPF** & Na. sonicated	4.2	0.35
011	**PMPF** & Na/Naphthalene	1.1	17
012	**PMPF** & Na/Naphthalene	1.2	19
015	**PMPF**, Na, cat. Naphth, sonic.	2.6	0.20
016	**PMPF** & TDAE	5.6	0.15
017	**PMPF** , TDAE, & sonication	2.3	2.3

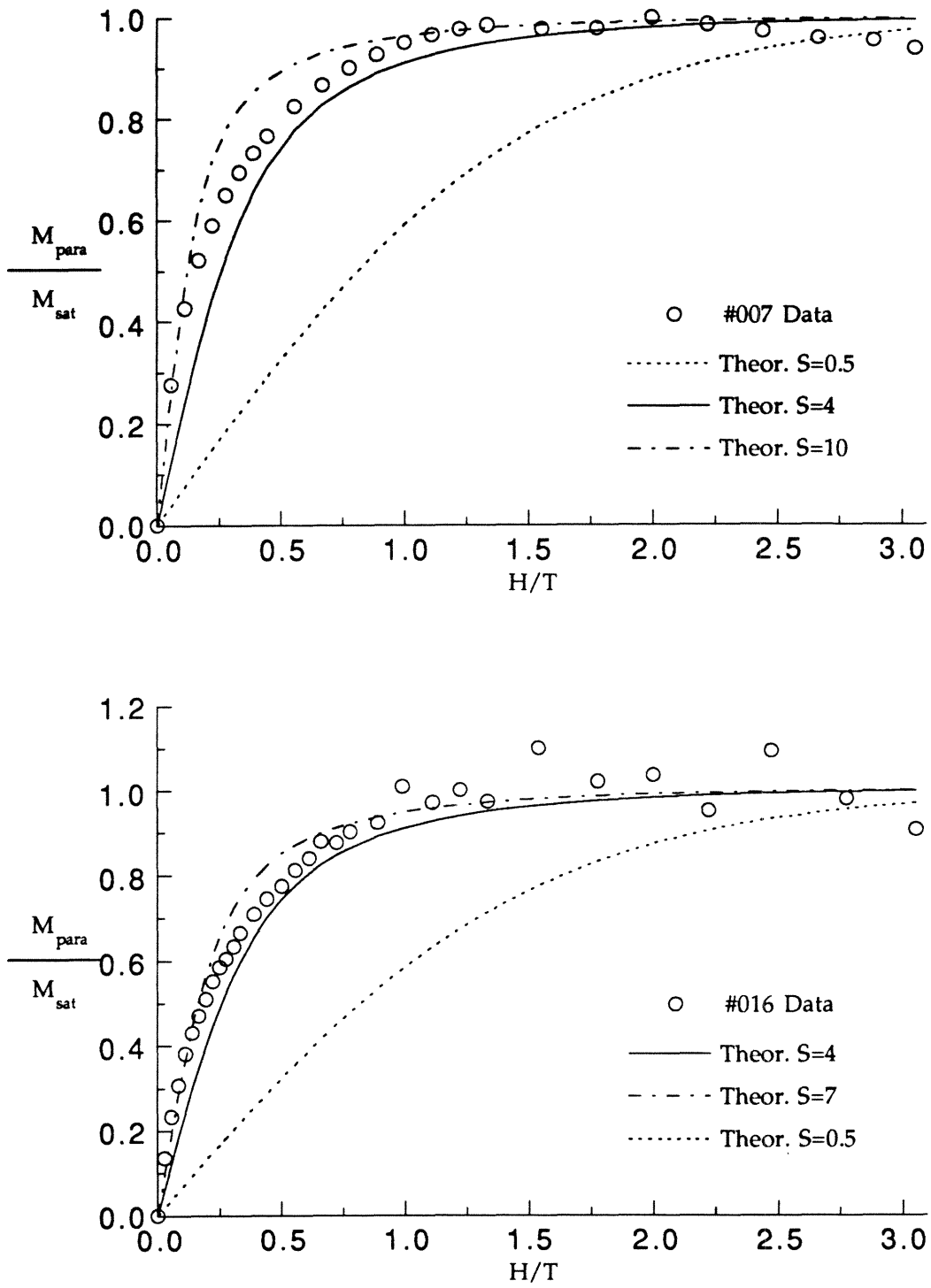

Figure 2.7: Typical Noisy, High *S*, Low % Spins Data for Chemically Doped **PMPF**. **A.** (top) #007, Na doping, best fit $S = 7.1$, spins 0.62%. **B.** (bottom) #016, TDAE doping, best fit $S = 5.6$, spins 0.15%.

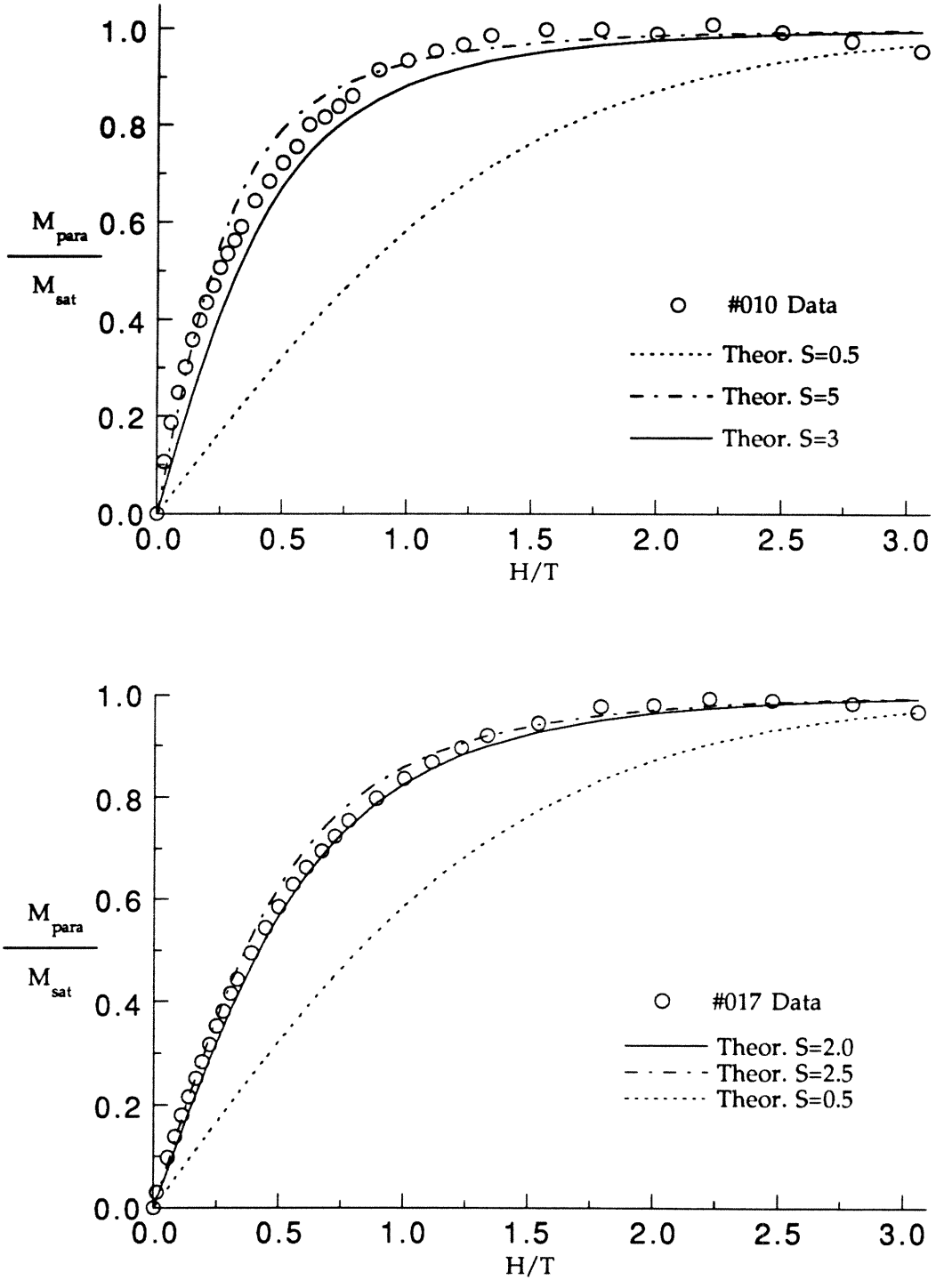

Figure 2.8: Sonication Combined with Chemical Doping of **PMPF**. **A.** (top) #010, Na doping, best fit S = 4.2, spin concentration 0.35%. **B.** (bottom) #017, TDAE doping, best fit S = 2.3, spin concentration 2.3%.

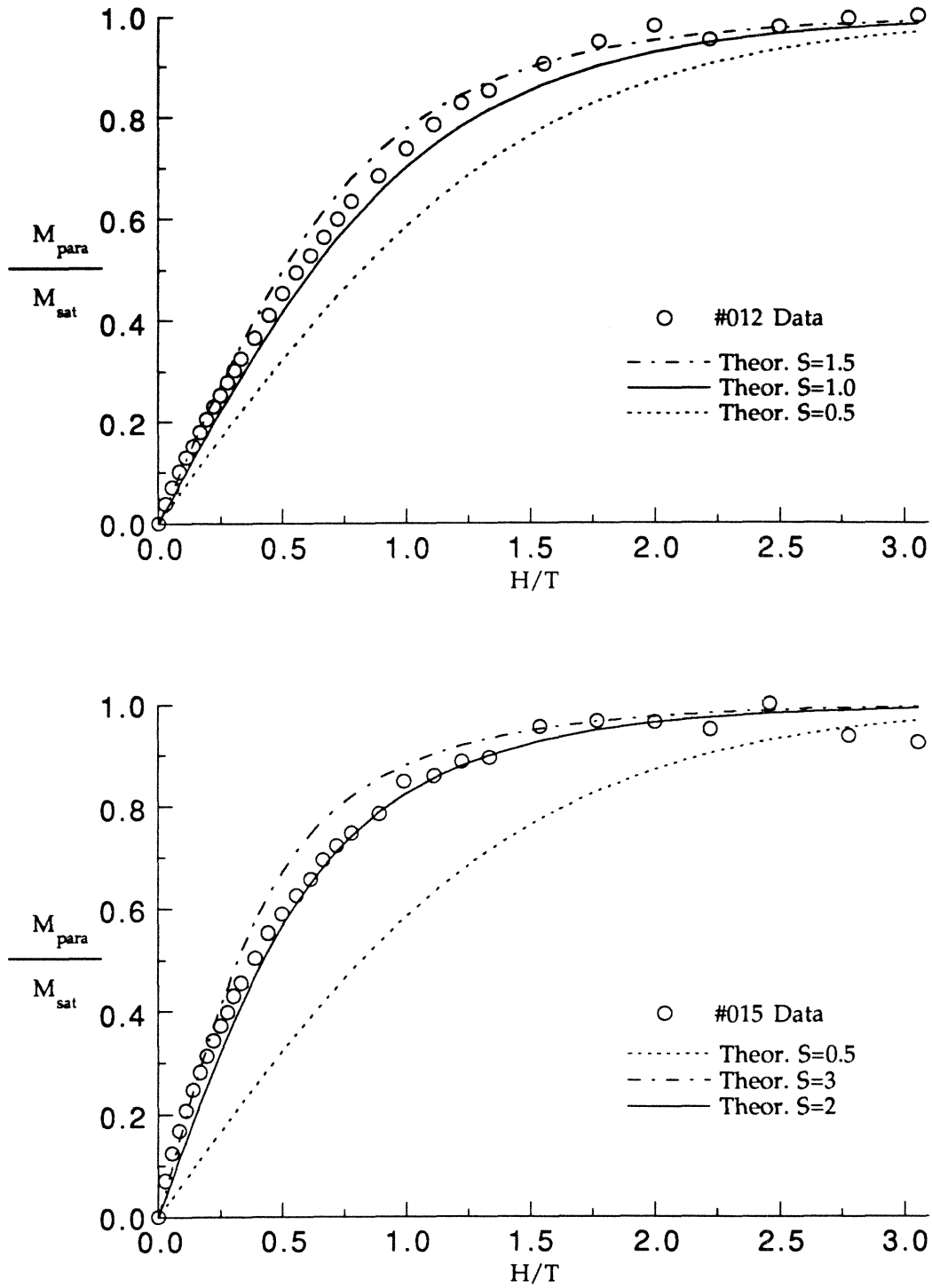

Figure 2.9: Sodium Naphthalide Doping of **PMPF**. **A.** (top) #012, best fit S = 1.2, spin concentration 19%. **B.** (bottom) #015, Na, catalytic amount of naphthalene, & sonication, best fit S = 2.6, spin concentration 0.20%.

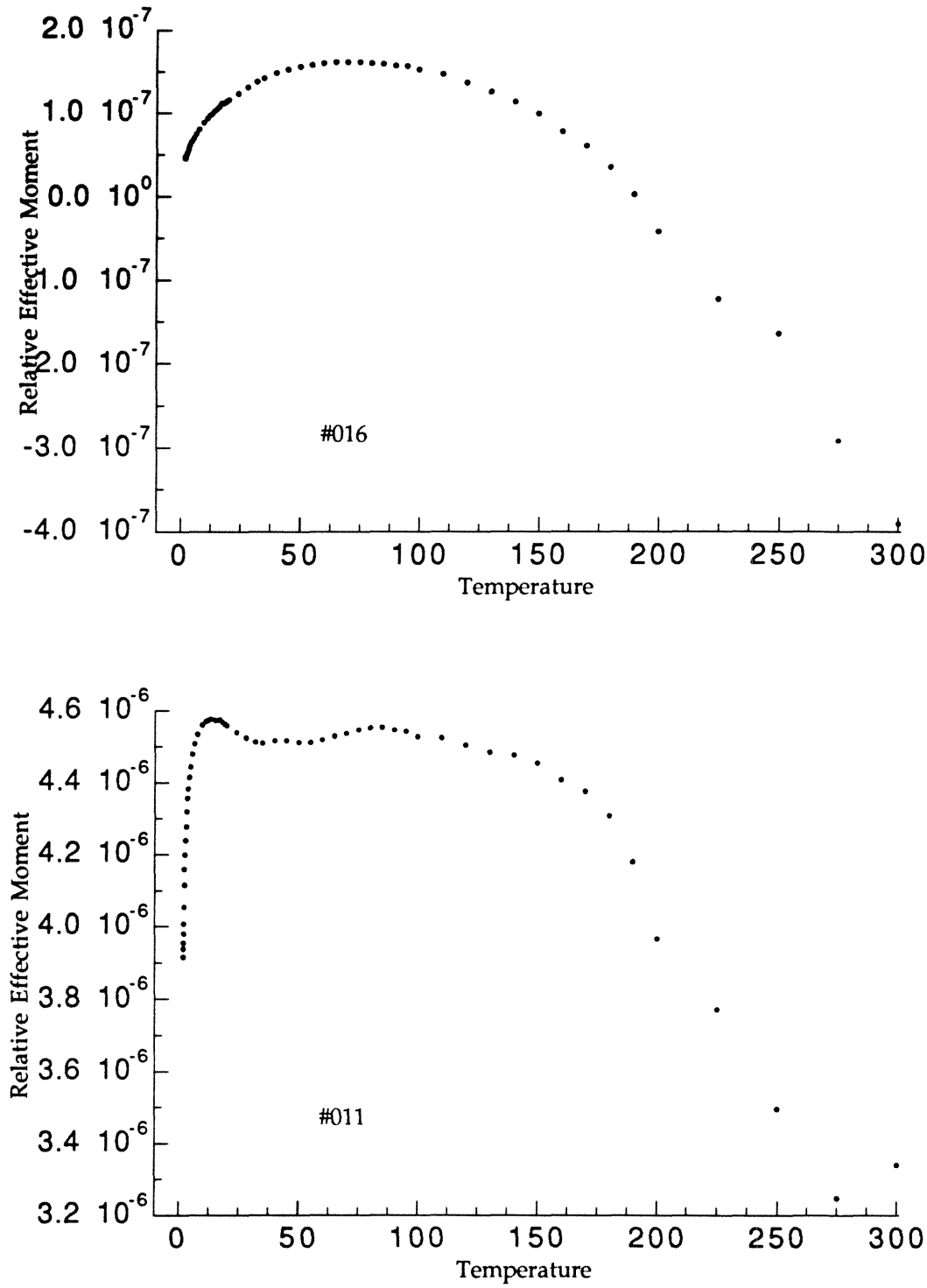

Figure 2.10: Relative Effective Moment Plots for Chemically Doped **PMPF**. **A.** (top) #016, typical plot for every sample except **B.** (bottom) #011, atypical plot for Na-naphthalide doped **PMPF**; note hump centered at 13 K.

Results of Electrochemical Doping

Results from electrochemical doping are substantially different (Table 2.3). There is a clear increase in both *S* value and spin concentration as the amount of electrochemical reduction increases (Figure 2.11), up to about 1.2 F/mol. A provisional interpretation is that *S* and spin concentration have leveled off or even begun to turn down at this point, but more data points would be needed for a firm conclusion. All of the electrochemical samples (except #506 **PMPF**, 0.3 F/mol, plot not shown) gave relatively noise-free data which fit the Brillouin function well, even though dilution in tetrabutylammonium perchlorate rendered their absolute moments comparable to those from the low spin %, chemically-doped **PMPF** samples.

The maximum *S* value observed is 2.0, at a spin concentration of 58% and doping extent of 1.24 F/mol (Figure 2.12A). Doping of control polymer **PPF** under the same conditions gave an *S* value of 0.55 with 6.8% spin concentration (Figure 2.12B).

Plots of relative effective magnetic moment versus temperature showed behavior similar to that of sodium naphthalide doped **PMPF**. Nearly all of the **PMPF** show a significant upturn in moment beginning by 30 K, peaking between 3-5 K, and then turning down (Figure 2.13A). Sample #523 did not turn down by 1.8 K. The effective moment versus temperature plot for doped samples of control polymer **PPF** showed the familiar inverted U shape, turning down at low and high temperature (Figure 2.13B). Figure 2.14 shows a stacked plot of all the electrochemically-doped **PMPF** relative effective moment data. The baselines have been adjusted to be coincident by correcting for absolute spin concentration, and the heights have been normalized to the peak of sample #522. The relative heights of the peaks reflect the raw data.

Table 2.3: Magnetic Characterization of Electrochemically Doped **PMPF & PPF**

Sample #	F/mol	*S* value	Spin concentration, %
506 **PMPF**	0.3[a]	0.84	7.7
523 **PMPF**	0.48[b]	0.92	12
525 **PMPF**	0.76[b]	1.2	25
521 **PMPF**	0.95[b]	1.4	23
524 **PMPF**	1.24[b]	2.0	58
522 **PMPF**	1.35[b]	2.0	51
520 **PMPF**	—c—	2.1	57
526 **PMPF**	1.70[b]	1.8	61
529 **PPF**	1.19[b]	0.55	6.8

F/mol values are from current measured in series with the working electrode, corrected for background current (after pre electrolysis but before adding polymer). a. ± 0.1 F/mol b. ± 0.02 F/mol c. > 0.9 F/mol

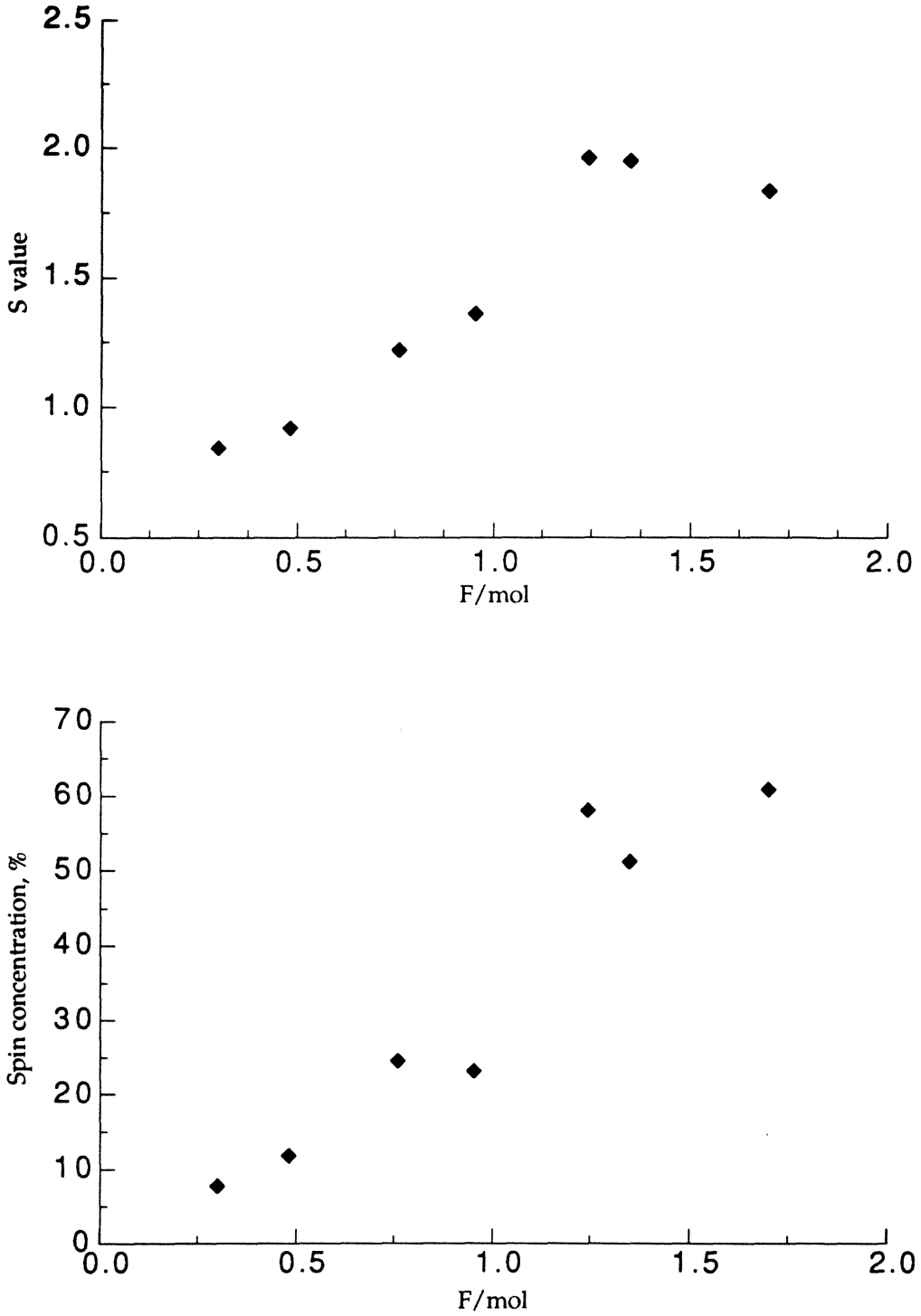

Figure 2.11: *S* Value and Spin Concentration Scale Positively with Electrochemical Doping Level in **PMPF**. **A.** (top) *S* value versus F/mol. **B.** (bottom) Spin concentration versus F/mol.

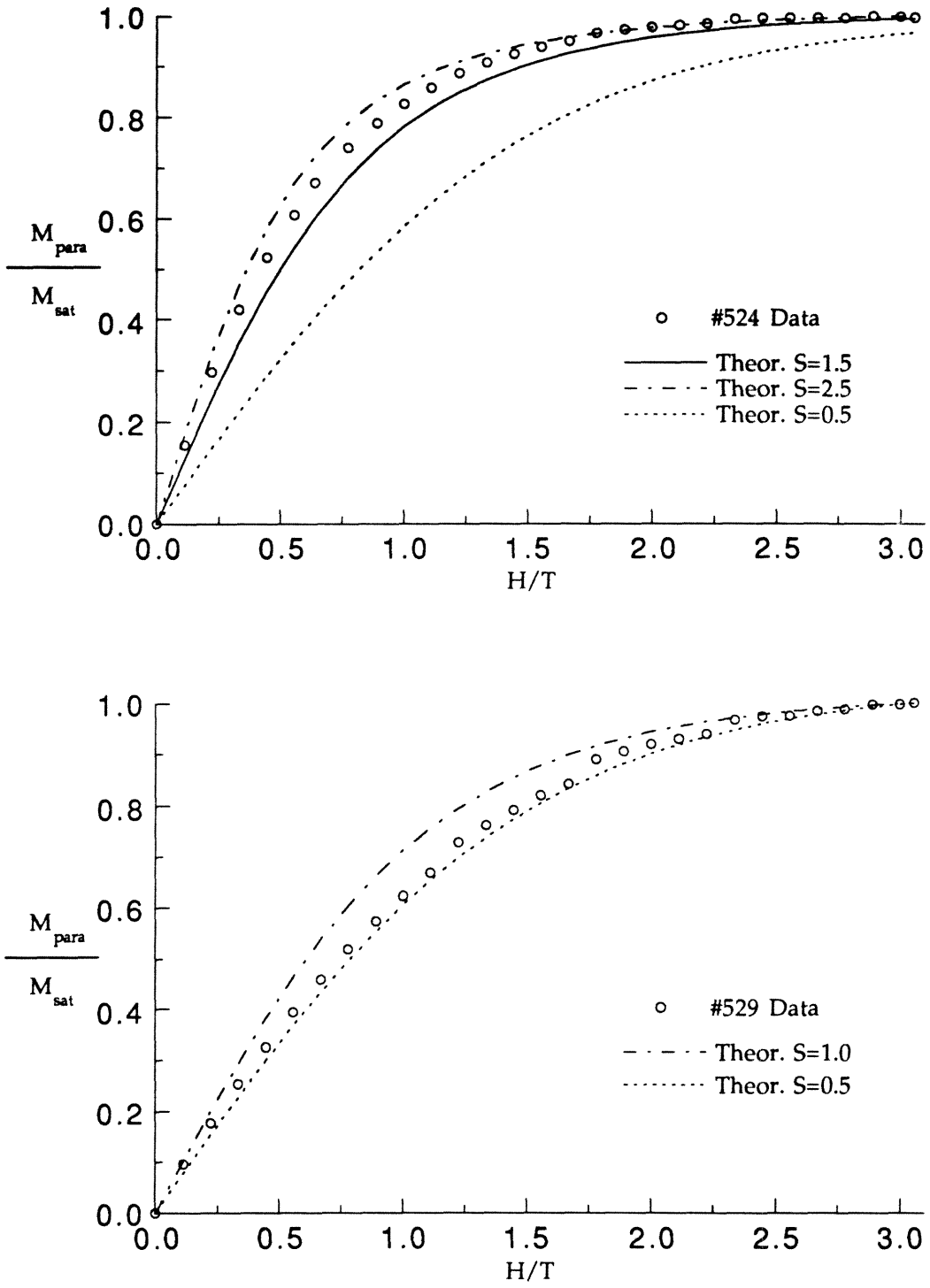

Figure 2.12: Typical Saturation Plots for Electrochemically Doped Polymer. **A.** (top) #524, **PMPF**, 1.24 F/mol, best fit S = 2.0, spin conc. 58%. **B.** (bottom) #529, **PPF**, 1.19 F/mol, best fit S = 0.55, spin conc. 6.8%.

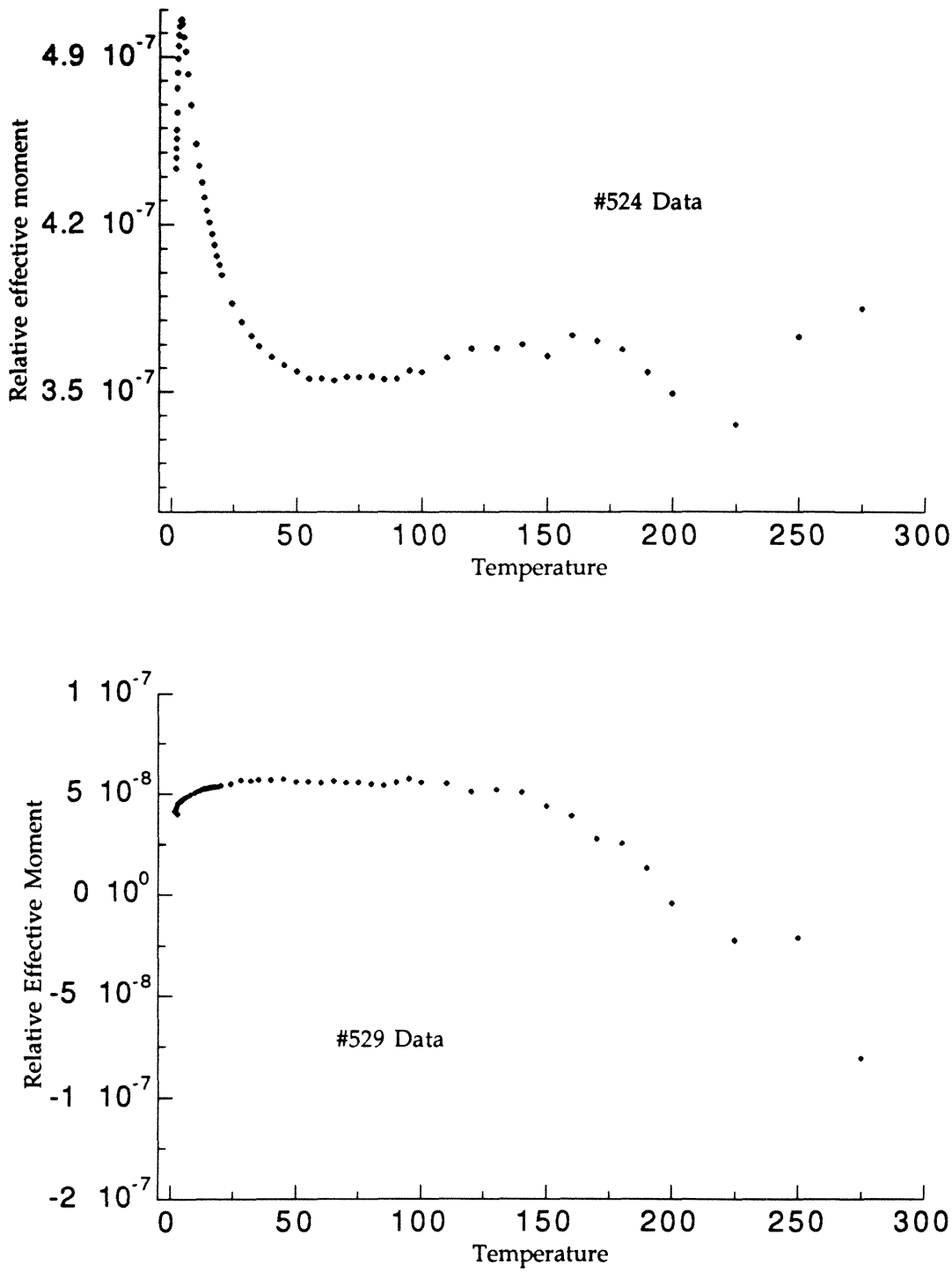

Figure 2.13: Relative Effective Moment Plots. **A.** (top) #524, **PMPF**, 1.24 F/mol. **B.** (bottom) #529, **PPF**, 1.19 F/mol.

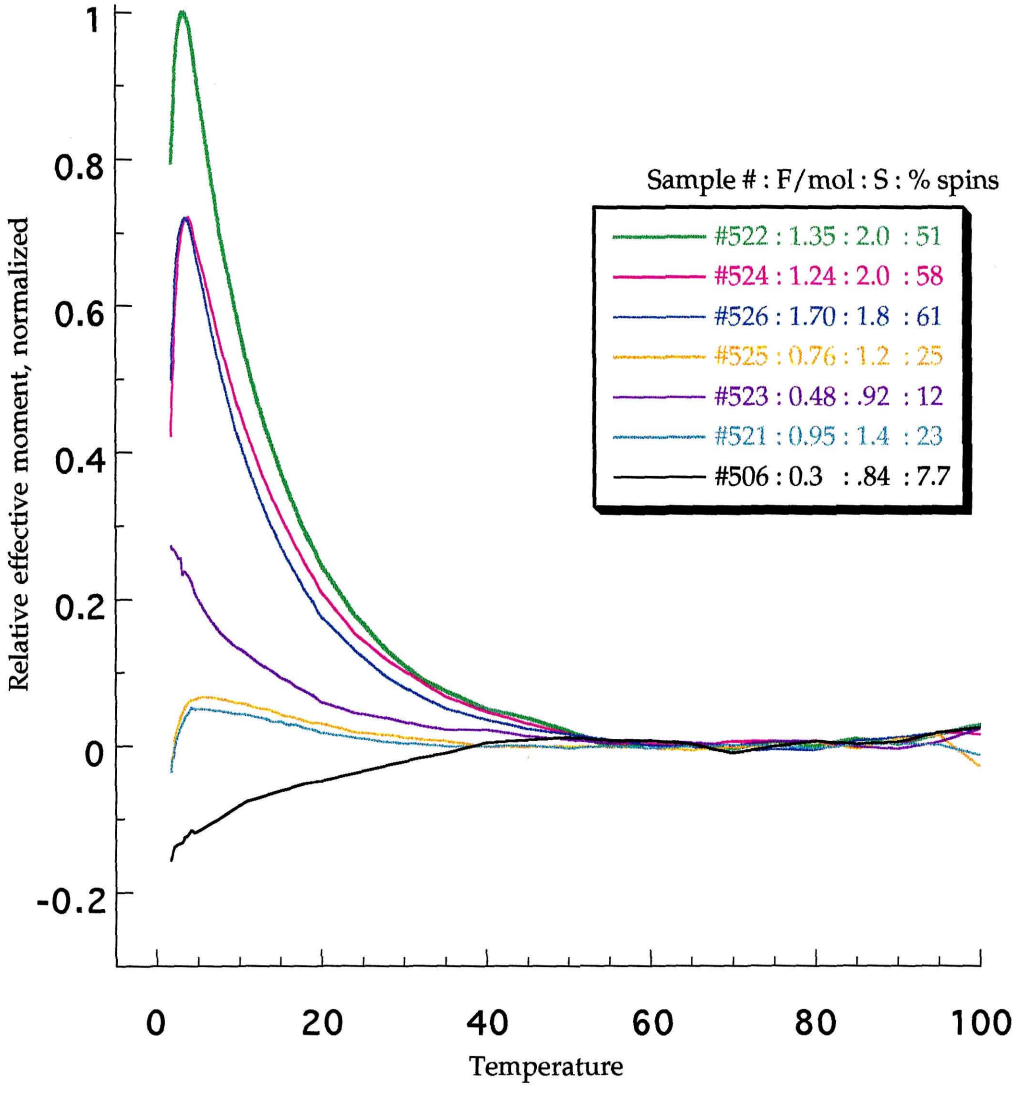

Figure 2.14: Stacked Relative Effective Moment Plots for **PMPF**. The baselines are adjusted to be coincident, but the relative heights reflect the raw data.

Discussion

This study provides a substantial increase in both performance and understanding of the one-dimensional polaronic ferromagnet paradigm. Previous work[1] generated some valuable insights, but also raised difficult questions; *S* values as high as 2.6 could be reproducibly generated, but only at extremely low spin concentration, while samples with moderate spin concentrations exhibited essentially no ferromagnetic coupling. For electrochemically doped, diluted **PMPF**, we have demonstrated a clear, positive relationship between *S* and spin concentration, culminating in an *S* of 2.0 at 58% spins. This represents an increase of nearly two orders of magnitude in spin concentration at this *S* value. While this is still far from our eventual goal of an organic ferromagnet, these significant results provide clear directions for future work.

Doping Issues

Chemical doping[9a,b] has proven problematical for these systems. There are few chemical dopants with potentials suitable for doping fuchsones. Tetrakis(dimethylamino)ethylene's reduction potential (-0.9 V) is probably too weak to generate significant amounts of unpaired electrons. Sodium's potential is well beyond the second, irreversible, reduction potential of fuchsones, yet sodium alone, with sonication, or with catalytic naphthalene and sonication did not react readily with **PMPF**. Furthermore, any strategy, such as extended sonication, that causes reaction with **PMPF** might simply over-dope the material. Sodium naphthalide did give some interesting results, but the deposition of metallic sodium upon solvent removal was troubling. Therefore, it is difficult to estimate the extent of reaction when using these dopants, and difficult to know whether poor results are due to under-doping, over-doping, or some other effect. One additional caveat for

the chemical doping results is that they are too good! The highest *S* value expected in the present study is no more than 3.5 since these **PMPF** samples are only seven repeat units long, yet values as high as 7.1 have been seen. It is difficult to interpret such confusing data. It is perhaps significant, however, that all of the $S > 3.5$ results also had spin concentrations well under one percent, and furthermore, had noisy data which fit poorly to the Brillouin function. Contamination is certainly possible, and although neat, undoped **PMPF** was diamagnetic, dopable impurities could still have been present. Control experiments using **PPF** could rule out such contamination, but were not performed with chemical doping since electrochemical doping appeared more promising.

Electrochemical doping,[9] by contrast, is much more effective and much easier to control. Increasing amounts of charge passed gave samples with increasing *S* value and spin concentration, up to a doping level of about 1.2 F/mol. Ideally, the *S* value and spin concentration should peak at 1.0 F/mol and decrease thereafter as spinless bipolaron defects are formed. We noticed, however, that after passing more than 1.0 F/mol, but still well below the second reduction potential, the current leveled off at a higher value than the initial background current (observed after pre-electrolysis but before adding polymer). One possible contribution is the oxidation of electrolyte solution at the counter electrode and the resultant clogging of the frit between the counter and working cells. It is difficult to find a proper correction for the rise in the apparent background current; however, assuming that the first reduction is done when the current levels off and that this current is not due to additional reduction to the fuchsone dianion, little decrease in the *S* value and spin concentration would be expected without using a more negative potential. Attempts were made to step to the second reduction potential in

order to see a definite turnover in *S* value and spin concentration, but this resulted in swift decomposition of the counter cell solution and plugged the frit.

Clearly, **PMPF** is pushing the limits of our electrochemical setup. THF is not an ideal solvent for bulk electrolysis; due to its relatively low dielectric constant, high concentrations of electrolyte are required to achieve a usably low cell resistance.[19] Even at 0.3 M tetrabutylammonium perchlorate, conductivity is impeded sufficiently at milliamp currents that the resulting high counter electrode potential swiftly decomposes the counter cell solution. Moreover, high electrolyte concentration noticeably limits the solubility of our polymers, impeding effective doping. It would be preferable to use a solvent with a higher dielectric constant, such as CH_3CN, which would allow higher conductivity at lower electrolyte concentrations. Of course, this would require the doped and undoped polymer to be soluble in the new solvent. Another way to minimize the potential difference between the counter and the working electrodes is to use electrodes with larger surface areas. Some relief would also be gained by using substrates whose doping potential is closer to zero.

S values and Spin Concentration

Intuitively, one might expect the *S* value to scale with spin concentration for moderate values of spin concentration in a homogeneously doped, finite, one-dimensional, ferromagnetic polymer.[20] For an ideal, infinite polymer, the *S* value might be expected to increase rapidly as the spin concentration nears its maximum. The highest *S* value expected in the present study is no more than 3.5 since these **PMPF** samples are only seven repeat units long. At a spin concentration of 58%, an *S* of 2.1 seems a reasonable value. Experimentally, it is possible that factors such as Coulomb

repulsions or geometry changes upon doping might prevent completely homogenous distribution of spins, leading to a nonlinear dependence of *S* upon spin concentration. This does not seem to be important in a system with as low a degree of polymerization as our **PMPF** samples (Figure 2.15).

An ideal, fully doped, antiferromagnetically linked polymer would have an *S* value and spin concentration of zero.[1] In practice, an *S* value of 0.5 and a low spin concentration should be observed due to isolated spins, which is essentially the behavior exhibited by **PPF**. This demonstrates conclusively that the high-spin, ferromagnetic coupling observed in doped **PMPF** is due solely to the doped polymer and is determined by its rationally designed *meta*-topology.

Balance of Ferromagnetic and Antiferromagnetic Interactions

The plots of relative effective moment versus temperature provide additional strong evidence for significant ferromagnetic coupling in electrochemically doped **PMPF**. As discussed previously, if the magnetic coupling strength is estimated by scaling the singlet-triplet gap in *meta*-xylylene by 2,6-di-*tert*-butylfuchsone radical anion spin densities, an increase in magnetic moment would be expected between 20 to 45 K.[13] We interpret the rise in moment beginning around 40 K as evidence of this intramolecular ferromagnetic coupling of polarons by the *meta*-phenylene coupling groups. The downturn observed below 3 K is interpreted as due to the emergence of weaker intermolecular antiferromagnetic interactions.[1e] Although the doped polymer is in a solid solution of tetrabutylammonium perchlorate electrolyte, the dilution factor is only about one polymer repeat unit to 20 to 30 electrolyte molecules. It is also possible that the polymer is not evenly distributed through the electrolyte. Moreover, even at infinite dilution an

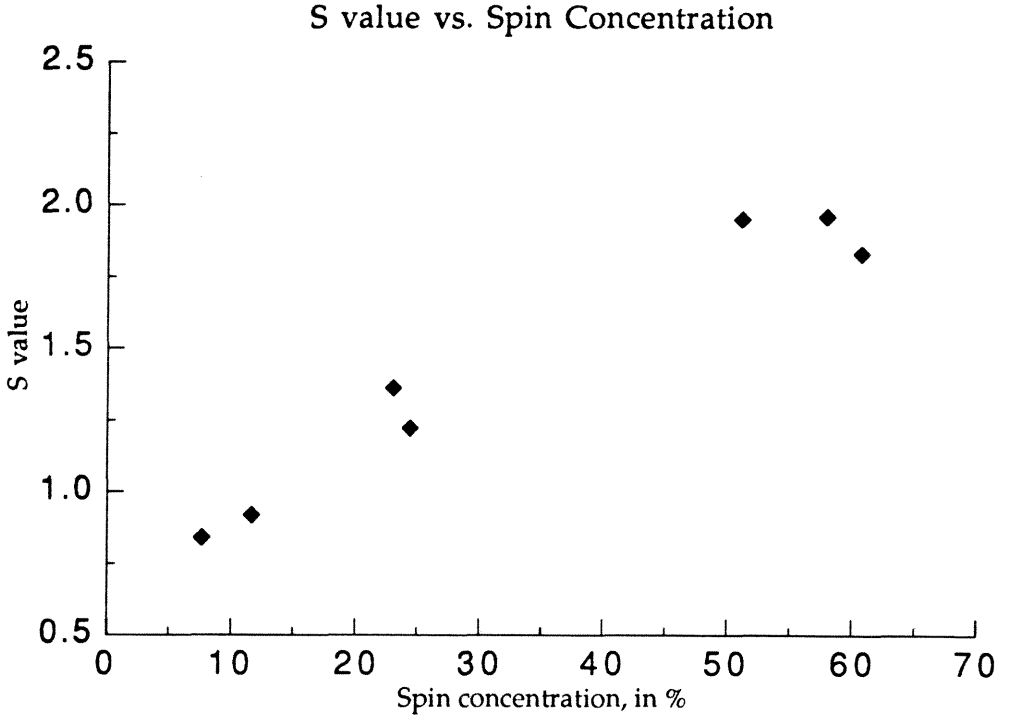

Figure 2.15: Variation of S value Versus Spin Concentration.

individual polymer strand may fold back on itself, allowing weak, through-space, antiferromagnetic interactions. Therefore, the appearance of antiferromagnetic interactions is entirely reasonable at sufficiently low temperatures.

The effective moment plot for control polymer **PPF** (Figure 2.13B) displays the inverted U shape we have observed in all of our previous studies,[1] and in nearly all of the chemically-doped **PMPF** samples. We had interpreted the downturn at high temperature as evidence for thermal disruption of the magnetic coupling, and the downturn at low temperature as due to weak intermolecular antiferromagnetic interactions, with the high moment at intermediate temperatures the result of intramolecular ferromagnetic coupling.[1] This interpretation is wanting, however, since the same behavior has been observed for a variety of samples regardless of their *S* value or their topology.

Comparison of the undiluted, chemically doped **PMPF** samples with the sodium naphthalide and electrochemically doped **PMPF** suggests an alternate explanation. It could be that in undiluted, doped samples, most spins produced are coupled antiferromagnetically throughout the entire range and are therefore undetected. The majority of observed spins are isolated monoradicals or islands of highly doped material, and as a result of their isolation, do not experience antiferromagnetic interactions until extremely low temperature. The number of islands of highly doped material are so few, as evidenced by spin concentrations less than one percent, that the onset of their ferromagnetic interactions is too small a contribution to the observed moment to be seen in the relative effective moment plot.

By contrast, the doped, diluted **PMPF** samples have substantially weakened intermolecular interactions, allowing the rise in moment due to

intramolecular ferromagnetic coupling to be observed. In addition, doped, diluted **PMPF** samples do not exhibit a downturn at higher temperature, but merely become noisy. It seems unlikely that chemically doped, undiluted **PMPF** would have a significantly stronger intramolecular coupling strength; therefore, the downturn it exhibits at high temperature may be due to some other unrelated effect.

If this interpretation is correct, the major reasons for the high *S* values and high spin concentrations seen are that doped **PMPF** is soluble, can be doped in a controlled manner, and can be diluted in a diamagnetic material. Since the doped polymers studied previously in the group tend to lose solubility,[1e] doping is difficult to control. Without effective dilution, intermolecular antiferromagnetic interactions overpower intramolecular ferromagnetic coupling. A specific test of this interpretation would be to dope one of the previously studied polymers in solution with a soluble, diamagnetic solid (tetrabutylammonium perchlorate, paraffin, etc.). If the doped polymer and the diamagnetic solid do not phase-separate upon solvent removal, magnetic characterization of the mixture should reveal increased *S* value and spin concentration, and a significant upturn in the relative effective moment at moderately low temperature. Certainly, other factors such as chemical stability and possibly greater spin density contribute to **PMPF**'s success. There are two central lessons, however; intermolecular antiferromagnetic interactions must be controlled in order to observe weak intramolecular ferromagnetic interactions, and polymers must be soluble in both doped and undoped forms to accomplish thorough, homogeneous doping.

Future Directions

How might these systems be improved? Several possibilities are suggested.

Increasing Solubility

Solubility is probably the greatest requirement in these systems after magnetic topology. Our current systems make use of long alkyl or ether chains attached to the *meta*-phenylene coupling unit to help their solubility.[1] The observation that doped **PMPF** is more soluble than undoped **PMPF**, even dissolving in CH_3CN, strongly suggests that *polar* solubility should be a target—in which case a long hydrocarbon chain may not be the best solubilizing group. The highest yields reported for palladium-catalyzed Suzuki polymerizations are from reactions conducted in polar solvents.[14] A polar solubilizing group might allow more efficient reaction and higher molecular weights. Moreover, if both doped and undoped polymer could remain in polar solution, doping might be vastly simplified by using CH_3CN, which is far superior to THF for electrochemical experiments.[19] CH_3CN would give lower cell resistance for a given concentration of supporting electrolyte and allow a choice of electrolytes. The resulting achievable decrease in cell resistance would make electrolysis considerably easier, likely reducing problems such oxidation of the counter cell solution and plugging of the frit. The higher currents then available would shorten the duration of a doping run. Finally, use of a more polar solvent would allow a wider range of electrolyte concentration, so the balance between ferromagnetic and antiferromagnetic interactions could be more easily investigated as a function of dilution.

Increasing solubility in polar solvents should be a simple matter of using a group such as carboxylate or sulfonate in place of the alkyl chain on

the *meta*-phenylene coupling unit (Figure 2.16). Precursors which can be converted into the desired monomers are commercially available.

Figure 2.16: Polar Solubilizing Groups

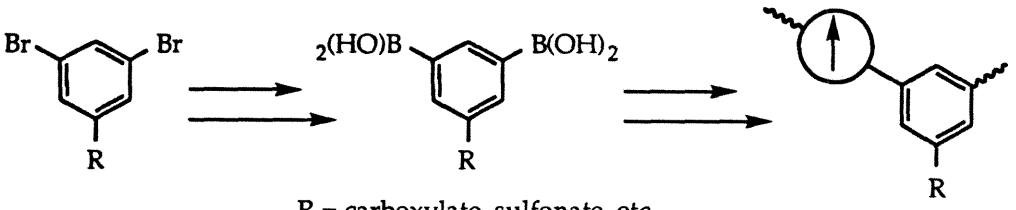

R = carboxylate, sulfonate, etc

Spin Density and Ferromagnetic Coupling Strength

One problem with the current design, **PMPF**, is that each spin is diluted over the four aryl rings in each repeat unit, weakening the coupling strength considerably relative to a model system like *meta*-xylylene.[4,13] Certainly, any future practical application of such materials would require coupling to exist at higher than cryogenic temperatures. More importantly, the use of dilution in this study emphasize the need for intramolecular ferromagnetic coupling to dominate intermolecular antiferromagnetic coupling, so this must be addressed if significant magnetic behavior is to be achieved in undiluted samples. This is an especially important consideration in crosslinked or hyperbranched designs, because even at infinite dilution, intramolecular (through space) antiferromagnetic interactions are possible.

By deleting some of the rings, structures of identical magnetic topology and higher spin density such as poly-*para*-*meta*-fuchsone (**PPMF**) and poly-*meta*-phenylenequinonemethide (**PMPQM**) can be designed (Figure 2.17). Given the spin density of 0.253 at the central carbon in the radical anion of 2,6-di-*tert*-butylfuchsone (Figure 2.5),[9a,b] scaling[13] the 10 kcal/mol singlet-triplet gap in *meta*-xylylene gives coupling strengths of 170 cal/mol and 640 cal/mol for PPMF and PMPQM. The corresponding temperatures for the

Figure 2.17: Reducing Spin Dilution With **PMPF** Analogs

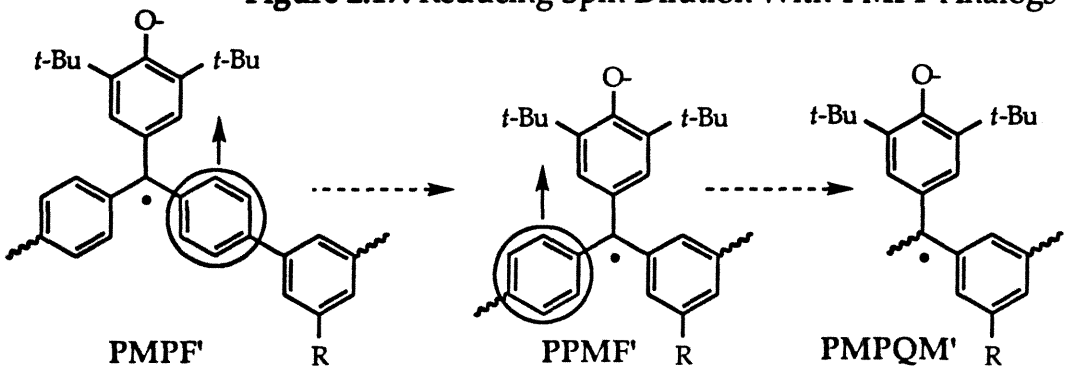

onset of intramolecular ferromagnetic coupling are 85 K and 320 K. Since the cyclic voltammetry of **PMPF** is essentially identical to that known for 2,6-di-*tert*-butylfuchsone,[9] we anticipate that **PPMF** would behave similarly; **PMPQM** might prove slightly more difficult to reduce.

Polymer **PPMF** might be synthesized by Suzuki polymerization of an AB monomer. Reaction of a 1,3-dibromobenzene (solubilizing group in the 5 position) with one equivalent of *tert*-butyllithium to create the monolithio derivative,[21] followed by addition of excess trimethylsilyl iodide, should give the 1-bromo-3-trimethylsilyl compound. This is isolated, then lithiated a second time, reacted with *para*-bromobenzaldehyde, and quenched to give the 4-bromo-3'-trimethylsilylbenzhydrol. Condensation with 2,6-di-*tert*-butylphenol and oxidation as before (Scheme 2.1) gives the 4-bromo-3'-trimethylsilyl fuchsone, which can then be reacted with boron tribromide to give the 4-bromo-3'-boro-fuchsone; aqueous workup would give the boric acid. Polymerization as before (Scheme 2.1) will give **PPMF**.

For **PMPQM**, although Suzuki coupling can work for vinyl halides, the yield is unacceptably low for polymerization. An alternate strategy (Scheme 2.5) begins by lithiating a 3-iodobenzaldehyde with *tert*-butyllithium and allowing it to react with itself. This sort of polymerization has been tried by forming the Grignard, but yields are low.[22] We have noticed for similar

Scheme 2.4: Possible Synthetic Route to Poly-*para-meta*-Fuchsone

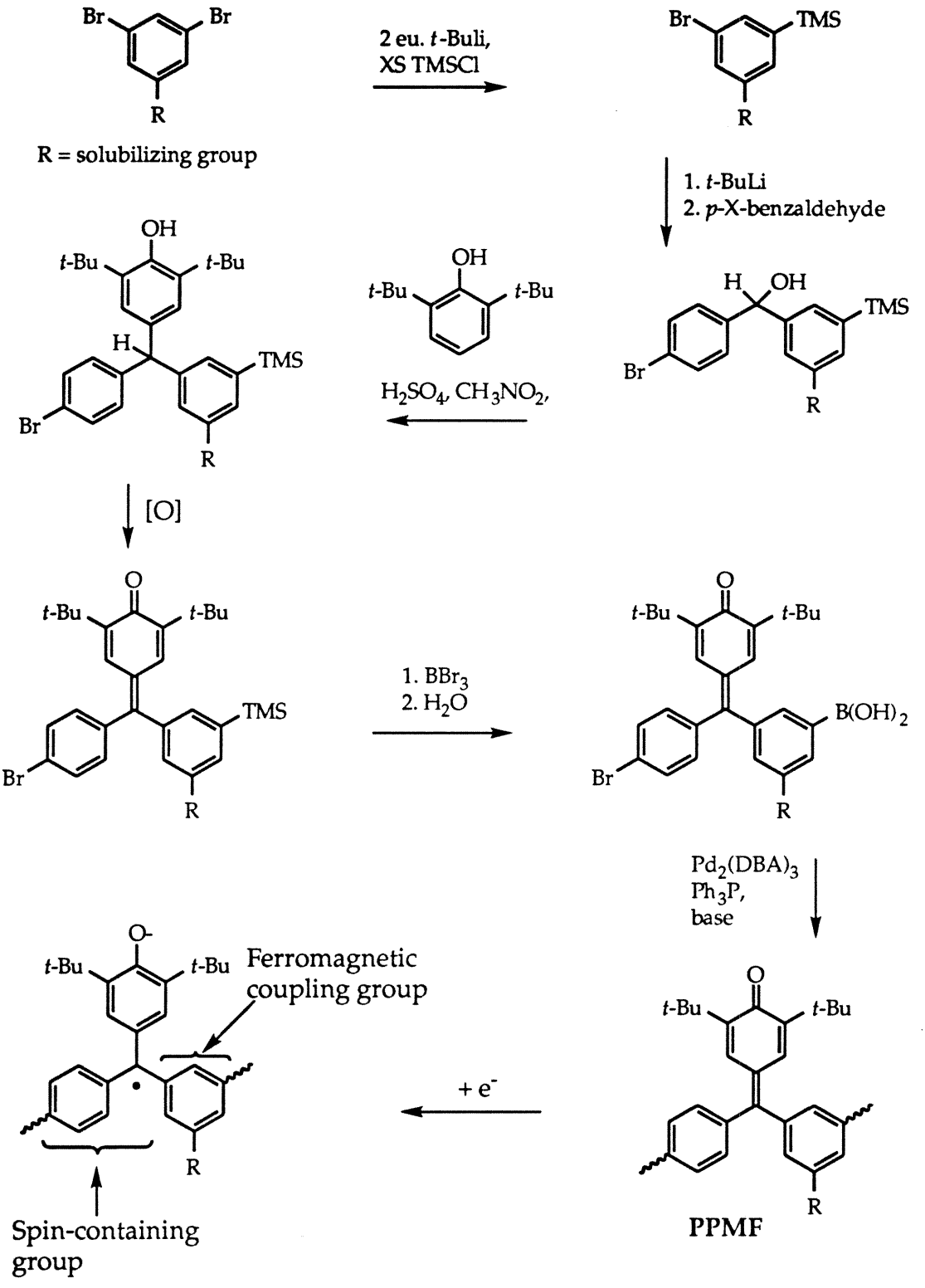

Scheme 2.5: Possible Route to Poly-*meta*-phenylenequinonemethide

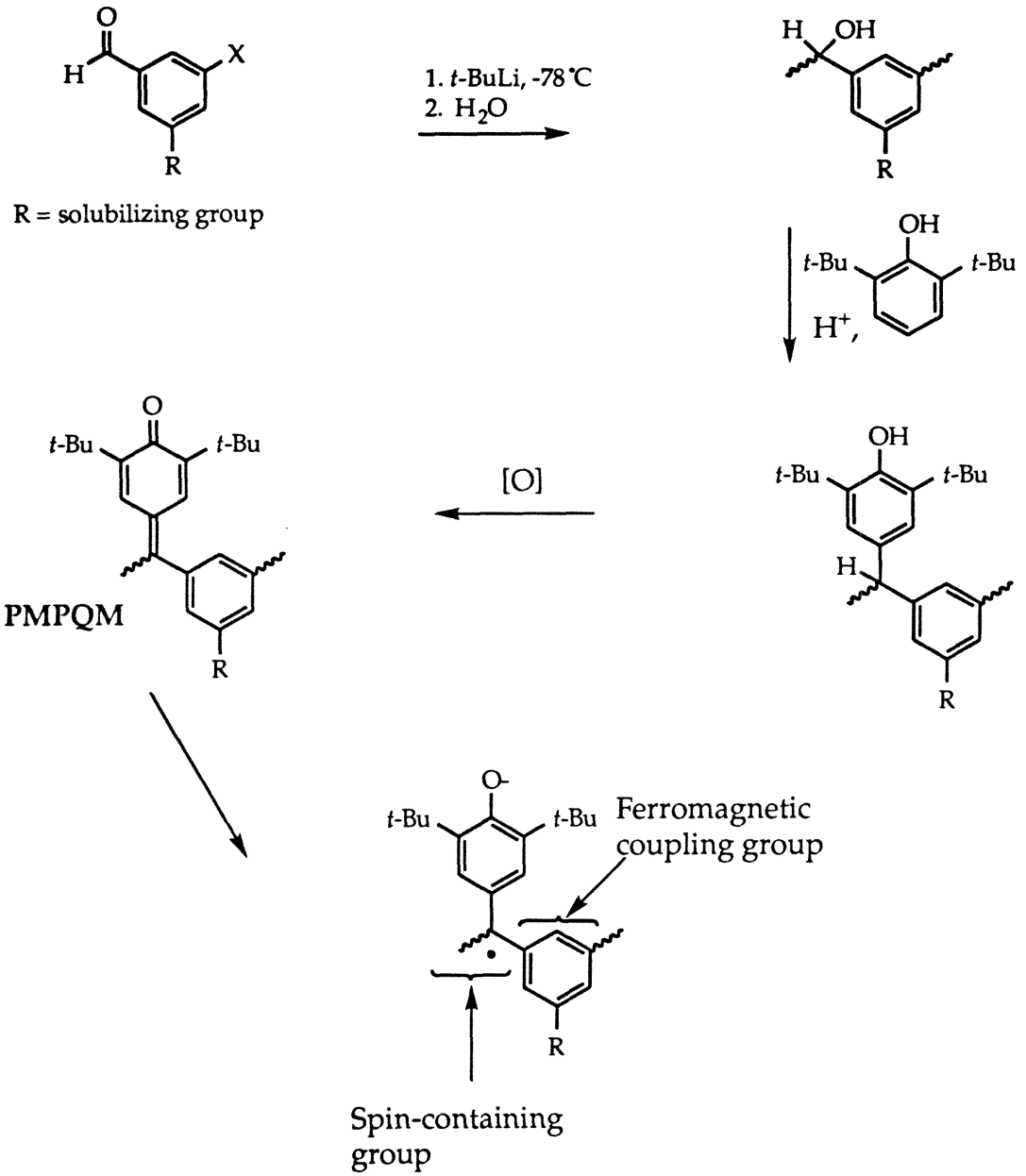

substrates that arylmagnesiumbromides are significantly less reactive than aryllithiums, so there is some hope that this modification might work.[22] The resulting poly-*meta*-phenylmethanol will then be condensed with 2,6-di-*tert*-butyl phenol and oxidized to give **PMPQM**. Certainly, this scheme is speculative; functionalizing a polymer in quantitative yield is difficult. For these initial investigations, however, small degrees of polymerization are acceptable, if not ideal.

One additional strategy possible with these monomer designs is to make a hyperbranched polymer, which may have better solubility than an otherwise identical linear polymer.[23] For example, an AB_2 monomer could be created by replacing the solubilizing R group in **PPMF**'s monomer with a boric acid group, a simple adaptation of Scheme 2.4.

Increasing Spin Concentration

A number of factors can decrease spin concentration. Certainly it is necessary to have an ultra-pure, dry, oxygen-free doping environment. While all possible care was taken during these investigations, additional desirable precautions include installation of a fresh catalyst bed and an oxygen meter on the doping glovebox. Additionally, a search for other stable organic radical cations and anions should be made, including reinvestigating, with dilution, some of the more stable units examined previously, such as indoloindole.[1] For **PMPF** and its analogs, stability might be increased and reduction eased by replacing *tert*-butyl with a strong electron donor such as nitro. Improvements in cell conductivity, as discussed under solubility, will certainly lead to better control of electrolysis, which may also improve spin concentration. Finally, experiments using increased dilution, perhaps with alternative diamagnetic diluents might reduce intermolecular antiferromagnetic interactions even further.

Higher Magnetic Order, Increasing *S* Value

Of course, the one-dimensional polaronic ferromagnet is only a model, and coupling in two or three dimensions will be required for higher magnetic ordering; the current finite, one-dimensional systems cannot be expected to display anything higher than paramagnetism. A hypothetical system with a degree of polymerization in the millions and a spin concentration of 100% would still be a paramagnet. Realistically, polymers with such high molecular weights might be achieved, but ensuring exactly zero defects in such long, linear chains is probably impossible (one defect in the middle of a chain will cut "S" in half). One alternate strategy would be to couple 1,3,5 through the phenylene coupling unit (Figure 2.18).[4b] In such a system, a small amount of defects will affect *S* much less than in a linear polymer because of the alternate coupling routes available. Certainly, this can reduce the solubility of a polymer, so only a small amount of the crosslinking monomer should be used. A subtle point is that hyperbranched[23] or dendrimeric[24] systems are distinct from crosslinked systems because they do not possess alternate paths, and therefore are just as susceptible to defects as linear systems.

Conclusions

Intramolecular ferromagnetic coupling in an all organic system, poly-*meta*-phenylenefuchsone, has been demonstrated as a model for the one-dimensional polaronic ferromagnet. The lack of ferromagnetic coupling exhibited by a *para* linked control polymer, poly-*para*-fuchsone proves that high-spin, ferromagnetic coupling in these systems is due solely to a rationally designed *meta*-topology. Electrochemistry has been shown to be a more effective and better controlled means of doping than chemical reduction. While this is still far from our eventual goal of an organic

Figure 2.18: Coupling 1,3,5 Through Phenylene to Overcome Effects of Defect Formation

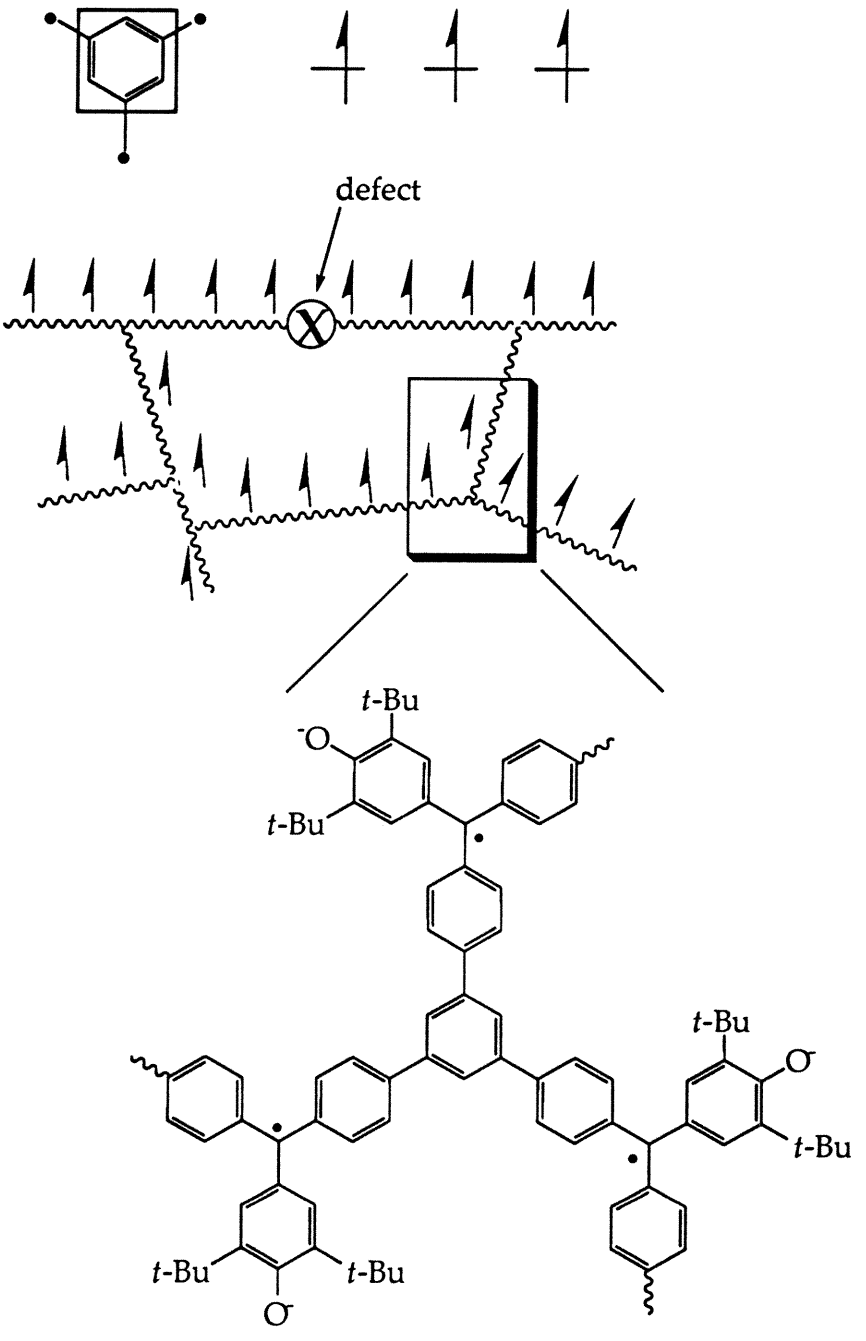

ferromagnet, these results are significant and have provided inspiration for future work. Solubility of both undoped and doped species is vital, not only for characterization but also for effective doping. Dilution of paramagnetic species with weak intramolecular ferromagnetic coupling may be necessary to overcome intermolecular antiferromagnetic coupling. These observations suggest a number of features which should be incorporated in future systems: solubility in a better electrochemical solvent such as CH_3CN; compact, stable, easily generated (redox potential near 0 V) spin containing groups which have high spin densities at connecting atoms; and a small amount of magnetic crosslinking.

Experimental

Unless otherwise noted, reactions were run under an atmosphere of dry argon using oven-dried glassware. THF, Et_2O, and benzene were distilled from sodium benzophenone ketyl. CH_2Cl_2, toluene, and CH_3CN were distilled from calcium hydride. Other solvents were used as received unless specified otherwise. Thin layer chromatography was performed on 0.25 mm silica-pre-coated glass plates visualized with UV light and molybdate stain. Flash chromatography was performed on 230-400 mesh silica gel. GC/MS data were obtained using a 70 eV EI Hewlett-Packard 5890/5970 GC/MS equipped with a 12 m X 0.2 mm HP-1 capillary column. High resolution mass spectrometry analyses were obtained on a ZAB 7070 instrument by the Mass Spectral Facility at the University of California, Riverside. NMR spectra were obtained on JEOL GX-400 (399.65 MHz ^1H, 100.4 MHz ^{13}C), or GE QE-300 at room temperature and referenced to residual protio solvent unless specified otherwise. IR spectra were obtained using a Perkin-Elmer 1600 Series FTIR. UV/Vis spectra were obtained using a Beckman DU-640 continuous wave

spectrophotometer. Melting and boiling points are uncorrected. Determination of polymer molecular weights by gel permeation chromatography was performed on a homemade instrument employing either three Shodex size Styragel columns, (KF 803, KF 804, and KF 805) or an American Polymer Standards 10-μm mixed-bed column, an Altex model 110A pump, a Knauer differential refractometer and a Kratos UV detector. CH_2Cl_2 was used as an eluant at a flow rate of 1 mL/min. Molecular weights are reported relative to narrow polystyrene standards; polymer solutions (ca. 1 mg/mL) were passed through a 0.5 μm filter before injection. Elemental analyses were performed by Galbraith Laboratories, Knoxville, Tennessee. All doping was carried out in a dry, oxygen-free, nitrogen-filled glovebox.

Electrochemical Doping Procedure

Electrochemical investigations were performed using a computer controlled potentiostat (EG&G-PAR Versastat). Due to instrument problems, current readings were collected manually at 1 min intervals from an external ammeter connected in series with the working electrode. The experiments were performed using a nitrogen-filled, dry, oxygen-free glovebox equipped with appropriate electrical connectors. The bulk electrolysis cell consisted of two chambers separated by a 0.5 cm fine glass frit. The counter cell was usually filled to a volume of 9 mL, and the working cell was filled about halfway, between 25 to 40 mL. The solvent was THF, distilled from sodium benzophenone ketyl, and thoroughly degassed before transferring it into the glovebox. The electrolyte was 99.9% tetrabutylammonium perchlorate, which was dried for 2 d in a vacuum desiccator over phosphorus pentoxide before transferring it to the glovebox. The concentration of electrolyte used was 0.3 M The counter electrode was a 2.5 X 2.5 cm piece of 100 mesh, 99.9% pure

platinum gauze attached to a platinum wire. The working electrode was a 10 X 2.5 cm piece of 52 mesh, 99.9% pure platinum gauze, which was shaped into a cylinder by two platinum wire hoops to a diameter a little less than that of the cell. Silver-silver chloride reference electrodes were constructed by plating a silver wire (1.0 or 2.0 mm in diameter, 99.9% pure) in concentrated hydrochloric acid at 0.22 V for 15-20 min. Before each experiment, all utensils, including the cell, electrodes, and Teflon-coated magnetic stirring bar were cleaned of extraneous metal (and everything else) with acid. The cell and frit were soaked thoroughly in concentrated nitric acid (CAUTION: extremely exothermic reaction occurs between nitric acid and polymer/electrolyte residue). Platinum electrodes were soaked in concentrated sulfuric acid. Silver electrodes and the stir bar were rinsed with concentrated hydrochloric acid. All other utensils were soaked in 1 M hydrochloric acid. After acid treatment, utensils were washing in succession with distilled water, neutralizing buffer, a solution of sodium ethylenediaminetetraacetate, and distilled water again, and finally, dried in an oven or in a vacuum desiccator. Before adding polymer, the electrolyte solution was pre-electrolyzed at -1.75 V for about 20-40 min, until background current had dropped under 50 μA; background current then measured at the first reduction potential of PMPF (-1.25 V) was less than 20 μA. At this point, faint yellowing of the counter cell solution and minor corrosion of the reference electrode was observed. An amount (ca. 30-100 mg) of polymer sufficient to make the concentration of the polymer's repeat unit between 1 to 4 mM was dissolved in the working cell. Even after stirring for several hours, no coloration of the frit or the counter cell solution due to dissolved polymer was observed. In the case of PPF, the polymer was first dissolved in a few milliliters of neat solvent and added to the electrolyte-containing solution

after pre-electrolysis. The reference potential was applied starting at -1.0 V, stepping to more negative potential slowly to maintain the current ≤ 3 mA, but never below a potential of -1.40 V. The reduction was stopped when the desired amount of charge had been passed. After only a few seconds of reduction at ~ 3 mA, the bright orange solution turned darker than any of the attempts at chemical reduction. Between 0.2 and 0.6 F/mol, solutions using **PMPF** were intensely black-green, almost opaque, with the color visible initially at the meniscus and later only by holding a microcapillary of the solution up to a bright light. After 0.8 F/mol, the color had become a deep, dark purple. For control polymer **PPF**, behavior was similar except the final color was not purple but an almost fluorescent green. In electrolyses where the amount of charge passed exceeded 1.0 F/mol, the current did not drop to the preelectrolysis background but leveled off at about 400 μA. In such prolonged experiments, the electrolyte solution in the counter cell had been significantly oxidized, turning dark brown, and often became an opaque, viscous gel. Replacing this with fresh electrolyte and allowing the system to stand for an hour decreased the current somewhat, but still not to the preelectrolysis background. After reduction, the solvent was removed by vacuum, leaving a dark black-green (**PPF**) or black-purple (**PMPF**) solid which was a mixture of the doped polymer and tetrabutylammonium perchlorate. These solids were loaded into sample tubes (the threads of which had been sealed with Apiezon M grease) and subjected to magnetic analysis without delay.

Problems and Troubleshooting

Be sure to check all wires and connections using a meter, and readjust the various metal clips. Check to see that none of the wires' bare metal is

touching another's, and that the wires are connected to the proper electrodes. Make sure the cell switch is on. If the voltage seems "frozen," try the following: turn the computer and potentiostat off, unplug them, switch them on, then off, plug them back in, and then restart. Avoid using the automatic bulk electrolysis options; instead, use "Immediate Mode" to control the experiment and acquire the data manually. The gas inlet solenoid for the drybox will occasionally cause the system to crash. Finally, be aware that the potentiostat's ability to pass current can be significantly hindered by measuring the current in series with an external meter. For example, the Keithly model 197 meter set to either "autorange" or "200 μA" in ammeter mode will limit the current substantially. Use of any of the other range settings allows about the same amount of current as the potentiostat alone says it is passing.

If the counter cell solution becomes significantly oxidized, it will begin to gel and plug the frit. This is imminent when the solution has turned opaque. One way to monitor this is to watch the voltage drop between the counter and working electrodes (measured using an external voltmeter); this should never be allowed to get past ± 20 V(the instrument's limit is about ± 23.5 V). This voltage must rise as the instrument passes increasing amounts of current. For the specific experimental conditions in this study, the current limit is about 3 mA. The ± 20 V limit is a more general limit for our instrument. Note that these points place a limit on the absolute amount of material that may be easily electrolyzed in a single experiment. Electrolysis should be performed as quickly as possible within the above restrictions, since the product may not be stable in solution.

Occasionally, the instrument will seem to be unable to control the potential, and/or the current displayed by the computer will not match the

current read in series with the working electrode using an external ammeter. If the potential was stepped too quickly, the current and counter/working potential are beyond the instrument's limits; the solution is to back away from the substrate's redox potential until control is regained. Alternatively, the reference electrode may have become too corroded or have a defect in its silver chloride layer; the solution is to use a fresh electrode. It may help to isolate the reference electrode by placing it in a tube tipped with a permeable material such as a glass frit or Vycor. I attempted this with a commercial Vycor-tipped tube, but the instrument could not maintain control of the potential, at least in this system (PMPF in 0.3 M tetrabutylammonium perchlorate/THF). This did work quite well, however, for a reduction of diquat carried out in 0.1 M tetrabutylammonium perchlorate/CH_3CN.[11] Perhaps the Vycor is not permeable enough in the THF system and a fine glass frit would work better.

Magnetization Studies[1,12,17,18]

Magnetic characterization was conducted using a Quantum Design MPMS Squid Magnetometer. Sample holders were two piece, threaded Delrin (polyethylene oxide) rods with a cavity capable of holding about 50-60 mg of organic solid. The diamagnetic correction (χ_{dia}) of the sample and holder could be determined from a plot of observed magnetic susceptibility (χ_{obs}) versus inverse temperature. The correction was estimated from the intercept upon extrapolation to infinite temperature. Variable temperature behavior was determined between 2 and 300 K at constant field (usually 10 kG); these plots were linear between 50 and 150 K. The magnetization of the sample was measured between 0 and 55 kG at constant temperature, (1.8 K), starting with the high field measurement to ensure saturation of

ferromagnetic impurities throughout the curve. An alternative means of determining the diamagnetic correction (χ_{dia}) of the sample and holder was from a three-parameter fit of the Brillouin function to this data. The spin states of the materials, S, and paramagnetic saturation moment M_{sat}, could be determined either from this fit or from a two-parameter fit upon data from which the Curie diamagnetic correction had been subtracted. No significant difference was observed between the two methods for the electrochemically doped samples. By contrast, application of the Curie diamagnetic correction to the chemically doped samples often gave physically unreasonable saturation plots; therefore, all reported numbers for both doping methods in this study are for the three-parameter fit.

The spin concentration was determined from the variable field plot. The saturation moment from the Brillouin fit (see Chapter 4 and Appendix D) in emu•G/g was converted to molar units by multiplying by the effective molecular weight, M^r, of the doped polymer's repeat unit (which is adjusted for dopant uptake with chemical doping experiments and electrolyte dilution for electrochemical doping experiments):

$$M_{sat}\,(\text{emu}\bullet\text{G/mol}) = M_{sat}\,(\text{emu}\bullet\text{G/g}) \times M^r(\text{g/mol}). \qquad (1)$$

The M_{sat} expected for a mole of molecules of a certain S is described by

$$M_{sat}\,(\text{emu}\bullet\text{G/mol}) = Ng\beta S, \qquad (2)$$

where N is Avogadro's number, g is the Landé splitting factor and β is the Bohr magneton. Assuming $g = 2$, this can be written as:

$$M_{sat}\,(\text{emu}\bullet\text{G/mol}) = 1.117 \times 10^4\, S. \qquad (3)$$

Thus for

$$S = \frac{1}{2}: \%\ \text{monomers doped} = \frac{M_{sat}\ (\text{emuG/mol})}{1.117 \times 10^4 \times 0.5} \times 100. \qquad (4)$$

Synthetic Procedures

4,4'-dibromobenzhydrol (2.1a)[9,15] 4,4' dibromobenzophenone (26.0 g, 0.0765 mol, Lancaster) was dissolved in 200 mL of boiling absolute ethanol. Sodium borohydride (3.47 g, 0.0917 mol) was suspended in absolute ethanol (75 mL) and added to the benzophenone solution over 5 min. The mixture was boiled for an additional 10 min, then poured into half-saturated NaCl soln (150 mL), and extracted with 3 X 75 mL of Et_2O. The Et_2O extracts were combined, dried over $MgSO_4$, filtered, and put on a rotary evaporator to remove the solvent. The residue was recrystallized from 95% ethanol to give 26.2 g (quantitative yield) of fine white needles. GC/MS, 50-250 °C, 10 °C/min, m/z 342 (M^+) @ 19.9 min.

(3,5-di-*tert*-butyl-4-hydroxyphenyl)-di-(4-bromophenyl)methane (2.1b)[9,15] 4,4'-Dibromobenzhydrol (5.65 g, 0.0165 mol) and 2,6-di-*tert*-butylphenol (3.40 g, 0.0165 mol) were added to nitromethane (25 mL); the mixture did not go completely into solution. Upon adding concentrated sulfuric acid (1.65 mL) all at once, the solution turned pale orange. After stirring for an additional 5 min, the mixture was poured into half-saturated NaCl soln (100 mL) and extracted with 3 X 75 mL of Et_2O. The combined extracts were washed with saturated $NaHCO_3$ soln (50 mL), dried over $MgSO_4$, filtered, and put on a rotary evaporator to remove the solvent. The residue was recrystallized from 95% ethanol to give 7.90 g (90.3%) of large white crystals. TLC, orange-brown spot at RF 0.5, molybdate stain, 5% ethyl acetate/petroleum ether. GC/MS, 50-

250°C, 10°C/min, m/z 530 (M^+) @ 30.8 min. 300 MHz ^1H NMR, $CDCl_3$, δ = 1.29 ppm, s, 18H; 5.15, s, 1H; 5.47, s, 1H; 6.87, s, 2H; 6.98, m, 8H. 300 MHz ^{13}C NMR, $CDCl_3$, δ = 30.4, 34.5, 55.8, 120.3, 125.9, 131.1, 131.4, 133.1, 135.9, 143.4, 152.5 ppm. FTIR, NaCl, ν = 3624 (sharp), 2955, 2908, 2872, 1484, 1431, 1396, 1361, 1314, 1232, 1491, 1120, 1073, 1002 cm^{-1}.

2,6-di-*tert*-butyl-4',4''-dibromofuchsone (2.1c)[9,15] Triarylmethane (4.95 g, 0.00933 mol) and 2,3-dichloro-5,6-dicyano-1,4-benzoquinone (DDQ, 2.33 g, 0.0103 mol) were each dissolved separately in 100 mL of benzene. The DDQ solution was added over 5 min to the phenol solution and the resulting mixture was stirred for an additional 55 min. The reaction mixture was then poured through a plug of silica gel, followed by an additional 150 mL of benzene. The solvent was removed on a rotary evaporator and the residue was recrystallized from isopropyl alcohol and toluene to give 4.78 g (96.9%) of bright orange crystals. TLC, visible orange spot at RF = 0.6, no stain, 5% ethyl acetate/petroleum ether. HRMS, DEI/PFK found MW = 526.049900, calculated MW = 526.050688 for $M^+ = C_{27}H_{28}OBr_2$ (for ^{79}Br). GC/MS, 50-250°C, 10°C/min, m/z 528 (M^+) @ 33.8 min. 300 MHz ^1H NMR, $CDCl_3$, δ = 1.25 ppm, s, 18H; 7.12, s, 2H; 7.11, m, 4H; 7.56, m, 4H. 300 MHz ^{13}C NMR, $CDCl_3$, δ = 29.6, 35.5, 124.0, 128.4, 130.4, 131.5, 133.6, 139.3, 148.3, 152.5, 186.1 ppm. FTIR, NaCl, ν = 2945, 2865, 1603, 1578, 1477, 1452, 1386, 1357, 1332, 1251, 1166, 1065, 1020, 1005, 965, 874, 814, 754 cm^{-1}. UV/Vis, λ_{max} = 279, 373 nm. MP = 204-205 °C. Elemental analysis: calculated for $C_{27}H_{28}Br_2O$, C, 61.38; H, 5.34; Br, 30.25; O, 3.03. Found: C, 61.72; H, 5.61; Br, 29.63; O, 3.21.

Poly-*meta*-(*para*-tetradecyl)phenylene-4',4''-fuchsone (PMPF)[1,14] Dibromofuchsone **2.1c** (0.742 g, 0.00140 mol), triphenylphosphine (0.0088 g, 0.000034 mol), 5-tetradecylbenzene-1,3-bis-(1,3,2-benzodioxaborole) **2.2d** (0.717

g, 0.0014 mol), tris(dibenzylideneacetone)dipalladium(0) (0.0030 g, 0.0000033 mol) and K_2CO_3 (1.16 g, 0.0084 mol) were added to a flask containing water (10 mL) and THF (50 mL). The mixture was carefully degassed, protected from light, and refluxed for 7 d. Upon cooling to room temperature, hydrochloric acid (4 M, 25 mL) was added over 10 min, and the reaction was stirred an additional 10 min. This was poured into 100 mL of pH 7 buffer (1.20 mol potassium dihydrogen phosphate and 1.60 mol potassium hydrogen phosphate dissolved in 1L of water) and reduced to an orange residue using a rotary evaporator. The orange solid was purified three times by precipitation from chloroform by adding 95% ethanol. The orange residue was redissolved in chloroform and reduced by rotary evaporation followed by 24 h of a 0.1 Torr vacuum to give 0.897 g (quantitative) of a transparent orange film. MW by GPC, in CH_2Cl_2 vs. polystyrene standard, PDI = 1.29, M_n = 3580, M_w = 4620, corresponding to a degree of polymerization of 7. 300 MHz ^1H NMR, $CDCl_3$ δ = 0.86 ppm, s, 3H; 1.26, s, 18H; 1.29, s, 22H; 1.75, m(br), 2H; 2.79, m(br), 2H; 7.31, s, 2H; 7,41, d, J = 8 Hz, 4H; 7.53, s, 2H; 7.77, d, J= 8 Hz, 4H; 7.80, s, 1H. 300 MHz ^{13}C NMR, $CDCl_3$, δ = 14.3, 22.8, 29.7, 32.0, 35.5, 36.4, 102.6, 123.7, 126.7, 127.1, 130.1, 132.8 (m), 139.5 (m), 140.0, 140.9, 142.1, 143.8, 144.6, 147.6, 147.9, 154.0, 155.6, 186.2 ppm. FTIR, 2955, 2915, 2845, 1598, 1497, 1452, 1382, 1357, 1332, 1251, 1080, 1020, 965, 874, 814 cm^{-1}. UV/Vis, λ_{max} = 242, 302, 390 nm. Elemental analysis: calculated for $C_{47}H_{60}O$, C, 88.07; H, 9.43; O, 2.50. Found: C, 88.17; H, 9.23; O, 2.46.

2,6-Dibromo-4-tetradecylaniline (2.2a)[1e] 4-Tetradecylaniline (Aldrich, 100 g, 0.345 mol) was dissolved in acetic acid (1 L) using a mechanical stirrer. Subsequently, a solution of bromine (36.5 mL, 0.708 mol) in acetic acid (300 mL) was added over 30 min at room temperature, generating a yellow

precipitate. The pale yellow suspension was stirred for 2 h, then poured into water and the precipitate collected by vacuum filtration. The solid residue was recrystallized from isopropyl alcohol (the temperature must be kept ≤ 70 °C to prevent product decomposition) to give 150 g (97%) of tan needles. 300 MHz ^{1}H NMR, $CDCl_3$, δ = 0.90, t, 3H; 1.31, s, 22H; 1.51, t, 2H; 2.48, t, 2H; 4.41, s, 2H; 7.22, s, 2H. 300 MHz ^{13}C NMR, $CDCl_3$, δ = 14.1, 22.7, 29.0, 29.4, 29.5, 29.7 (2C), 31.4, 31.9, 34.4, 108.3, 131.5, 134.6, 139.5 ppm. FTIR, NaCl, ν = 3433, 3342, 2955, 2918, 2846, 1618, 1577, 1543, 1467, 864, 732, 712 cm^{-1}. MP = 79-80 °C. Elemental analysis: calculated for $C_{20}H_{33}Br_2N$: C, 53.70; H, 7.44; Br, 35.73; N, 3.13. Found: C, 53.74; H, 7.37; Br, 35.67; N, 3.18.

1,3-Dibromo-5-tetradecylbenzene (2.2b)[1e] A solution of *tert.*-butylnitrite (40.0 mL, 0.336 mol) in DMF (250 mL, distilled from calcium hydride and stored over molecular sieves) was purged with argon and heated to 50 °C. Solid dibromoaniline **2.2a** (67.0 g, 0.150 mol) was added over 20 min; delayed gas evolution followed each portion added. The resulting dark red solution was stirred for 1 h, cooled to room temperature, poured into half-saturated NH_4Cl soln (250 mL) and extracted with 3 X 300 mL of Et_2O. The combined extracts were dried over $MgSO_4$, passed through a short silica gel plug to remove most colored impurities and reduced to a pale yellow oil using a rotary evaporator. Upon standing at room temperature and atmospheric pressure overnight, the oil crystallized to give 43.0 g (66%) of off-white crystals. TLC, blue spot at RF 0.8-0.9, molybdate stain, 5% ethyl acetate/petroleum ether. GC/MS, 50-250°C, 10°C/min, m/z 432 (M^+) @ 23.4 min. 300 MHz ^{1}H NMR, $CDCl_3$, δ = 0.91, t, 3H; 1.32, s, 22H; 1.59, t, 2H; 2.56, t, 2H; 7.29, s, 2H; 7.49, s, 1H. 300 MHz ^{13}C NMR, $CDCl_3$, δ = 14.2, 22.8, 29.5 (m), 31.1, 32.0, 35.5, 122.7, 130.3, 131.3, 147.0

ppm. FTIR, NaCl, ν = 2925, 2855, 1585, 1553, 1422, 849, 740 cm^{-1}. MP = 37-38 °C.

1,3 -Bis(trimethylsilyl)-5-tetradecylbenzene (2.2c)[1e] Dibromide **2.2b** (47.1 g, 0.109 mol) and trimethylsilyl chloride (83 mL, 0.65 mol, freshly distilled from calcium hydride) were added to a stirred mixture of magnesium turnings (5.30 g, 0.218 mol) in THF (450 mL). The reaction was refluxed for 15 h, then quenched by cooling with an ice water bath and carefully adding water (25 mL). The mixture was poured into saturated NH_4Cl soln (400 mL), shaken vigorously, and separated. The organic layer was dried over $MgSO_4$, filtered, and reduced to a light brown oil on a rotary evaporator. This oil was distilled at 0.8 Torr and 240 °C using a vacuum-jacketed Vigreaux column to give 23.9 g (57%) of a clear, colorless oil. GC/MS, 50-250°C, 10°C/min, m/z 418 (M^+) @ 21.9 min. 300 MHz ^1H NMR, $CDCl_3$, δ = 0.32 ppm, s, 18H; 0.94, t, 3H; 1.33, s, 22H; 1.68, broad s, 2H; 2.66, t, 2H;, 7.40, s, 2H; 7.55, s, 1H. 300 MHz ^{13}C NMR, $CDCl_3$, δ = -1.0, 14.2, 22.8, 29.6 (m), 31.3, 32.0, 36.3, 133.5, 134.0, 136.5, 139.2, 141.1 ppm.

5-Tetradecylbenzene-1,3-bis-(1,3,2-benzodioxaborole) (2.2d)[1e] Bis-trimethylsilyl compound **2.2d** (12.69 g, 0.0303 mol) was added to CH_2Cl_2 (200 mL), stirred. and cooled to -50 °C. A solution of boron tribromide in CH_2Cl_2 (1.0 M, 66 mL, 0.066 mol) was added via syringe over 20 min. This cloudy yellow mixture was allowed to rise to room temperature, then refluxed for 12 h. The resulting brown-red solution was cooled with an ice-water bath, and catechol (7.34 g, 0.0667 mol) was added in one portion. After stirring for 3 h, the mixture was poured into 250 mL of aqueous pH 7 buffer (1.20 mol potassium dihydrogen phosphate and 1.60 mol potassium hydrogen phosphate dissolved in 1L of water), shaken vigorously, and extracted with 3

X 200 mL of CH_2Cl_2. Additional CH_2Cl_2 was added (to a total volume of 2.5 L) until all solid had dissolved. This was then dried over $MgSO_4$, filtered through a short plug of neutral alumina, and reduced to about 150-200 mL using a rotary evaporator. This mixture was cooled overnight at about -10 °C, and the precipitate collected on a glass frit and washed with 3 X 100 mL of cold CH_2Cl_2. The solid residue was recrystallized from chloroform three times to give 7.42 g (48.1%) of small white crystals. HRMS, DEI/PFK, found MW = 510.310100, calculated MW = 510.311326, for $MH^+ = C_{32}H_{41}B_2O_4$. 300 MHz ^1H NMR, $CDCl_3$, δ = 0.88 ppm, broad m, 3H; 1.28, s, 22H; 1.70, broad s, 2H; 2.76, t, J = 7.8 Hz, 2H; 7.18, dd, J = 3.4, 2.4 Hz, 4H; 7.37, dd, J = 3.4, 2.4 Hz, 4H; 8.12, s, 2H; 8.67, s, 1H. 300 MHz ^{13}C NMR, $CDCl_3$, δ = 14.1, 22.8, 29.6 (m), 31.5, 31.9, 36.0, 112.7, 122.8, 125.9, 138.9, 139.3, 142.6, 148.7 ppm. FTIR, KBr, ν = IR 3033, 2919, 2872, 1601, 1473, 1454, 1397, 1303, 1235, 1136, 914, 862, 811, 741 cm^{-1}. MP = 144-145°C. Elemental analysis: calculated for $C_{32}H_{40}B_2O_4$, C, 75.32; H, 7.90; B, 4.24. found, C, 75.36; H, 7.94; B, 4.10.

Chapter 2 References

1. (a) Kaisaki, D. A.; Dougherty, D. A. *Tetrahedron Lett.* **1987**, *28*, 5263-5266. (b) Dougherty, D. A.; Kaisaki, D. A. *Mol. Cryst. Liq. Cryst.* **1990**, *183*, 71-79. (c) Dougherty, D. A.; Grubbs, R. H.; Kaisaki, D. A.; Chang, W.; Jacobs, S. J.; Shultz, D. A.; Anderson, K. K.; Jain, R.; Ho, P. T.; Stewart, E. G. In *Magnetic Molecular Materials*; D. Gatteschi, O. Kahn, J. S. Miller and F. Palacio, Ed.; Kluwer Academic Publishers: The Netherlands, 1991; pp 105-120. (d) Kaisaki, D. A.; Chang, W.; Dougherty, D. A. *J. Am. Chem. Soc.* **1991**, *113*, 2764-2766. (e) Murray, M. M.; Kaszynski, P.; Kaisaki, D. A.; Chang, W.; Dougherty, D. A. *J. Am. Chem. Soc.* **1994**, *116*, 8152-8161. (f) Dougherty, D. A. *Acc. Chem. Res.* **1991**, 23, 88-94.

2. Hurd, C. M. *Contemp. Phys.* **1982,** *23,* 469-493.

3. For reviews of the field see: (a) Dowd, P. *Acc. Chem. Res.* **1972,** *5,* 242-248. (b) Borden, W. T. *Diradicals;* John Wiley & Sons: New York, 1982, pp 321. (c) Salem, L.; Rowland, C. *Angew. Chem. Internat. Edit.* **1972,** *11,* 92-111. (d) Borden, W. T.; Davidson, E. R. *J. Am. Chem. Soc.* **1977,** *99,* 4587-4594. (e) Borden, W. T.; Davidson, E. R. *Acc. Chem. Res.* **1981,** *14,* 69-76.

4. (a) Itoh, K. *Pure & Appl. Chem.* **1978,** *50,* 1251-1259. (b) Yoshizawa, K.; Chano, A.; Ito, A.; Tanaka, K.; Yamabe, T.; Fujita, H.; Yamauchi, J. *Chem. Lett.* **1992,** 369-372. (c) Nakamura, N.; Inoue, K.; Iwamura, H. *Angew. Chem. Int. Ed. Engl.* **1993,** *32,* 872-874. (d) Wasserman, E.; Schueller, K.; Yager, W. A. *Chem. Phys. Lett.* **1968,** *2,* 259-260.

5. (a) Baseman, R. J.; Pratt, D. W.; Chow, M.; Dowd, P. *J. Am. Chem. Soc.* **1976,** *98,* 5726-5727. (b) Dowd, P.; Chow, M. *J. Am. Chem. Soc.* **1977,** *99,* 6438-6440. (c) Dowd, P. *Acc. Chem. Res.* **1972,** *5,* 242-248. (d) Dowd, P.; Gold, A.; Sachdev, K. *J. Am. Chem. Soc.* **1968,** *90,* 2715-2716. (e) Dowd, P. *J. Am. Chem. Soc.* **1966,** *88,* 2587-2589. (f) Dowd, P.; Chow, M. *Tetrahedron* **1982,** *38,* 799-807.

6. (a) Coms, F. D.; Dougherty, D. A. *Tetrahedron Lett.* **1988,** *29,* 3753-3756. (b) Sponsler, M. B.; Jain, R.; Coms, F. D.; Dougherty, D. A. *J. Am. Chem. Soc.* **1989,** *111,* 2240-2252. (c) Pranata, J.; Dougherty, D. A. *J. Phys. Org. Chem.* **1989,** *2,* 161-176. (d) Pranata, J.; Dougherty, D. A. *Synthetic Metals* **1987,** *22,* 171-178. (e) Jain, R.; Sponsler, M. B.; Coms, F. D.; Dougherty, D. A. *J. Am. Chem. Soc.,* **1988,** *110,* 1356-1366.

7. (a) *Handbook of Conducting Polymers, Vol. 1;* Skotheim, T. A., Ed.; Marcel Dekker, Inc.: New York, 1986; Vol. 1. (b) *Handbook of Conducting Polymers, Vol. 2;* Skotheim, T. A., Ed.; Marcel Dekker, Inc.: New York, 1986; Vol. 2.

8. Fukutome, H.; I., T.; Ozaki, M. *Chem. Phys. Lett.* **1987,** *133,* 34-38.

9. (a) Prokof'ev, A. I.; Solodovnikov, S. P.; Rasuleva, D. Kh.; Volod'kin, A. A.; Ershov, V. V. *Izv. Akad. Nauk. SSSR, Ser. Khim.* **1970**, *7*, 1656-1658. (b) Kudinova, L.I.; Volod'kin, A. A.; Ershov, V. V.; Prokof'ev, A. I. *Izv. Akad. Nauk. SSSR, Ser. Khim.* **1978**, *7*, 1503-1508. (c) Merete, F. N.; Spriggs, S.; Utley, J. H. P.; Gao, Y. *J. Chem. Soc., Chem. Commun.* **1994**, *11*, 1395-1397. (d) Goulart, M. O. F.; Utley, J. H. P. *J. Org. Chem.* **1988**, *53*, 2520-2525. (e) Veciana, J.; Martinez, A. D.; Armet, O. *Rev. Chem. Interm.* **1988**, *10*, 35-70.

10. See Chapter 3 in this thesis.

11. Murray, M. M., California Institute of Technology, personal communication.

12. See Chapter 4 in this thesis.

13. Jacobs, S. J.; Shultz, D. A.; Jain, R.; Novak, J.; Dougherty, D. A. *J. Am. Chem. Soc.* **1993**, *115*, 1744-1753.

14. (a) Wallow, T. I.; Novak, B. M. *J. Am. Chem. Soc.* **1991**, *113*, 7411-7412. (b) Wallow, T. I.; Novak, B. M. *J. Org. Chem.* **1994**, *59*, 5034-5037.

15. Becker, H.-D. *J. Org. Chem.* **1967**, *32*, 2115-2124. Becker, H.-D. *J. Org. Chem.* **1967**, *32*, 2124-2130.

16. Miller, S. A., California Institute of Technology, unpublished results.

17. (a) Carlin, R. L. *Magnetochemistry*; Springer-Verlag: New York, 1986. (b) Iwamura, H.; Koga, N. *Acc. Chem. Res.* **1993**, *26*, 346-351.

18. Jacobs, S. J. Ph.D. Thesis, California Institute of Technology, Pasadena, California, 1994.

19. (a) Mann, C. K. *Electroanal. Chem.* **1969**, *3*, 57-134. (b) Mann, C. K.; Barnes, K. K. *Electrochemical Reactions in Nonaqueous Systems*; Marcel Dekker: New York, 1970. (c) *Organic Electrochemistry*; Baizer, M. M., Lund, H., Eds.; Marcel Dekker: New York, 1983.

20. A model has been developed which bears out these qualitative expectations for *S* versus spin concentration: Miller, S. A. California Institute of Technology, unpublished results.

21. Clites, J. A. California Institute of Technology, unpublished results.

22. See "Research towards a stable analog of non-Kekulé benzene" in Appendix C of this thesis.

23. Webster, O. W.; Kim, Y. H. *J. Am. Chem. Soc.* **1990**, *112*, 4592-4593.

24. Miller, T. M.; Neenan, T. X.; Zayas, R.; Bair, H. *J. Am. Chem. Soc.* **1992**, *114*, 1018-1025.

Chapter 3. Design, Synthesis, and Attempted Observation of a Tetraphenoxyl Tetraradical: Facile Rearrangement of a Substituted Bicyclobutane

Introduction

The preparation of room-temperature stable, high-spin organic polyradicals is part of our long-term goal of producing an organic ferromagnet.[1] Previously, this group has demonstrated that tetraradical **A**,

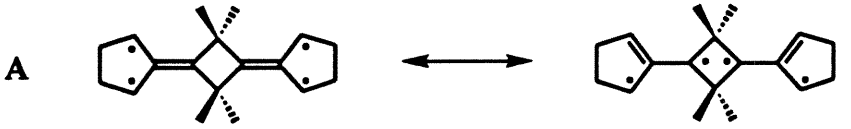

Figure 3.1: A Rationally Designed Quintet Tetraradical

which incorporates both trimethylenemethane and cyclobutanediyl aspects in its resonance structures, is a ground state quintet.[2] The generation of **A** is nontrivial, however, requiring the construction and photolysis in solid matrix of an appropriate bisdiazene precursor. Additionally, **A** is not stable in fluid media. Inspired by stable radicals like BHT, galvinoxyl,[3] and Yang's

Figure 3.2: Stable Phenoxyl Radicals

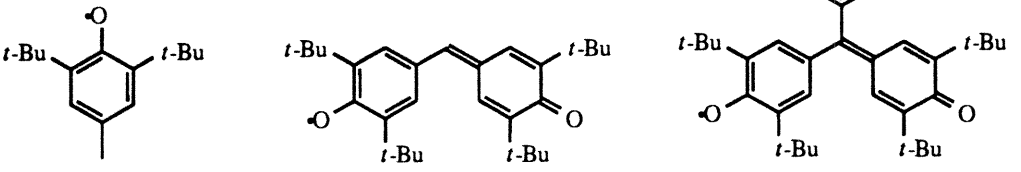

BHT Galvinoxyl Yang's biradical

biradical,[3] we wondered if a tetraphenoxyl radical could be obtained by oxidation of tetraphenol **I** that would be stable and more easily generated than

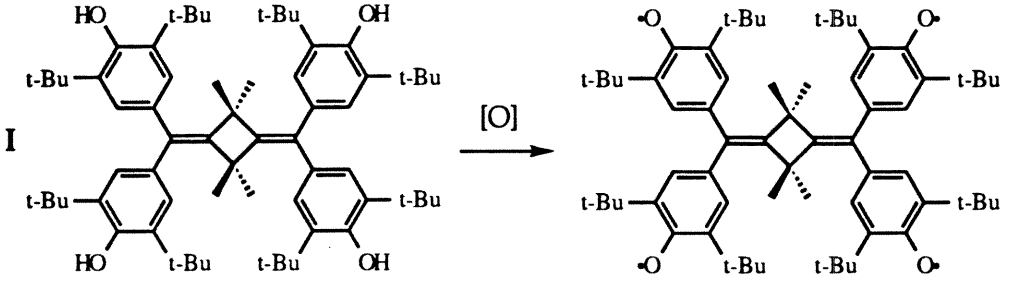

Figure 3.3: A Rationally Designed, Room Temperature Quintet?

the (magnetically) topologically identical **A**. We anticipated that this tetraradical might close to form a substituted bicyclobutane, as Hünig et al. have observed in similar systems.[4-9] In this case it might be possible to observe true magnetooptical switching between the ring-opened tetraradical and the ring-closed biradical by irradiation at appropriate wavelengths, a process this group has demonstrated previously[10] using the triplet biradical

Figure 3.4: Magnetooptical Switching in 2,4-Dimethylene-1,3-cyclobutanediyl

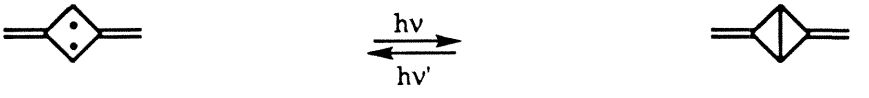

2,4-dimethylene-1,3-cyclobutanediyl, the non-Kekulé isomer of benzene. Unfortunately (for our purposes) the major isolated product from the oxidation of **I** is the rearranged bisgalvinol butadiene **V**, which presumably goes through an unstable bicyclobutane intermediate (Figure 3.5). The novel feature of this rearrangement, which occurs for unsubstituted bicyclobutane at

Figure 3.5: Bicyclobutane Formation and Rearrangement

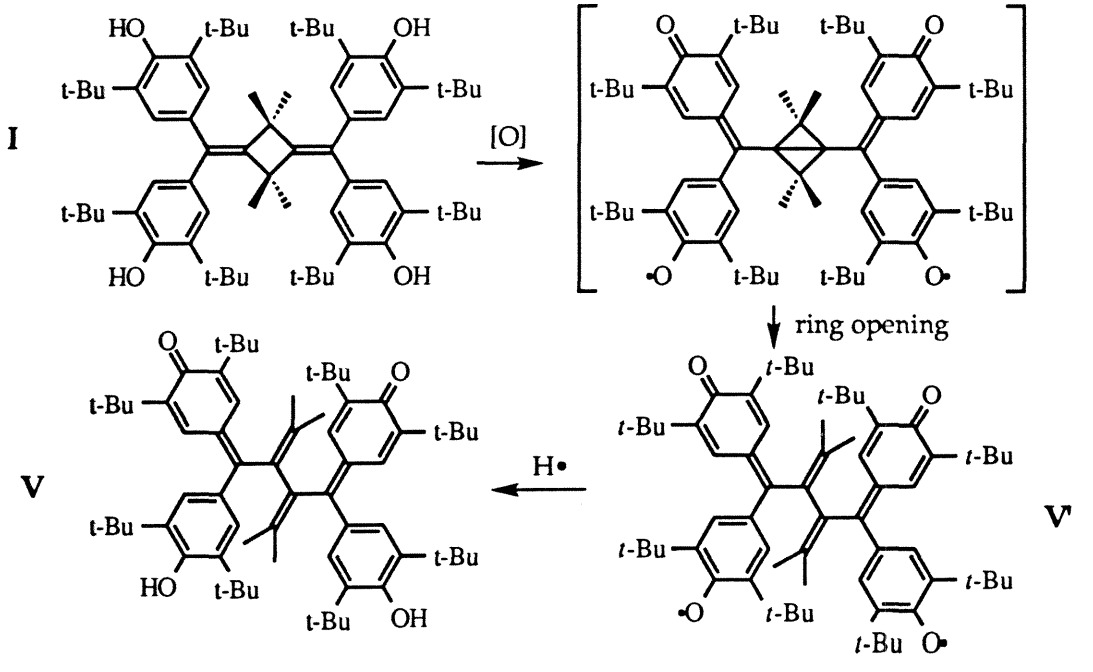

~200°C[11] and for Hünig's substituted bicyclobutanes at ~40°C,[4-9] is that it proceeds readily in our system even under very mild conditions. Thus, we have not observed any evidence of high spin nor have we been able to isolate a bicyclobutane derivative.

Target Structures and Synthetic Strategies

Tetraphenol **I** was obtained on a multi-gram scale in 7% overall yield (based on 2,6-di-*tert*-butylphenol) using fairly conventional chemistry as shown in Scheme 3.1. Bisphenol **3.1a** was obtained in 64% yield by coupling 2,6-di-*tert*-butylphenol with formaldehyde using KOH in ispropanol.[12] The phenol hydroxyl was protected as a methyl ether using sodium hydride and methyl iodide,[13] giving bisanisole **3.1b** in 36% yield. Despite the low yield and the subsequent difficulty of deprotection, this step was necessary as other protecting groups did not survive the rest of the sequence. Bisanisole **3.1b** was then oxidized with cerium (IV) ammonium nitrate[14] to give benzophenone **3.1c** in 74% yield. Formation of hydrazone **3.1d** in 95% yield was accomplished with anhydrous hydrazine.[15] In the key step,[4,15,16] diazomethane **3.1e**, prepared *in situ* by oxidation of **3.1d** with activated mercuric oxide,[17] was added to 2,2,4,4-tetramethylcyclobutanedithione (**3.1f**) to give bisepisulfide **3.1g** in 75% yield based on hydrazone **3.1d**. Desulfurization was accomplished by refluxing with triphenylphosphine to give tetraanisole **3.1h** in 95% yield.[18] In the final step, heating the tetraanisole at 85°C in a 1.5 M CH_3SLi/HMPA soln for 10 days removed the methyl ether protecting groups,[19] giving tetraphenol **I** in 60% yield. Tetraphenol **I** is a white solid, sparingly soluble in THF, benzene, and chlorinated solvents, and apparently immune to significant air oxidation, even when heated over 360°C in a melting point apparatus.

Scheme 3.1: Synthesis of Phenol **I**

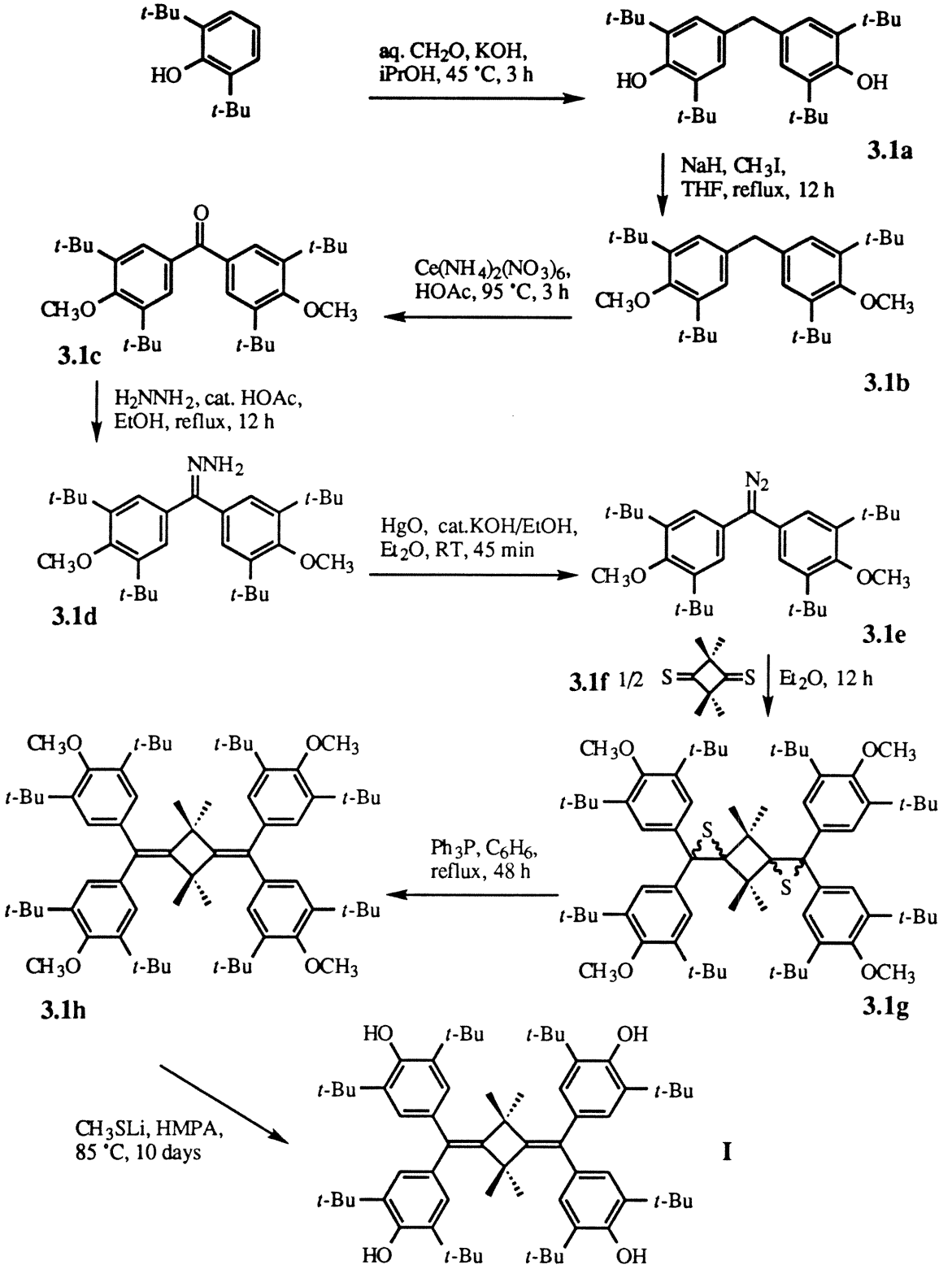

Bisphenol **II** (Scheme 3.2) was obtained in 12% overall yield (based on 2,6-di-*tert*-butylphenol) in a similar sequence by taking advantage of the stepwise nature of the Barton-Kellogg reaction[4,16] on these substrates. First, one equivalent of diphenyldiazomethane was added to dithione **3.1f**, giving monoepisulfide **3.2b** in 94% isolated yield; the crude reaction mixture could be combined with substituted diphenyldiazomethane **3.1e**, giving hetero-bisepisulfide **3.2c** in 98% yield based on **3.1e**. Desulfurization was accomplished as before in 98% yield. For the deprotection step, we found that EtSLi solution in DMF[19] was effective on bisanisole **3.2d**, giving **II** in 79% yield, avoiding HMPA as a solvent (for deprotection of **3.1h**, the DMF solution was much less effective). Bisphenol **II** is a white solid, soluble in THF, benzene, and chlorinated solvents, and slightly soluble in CH_3CN.

Phenols **III** and **IV** (Schemes 3.3 & 3.4) were designed and synthesized to help explain some of the initially puzzling oxidation/EPR results of phenols **I** and **II**. Bisphenol **III** was obtained by addition of isopropyl magnesium chloride to benzophenone **1c** followed by dehydration to **3.3a** (92% yield). Subsequent deprotection using the EtSLi solution in DMF gave **III** in 51% isolated yield. Bisphenol **III** is a white solid, freely soluble in most organic solvents, but sensitive to oxygen; a sample of white powder turned yellow in a few minutes in air.

Phenol **IV** was synthesized by a similar sequence. First, *tert*-butyllithium was added to bromoanisole **3.4b**, creating aryllithium **3.4c** *in situ*, followed by addition of isobutyrophenone. Subsequent acidic dehydration gave anisole **3.4d** in 47% yield. Deprotection with EtSLi in DMF gave **IV** in 63% isolated yield. As with **III**, phenol **IV** is a soluble, air-sensitive white solid.

Scheme 3.2: Synthesis of Phenol **II**

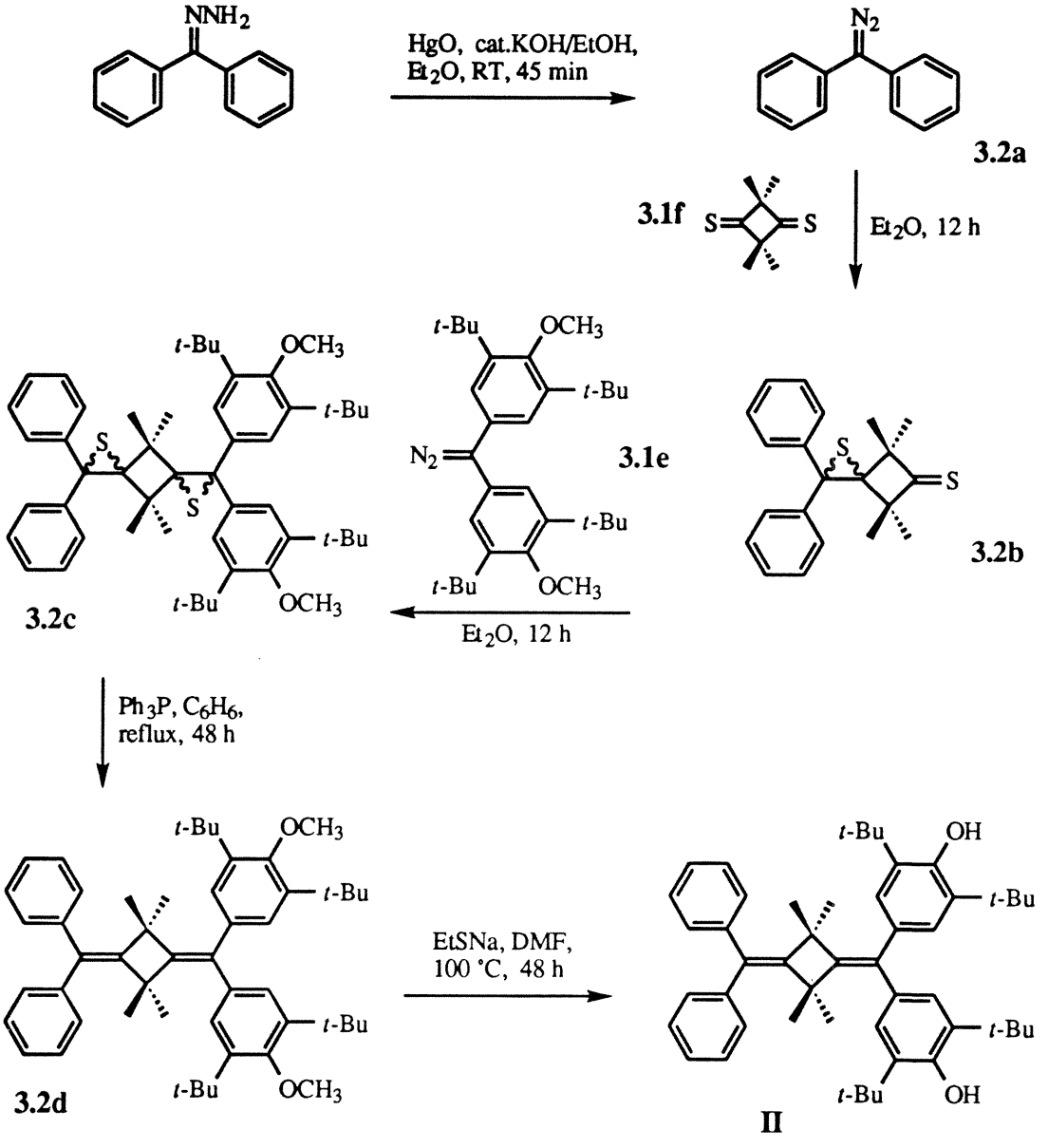

Scheme 3.3: Synthesis of Phenol **III**

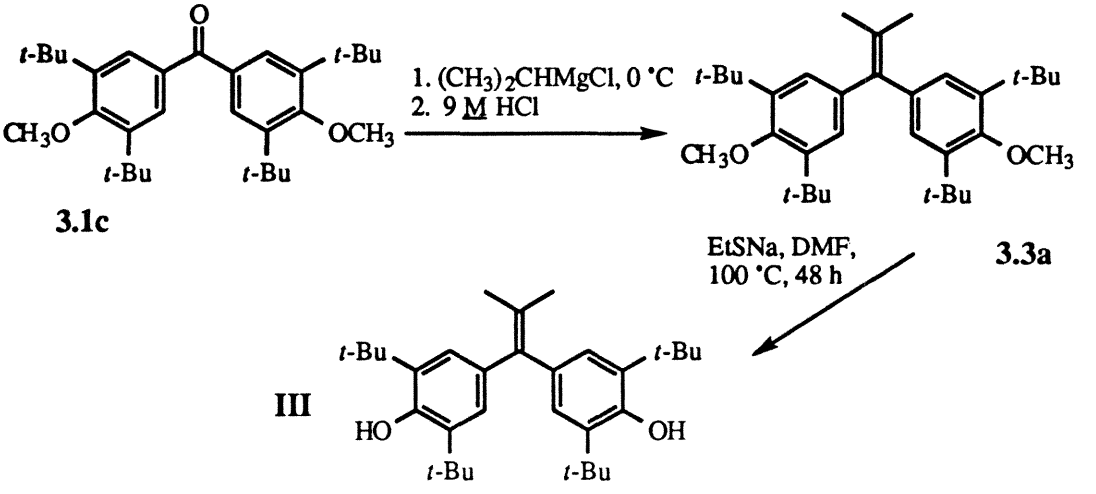

Scheme 3.4: Synthesis of Phenol **IV**

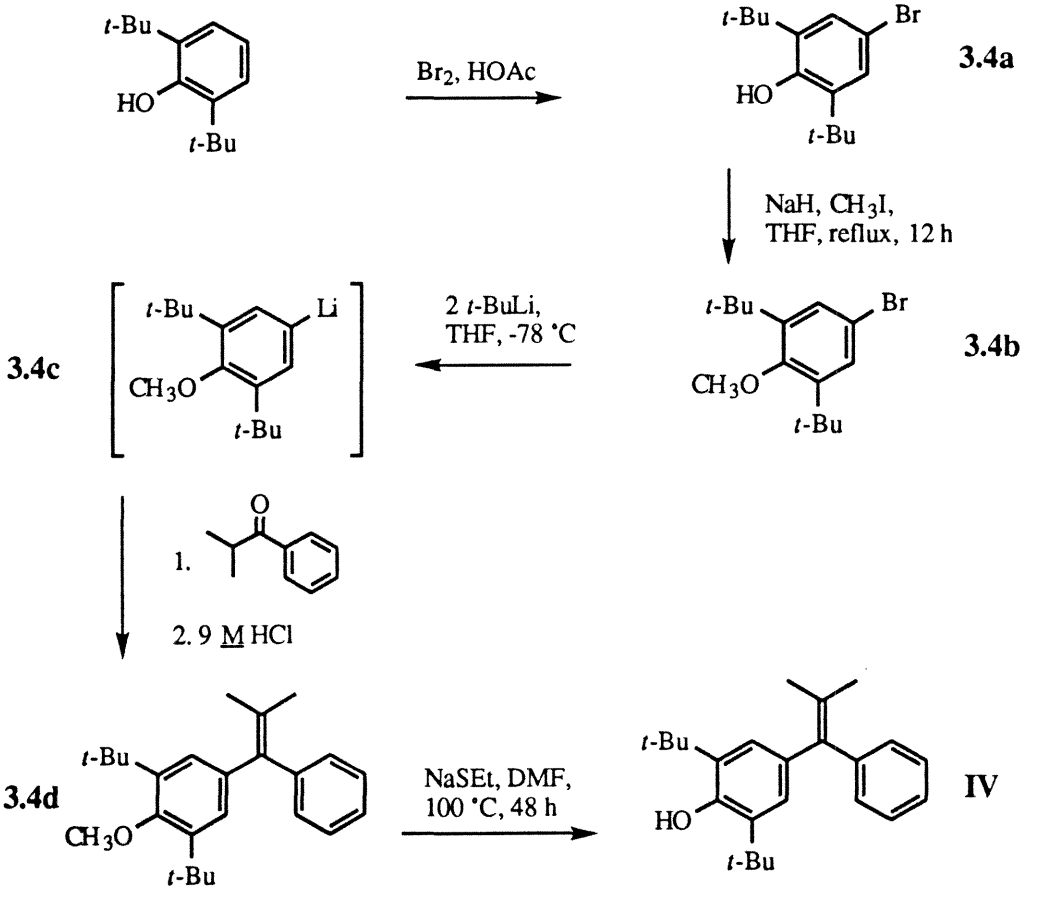

Results and Discussion

A variety of chemical oxidants including potassium ferricyanide (+0.36 V versus SHE), iodine (+0.54 V), activated nickel peroxide (+1.68 V), 2,3-dichloro-5,6-dicyanobenzoquinone (+1.68 V), lead dioxide (+1.69 V), and silver(II)oxide (+1.98 V) were used in this study.[3,20] Representative experimental EPR[21] spectra and computer simulated[22] spectra are shown in Figures 3.6-3.12.

The room temperature EPR spectrum obtained from phenol **III** (Figure 3.6) upon oxidation with lead dioxide is composed of 15 lines and is 28 G wide. Computer simulation[22] of hyperfine splitting showed that a similar, though not precisely superimposable spectrum could be generated by two meta hydrogens, a_H = 1.7 G, and six allylic hydrogens, a_H = 3.1 G.[23] Frozen matrix spectra at 77 K gave a single line 17.5 G wide (not shown, see Figure 3.12 for representative spectrum), with no sign of a $\Delta M_S = 2$ transition or any other indications of higher than a doublet spin state. The behavior of phenol **III** upon oxidation with potassium ferricyanide under basic, biphasic conditions was more complex. Aliquots of the organic layer were separated after 5-10 minutes of oxidation and frozen at 77 K until spectra were taken. These gave a 15 line, 28 G wide spectrum at room temperature and a single line, 20.5 G wide spectrum at 77 K, similar to the PbO_2 oxidation. Conversely, samples taken after 45 min of oxidation gave a five line spectrum (Figure 3.7) consistent with a galvinoxyl doublet radical split by four meta hydrogens, a_H = 1.35 G.[3] The spectrum in frozen matrix was composed of a single line 10.9 G wide, with no sign of a $\Delta M_S = 2$ transition or any other indications of higher than a doublet spin state. Samples which generated the 15 line spectrum did not transform into the 5 line spectrum when isolated from the

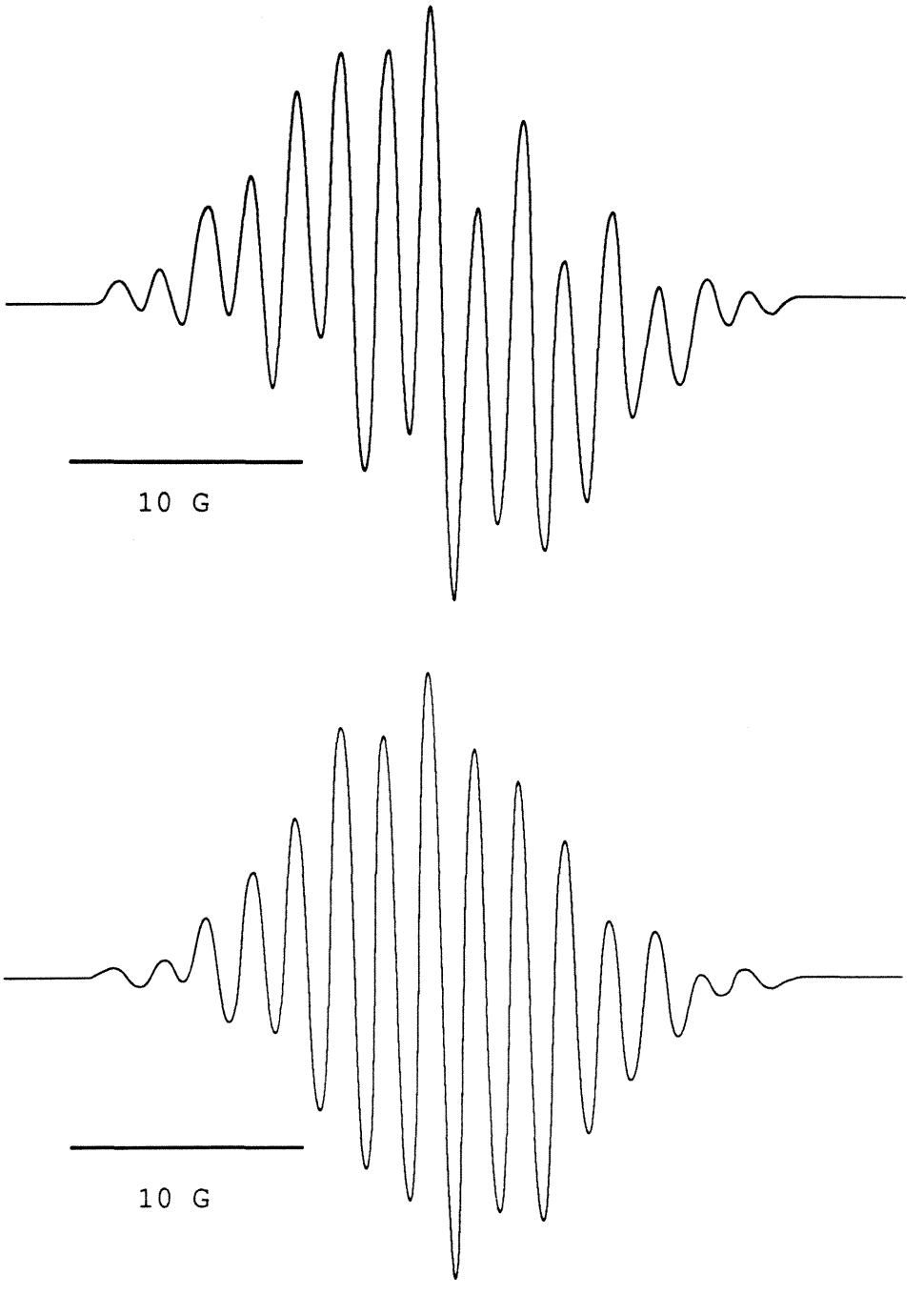

Figure 3.6: 15 line EPR Spectra for **III'**.

Top: **III** oxidized by PbO_2

Bottom: Computer simulation[22] using 2H, a_H = 1.7 G & 6H, a_H = 3.1 G.[23]

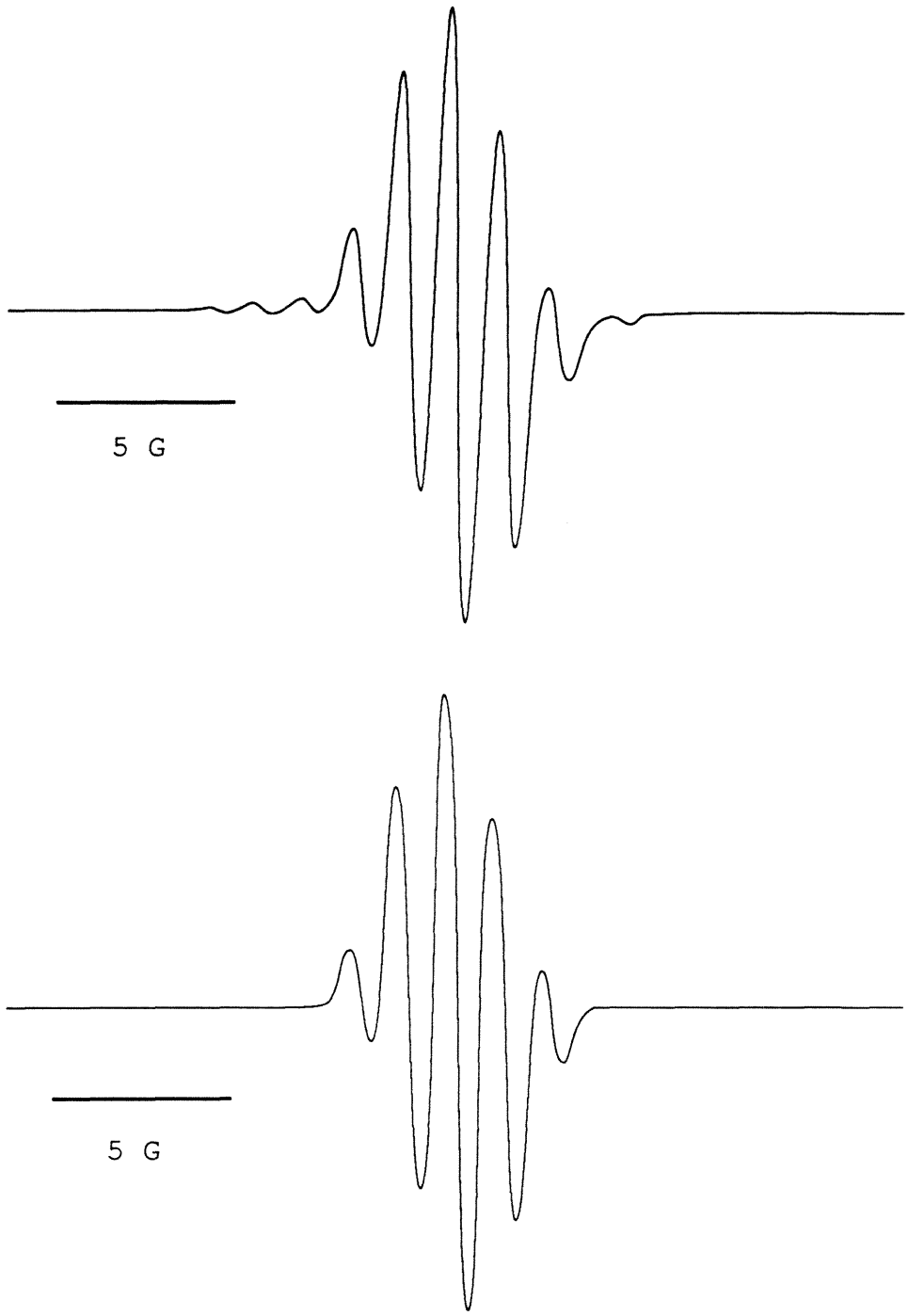

Figure 3.7: 5 line EPR Spectra for **III->VI'**.

Top: **III** after 30 min biphasic $K_3Fe(CN)_6$/NaOH oxidation

Bottom: Computer simulation[22] using 4H, a_H = 1.35 G.[23]

oxidant. The behavior of phenol **III** upon oxidation with silver (II) oxide was similar. Room temperature spectra taken after 1 hour exhibited the 15 line spectrum which transformed over 24 hours (in contact with the oxidant) into a broad five line spectrum. Frozen matrix spectra at 77 K gave a single line with no sign of a $\Delta M_S = 2$ transition or any other indications of higher than a doublet spin state.

Phenoxyl radical **III'** (Scheme 3.5), obtained by partial oxidation of phenol **III**, is the likely source of the observed 15 line spectrum. The five-line galvinoxyl-type spectrum obtained after prolonged oxidation could be due to either a dimer or to galvinoxyl **VI'**. Since the only galvinol isolated after the reaction is **VI**, which generates the five line spectra upon reoxidation (Figure 3.8), the original spectrum is assigned to **VI'**. One possible path from **III'** to **VI'** involving disproportionation (not shown) is contradicted by the fact that the 15 line phenoxyl spectrum obtained after 5-10 minutes of biphasic potassium ferricyanide oxidation does not transform into the five line spectrum in the absence of oxidant. This also suggests that oxidation of the second phenol is either necessary for abstraction of one of the allylic hydrogens or is only possible after the galvinol intermediate is generated. No evidence of triplet spin was observed, nor any hyperfine that could be assigned to biradical **III''**. Thus, if **III''** were produced, it is either a singlet or has a very short lifetime. This leaves two possible mechanisms; either formation of **III''** which rapidly loses an allylic hydrogen, or loss of an allylic hydrogen from **III'** to give the galvinol **VI** which is then further oxidized.

SCHEME 3.5: Pathway to Galvinol **VI**

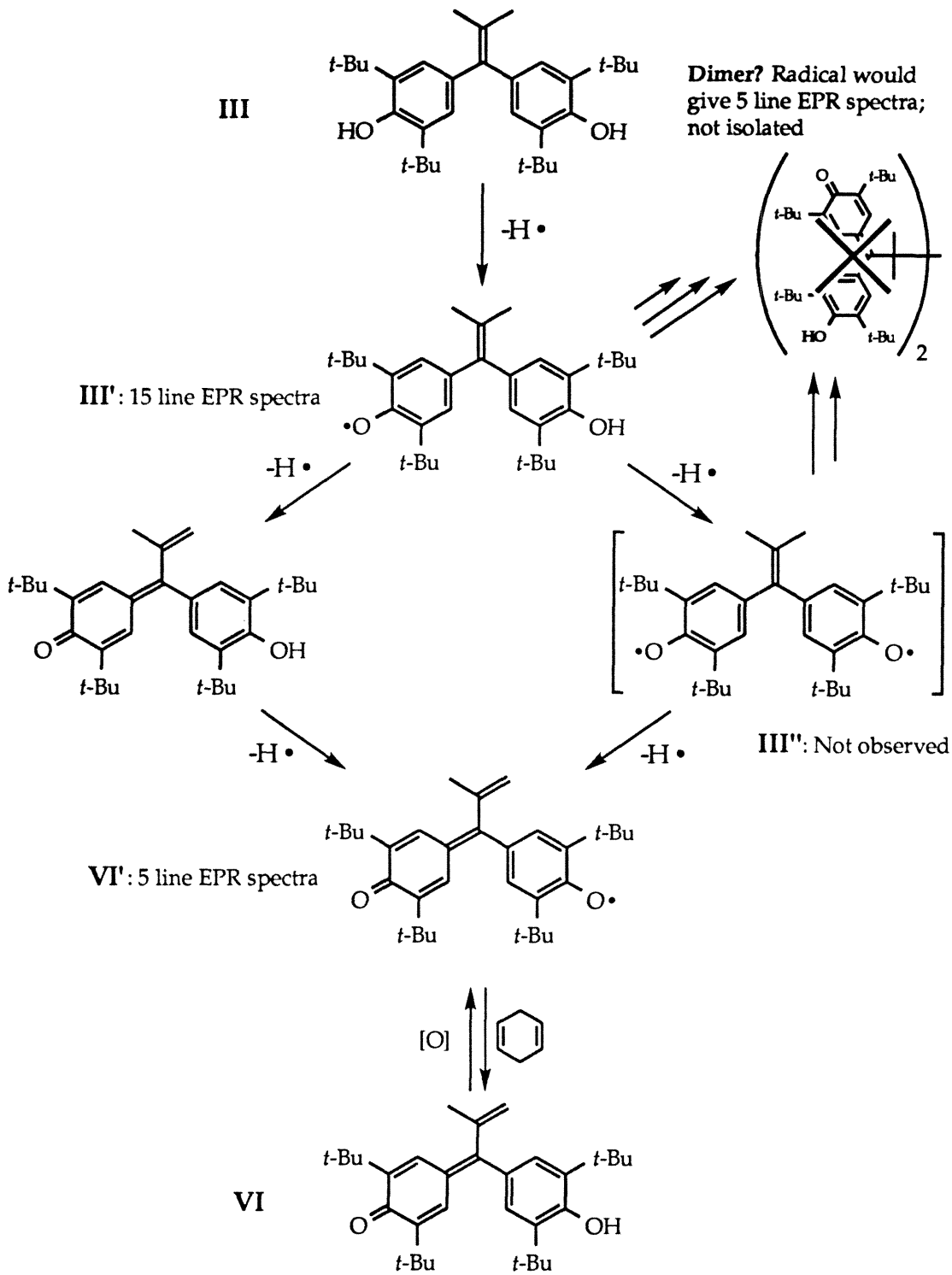

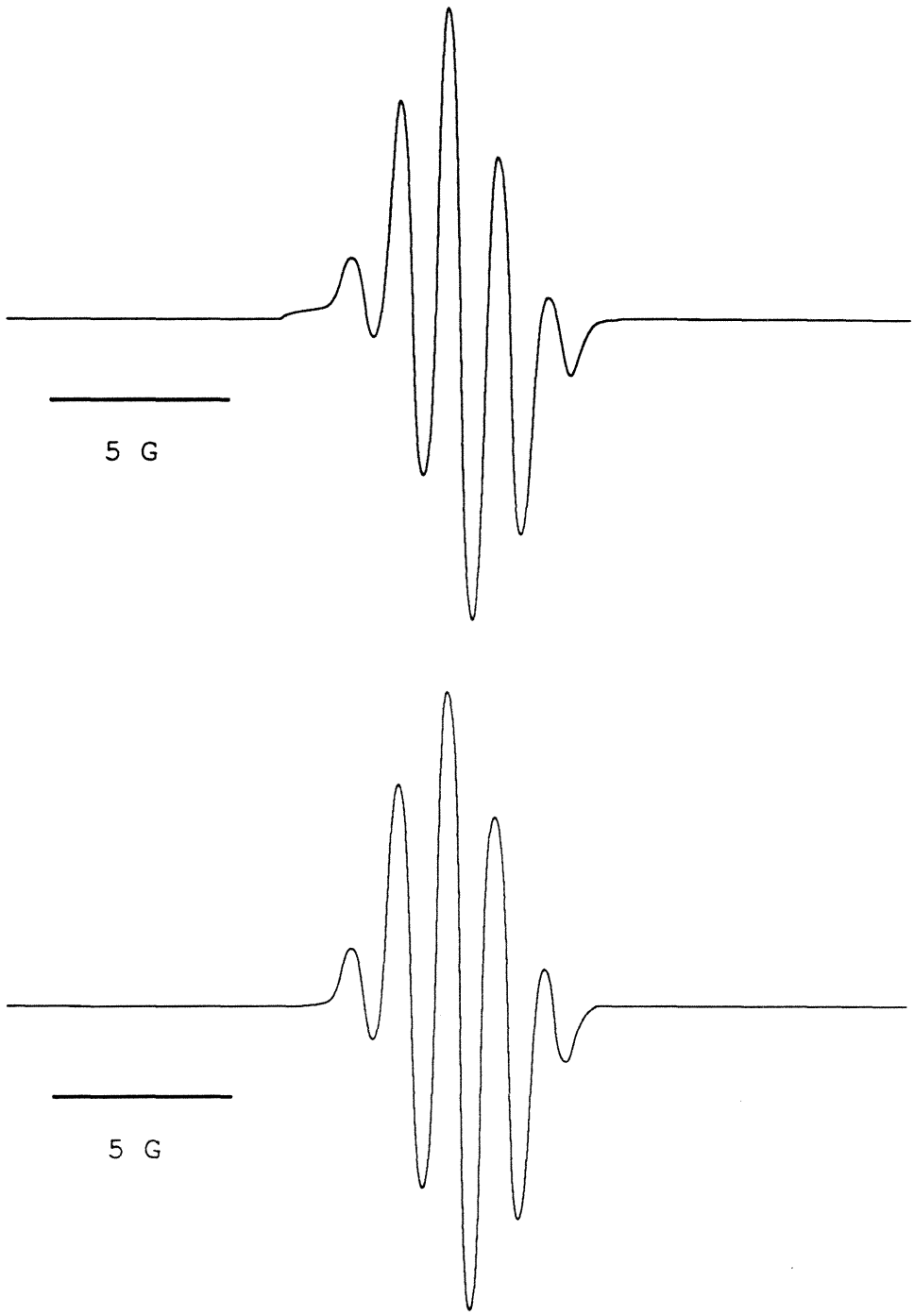

Figure 3.8: 5 line EPR Spectra From Isolated **VI**.

Top: **VI** oxidized by AgO

Bottom: Computer simulation[22] using 4H, a_H = 1.35 G.[23]

The room temperature EPR spectra of phenol **IV** (Figure 3.9) upon oxidation with either lead dioxide or silver (II) oxide are identical and consist of 26 G wide, 15 line spectra which are essentially identical to the 15 line spectra obtained from **III**. Computer simulation[22] of hyperfine splitting showed that similar, though not superimposable spectra could be generated by two meta hydrogens, a_H = 1.6 G and six allylic hydrogens, a_H = 2.9 G.[23] Frozen matrix spectra at 77 K gave a single line 20.5 G wide. The room temperature spectrum of phenol **IV** upon oxidation with potassium ferricyanide under basic, biphasic conditions[20] is more complex. Aliquots of the organic layer were separated after 5-10 minutes of oxidation and frozen at 77 K until spectra were taken. These gave a 15 line, 26 G wide spectrum at room temperature that that was qualitatively identical to those produced by the lead and silver oxidations. Conversely, room temperature samples taken after 45 min of oxidation gave weak, broadened 3 line spectra (not shown) consistent with a phenoxyl doublet radical split by two meta hydrogens, a_H = 1.9 G.[23] Samples which generated the 15 line spectrum did not transform into the 3 line spectrum when isolated from the oxidation reaction.

Clearly, phenoxyl radical **IV'**, obtained by oxidation of phenol **IV** (Scheme 3.6), is the source of the observed 15 line spectrum due to the unpaired electron being split by the two meta hydrogens and the six allylic hydrogens. The latter indicates that spin density is not localized to the

Scheme 3.6: Oxidation of **IV**

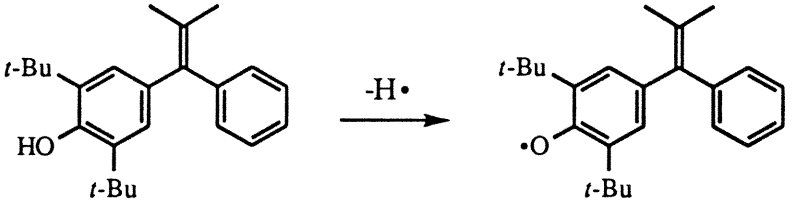

IV **IV'**: 15 line EPR spectra

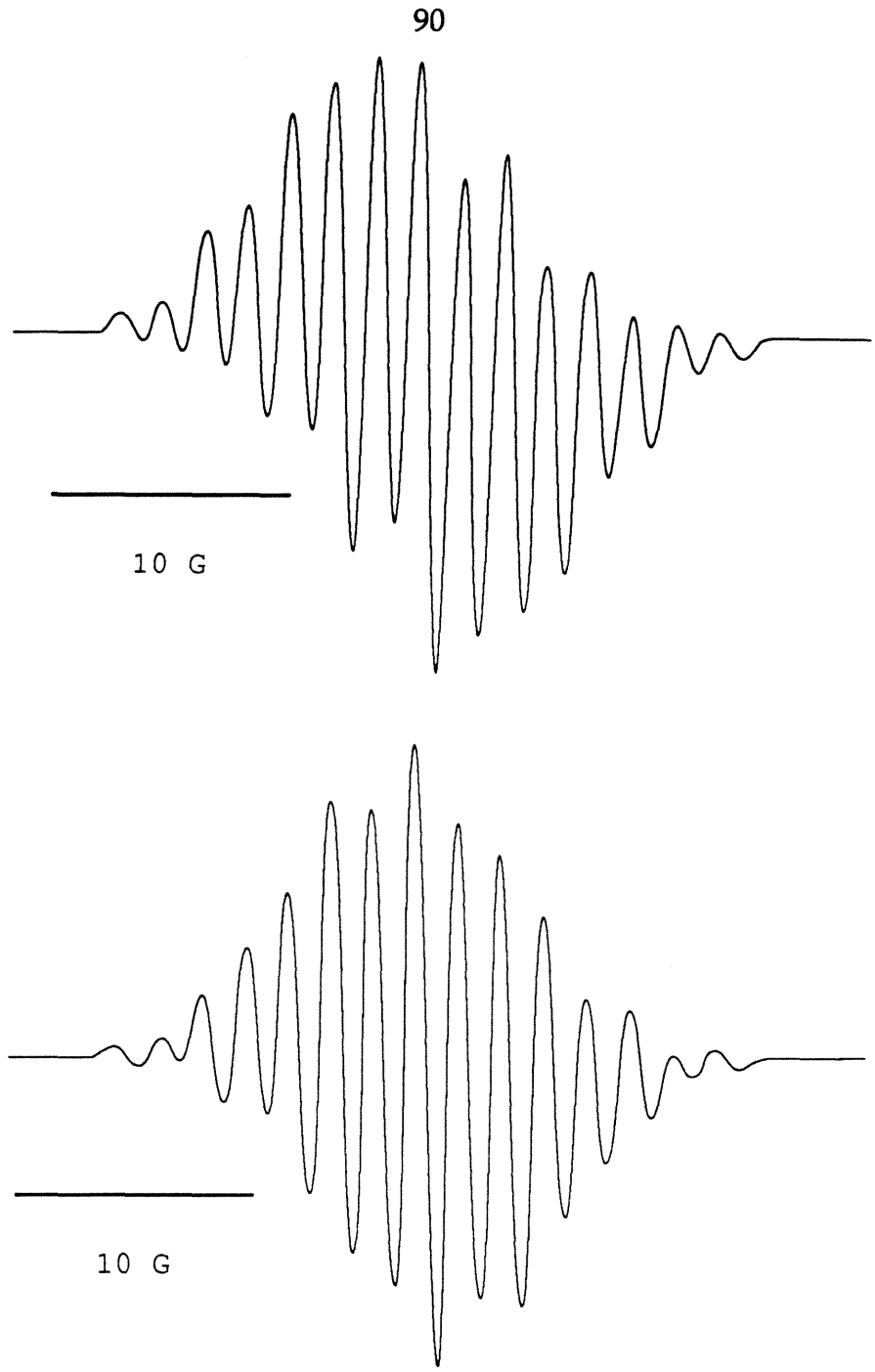

Figure 3.9: 15 line EPR Spectra for **IV'**.

Top: **IV** oxidized by PbO_2

Bottom: Computer simulation[22] using 2H, a_H = 1.58 G & 6H, a_H = 2.88 G.[23]

phenoxyl ring. The weak three line spectrum observed after prolonged biphasic oxidation with potassium ferricyanide is likely due to a decomposition product of **IV'** or other phenol impurities. The 77 K spectra show no evidence of anything but a doublet spin state, as expected.

Initial attempts to oxidize tetraphenol **I** and bisphenol **II** under a wide variety of conditions were frustrating, displaying EPR spectra consistant with one isolated di-*tert*-butylphenoxyl radical. For both, oxidation either alone in 2-methyltetrahydrofuran or after exposure to base (organolithiums, metal hydrides, or using pyridine as solvent) gave room temperature spectra composed of three lines (Figure 3.10) consistent with an isolated phenoxyl doublet radical split by two meta hydrogens, a_H = 1.7 G.[23] Frozen matrix spectra at 77 K are composed of a single line 7.2 G wide, with no sign of a ΔM_S = 2 transition or any other indications of higher than a doublet spin state. There was no evidence of a spin or spins acting between phenoxyl rings or across the bicyclobutane.

Our initial interpretation was that the phenol groups in **I** and **II** were so twisted that no communication was possible. Unsuccessful attempts at hydrogen-deuterium exchange of the four phenol protons using these strong bases, however, indicated a different problem. We doubted that these protons were significantly less acidic than typical 2,6-di-*tert*-butylphenols; the remaining possibility was suggested by the limited solubility of **I** itself. The use of a milder base with a more soluble organic counterion, tetrabutylammonium hydroxide,[28] showed immediate results. Not only did tetrabutylammonium hydroxide draw **I** into many solvents it would otherwise be insoluble in, such as methanol, it also suggested, through the rapid development of a deep blue color, that deprotonated **I** was easily air-oxidized. Further experiments with tetrabutylammonium hydroxide

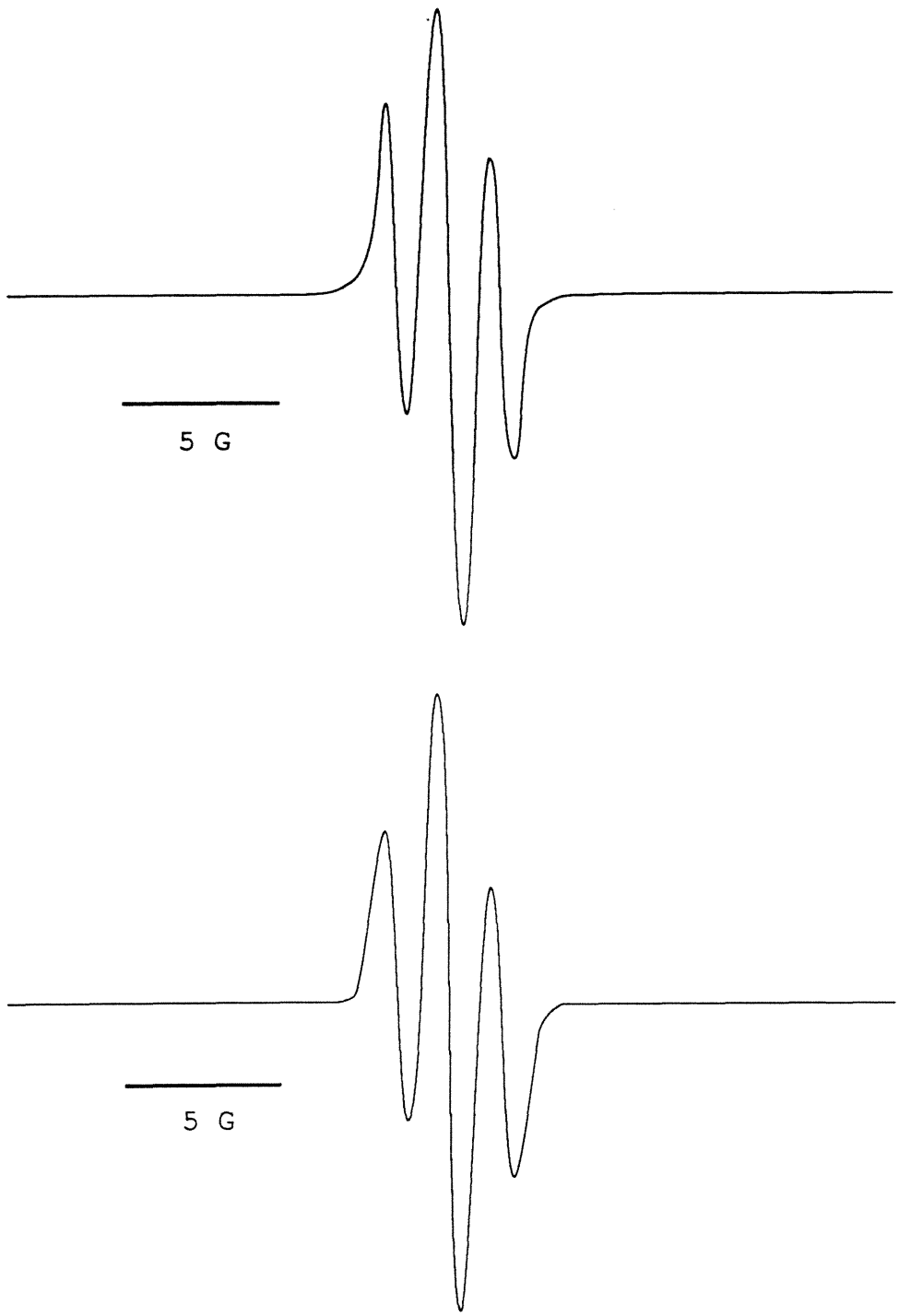

Figure 3.10: Representative 3 line EPR Spectra for **I′** and **II′**.

Top: **I** oxidized by AgO

Bottom: Computer simulation[22] using 2H, a_H = 1.7 G.[23]

demonstrated that all four phenol protons could be exchanged for deuterium or trimethylsilyl groups, which we had been unable to demonstrate with other bases. Oxidation of I with varying amounts of iodine in the presence of stoichiometric or excess amounts of tetrabutylammonium hydroxide showed markedly different behavior from attempts without this base (Figure 3.11). At less than one equivalent of electrons removed, the room-temperature EPR spectrum displays the same isolated phenoxyl spectrum as before. Between one and three equivalents of electrons removed, the simple three line spectrum is again exhibited, but other lines are beginning to emerge. At four equivalents of electrons removed, a five line spectrum is observed, consistent with a galvinoxyl-type radical split by four meta hydrogens.[3,23] We were greatly encouraged by this result despite that the 77 K spectra indicated only a doublet spin state, since we thought it possible that this signal was due to a bisgalvinoxyl bicyclobutane (see Figure 3.5). If this were the case, it might be possible to break the central bond of the bicyclobutane by irradiation at an appropriate wavelength, but exposure to a variety of wavelengths did not change the 77 K spectra. This was puzzling, but we expected that a bicyclobutane structure, if formed during the original oxidation, could ring-open to the butadiene near room temperature.[4-9,11] Accordingly, the base-assisted oxidation was conducted in a dry-ice bath at the preparatory scale and near the freezing point of THF in the EPR cavity. Both yielded results essentially identical to the room-temperature studies. Simple analysis techniques such as IR, UV/Vis, and mass spectrometry applied to the isolated product of these reactions could not distinguish between either a bicyclobutane or a ring-opened butadiene structure. The ^{1}H NMR spectrum (Figure 3.13) of the product is exceedingly complicated, no doubt due in part to the number of rotomers possible. A spectrum of the dianion in d6-acetone

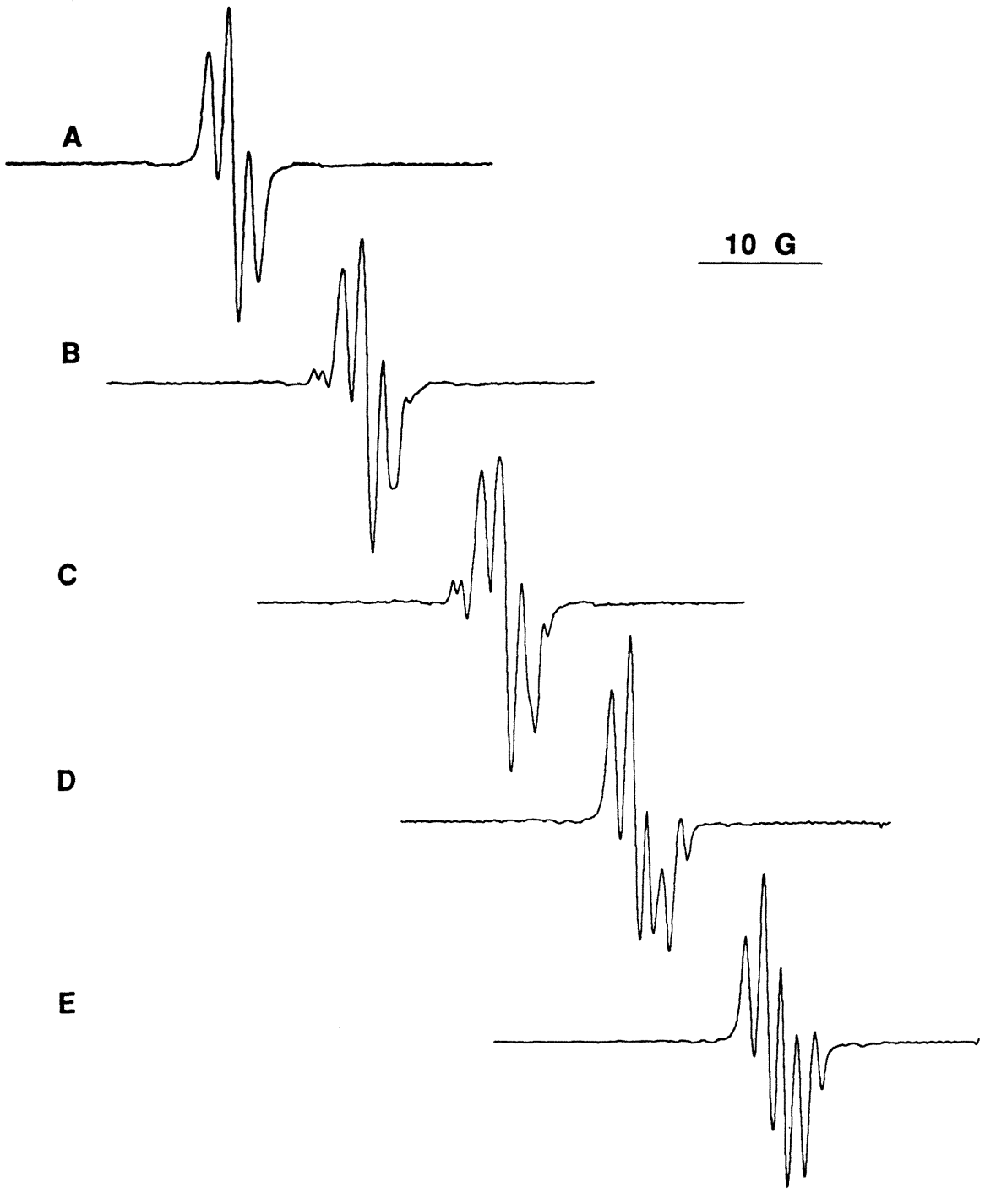

Figure 3.11: Representative 3->5 line EPR Spectra for I_2/Tetrabutylammonium Hydroxide Oxidations of **I** and **II**. **I** and XS tetrabutylammonium hydroxide after oxidation of: **A.** < 1 e^- **B.** 1 e^- **C.** 2 e- **D.** 3 e^- **E.** > 4 e^-.

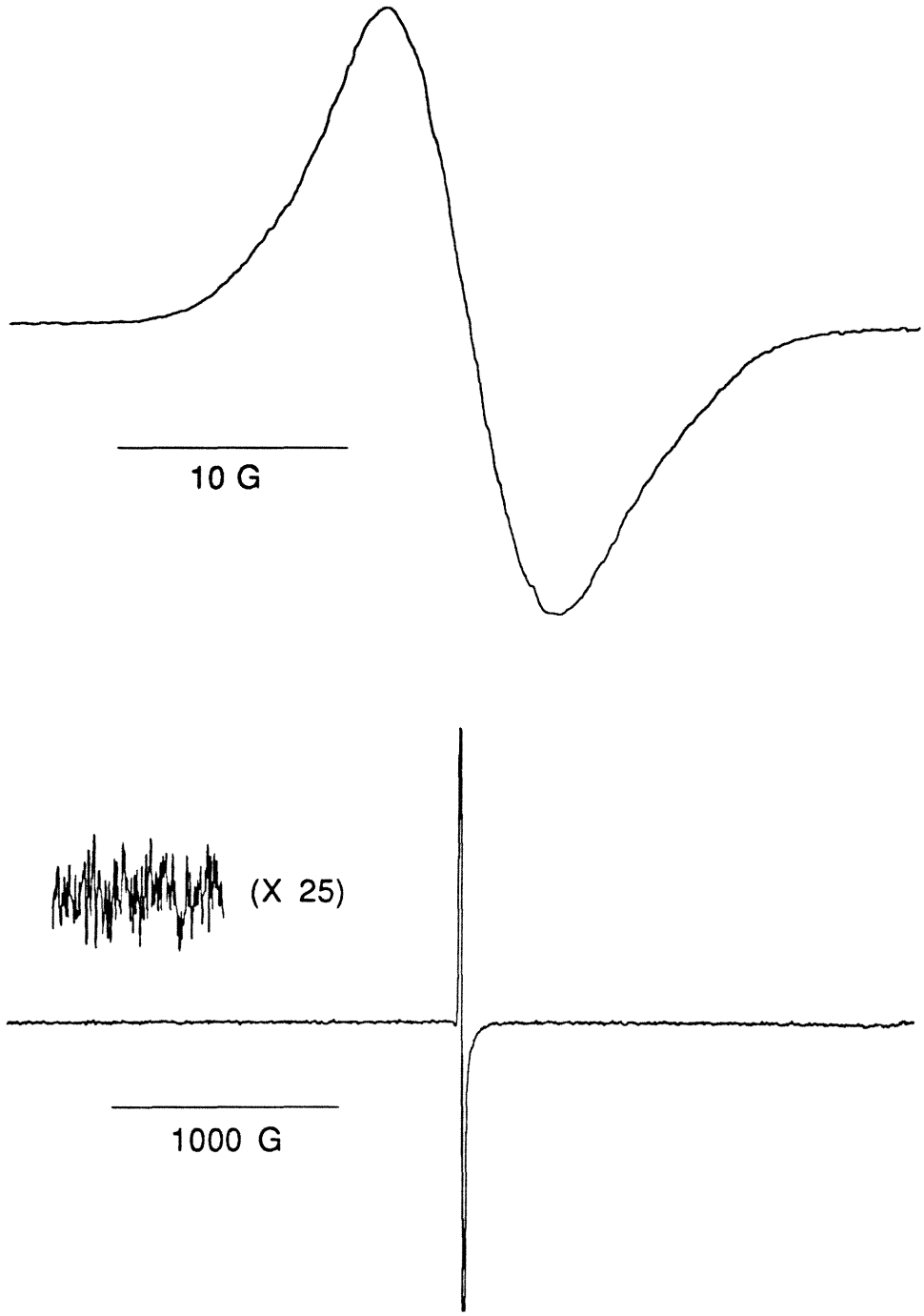

Figure 3.12: Representative 77 K Spectra.

Top: 40 G scan of I_2/tetrabutylammonium hydroxide oxidation of **I** (same as **11E**) Bottom: 4000 G scan. Note lack of signal in $\Delta M_S = 2$ region at half field.

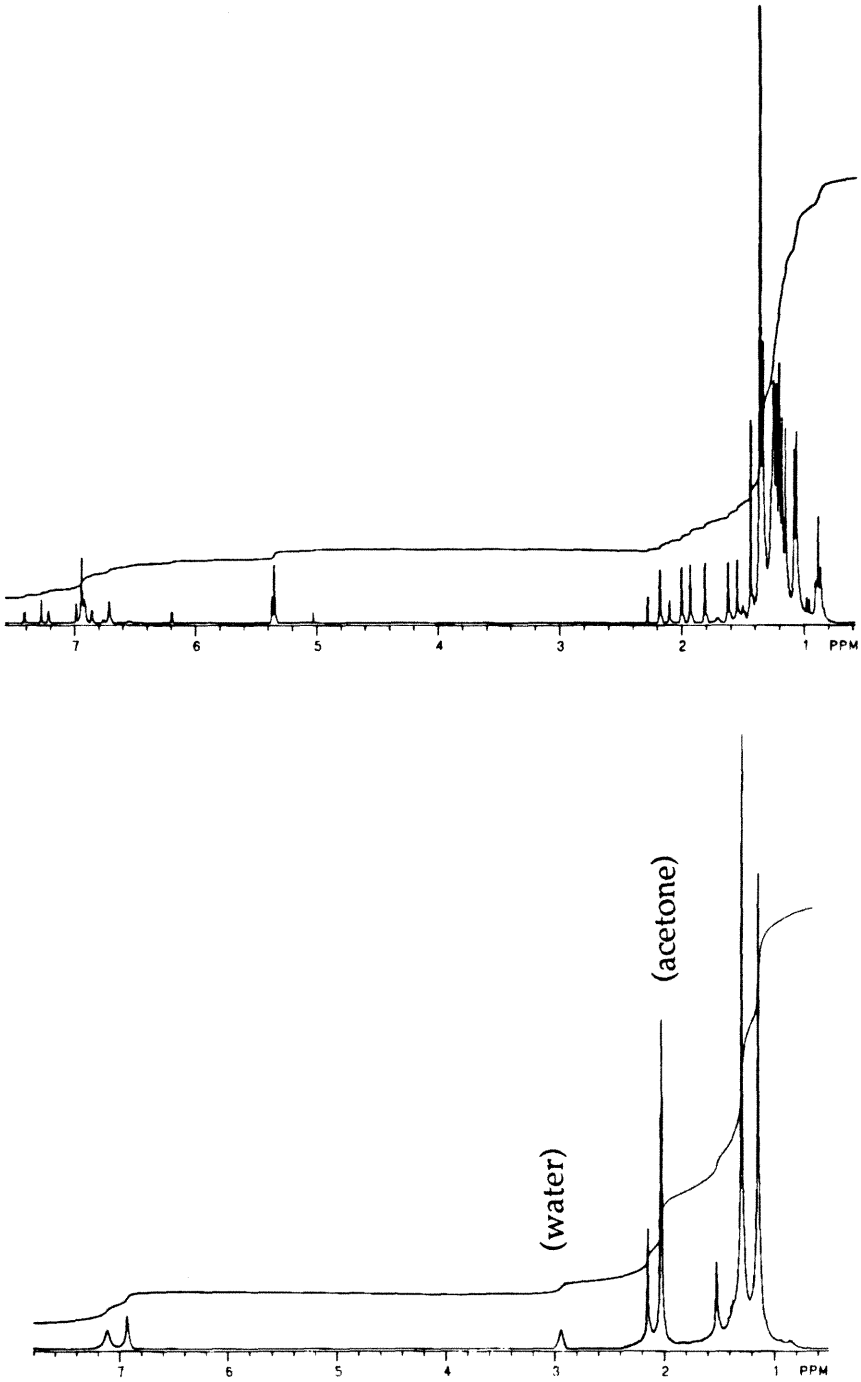

Figure 3.13: 300MHz ^{1}H NMR Spectra of Bisgalvinol **V**. Top: **V** in $CDCl_3$. Bottom: **V** with slight excess of LiOD in acetone-d_6.

showed that the peaks could be collapsed to six singlets, and variable temperature ^{1}H NMR (not shown) in toluene-d_8 showed some coalescence by 100°C; both were reversible. None of these spectra was obviously indicative of or inconsistant with either structure. A single crystal of the product, recrystallized from methanol, was submitted to X-ray analysis, definitively assigning the structure to the ring-opened bisgalvinol **V** (Figure 3.14, see also Appendix B). Though Hünig's similarly substituted bicyclobutanes are reported to ring-open in hot, polar solvents,[4-9] the methanol recrystallization is not responsible since unheated product displays the same NMR behavior. Additional support is lent by the fact that the five-line EPR spectrum obtained by lead dioxide oxidation of **V** (Figure 3.15) is identical to that obtained from the unheated product (not shown).

One plausible route from tetraphenol **I** is shown in Scheme 3.7. The initial three line EPR spectrum is due to singly oxidized tetraphenol, either as the neuteral (not shown) or the trianion monoradical **I'**. Oxidation of a second phenol across the cyclobutane ring offers a chance for formation of the bicyclobutane bond[4-9] and subsequent ring opening to the bisgalvinol anion, which can then be further oxidized to a bisgalvinoxyl radical displaying five line spectra. A mixture of galvinoxyl and phenoxyl species could be expected to display some combination of three and five lines, as observed in Figure 3.11-B, C, and D. Our inability to observe higher than doublet spin could be due to a combination of factors. Although the bracketed intermediates in Scheme 3.7 are hypothetical and have not been observed directly, some sort of bicyclobutane intermediate must form since its bridging bond becomes the central bond of the product **V**. Our inability to observe or isolate such a structure could be due its instability in the presence of methanol, iodine/iodide, or trace hydroxide from the oxidation, or perhaps simply the

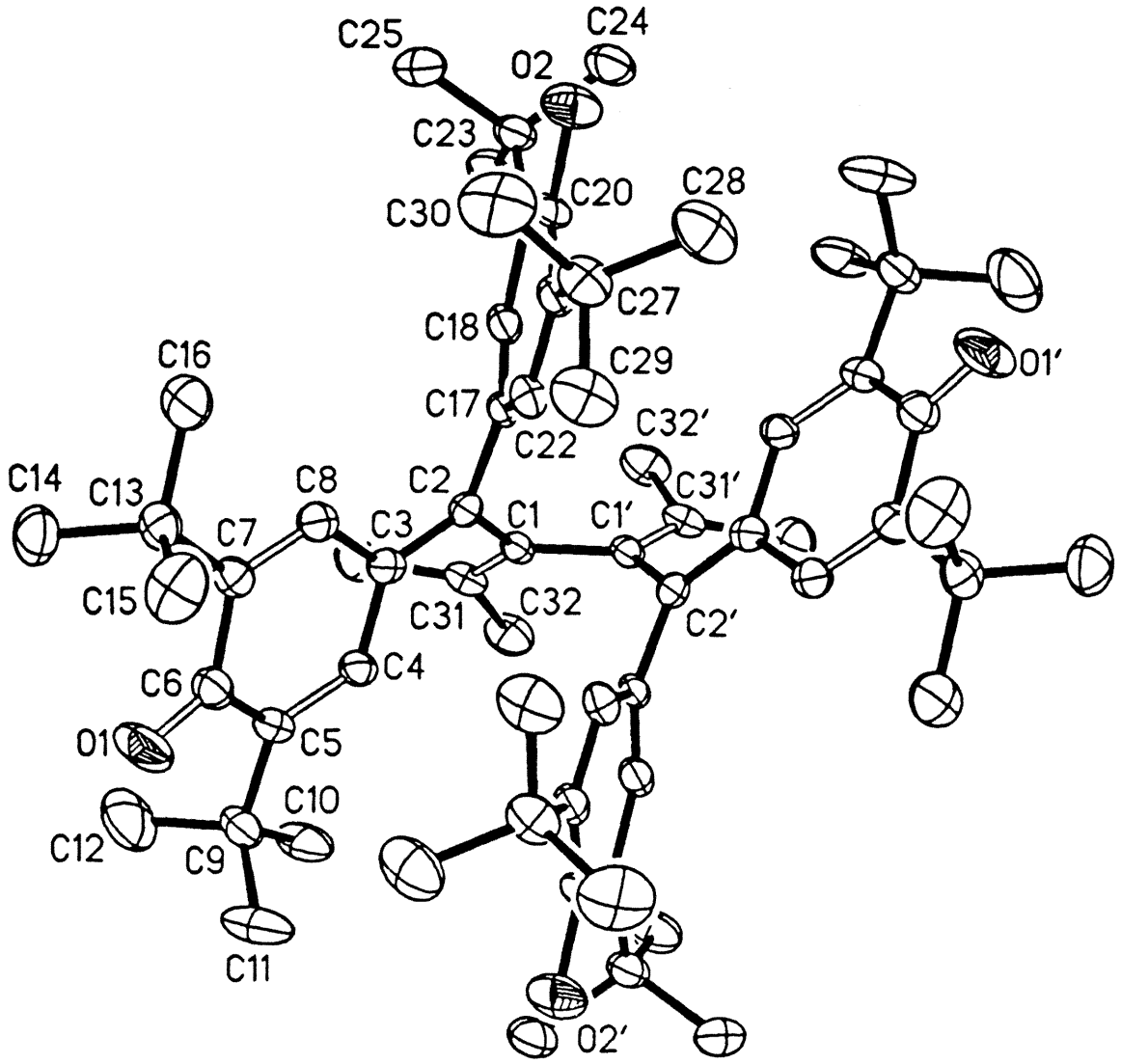

Figure 3.14: X-ray Structure of Bisgalvinol **V** (details in Appendix B).

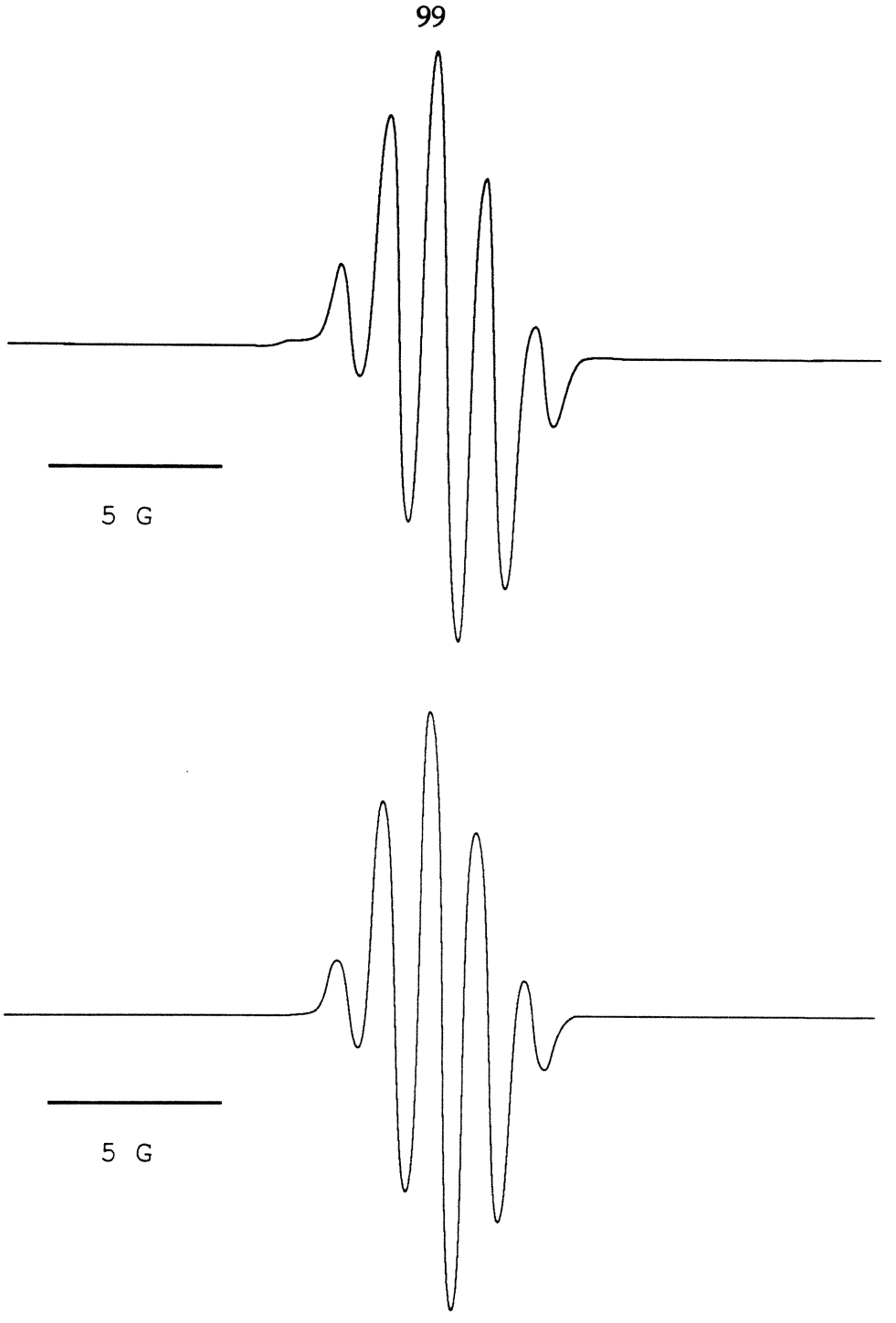

Figure 3.15: 5 line EPR Spectra of Bisgalvinol **V**.

Top: **V** oxidized by PbO_2

Bottom: Computer simulation[22] using 4H, a_H = 1.35 G.[23]

SCHEME 3.7: A Possible Pathway to Bisgalvinol **V**

(bracketed structures are hypothetical)

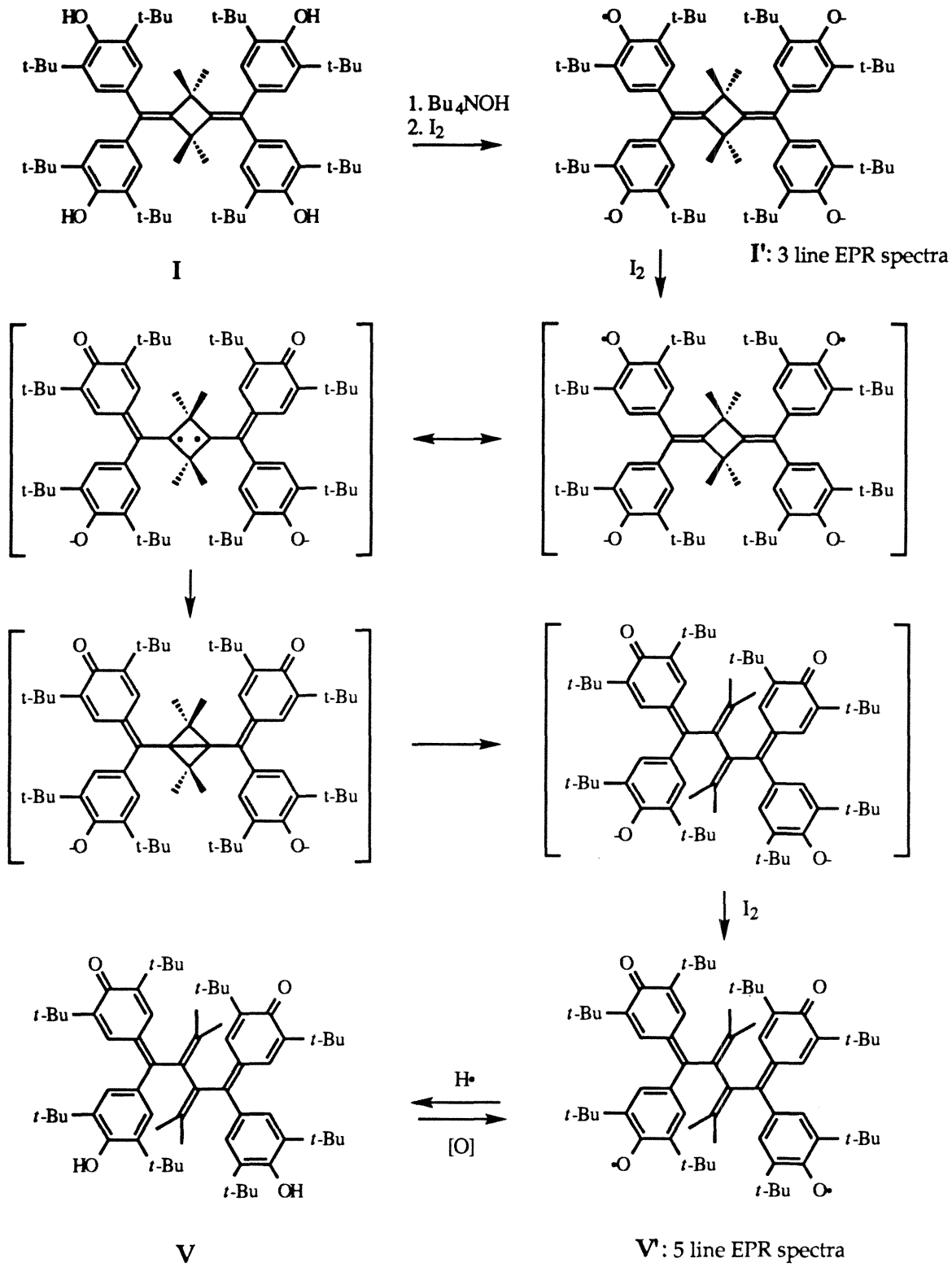

steric strain that must be present in such a crowded system. Finally, there is the possibility that a high spin species is present, but displays only a single narrow line at 77 K because its electrons are so delocalized that zero-field splitting is negligible.[21]

It has been reported that alkylated phenoxyl radicals may be generated via photolysis of a 2-mercaptopyridine-N-oxide derivative.[24] Since this

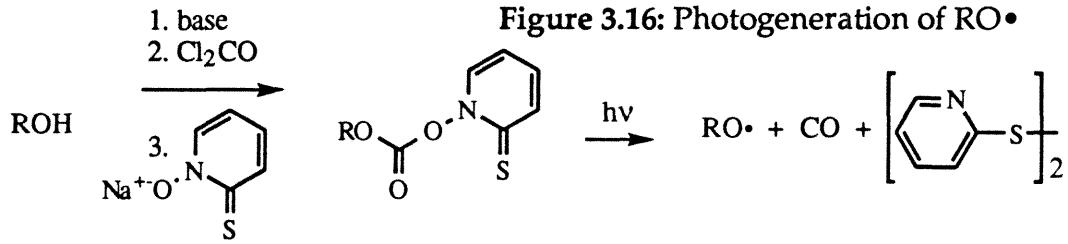

Figure 3.16: Photogeneration of RO•

reaction is reported to be less than quantitative yield, making tetra-derivatization of I less than certain, we first attempted to optimize the reaction using BHT as a model substrate. This revealed some interesting chemistry (Figure 3.17). The delocalized phenol anion can react with phosgene to form a chloroformate at either the oxygen or the 2, 4, or 6 carbons

Figure 3.17: Chloroformylation of BHT anion

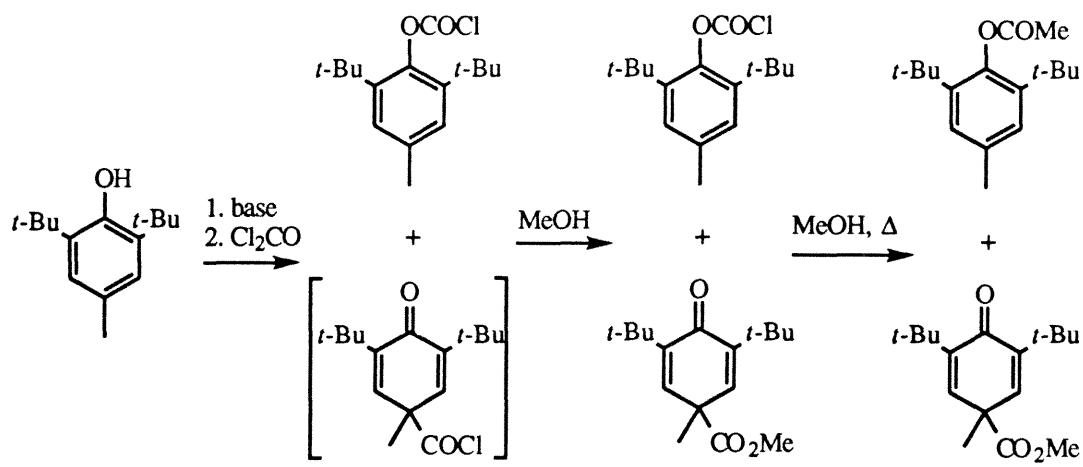

(in practice, the meta positions are too hindered by the *t*-butyl groups for significant reaction). Quenching of this solution with room temperature

methanol gives two products by GC/MS, one with m/z of the expected methyl ester and one with m/z corresponding to an unquenched chloroformate! Upon refluxing for several hours in methanol, the m/z corresponding to the chloroformate disappeared and an additional peak of the same m/z of the methyl ester, but at a different retention time, appeared. Proton NMR of this residue (not shown) gave a clean spectrum which can be assigned to a mixture of the O- and 4- substituted compounds. The explanation for this behavior is simple; consideration of a space-filling model of the O-chloroformate shows that the carbonyl carbon is buried by the *tert*-butyls and the chlorine.

Photolysis of either of the corresponding 2-mercaptopyridine-N-oxide derivatives would generate the same phenoxyl radical, so the 4-substitution would not be a barrier for our purposes. The low reactivity of the O-chloroformate, however, indicates a serious obstacle to optimizing the synthesis of 2-mercaptopyridine-N-oxide derivatives of these substrates; since the products are heat-sensitive, refluxing to convert the O-chloroformate is not a viable option. We concluded that the effort necessary to optimize this sequence to the degree necessary to synthesize tetra-derivatized **I** was not justifiable.

Conclusions

This project attempted to stabilize known tetraradical **A** by substituting di-*tert*-butyl phenoxyls as spin containing groups. Instead of the target tetraradical, an interesting rearrangement was observed. It might be possible to improve syntheses of photochemical precursors in order to generate the target tetraradical in solid matrix, or optimize oxidation conditions (e.g, EPR flow studies) in order to observe some of the proposed intermediates in the

pathway from tetraphenol **I** to bisgalvinol **V**. It is clear, however, that **I** will not fulfill our goal as a room-temperature stable, easily generated, quintet tetraradical.

Experimental

Unless otherwise noted, reactions were run under an atmosphere of dry argon using oven-dried glassware. THF, Et_2O, and benzene were distilled from sodium benzophenone ketyl. CH_2Cl_2, toluene, and CH_3CN were distilled from calcium hydride. Other solvents were used as received unless specified otherwise. Thin layer chromatography was performed on 0.25 mm silica-precoated glass plates visualized with UV light and molybdate stain. Flash chromatography was performed on 230-400 mesh silica gel. GC/MS data were obtained using a 70 eV EI Hewlett-Packard 5890/5970 GC/MS equipped with a 12 m X 0.2 mm HP-1 capillary column. High resolution mass spectrometry analyses were obtained on a ZAB 7070 instrument by the Mass Spectral Facility at the University of California, Riverside. NMR spectra were obtained on JEOL GX-400 (399.65 MHz ^1H, 100.4 MHz ^{13}C), GE QE-300, or Varian EM-390 spectrometers at room temperature and referenced to residual protio solvent unless specified otherwise. IR spectra were obtained using a Perkin-Elmer 1600 Series FTIR. UV/Vis spectra were obtained using a Beckman DU-640 continuous wave spectrophotometer. Melting and boiling points are uncorrected. Elemental analyses were performed by Galbraith Laboratories, Knoxville, Tennessee. EPR spectra were obtained on a Varian E-Line Century Series spectrometer operating at X-Band ($\nu \approx 9.27$ GHz). EPR samples were generally prepared in 2-methyltetrahydrofuran, vacuum transferred from sodium benzophenone ketyl in the strict absence of oxygen. Some EPR samples were prepared in other solvents such as THF, toluene,

benzene, or Et_2O. All samples were carefully degassed on a vacuum line by the freeze-pump-thaw method. A liquid nitrogen-filled finger dewar was used for spectra taken at 77 K.

Bis-(3,5-di-*tert*-butyl-4-hydroxyphenyl)methane (3.1a)[12] A mixture of 2,6-di-*tert*-butylphenol (12.0 g, 0.0582 mol), 37% aq formaldehyde (2.2 mL, 0.20 mol), and 25 mL of isopropyl alcohol was purged with argon. After adding KOH (0.326 g, 0.00581 mol), the mixture was stirred for 3 h at 45 °C, then cooled to room temperature. The resulting white precipitate was recovered by vacuum filtration, washed with ice cold ethanol to remove all traces of purple, and dried to give bis-(3,5-di-*tert*-butyl-4-hydroxyphenyl)methane (7.86 g, 0.0185 mol) in 64% yield as a white solid. GC/MS, 50-250 °C, 10 °C/min, m/z 424 (M^+) @ 28.8 min. MP = 155 °C (lit.[12] 153-154 °C).

Bis-(3,5-di-*tert*-butyl-4-methoxyphenyl)methane (3.1b)[13] Under an argon atmosphere, a solution of **3.1a** (7.86 g, 0.0185 mol) and iodomethane (18.4 mL, 0.296 mol) in THF (100 mL) was added over 15 min to a stirred suspension of sodium hydride (2.66 g, 0.111 mol) in THF (25 mL). The mixture was stirred and refluxed for 12 h, over which time the color turned from light yellow to bright red to light purple. After cooling to room temperature, the excess sodium hydride was quenched by carefully adding 18 mL of water, followed by 200 mL of 1 M hydrochloric acid. The mixture was extracted with 3 X 200 mL of CH_2Cl_2. The combined extracts were dried over $MgSO_4$, filtered, and put on a rotary evaporator to remove the solvent. Recrystallization of the residue from 95% ethanol gave bis-(3,5-di-*tert*-butyl-4-methoxyphenyl)methane (2.98 g, 0.00659 mol) in 36% yield as fine, white crystals. TLC, bright violet spot at RF 0.6, molybdate stain, 5% ethyl acetate/petroleum ether. GC/MS, 60-250 °C, 20 °C/min, m/z 452 (M^+) @ 15.0 min. MP = 158 °C (lit.[13] 158-159 °C).

Bis-(3,5-di-*tert*-butyl-4-methoxyphenyl)methanone (3.1c)[14] A mixture of **3.1b** (35.0 g, 0.0773 mol) and cerium (IV) ammonium nitrate (170 g, 0.309 mol) in glacial acetic acid (800 mL) was stirred and slowly heated to 95 °C. After 3 h, the mixture was poured into ice water and extracted with 3 X 300 mL of Et_2O. The combined extracts were washed with saturated Na_2CO_3 soln, dried over $MgSO_4$, filtered, and put on a rotary evaporator to remove the solvent. The glassy orange residue was recrystallized from methanol to give bis-(3,5-di-*tert*-butyl-4-methoxyphenyl)methanone (26.7 g, 0.0572 mol) in 74% yield as pale yellow crystals. TLC, faint yellow spot at RF 0.6, molybdate stain, 5% ethyl acetate/petroleum ether. GC/MS, 50-250 °C, 10 °C/min, m/z 466 (M^+) @ 24.1 min. 300 MHz ^1H NMR, $CDCl_3$, δ = 1.42 ppm, s, 36H; 3.76, s, 6H; 7.43, s, 4H. FTIR, KBr, ν = 2954, 2869, 1655, 1590, 1458, 1412, 1362, 1307, 1258, 1224, 1115, 1010, 888, 770 cm^{-1}. MP = 165-167 °C (lit.[19] 165 °C).

Bis-(3,5-di-*tert*-butyl-4-methoxyphenyl)methylhydrazone (3.1d)[15]

Anhydrous hydrazine (2.8 mL, 0.087 mol), **3.1c** (4.08 g, 0.00874 mol), and a few drops of glacial acetic acid were added to absolute ethanol (100 mL). After refluxing for 12 h, the mixture was cooled to room temperature and the solvent was removed on a rotary evaporator. Recrystallization from methanol gave diarylhydrazone **3.1d** (3.99 g, 0.00831 mol) in 95% yield as pale yellow crystals. TLC, grey-blue spot at RF 0.3, molybdate stain, 33% Et_2O/petroleum ether. GC/MS, 50-250 °C, 10 °C/min, m/z 480 (M^+) @ 28.0 min. 300 MHz ^1H NMR, $CDCl_3$, δ = 1.38 ppm, s, 18H; 1.44, s, 18H; 3.71, s, 3H; 3.77, s, 3H; 5.2 broad s, 2H; 7.20, s, 2H; 7.43, s, 2H. FTIR, NaCl, ν = 3387, 2955, 2869, 1590, 1458, 1412, 1392, 1358, 1308, 1257, 1221, 1115, 1006, 889, 770 cm^{-1}.

Bis-(3,5-di-*tert*-butyl-4-methoxyphenyl)diazomethane (3.1e)[15] A mixture of **1d** (2.59 g, 0.00539 mol), freshly activated mercury (II) oxide (2.85 g, 0.0132

mol), sodium sulfate (1.22 g, 0.00862 mol), 5 drops of saturated KOH/absolute ethanol soln, and Et_2O (100 mL) was stirred under a drying tube for 45 min. The intensely purple mixture was vacuum filtered through a fine glass sinter. After removing the solvent on a rotary evaporator, the purple residue was used in the next step without further purification. The residue was presumably bis-(3,5-di-*tert*-butyl-4-methoxyphenyl)-diazomethane: TLC, violet spot at RF 0.7, no stain, 33% ether/petroleum ether. FTIR, NaCl, ν = 2961, 2869, 2031, 1590, 1448, 1420, 1394, 1361, 1262, 1224, 1173, 1115, 1011, 888 cm^{-1}.

Activation of mercury (II) oxide[17] Mercury(II) oxide (5.0 g, 0.023 mol) was dissolved, with stirring, in concentrated perchloric acid. After cooling the mixture in an ice bath, 50% NaOH was added dropwise until the mixture was basic. The orange precipitate was collected by vacuum filtration and dried to give activated mercury(II) oxide (4.9 g, 0.023 mol).

Bisepisulfide 3.1g [4,16] Diaryldiazomethane **3.1e** (2.58 g, 0.00539 mol) and 2,2,4,4-tetramethyl-1,3-cyclobutanedithione (**3.1f**, 0.464 g, 0.00269 mol) were added to Et_2O (50 mL). Slight warming and gas evolution was observed. Upon stirring overnight, the color went from deep purple to light gold. The solid precipitated by cooling to 0 °C was collected by vacuum filtration and washed with a minimum of ice cold ether. Drying gave bis-episulfide **3.1g** (2.17 g, 0.00202 mol) in 75% yield as a white powder. TLC, brown spot at RF 0.4, vanillin stain, 33% CH_2Cl_2/petroleum ether. 90 MHz ^1H NMR, $CDCl_3$, δ = 0.46,ppm, s, 3H; 0.66, s, 3H;, 0.95, s, 3H; 1.21, s, 3H; 1.40, s, 72H; 3.61, s, 12H; 7.74, s, 8H. FTIR, NaCl, ν = 2962, 1466, 1414, 1362, 1267, 1224, 1114, 1009, 897, 826 cm^{-1}. Elemental analysis: calculated for $C_{70}H_{104}O_4S_2$, C, 78.30; H, 9.76; O, 5.96; S, 5.97. Found: C, 78.03; H, 10.01; O, 5.95; S, 5.87.

2,2,4,4-tetramethyl-1,3-cyclobutanedithione (3.1f)[25] Under an argon atmosphere, 2,2,4,4-tetramethyl-1,3-cyclobutanedione (2.00 g, 0.0143 mol) and phosphorous pentasulfide (1.59 g, 0.00357 mol) were added to sieve-dried pyridine (150 mL) and stirred at 95 °C for 48 h. The mixture was cooled to room temperature, poured into water, and extracted with 3 X 75 mL of petroleum ether. The combined extracts were dried over $MgSO_4$, filtered, and put on a rotary evaporator to remove the solvent (since the product readily sublimes, the source flask was cooled with an ice water bath). The solid residue was purified by flash chromatography (the second red band is monothione) using petroleum ether as the elutant to give 2,2,4,4-tetramethyl-1,3-cyclobutanedithione **3.1f** (0.763 g, 0.00443 mol) in 31% yield (> 90% yield if starting material and monothione are recycled) as odoriferous, bright red crystals. TLC, bright red spot at RF 0.6, no stain, 100% petroleum ether. GC/MS, 50-250 °C, 10 °C/min, m/z 172 (M^+) @ 5.9 min. 300 MHz ^1H NMR, $CDCl_3$, δ = 1.41, s, 12H. 300 MHz ^{13}C NMR, $CDCl_3$, δ = 25.8, 80.5, 107.4 ppm. FTIR, NaCl, ν = 2965, 2915, 2845, 1452, 1347, 1266, 1070, 1000, 904, 728, 698 cm^{-1}. UV/Vis, λ_{max} = 240 nm.

1,3-Bis-(bis-(3,5-di-*tert*-butyl-4-methoxyphenyl)methylene)-2,2,4,4,-tetramethylcyclobutane (3.1h)[18] Under an argon atmosphere, bis-episulfide **3.1g** (1.35 g, 0.00126 mol) and triphenylphosphine (0.66 g, 0.0025 mol) were added to 100 mL of dry, distilled benzene and refluxed with stirring for 48 h. The solid residue collected after removing the benzene on a rotary evaporator was boiled for 10 min in 50 mL of a 1:1 solution of carbon tetrachloride and 95% ethanol. After removing the solvent on a rotary evaporator, the solid residue was washed with 95% ethanol and dried to give the tetraanisole (1.21 g, 0.00120 mol) in 95% yield as a white powder. TLC, blue purple spot at RF

0.6, vanillin stain, 33% CH_2Cl_2/petroleum ether. HRMS, found MW = 1008.7924, calculated MW = 1008.7935, for $M^+ = C_{70}H_{104}O_4$. 300 MHz ^1H NMR, $CDCl_3$, δ = 0.97 ppm, s, 12H; 1.44, s, 72H; 3.74, s, 12H; 6.95, s, 8H. 300 MHz ^{13}C NMR, $CDCl_3$, δ = 27.7, 32.2, 35.5, 49.6, 64.2, 127.1, 136.4, 136.9, 142.2, 154.3, 157.8 ppm. FTIR, NaCl, ν = 3012, 2960, 2868, 1590, 1458, 1448, 1413, 1395, 1360, 1258, 1220, 1155, 1116, 1013, 892, 827, 688, 628 cm^{-1}. Mp > 360 °C. Elemental analysis: calculated for $C_{70}H_{104}O_4$, C, 83.28; H, 10.38; O, 6.34. Found: C, 83.39; H, 10.26; O, 6.29.

1,3-Bis-(bis-(3,5-di-*tert*-butyl-4-hydroxyphenyl)methylene)-2,2,4,4,-tetramethyl-cyclobutane (I)[19] Under an argon atmosphere, 9.6 mL (0.014 mol) of 1.5 M CH_3SLi in HMPA was added to tetraanisole **3.1h** (1.21 g, 0.00120 mol). (*Note*: Oxygen and water must be rigorously excluded.) The mixture was stirred and heated to 85 °C. Because the product cannot be easily purified by column chromatography or recrystallization, the reaction was run until no methoxy compounds were visible by TLC (removal of each methyl results in spots at successively lower RFs), although this resulted in some product decomposition. After 10 days, the reaction, which had turned green, was quenched with water (10 mL), stirred for 5 min while the green color disappeared, and stirred for 1 h with concentrated hydrochloric acid (20 mL) to destroy the HMPA. The mixture was extracted with 3 X 100 mL of CH_2Cl_2, dried over $MgSO_4$, filtered, and the solvent removed on a rotary evaporator. The solid residue was washed on a fine glass sinter with 500 mL each of boiling water and boiling CH_3CN. Drying gave tetraphenol **I** (0.686 g, 0.000719 mol) in 60% yield as a white powder. TLC, blue grey spot at RF 0.25, molybdate stain, 5% ethyl acetate/petroleum ether. HRMS, FAB, found MW = 952.731600, calculated MW = 952.730862 for $M^+ = C_{66}H_{96}O_4$. 400 MHz ^1H

NMR, d_8-THF, δ = 0.97 ppm, s, 12H; 1.37 ppm, s, 72H; 5.90 ppm, s, 4H; 7.11 ppm, s, 8H. 400 MHz ^{13}C NMR, d_8-THF, δ = 28.5, 31.1, 35.3, 50.6, 126.1, 135.3, 137.1, 138.5, 153.3, 155.0. FTIR, NaCl, ν = 3641, 3618, 3077, 2954, 2872, 1435, 1360, 1308, 1232, 1155, 1120, 892, 830, 787, 770, 704, 661, 634 cm^{-1}. UV/Vis, λ_{max} = 241 nm. MP > 360 °C. Elemental analysis: calculated for $C_{66}H_{96}O_4$, C, 83.14; H, 10.15; O, 6.71. Found: C, 83.25; H, 10.21; O, 6.24.

Preparation of 1.5 M CH_3SLi in HMPA[19] Under an argon atmosphere, 125 mL of hexamethyl-phosphoramide was distilled from barium oxide at 75 °C and 0.4 torr onto lithium hydride (4.58 g, 0.576 mol). Methanethiol (35.3 mL, 0.188 mol) was collected at -78 °C and cannulated into the reaction mixture, which was cooled with an ice water bath during the addition. After stirring at room temperature for 12 h, the mixture was vacuum filtered through a Schlenk line fine glass sinter. The concentration of this solution was determined to be 1.50±0.01 M by titration with 0.1501 M potassium hydrogen pthalate.

Bisgalvinol V[3,20] Tetraphenol **I** (0.287 g, 0.000301 mol) was stirred in benzene (50 mL) and purged thoroughly with argon. Next, a solution of tetrabutylammonium hydroxide in methanol (1.0 M, 3.6 mL, 0.0036 mol) was added. The mixture was allowed to stir until **I** had dissolved completely, about 5 min. Ath this point the solution was light blue in color, probably due to oxidation by residual oxygen. A solution of iodine in benzene (0.0301 M, 20.3 mL, 0.000612 mol) was added via syringe, resulting immediately in a dark blue-purple color. The reaction was allowed to stir for an additional 10 min and then quenched by carefully adding half-saturated NH_4Cl soln (20 mL). The organic layer was separated, dried over $MgSO_4$, and the solvent removed on a rotary evaporator. The residue was purified by column chromatography using 1-10% Et_2O/petroleum ether as elutant. A portion of the orange solid

was recrystallized from methanol for X-ray analysis. TLC, visibly yellow spot at RF 0.2, no stain, 5% ethyl acetate/petroleum ether. HRMS, FAB, found MW = 952.731600, calculated MW = 952.730862, for $MH^+ = C_{66}H_{95}O_4$. 300 MHz ^1H NMR (see also Figure 3.13), acetone-d_6 with slight excess of LiOD, δ = 1.15 ppm, s, 36H; 1.30, s, 36H; 1.52, s, 6H; 2.16, s, 6H; 6.93, s, 4H; 7.11, s, 4H. FTIR, NaCl, ν = 3636 (sharp), 2957, 1602, 1434, 1360, 758 cm^{-1}. UV/Vis, neuteral, λ_{max} = 395 nm, ε = 36,950; dianion, λ_{max} = 602 nm, ε = 110,830. MP = 175-176 °C. Elemental analysis: calculated for $C_{66}H_{94}O_4$, C, 83.32; H, 9.96; O, 6.73. Found: C, 83.02; H, 10.07; O, 6.79.

Diphenyldiazomethane (3.2a)[15] A mixture of benzophenone hydrazone (0.580 g, 0.00295 mol), freshly activated mercury (II) oxide (1.92 g, 0.00886 mol), sodium sulfate (0.630 g, 0.00443 mol), 5 drops of saturated KOH/absolute ethanol soln, and Et_2O (100 mL) was stirred under a drying tube for 45 min. The red-purple mixture was vacuum filtered through a fine glass sinter. After removing the solvent on a rotary evaporator, the residue was used in the next step without further purification or characterization. The residue was presumably diphenyl-diazomethane: TLC, rose spot at RF 0.7, no stain, 33% ether/petroleum ether.

Monoepisulfide 3.2b[4,16] 2,2,4,4-Tetramethyl-1,3-cyclobutanedithione (**3.1f**, 0.514 g, 0.00298 mol) and diphenyldiazomethane (**3.2a**, 0.580 g, 0.00295 mol) were added to Et_2O (200 mL). Slight warming and gas evolution was observed. As the mixture was stirred overnight, the color went from deep purple to light pink. Removal of the solvent on a rotary evaporator gave the mono-episulfide (2.17 g, 0.00202 mol) in 94% yield as a pink solid. TLC, dark blue spot at RF 0.5, vanillin stain, 5% ethyl acetate/petroleum ether. GC/MS,

50-250 °C, 10 °C/min, m/z 338 (M^+) @ 21.2 min. 90 MHz ^1H NMR, $CDCl_3$, δ = 1.25 ppm, s, 12H; 7.3, m, 10H.

Bisepisulfide 3.2c[4,16] Diarydiazomethane **3.1e** (1.34 g, 0.00280 mol) and mono-episulfide **3.2b** (0.948 g, 0.00280 mol) were added to Et_2O (75 mL). Slight warming and gas evolution was observed. As the mixture was stirred overnight, the color went from deep purple to clear gold. The solid precipitated by cooling to 0 °C was collected by vacuum filtration, washed with a minimum of ice cold ether, and dried to give the bis-episulfide **2c** (2.16 g, 0.00274 mol) in 98% yield as a white powder. TLC, brick red spot at RF 0.5, vanillin stain, 5% ethyl acetate/petroleum ether. 300 MHz ^1H NMR, $CDCl_3$, δ = 0.4-1.3 ppm, m, 12H; 1.45, s, 36H; 3.6, s, 6H; 7.2-7.7, m, 18H. Elemental analysis: calculated for $C_{52}H_{68}O_2S_2$, C, 79.14; H, 8.68; O, 4.05; S, 8.12. Found: C, 79.02; H, 8.58; O, 4.09; S, 8.11.

1-(diphenylmethylene)-3-(bis-(3,5-di-*tert*-butyl-4-methoxyphenyl)methylene)-2,2,4,4,-tetramethylcyclobutane (3.2d)[18] Under an argon atmosphere, bisepisulfide **3.2c** (1.22 g, 0.00155 mol) and triphenylphosphine (0.813 g, 0.00310 mol) were added to benzene (75 mL) and refluxed with stirring for 48 h. The solid residue collected after removing the benzene on a rotary evaporator was boiled for 10 min in 50 mL of a 1:1 solution of carbon tetrachloride and 95% ethanol. After removing the solvent on a rotary evaporator, the solid residue was washed with 95% ethanol and dried to give bisanisole **3.2d** (1.10 g, 0.00152 mol) in 98% yield as a white powder. TLC, blue purple spot at RF 0.5, molybdate stain, 33% ethyl acetate/petroleum ether. HRMS, found MW = 724.519500, calculated MW = 724.521932, for M+ = $C_{52}H_{68}O_2$. 300 MHz ^1H NMR, $CDCl_3$, δ = 1.00 ppm, s, 12H; 1.42, s, 36H; 3.62, s, 6H; 7.15-7.35, m, 14H. 300 MHz ^{13}C NMR, $CDCl_3$, δ = 28.0, 32.3, 35.6, 49.8, 64.1, 64.8, 107.5, 126.4, 127.2,

127.8, 129.0, 129.1, 136.4, 136.6, 142.3, 142.4, 154.1, 158.0 ppm. Elemental analysis: calculated for $C_{52}H_{68}O_2$, C, 86.13; H, 9.45; O, 4.41. Found: C, 85.96; H, 9.58; O, 4.30.

1-(diphenylmethylene)-3-(bis-(3,5-di-*tert*-butyl-4-hydroxyphenyl)methylene)-2,2,4,4,-tetramethylcyclobutane (II)[19] (*Note*: Oxygen and water must be rigorously excluded.) Ethanethiol (0.5 mL, 0.01 mol) was added to a stirred suspension of sodium hydride (0.260 g, 0.0108 mol) in DMF (75 mL, distilled from calcium hydride and stored over molecular sieves). After the bubbling ceased, bisianisole **3.2d** (1.62 g, 0.00223 mol) was added and the mixture was heated to 100 °C for two days. The reaction, which had turned dark brown, was quenched by carefully adding water (10 mL), stirred for 5 min, and stirred for 1 h with 6 M hydrochloric acid (100 mL). The mixture was poured into 750 mL of water, extracted with 3 X 100 mL of CH_2Cl_2, dried over $MgSO_4$, filtered, and the solvent removed on a rotary evaporator. The solid residue was washed on a fine glass sinter with 100 mL each of water and CH_3CN. Drying gave bisphenol II (1.23 g, 0.00176 mol) in 79% yield as a white powder. TLC, blue grey spot at RF 0.4, molybdate stain, 5% ethyl acetate/petroleum ether. HRMS, found MW = 696.488900, calculated MW = 696.490632, for M+ = $C_{50}H_{64}O_2$. 300 MHz ^{1}H NMR, $CDCl_3$, δ = 1.02 ppm, s, 12H; 1.43 ppm, s, 36H; 5.01 ppm, s, 2H; 7.11-7.34 ppm, m, 14H. 300 MHz ^{13}C NMR, δ = 27.7, 30.2, 34.0, 49.6, 125.2, 126.0, 127.4, 128.8, 133.4, 134.5, 135.2, 136.9, 142.1, 151.9, 153.9, 155.5 ppm. FTIR, NaCl, ν = 3639 (sharp), 2955, 2865, 1432, 1392, 1352, 1306, 1226, 1146, 1115, 1070, 889, 824, 724, 698 cm^{-1}. UV/Vis, λ_{max} = 239 nm. Elemental analysis: calculated for $C_{50}H_{64}O_2$, C, 86.16; H, 9.25; O, 4.59. Found: C, 85.89 H, 9.46; O, 4.37.

1,1-Dimethyl-2,2-bis(3,5-di-*tert*-butyl-4-methoxyphenyl)ethylene (3.3a)[26,27] Benzophenone **3.1c** (2.17 g, 0.00465 mol) was dissolved in THF (50 mL) and cooled to 0 °C. To this was added isopropyl magnesium chloride (2.0 M, 2.3 mL, 0.0047 mol). The resulting green solution turned clear gold after stirring for 2 h at room temperature. The reaction was colled with an ice water bath, quenched by carefully adding water (10 mL), and the alcohol intermediate dehydrated by adding concentrated hydrochloric acid (10 mL). This mixture was extracted with 3 X 75 mL of Et_2O, dried over $MgSO_4$, filtered, and put on a rotary evaporator to remove the solvent. Recrystallization of the residue from methanol gave bisanisole **3.3a** (2.06 g, 0.00418 mol) in 92% yield as white crystals. TLC, midnight blue spot at RF 0.7, molybdate stain, 5% ethyl acetate/petroleum ether. GC/MS, 50-250 °C, 10 °C/min, m/z 492 (M^+) @ 22.4 min. 400 MHz ^1H NMR, $CDCl_3$, δ = 1.33 ppm, s, 36H; 1.81, s, 6H; 3.63, s, 6H;, 6.94, s, 4H. 400 MHz ^{13}C NMR, $CDCl_3$, δ = 23, 33, 37, 65, 129, 130, 138, 143, 158 ppm.

1,1-Dimethyl-2,2-bis(3,5-di-*tert*-butyl-4-hydroxyphenyl)ethylene (III)[19] (*Note*: Oxygen and water must be rigorously excluded.) Ethanethiol (2.3 mL, 0.044 mol) was added to a stirred suspension of sodium hydride (1.15 g, 0.0479 mol) in DMF (75 mL, distilled from calcium hydride and stored over molecular sieves). After the bubbling ceased, 1,1-dimethyl-2,2-bis(3,5-di-*tert*-butyl-4-methoxyphenyl)-ethylene (1.48 g, 0.00318 mol) was added and the mixture was heated to 100 °C for two days. The reaction, which had turned dark brown, was quenched by carefully adding water (10 mL), stirred for 5 min, and stirred for 1 h with 6 M hydrochloric acid (100 mL). The mixture was poured into 750 mL of water, extracted with 3 X 100 mL of Et_2O, dried over $MgSO_4$, filtered, and the solvent removed on a rotary evaporator. Recrystallization of

the residue from methanol gave bisphenol **III** (0.753 g, 0.00162 mol) in 51% yield as air-sensitive white microcrystals (these slowly turned yellow even in a glovebox). TLC, blue purple spot at RF 0.5, molybdate stain, 5% ethyl acetate/petroleum ether. GC/MS, 50-250 °C, 10 °C/min, m/z 464 (M^+) @ 23.8 min. 300 MHz ^1H NMR, $CDCl_3$, δ = 1.41 ppm, s, 36H; 1.81, s, 6H;, 5.06, s, 2H; 6.96, s, 4H. 300 MHz ^{13}C NMR, $CDCl_3$, δ = 22.9, 30.5, 24.4, 108, 126.3, 129.5, 134.7, 151.5 ppm. Elemental analysis: calculated for $C_{32}H_{48}O_2$, C, 82.70; H, 10.41; O, 6.89. Found: C, 81.61; H, 10.47; O, 6.63.

Galvinol VI[3,20] Bisphenol **3.3b** (0.155 g, 0.000333 mol), potassium ferricyanide (0.384 g, 0.00117 mol) and a few pellets of KOH were added to a flask containing water (10 mL) and benzene (10 mL). The mixture was purged carefully with argon and then stirred vigorously. Within several seconds a dark blue color appeared and turned the reaction opaque by 1 min. After 30 min, the color was brown-gold, and the aqueous layer was removed. The organic layer was washed with 3 X 30 mL of aqueous pH 7 buffer (1.20 mol potassium dihydrogen phosphate and 1.60 mol potassium hydrogen phosphate dissolved in 1L of water), dried over $MgSO_4$, filtered, and reduced to a brown solid residue using a rotary evaporator. The residue was redissolved in benzene (10 mL) and an excess of 1,4-cyclohexadiene (0.5 mL, 0.005 mol) was added. The dark brown solution was carefully degassed, and then heated in an oil bath at 65 °C for 1 h, at which point the color had changed to light red-orange. The solvent was removed by rotary evaporation and the residue pumped on at < 0.1 Torr for 24 h. The residue was then dissolved in hexanes and purified on a Chromatatron (Harrison Research) using 1% Et_2O in hexanes. The fractions containing product, which were still impure, were reduced to a solid on a rotary evaporator and then recrystallized

from petroleum ether to give 0.103 g (67%) of fine yellow crystals. TLC, visibly yellow spot at RF 0.4, no stain, 5% ethyl acetate/petroleum ether. HRMS, DCI/NH_3, found MW = 463.356700, calculated MW = 463.357606, for $MH^+ = C_{32}H_{47}O_2$. 300 MHz ^1H NMR, C_6D_6, δ = 1.33 ppm, s, 18H; 1.42, s, 9H; 1.44, s, 9H; 1.73, s, 3H; 5.07, s, 1H; 5.19, s, 1H; 5.28, s, 1H; 7.41, s, 2H; 7.51, s, 1H; 7.75, s, 1H. 300 MHz ^{13}C NMR, $CDCl_3$, δ = 23.4, 29.7, 30.2, 30.5, 34.5, 35.4, 102.6, 120.3, 127.8, 128.4, 132.0, 135.5, 144.8, 146.2, 146.9, 155.2, 160.4, 186.7 ppm. FTIR, NaCl, ν = 3635 (sharp), 2958, 2908, 2867, 1604, 1508, 1437, 1356, 1255, 1237 cm^{-1}. UV/Vis, λ_{max} = 387 nm. MP = 175-176 °C. Elemental analysis: calculated for $C_{32}H_{46}O_2$, C, 83.06; H, 10.02; O, 6.92. Found: C, 82.74; H, 10.01; O, 6.51.

4-Bromo-2,6-di-*tert*-butylphenol (3.4a)[29] Bromine (13.7 mL, 0.265 mol) was added over 5 min to a solution of 2,6-di-*tert*-butylphenol (52.2 g, 0.253 mol) in glacial acetic acid (150 mL) which was cooled by an ice water bath. After stirring for 1 h, the reaction was poured into 500 mL of ice water. The resulting white precipitate was collected by vacuum filtration, washed with water (500 mL), and dried to give 4-bromo-2,6-di-*tert*-butylphenol (72.1 g, 0.253 mol) in quantitative yield. GC/MS, 50-250 °C, 10 °C/min, m/z 137 (M^+) @ 15.6 min.

4-Bromo-2,6-di-*tert*-butylanisole (3.4b)[13,30] A solution of **3.4a** (72.1 g, 0.253 mol) and iodomethane (31.5 mL, 0.506 mol) in THF (500 mL) was added over 15 min to a stirred suspension of sodium hydride (12.1 g, 0.505 mol) in THF (25 mL). The mixture was stirred and refluxed for 12 h, over which time the color turned from light yellow to bright red to light purple. After cooling to room temperature, the excess sodium hydride was quenched by carefully adding water (25 mL), followed by 1 M hydrochloric acid (250 mL). The mixture was extracted with ether, dried over $MgSO_4$, filtered, and put on a

rotary evaporator to remove the solvent. Vacuum distillation using a 30 cm Vigreaux column gave 4-bromo-2,6-di-*tert*-butylanisole (57.7 g, 0.193 mol) in 76% yield as a light yellow oil, BP 110 °C at 1 Torr. GC/MS, 50-250 °C, 10 °C/min, m/z 298 (M^+) @ 14.8 min. 90 MHz ^1H NMR, δ = 1.3 ppm, s, 18H; 3.6, s, 3H; 7.2, s, 2H.

1,1-Dimethyl-2-(3,5-di-*tert*-butyl-4-methoxyphenyl)-2-phenylethylene (3.4d)[26,27] *tert*-Butyllithium (1.7 M in hexanes, 19.7 mL, 0.033 mol) was added to a solution of **3.4b** (5.00 g, 0.0167 mol) in THF (75 mL) which was cooled to -78 °C by a dry ice/acetone bath. After stirring for 1 h, isobutyrophenone (2.49 mL, 0.0167 mol) was added. The reaction was allowed to stir at -78 °C for 1 h, then allowed to rise to 0 °C. Hydrolysis of the alcohol intermediate was accomplished by slowly adding hydrochloric acid (6 M, 100 mL) and stirring for 4 h. The resulting mixture was extracted with ether, washed with saturated Na_2CO_3, dried over $MgSO_4$, and put on a rotary evaporator to remove the solvent. Upon standing overnight, the resulting oil crystallized to give pure **3.4d** (2.75 g, 0.00784 mol) in 47% yield as large colorless crystals. TLC, midnight blue spot at RF 0.7, molybdate stain, 5% ethyl acetate/petroleum ether. GC/MS, 50-250 °C, 10 °C/min, m/z 350 (M^+) @ 20.3 min. 300 MHz ^1H NMR, $CDCl_3$, δ = 1.43 ppm, s, 18H; 1.83, s, 3H; 1.87, s, 3H; 3.72, s, 3H; 7.03, s, 2H; 7.25-7.45, m, 5H. 300 MHz ^{13}C NMR, $CDCl_3$, δ = 22.8, 32.3, 35.8, 64.2, 107.4, 125.9, 127.8, 128.3, 129,9, 130.3, 137.3, 137.8, 142.4, 143.9, 157.7 ppm.

1,1-Dimethyl-2-(3,5-di-*tert*-butyl-4-hydroxyphenyl)-2-phenylethylene (IV)[19]

(*Note*: Oxygen and water must be rigorously excluded.) Ethanethiol (1.9 mL, 0.025 mol) was added to a stirred suspension of sodium hydride (0.70 g, 0.029 mol) in DMF (50 mL, distilled from calcium hydride and stored over

molecular sieves). After the bubbling ceased, monoanisole **3.4d** (1.25 g, 0.00358 mol) was added and the mixture was heated to 100 °C for 12 h. The reaction, which had turned dark brown, was quenched by carefully adding water (10 mL), stirred for 5 min, and stirred for 1 h with 6 M hydrochloric acid (100 mL). The mixture was poured into 500 mL of water, extracted with ether, dried over $MgSO_4$, filtered, and the solvent removed on a rotary evaporator. Recrystallization from methanol gave **IV** (0.759 g, 0.00226 mol) in 63% yield as air-sensitive white microcrystals. TLC, purple spot at RF 0.5, molybdate stain, 5% ethyl acetate/petroleum ether. GC/MS, 50-250 °C, 10 °C/min, m/z 336 (M^+) @ 20.0 min. 300 MHz ^1H NMR, $CDCl_3$, δ = 1.43 ppm, s, 18H; 1.83, s, 3H; 1.86, s, 3H; 5.02, s, 1H; 6.98, s, 2H; 7.25-7.45, m, 5H. Elemental analysis: calculated for $C_{24}H_{32}O$, C, 85.66; H, 9.59; O, 4.75. Found: C, 85.50; H, 9.53; O, 4.91.

General procedure for biphasic potassium ferricyanide oxidations: Under an argon atmosphere, a solution of phenol (10^{-3}-10^{-4} M, 5 ml) and excess potassium ferricyanide were added to a dilute solution of NaOH (5 mL, ca. 1M). After stirring for a desired length of time, a 0.5 mL aliquot of the ether solution was transferred into an EPR tube. The ether was removed under vacuum and replaced with about 0.5 mL of 2-methyl THF.

General procedure for heterogeneous oxidations: Under an argon atmosphere, 1 mg of phenol and an excess of a solid oxidant (lead dioxide, silver (II) oxide, nickel peroxide, etc.) were added to a dry EPR tube. The tube was evacuated and about 0.5 mL of 2-methyl THF was condensed in the tube. The mixture was agitated for a few minutes and allowed to settle before measurement. Alternatively, a solution of argon purged phenol in THF,

toluene, or benzene (10^{-3}-10^{-4} M, 0.5 ml) and an excess of solid oxidant were added to an EPR tube under argon.

General procedure for iodine/tetrabutylammonium hydroxide oxidations: Under an argon atmosphere, solutions of a phenol (10^{-3}-10^{-4} M), tettrabutylammonium hydroxide, and iodine in THF were added to EPR tubes. The deep blue solutions were then carefully degassed.

Chapter 3 References

1. Dougherty, D. A. *Acc. Chem. Res.* **1991**, *24*, 88-94.

2. (a) Novak, J. A.; Jain, R.; Dougherty, D. A. *J. Am. Chem. Soc.* **1989**, *111*, 7618-7619. (b) Jacobs, S. J.; Shultz, D. A.; Jain, R.; Novak, J.; Dougherty, D. A. *J. Am. Chem. Soc.* **1993**, *115*, 1744-1753.

3. (a) Willigen, H. V.; Kirste, B. *Isr. J. Chem.* **1989**, *29*, 93-98. (b) Kirste, B.; Harrer, W.; Kurreck, H. *Angew. Chem. Int. Ed. Engl.* **1981**, *20*, 873-874. (c) Grimm, M.; Kirste, B.; Kurreck, H. *Angew. Chem. Int. Ed. Engl.* **1986**, *25*, 1097-1098. (d) Kirste, B.; Kurreck, H.; Sordo, M. *Chem. Ber.* **1985**, *118*, 1782-1797. (e) Kirste, B.; Harrer, W.; Kurreck, H.; Schubert, K.; Bauer, H.; Gierke, W. *J. Am. Chem. Soc.* **1981**, *103*, 6280-6286. (f) Kirste, B.; Kurreck, H.; Schubert, K. *Tetrahedron* **1980**, *36*, 1985-1991. (g) Mukai, K.; Tamaki, T. *Bull. Chem. Soc. Jap.* **1977**, *50*, 1239-1244. (h) Mukai, K.; Sogabe, A. *J. Chem. Phys.* **1980**, *72*, 598-601. (i) Awaga, K.; Sugano, T.; Kinoshita, M. *J. Chem. Phys.* **1986**, *85*, 2211-2218. (j) Chiang, L. Y.; Upasani, R. B.; Sheu, H. S.; Goshorn, D. P.; Lee, C. H. *J. Chem. Soc., Chem. Commun.* **1992**, 959-961. (k) Nishide, H.; Yoshioka, N.; Kaneko, T.; Tsuchida, E. *Macromolecules* **1990**, *23*, 4487-4488. (l) Yoshioka, N.; Nishide, H.; Kaneko, T.; Yoshiki, H.; Tsuchida, E. *Macromolecules* **1992**, *25*, 3838-3842. (m) Mukai, K.; Kamata, T.; Tamaki, T.; Kazuhiko, I. *Bull. Chem. Soc. Jap.* **1976**, *49*, 3376-3381.

4. (a) Yang, N. C.; Castro, A. J. *J. Am. Chem. Soc.* **1960**, *82*, 6208. (b) Mukai, K.; Mishina, T.; Ishizu, K. *J. Chem. Phys.* **1977**, *66*, 1680-1684. (c) Mukai, K. *Bull. Chem. Soc. Jpn.* **1979**, *52*, 1911-1915. (c) Mukai, K.; Ishizu, K.; Nakahara, M.; Deguchi, Y. *Bull. Chem. Soc. Jpn.* **1980**, *53*, 3363-3364. (d) Mukai, K. *Bull. Chem. Soc. Jpn.* **1978**, *51*, 313-314.

5. Freund, F.; Hünig, S. *J. Org. Chem.* **1987**, *52*, 2154-2161.

6. Freund, F.; Hünig, S. *Helv. Chim. Acta* **1987**, *70*, 929-941.

7. Horner, M.; Hünig, S. *J. Am. Chem. Soc.* **1977**, *99*, 6120-6122.

8. Horner, M.; Hünig, S. *J. Am. Chem. Soc.* **1977**, *99*, 6122-6124.

9. Horner, M.; Hünig, S. *Liebigs. Ann. Chem.* **1983**, 70-97.

10. (a) Jain, R.; Snyder, G. J.; Dougherty, D. A. *J. Am. Chem. Soc.*. **1984**, *106*, 7294-7295. (b) Snyder, G. J.; Dougherty, D. A. *J. Am. Chem. Soc.* **1985**, *107*, 1774-1775. (c) Snyder, G. J.; Dougherty, D. A. *J. Am. Chem. Soc.* **1986**, *108*, 299-300. (d) Snyder, G. J.; Dougherty, D. A. *J. Am. Chem. Soc.* **1989**, *111*, 3942- 3954. (e) Snyder, G. J.; Dougherty, D. A. *J. Am. Chem. Soc.* **1989**, *111*, 3927- 3942.

11. Wiberg, K.B. *Adv. Alicyclic Chem.* **1968**, *2*, 185-254.

12. Coffield, T. H.; Ecke, G. G.; Filbey, A. H.; Kolka, A. J. *J. Am. Chem.Soc.* **1957**, *79*, 5019-5023.

13. Benoitin, N. L.; Stoochnoff, B. A. *Tetrahedron Lett.* **1973**, *1*, 21-24.

14. Syper, L. *Tetrahedron Lett.* **1966**, *37*, 4493-4498.

15. (a) Howard, K. L.; Smith, L. I. *Org. Syn.* coll. vol. III, 351-352. (b) Miller, J. B. *J. Org. Chem.* **1959**, *24*, 560-561.

16. Abeguz, B.; Krapcho, A. P.; Rao, D. R.; Silvon, M. P. *J. Org. Chem.* **1971**, *36*, 3885-3890.

17. Armarego, W. L.; Perrin, D. D. *Purification of Laboratory Chemicals*; 3rd ed., Pergamon: New York, 1988; p 332.

18. Dali, B. B.; Kelly, T. R.; Tsang, W. G. *Tetrahedron Lett.* **1977**, 3859-3862.

19. Colegate, S. M.; Hewgill, F. R.; Howie, G. B. *Aust. J. Chem.* **1975**, *28*, 343-353.

20. Cook, C. D.; Gilmour, N. D. *J. Org. Chem.* **1960**, *25*, 1429-1431.

21. Dougherty, D. A. In *Kinetics and Spectroscopy of Carbenes and Biradicals*; Platz, M. S., Ed.; Plenum: New York, 1990; pp 117-142.

22. Simulations performed using ESRa Version 1.0, Calleo Scientific Software Publishers.

23. Bielski, B. H. J.; Gebicki, J. M. *Atlas of Electron Spin Resonance Spectra*; Academic: New York, 1967; pp 441-465.

24. Togo, Y.; Nakamura, N.; Iwamura, H. *Chem. Lett.* **1991**, 1201-1204, and references therein.

25. Griedanus, J. W. *Can. J. Chem.* **1970**, *48*, 3530-3536.

26. Hoye, T. R.; Martin, S. J.; Peck, D. R. *J. Org. Chem.* **1982**, *47*, 331-337.

27. Carey, F. A.; Sundberg, R. J. *Advanced Organic Chemistry*; Plenum: New York, 1990, Part A, p 454.

28. (a) Harlow, G. A.; Wyld, G. E. A. *Anal. Chem.* **1962**, *34*, 172-173. (b) Cundiff, R. H.; Markunas, P. C. *Anal. Chem.* **1962**, *34*, 584-585.

29. (a) Adams, R.; Marvel, C. S. *Org. Syn.*, coll. vol. I, 128-131. (b) Karhu, M. *J. Chem. Soc., Perkin Trans. 1* **1981**, 303-306.

30. Dhami, Kewal S.; Stothers, J. B. *Can. J. Chem.* **1966**, *44*, 2855-2866.

Chapter 4. Introduction to Ferromagnetic Coupling in Organic Systems: Theory, Design Strategies, and Magnetic Characterization

Introduction

Magnetism has fascinated and confounded humanity for several millenia.[1,2] Despite efforts by many of the great minds of classical science, an understanding of magnetism was not possible until the twentieth century and the advent of quantum mechanics. Furthermore, despite the explanatory power allowed by the concepts of electron spin and the Pauli exclusion principle, new experimental observations of exotic magnetic phenomena continue to challenge and develop the theory of magnetism.[3] To call the field nonintuitive, then, is no overstatement.

When beginning my research in magnetic materials, I found that much of the necessary theory was widely scattered, employed conflicting jargon, and was not particularly geared towards organic chemists or understanding magnetic interactions in organic compounds. Here I have tried to collect, summarize, and reinterpret these various sources. My goal is to provide a coherent introduction for organic chemists who have had some introduction to quantum mechanics. Certainly, more detailed, higher level treatments are available. Dirac's formulation of quantum mechanics derives spin explicitly from relativistic considerations.[4] Such high level theory, however, can be unwieldy, and the Schrodinger formulation,[5,6] where electron spin is an *ad hoc* assumption, is entirely adequate for our purposes.

The goal of this chapter is to provide a reasonably detailed understanding of spin behavior and magnetic coupling at the quantum mechanical level, followed by practical strategies for designing organic compounds with interesting magnetic properties, and finally, an examination of experimental behavior and magnetic characterization. The chapter begins with an examination of a two-electron system, exploring the concepts of electron spin, the Pauli exclusion principle, and exchange interactions. The

following section examines spin angular momentum in some detail. Next, analytic expressions for singlet-triplet gaps in two simple systems, hydrogen and atomic carbon, are derived. The origin of the triplet ground state in 1,3-cyclobutanediyls is discussed in terms of molecular orbital theory. Simpler rules for designing high-spin interactions follow from these considerations. Finally, the experimental characterization of paramagnetic materials is introduced.

Indistinguishability, the Pauli Principle and Electron Exchange[5-7]

It is a postulate of quantum mechanics that electrons are indistinguishable particles. In classical mechanics, electrons are identical but distinguishable because the paths the electrons take can be exactly known. In quantum mechanics, the Heisenberg Uncertainty Principle states that the momentum and the position cannot be simultaneously known exactly. Whenever the wavefunctions associated with each electron overlap, it becomes impossible to tell them apart. Of course, the electrons can be distinguished if they are separated by a great distance and constrained so that their wavefunctions never overlap. In any multielectron atom or molecule, however, the electrons are continually interacting under the umbrella of uncertainty and are thus indistinguishable. Therefore, the eigenvalues generated from an accurate quantum mechanical description of a multielectron system must be independent of any interchange of electron coordinates.

Consider the following two-electron wavefunction. Because the electron labels denote sets of coordinates, application of the permutation operator $\mathbf{P}_{12}$ means each spin orbital becomes a function of a different set of

variables. Eigenvalues obtained from this permuted function will be different, so Ψ is not an acceptable two-electron wavefunction.

$$\Psi = \psi(1)\alpha(1)\psi(2)\beta(2) \tag{1}$$

$$\mathbf{P}_{12}\Psi = \psi(2)\alpha(2)\psi(1)\beta(1) = \Psi_P \neq \Psi \tag{2}$$

If the eigenvalues of the function are to remain the same upon permutation, the square of the wavefunction must be invariant under such an interchange. This is true only if the permuted wavefunction is symmetric (S) or antisymmetric (A).

$$\left(\mathbf{P}_{12}\Psi_S\right)^2 = \left(\Psi_S\right)^2 = \Psi_S^{\,2} \tag{3}$$

$$\left(\mathbf{P}_{12}\Psi_A\right)^2 = \left(-\Psi_A\right)^2 = \Psi_A^{\,2} \tag{4}$$

We can construct symmetric and antisymmetric linear combinations of Ψ and Ψ_P which retain the electron labels for mathematical clarity but also render the electrons indistinguishable.

$$\Psi_S = \Psi + \Psi_P = \psi(1)\alpha(1)\psi(2)\beta(2) + \psi(2)\alpha(2)\psi(1)\beta(1) \tag{5}$$

$$\Psi_A = \Psi - \Psi_P = \psi(1)\alpha(1)\psi(2)\beta(2) - \psi(2)\alpha(2)\psi(1)\beta(1) \tag{6}$$

Both of these appear to be acceptable. It turns out, however, that half integral spin particles (fermions) such as electrons, protons and neutrons are described only by antisymmetric wavefunctions, while zero and integer spin particles (bosons) such as α particles, photons and deuterons are described only by symmetric wavefunctions. Because we will only be discussing electrons, all of the *total* wavefunctions we will consider will be antisymmetric.

A useful technique for constructing an antisymmetric total wavefunction for a multielectron system is to take the determinant of a matrix, where the rows follow the electron numbers and the columns follow the one-electron spin orbitals.

$$\Psi_A = \frac{1}{\sqrt{(2n)!}} \begin{vmatrix} \psi_1(1)\alpha(1) & \psi_1(1)\beta(1) & \psi_2(1)\alpha(1) & \cdots & \psi_n(1)\beta(1) \\ \psi_1(2)\alpha(2) & \cdots & & & \\ \vdots & & & & \\ \psi_1(2n)\alpha(2n) & \cdots & & & \psi_n(2n)\beta(2n) \end{vmatrix} \tag{7}$$

This expression is known as a Slater determinant.

The usual expressions of the Pauli Principle arise naturally from the properties of determinants. Interchanging two rows of the matrix changes the sign of the determinant, as interchanging the coordinates of two electrons with P_{12} changes the sign of the wavefunction. Also, if two columns are identical, the determinant is zero, which is the same as saying no two electrons can occupy the same spin orbital.

The concept of exchange arises naturally from the properties of symmetric and antisymmetric space functions. Consider the total two-electron wavefunction we constructed,

$$\Psi_A = \psi(1)\alpha(1)\psi(2)\beta(2) - \psi(2)\alpha(2)\psi(1)\beta(1), \tag{8}$$

applied to a system where we will neglect explicit electron interactions like coulomb repulsions. Because the spin functions and the space functions do not depend on the same coordinate systems, we can separate the total wavefunction into two parts.

$$\Psi_{total} = \left[\Psi_{space}\right] \times \left[\Psi_{spin}\right] \tag{9}$$

For the singlet state, where the electrons are paired antiparallel, there is only one acceptable spin function (remember that $\alpha\beta$ alone is unacceptable due to the requirement of indistinguishability).

$$\alpha\beta - \beta\alpha \tag{10}$$

For the triplet state, there are three acceptable spin functions.

$$\alpha\alpha,\ \alpha\beta + \beta\alpha,\ \beta\beta \tag{11}$$

Because the singlet spin function is antisymmetric, its space function must be symmetric to give an antisymmetric total wavefunction. Similarly, because the triplet's spin functions are symmetric, its space function must be antisymmetric.

$${}^{1}\Psi = \left[\psi(1)\psi(2) + \psi(2)\psi(1)\right] \times \left[\alpha\beta - \beta\alpha\right] \tag{12}$$

$${}^{3}\Psi = \left[\psi(1)\psi(2) - \psi(2)\psi(1)\right] \times \left[\alpha\alpha,\ \alpha\beta + \beta\alpha, \text{ or } \beta\beta\right] \tag{13}$$

Consider the case for the triplet state when the electrons are close together, that is, their coordinates are almost identical. Then,

$$\psi(1) \approx \psi(2) \tag{14}$$

$$\psi(1)\psi(2) \approx \psi(2)\psi(1) \tag{15}$$

$${}^{3}\Psi = \left[\psi(1)\psi(2) - \psi(2)\psi(1)\right] \approx 0 \tag{16}$$

$${}^{3}\Psi^{*}\,{}^{3}\Psi \equiv 0. \tag{17}$$

In this situation, the space function for the triplet is very small, so its probability density is essentially zero. Thus, electrons in the triplet state *act* as if they repel each other. This repulsion is not due to Coulomb interactions

but is simply a characteristic of antisymmetric space functions. Conversely, the space function and the probability density for the singlet state will be high and thus electrons in the singlet state act as if they attract each other.

By requiring an antisymmetric wavefunction, the Pauli Principle leads to a coupling between the space and spin variables. This coupling produces a force called exchange (to be treated more rigorously in the next section) which is purely quantum mechanical in origin and has no classical counterpart. Although exchange is not due to Coulomb repulsions, by correlating electrons in the triplet state, it gives reduced Coulomb repulsions relative to the singlet state. Therefore, exchange interactions should be considered when designing high spin molecules.

Spin Angular Momentum[6,8]

Electron spin, a nonclassical concept, behaves as if it were angular momentum. This is curious, to say the least; the rotational velocity necessary to cause a classical particle the mass and size of the electron to exhibit spin angular momentum leads to several jarring paradoxes. Electron spin, then, does not correspond to an actual, physical rotation, yet its effects can be described exactly as if they were the consequences of angular momentum. This section demonstrates how spin and spin states can be derived entirely from commutation relations, angular momentum operators, and elements of quantum mechanics. A review of a few basic principles of quantum mechanics may be helpful. To every observable value of a function there exists a corresponding operator, which must be linear.

$$\mathbf{A}(a\mathbf{f} + b\mathbf{g}) = a(\mathbf{A}\mathbf{f}) + b(\mathbf{A}\mathbf{g}) \tag{18}$$

Here **A** is an operator, a and b are constants, and **f** and **g** are functions. Operators must also obey the distributive and associative laws.

$$(\mathbf{A} + \mathbf{B})\psi = \mathbf{A}\psi + \mathbf{B}\psi \tag{19}$$

$$(\mathbf{AB})\psi = \mathbf{A}(\mathbf{B}\psi) \tag{20}$$

It is possible, however, that they do not commute.

$$\mathbf{AB}\psi \neq \mathbf{BA}\psi \tag{21}$$

This leads us to define a quantity relating two operators, called the commutator.

$$[\mathbf{A}, \mathbf{B}] = \mathbf{AB} - \mathbf{AB} \tag{22}$$

When the commutator is zero, **A** and **B** are said to commute—that is, they obey the commutative law.

Quantum mechanical operators must also be Hermitian. This means that all eigenvalues must be real, because those eigenvalues correspond to observable quantities. A Hermitian operator will satisfy the following relation.

$$\langle\psi|\mathbf{A}|\psi\rangle = \langle\mathbf{A}\psi|\psi\rangle \tag{23}$$

Another quality of Hermitian operators is that their squares generate real, nonnegative eigenvalues.

$$\langle\psi|\mathbf{A}^2|\psi\rangle \geq 0 \tag{24}$$

Commutation Rules and Angular Momentum

The quantum mechanical operator for angular momentum is given by

$$\mathbf{L} = \frac{-ih}{2\pi}\sum_k \mathbf{r}_k \times \nabla_k \tag{25}$$

where $\mathbf{r}_k$ is the coordinate vector of particle k and $\frac{-ih}{2\pi}\nabla_k$ is its linear momentum (inatomic units). The x, y, and z components of **L** are shown below.

$$\mathbf{L}_x = \frac{-ih}{2\pi}\sum_k \left(y_k \frac{\partial}{\partial z_k} - z_k \frac{\partial}{\partial y_k}\right) \tag{26}$$

$$\mathbf{L}_y = \frac{-ih}{2\pi}\sum_k \left(z_k \frac{\partial}{\partial x_k} - x_k \frac{\partial}{\partial z_k}\right) \tag{27}$$

$$\mathbf{L}_z = \frac{-ih}{2\pi}\sum_k \left(x_k \frac{\partial}{\partial y_k} - y_k \frac{\partial}{\partial x_k}\right) \tag{28}$$

The commutation relations between L_x, L_y, and L_z are shown below.

$$[\mathbf{L}_y, \mathbf{L}_z] = \mathbf{L}_y\mathbf{L}_z - \mathbf{L}_z\mathbf{L}_y = i\mathbf{L}_x \tag{29}$$

$$[\mathbf{L}_z, \mathbf{L}_x] = \mathbf{L}_z\mathbf{L}_x - \mathbf{L}_x\mathbf{L}_z = i\mathbf{L}_y \tag{30}$$

$$[\mathbf{L}_x, \mathbf{L}_y] = \mathbf{L}_x\mathbf{L}_y - \mathbf{L}_y\mathbf{L}_x = i\mathbf{L}_z \tag{31}$$

$$\mathbf{L} \times \mathbf{L} = i\mathbf{L} \tag{32}$$

These relations are assumed to apply to spin angular momentum.

$$\mathbf{S} = \sum_k \mathbf{S}_k \tag{33}$$

$$\mathbf{S} \times \mathbf{S} = i\mathbf{S} \tag{34}$$

This assumption is borne out by experiment. Because spin has no classical counterpart, the coordinate space in which it operates can be considered independently of that in which **L** operates. Therefore, the components of **L** commute with those of **S**, although as for **L**, the components of **S** do not

commute among themselves. A total angular momentum operator can be defined.

$$\mathbf{I} = \mathbf{L} + \mathbf{S} \tag{35}$$

This operator and its components follow the same commutation relations as **L** and **S**. Using this relation, it can be shown that $\mathbf{I}^2 = \mathbf{I}_x^2 + \mathbf{I}_y^2 + \mathbf{I}_z^2$ commutes with any one of its components (say $\mathbf{I}_z$). It can also be shown that $\mathbf{I}^2$ (and thus $\mathbf{L}^2$ and $\mathbf{S}^2$) commutes with **H**. Therefore, we can consider a function ψ which is a simultaneous eigenfunction of **H**, $\mathbf{S}^2$, and $\mathbf{S}_z$,

$$\mathbf{H}\psi = \alpha\psi \tag{36}$$

$$\mathbf{S}^2\psi = \lambda\psi \tag{37}$$

$$\mathbf{S}_z\psi = \mu\psi \tag{38}$$

where α, λ, and μ are the respective eigenvalues. Let us also define the raising ($\mathbf{S}_+$) and lowering ($\mathbf{S}_-$) operators.

$$\mathbf{S}_+ = \mathbf{S}_x + i\mathbf{S}_y \tag{39}$$

$$\mathbf{S}_- = \mathbf{S}_x - i\mathbf{S}_y \tag{40}$$

The following commutation relations hold.

$$\mathbf{S}_z\mathbf{S}_+ - \mathbf{S}_+\mathbf{S}_z = \mathbf{S}_+ \tag{41}$$

$$\mathbf{S}_z\mathbf{S}_- - \mathbf{S}_-\mathbf{S}_z = -\mathbf{S}_- \tag{42}$$

$$\mathbf{S}_+\mathbf{S}_- - \mathbf{S}_-\mathbf{S}_+ = 2\mathbf{S}_z \tag{43}$$

Applying $\mathbf{S}_+$ to $\mathbf{S}_z\psi$ gives

$$S_+S_z\psi = \mu S_+\psi. \tag{44}$$

Because $S_+S_z = (S_z - 1)S_+$, we have

$$(S_z - 1)S_+\psi = \mu S_+\psi \tag{45}$$

$$S_zS_+\psi = (\mu + 1)S_+\psi. \tag{46}$$

Therefore, $S_+\psi$ is an eigenfunction of S_z with eigenvalue $\mu + 1$. Similarly, $S_-\psi$ is an eigenfunction of S_z with eigenvalue $\mu - 1$. And, because S_- and S_+ commute with H and S^2, $S_+\psi$ and $S_-\psi$ are simultaneous eigenfunctions of H and S^2 with the same eigenvalues that belong to the original ψ (i.e., α and λ). Repeated application of S_- and S_+ (known as the "ladder" operators) gives a series of new eigenfunctions and eigenvalues.

$$\begin{array}{ccc}
 & \vdots & \\
S_+^3\psi & _____ & \mu + 3 \\
S_+^2\psi & _____ & \mu + 2 \\
S_+\psi & _____ & \mu + 1 \\
\psi & _____ & \mu \\
S_-\psi & _____ & \mu - 1 \\
S_-^2\psi & _____ & \mu - 2 \\
S_-^3\psi & _____ & \mu - 3 \\
 & \vdots &
\end{array} \tag{47}$$

This series appears to stretch infinitely in either direction. Actually, however, its extent is finite and is determined by the eigenvalue λ of S^2. Consider the product S_-S_+.

$$S_-S_+ = (S_x - iS_y)(S_x + iS_y) = S_x^2 + S_y^2 + i(S_xS_y - S_yS_x) \tag{48}$$

It can then be shown that

$$\mathbf{S_-S_+} = \mathbf{S^2} - \mathbf{S_z^2} - \mathbf{S_z} \tag{49}$$

and consequently,

$$\mathbf{S_-S_+}\psi = (\lambda - \mu^2 - \mu)\psi. \tag{50}$$

Although $\mathbf{S_-}$ and $\mathbf{S_+}$ are not Hermitian, their elements $\mathbf{S_x}$ and $\mathbf{S_y}$ are. Using this fact, it can be shown that the integral

$$\langle\psi|\mathbf{S_-S_+}|\psi\rangle = \langle\psi|(\mathbf{S_x} - i\mathbf{S_y})(\mathbf{S_x} + i\mathbf{S_y})|\psi\rangle \tag{51}$$

is equivalent to

$$\langle\psi|\mathbf{S_x} + i\mathbf{S_y}|^2\psi\rangle \geq 0 \tag{52}$$

which is necessarily nonnegative, so its eigenvalues are nonnegative.

$$\lambda - \mu^2 - \mu \geq 0 \tag{53}$$

Because λ is nonnegative,

$$\lambda = \frac{\langle\psi|\mathbf{S^2}|\psi\rangle}{\langle\psi|\psi\rangle}, \tag{54}$$

the upper limit on μ is given by

$$\lambda \geq \mu^2 + \mu. \tag{55}$$

Having shown that μ_{max} exists, we can evaluate λ in terms of μ_{max}. By definition, $\mathbf{S_+}\psi(\mu_{max})$ cannot generate an eigenvalue $\mu_{max}+ 1$. Therefore, $\mathbf{S_+}\psi(\mu_{max})$ must vanish.

$$\mathbf{S_-S_+}\psi(\mu_{max}) = 0 = (\lambda - \mu_{max}^2 - \mu_{max})\psi(\mu_{max}) \tag{56}$$

$$\lambda = \mu_{max}^2 + \mu_{max} \tag{57}$$

Similarly, beginning from S_+S_- instead of S_-S_+, it can be shown that

$$\lambda = \mu_{min}^2 - \mu_{min} \tag{58}$$

Therefore, $\mu_{max} = \mu_{min}$. What are these values? Eigenvalue μ corresponds to M_S and μ_{max} is S. The symmetry of the eigenvalues about zero combined with their unit spacing gives 2S + 1 values of M_S.

The Quantum Mechanical Basis of Ferromagnetic Coupling[9-12]

Consider atomic carbon, a ground state triplet. This is in accordance with Hund's rule, which says that weakly interacting electrons in different, degenerate orbitals are ferromagnetically, or high-spin, coupled (Figure 4.1).

Figure 4.1: Triplet Ground State of Atomic Carbon

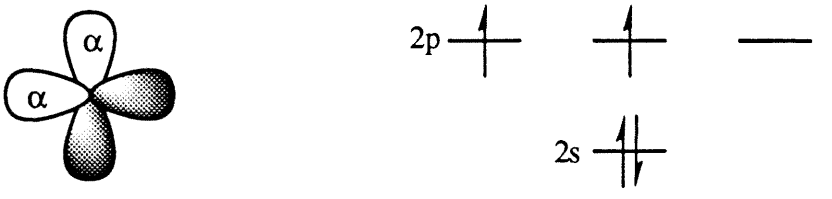

It is tempting to apply this reasoning to molecules; however, consider that H_2, the simplest molecule, is a singlet at all separations **r** (Figure 4.2)!

Figure 4.2: H_2 has a Singlet Ground State for all **r**

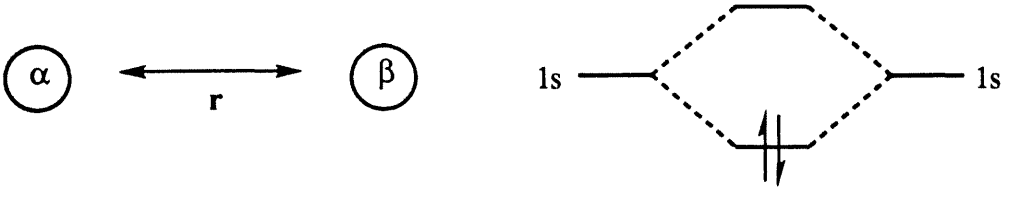

The problem is that Hund's rule is an empirical statement developed for atoms, not molecules. To understand the requirements for ferromagnetic coupling of spins in organic molecules, we need a better, i.e., quantum

mechanical, explanation for the triplet preference of atomic carbon. We start with the following singlet and triplet wavefunctions for atomic carbon, where the two 2p orbitals are represented by *a* and *b*, and the core 1s and 2s electrons are neglected.

$$^{1}\Psi = \frac{1}{\sqrt{2}}[ab + ba] \times [\alpha\beta - \beta\alpha] \tag{59}$$

$$^{3}\Psi = [ab - ba] \times \left[\alpha\alpha, \frac{1}{\sqrt{2}}(\alpha\beta + \beta\alpha), \text{ or } \beta\beta\right] \tag{60}$$

The energy ^{x}E for each state x is given by

$$^{x}E = \frac{\langle {}^{x}\Psi | H | {}^{x}\Psi \rangle}{\langle {}^{x}\Psi | {}^{x}\Psi \rangle}. \tag{61}$$

Because the wavefunction is normalized and the 2p orbitals are orthogonal, the denominator is unity. Also, because the spin functions do not interact with the hamiltonian, they can be integrated separately; and because they are normalized, they too are unity. The energy expressions then become

$$^{1}E = \frac{1}{2}\langle ab + ba|H|ab + ba\rangle = \frac{1}{2}(\langle ab|H|ab\rangle + \langle ab|H|ba\rangle + \langle ba|H|ab\rangle + \langle ba|H|ba\rangle) \tag{62}$$

$$^{3}E = \frac{1}{2}\langle ab - ba|H|ab - ba\rangle = \frac{1}{2}(\langle ab|H|ab\rangle - \langle ab|H|ba\rangle - \langle ba|H|ab\rangle + \langle ba|H|ba\rangle). \tag{63}$$

Because the 2p orbitals are homosymmetric (can be converted by a symmetry operation), the following relations apply, and the energy expressions can be further condensed.

$$\langle ab|H|ab\rangle = \langle ba|H|ba\rangle \qquad \langle ab|H|ba\rangle = \langle ba|H|ab\rangle \tag{64}$$

$$^{1}E = \langle ab|H|ab\rangle + \langle ab|H|ba\rangle \tag{65}$$

$$^{3}E = \langle ab|H|ab\rangle - \langle ab|H|ba\rangle \tag{66}$$

The hamiltonian which applies here is composed of two one-electron terms ($\mathbf{h}_1$ and $\mathbf{h}_2$) containing kinetic and potential energy operators and one two-electron term $\left(\frac{1}{r_{12}}\right)$.

$$\mathbf{H} = \mathbf{h}_1 + \mathbf{h}_2 + \frac{1}{r_{12}} \tag{67}$$

Substituting the applicable operators in and expanding,

$${}^1\mathbf{E} = \langle ab|\mathbf{h}_1|ab\rangle + \langle ab|\mathbf{h}_2|ab\rangle + \left\langle ab\left|\frac{1}{r_{12}}\right|ab\right\rangle + \left\langle ab\left|\frac{1}{r_{12}}\right|ba\right\rangle \tag{68}$$

$${}^3\mathbf{E} = \langle ab|\mathbf{h}_1|ab\rangle + \langle ab|\mathbf{h}_2|ab\rangle + \left\langle ab\left|\frac{1}{r_{12}}\right|ab\right\rangle - \left\langle ab\left|\frac{1}{r_{12}}\right|ba\right\rangle. \tag{69}$$

Both one-electron integrals in each expression are equivalent (i.e., electrons are indistinguishable) and are evaluated as one-electron energies. The first two-electron integral represents the electrostatic repulsion between the a^*a and b^*b electron distributions. It is called the coulomb integral, or J, and is always positive. The second two-electron integral, called the exchange integral, or K, represents the electrostatic repulsion between the a^*b^* and ab overlap distributions and is always positive.

$$\langle ab|\mathbf{h}_1|ab\rangle = \langle ab|\mathbf{h}_2|ab\rangle = \mathbf{h}_{aa} = \mathbf{h}_{bb} \tag{70}$$

$$\left\langle ab\left|\frac{1}{r_{12}}\right|ab\right\rangle = \mathbf{J}_{ab} \tag{71}$$

$$\left\langle ab\left|\frac{1}{r_{12}}\right|ba\right\rangle = \mathbf{K}_{ab} \tag{72}$$

Using these definitions, we can rewrite the energy expressions.

$${}^1\mathbf{E} = 2\mathbf{h}_{aa} + \mathbf{J}_{ab} + \mathbf{K}_{ab} \tag{73}$$

$${}^3\mathbf{E} = 2\mathbf{h}_{aa} + \mathbf{J}_{ab} - \mathbf{K}_{ab} \tag{74}$$

The singlet-triplet gap is then

$$^1\mathbf{E} - {}^3\mathbf{E} = 2\mathbf{h}_{aa} - 2\mathbf{h}_{aa} + \mathbf{J}_{ab} - \mathbf{J}_{ab} + \mathbf{K}_{ab} + \mathbf{K}_{ab} = 2\mathbf{K}_{ab}. \quad (75)$$

Because **K** is never negative, we see that in atomic carbon, the triplet is stabilized relative to the singlet by $2\mathbf{K}_{ab}$ (a subtle point here is that $^1\mathbf{J}_{ab} \neq {}^3\mathbf{J}_{ab}$, although the difference decreases at higher levels of theory. Regardless, $\Delta^{1\text{-}3}\mathbf{J}_{ab}$ is small compared to $2\mathbf{K}_{ab}$).

What about H_2? Using the same notation, where *a* and *b* are the hydrogen 1s orbitals, the singlet and triplet wavefunctions are again

$$^1\Psi = \frac{1}{\sqrt{2}}[ab + ba] \times [\alpha\beta - \beta\alpha] \quad (76)$$

$$^3\Psi = [ab - ba] \times \left[\alpha\alpha, \frac{1}{\sqrt{2}}(\alpha\beta + \beta\alpha), \text{ or } \beta\beta\right]. \quad (77)$$

In the energy expressions, the spin functions are again unity. But, because *a* and *b* are not orthogonal, the denominator is no longer unity. Using the singlet state as an example,

$$^1\mathbf{E} = \frac{\langle {}^1\Psi|\mathbf{H}|{}^1\Psi\rangle}{\langle {}^1\Psi|{}^1\Psi\rangle} = \frac{\langle ab + ba|\mathbf{H}|ab + ba\rangle}{\langle ab + ba|ab + ba\rangle} = \frac{\langle ab|\mathbf{H}|ab\rangle + \langle ab|\mathbf{H}|ba\rangle + \langle ba|\mathbf{H}|ab\rangle + \langle ba|\mathbf{H}|ba\rangle}{\langle ab|ab\rangle + \langle ab|ba\rangle + \langle ba|ab\rangle + \langle ba|ba\rangle}. \quad (78)$$

Because the orbitals are homosymmetric, the following relations apply, and the energy expressions can be further condensed.

$$\langle ab|ab\rangle = \langle ba|ba\rangle \qquad \langle ab|ba\rangle = \langle ba|ab\rangle \quad (79)$$

$$^1\mathbf{E} = \frac{2(\langle ab|\mathbf{H}|ab\rangle + \langle ab|\mathbf{H}|ba\rangle)}{2(\langle ab|ab\rangle + \langle ab|ba\rangle)} = \frac{\langle ab|\mathbf{H}|ab\rangle + \langle ab|\mathbf{H}|ba\rangle}{\langle ab|ab\rangle + \langle ab|ba\rangle} \quad (80)$$

The integrals are evaluated as follows, where $\mathbf{h}_{xx}$ is a one-electron energy, $\mathbf{S}_{ab}$ is overlap, $\mathbf{J}_{ab}$ is coulomb repulsion, and $\mathbf{K}_{ab}$ is exchange.

$$\langle ab|ab\rangle = 1 \quad (81)$$

$$\langle ab|ba\rangle = S_{ab}^2 \tag{82}$$

$$\langle ab|H|ab\rangle = \left\langle ab\left|h_1 + h_2 + \frac{1}{r_{12}}\right|ab\right\rangle$$

$$= \langle ab|h_1|ab\rangle + \langle ab|h_2|ab\rangle + \left\langle ab\left|\frac{1}{r_{12}}\right|ab\right\rangle$$

$$= h_{aa} + h_{bb} + J_{ab} \tag{83}$$

$$\langle ab|H|ba\rangle = \langle ab|h_2|ba\rangle + \langle ab|h_2|ba\rangle + \left\langle ab\left|\frac{1}{r_{12}}\right|ba\right\rangle$$

$$= S_{ab}h_{ab} + S_{ab}h_{ab} + K_{ab} = 2S_{ab}h_{ab} + K_{ab} \tag{84}$$

Thus, the energy expression for the singlet is

$${}^1E = \frac{h_{aa} + h_{bb} + J_{ab} - 2S_{ab}h_{ab} + K_{ab}}{1 + S_{ab}^2}. \tag{85}$$

It can be shown that the corresponding expression for the triplet is

$${}^3E = \frac{h_{aa} + h_{bb} + J_{ab} - 2S_{ab}h_{ab} - K_{ab}}{1 - S_{ab}^2}. \tag{86}$$

The singlet-triplet energy gap is much more complex than the expression for atomic carbon.

$${}^1E - {}^3E = \frac{\left(1 - S_{ab}^2\right)\left(h_{aa} + h_{bb} + J_{ab} + 2S_{ab}h_{ab} + K_{ab}\right) - \left(1 + S_{ab}^2\right)\left(h_{aa} + h_{bb} + J_{ab} - 2S_{ab}h_{ab} - K_{ab}\right)}{\left(1 + S_{ab}^2\right)\left(1 - S_{ab}^2\right)}$$

$$= \frac{4S_{ab}h_{ab} + 2K_{ab} - 2S_{ab}^2h_{aa} - 2S_{ab}^2h_{bb} - 2S_{ab}^2J_{ab}}{1 - S_{ab}^4} \tag{87}$$

In the limit of zero overlap (S_{ab} -> 0), the energy expression reduces to what we saw in atomic carbon (where the 2p orbitals are orthogonal, so $S_{ab} = 0$).

$${}^1E - {}^3E = \frac{4(0)h_{ab} + 2K_{ab} - 2(0)^2h_{aa} - 2(0)^2h_{bb} - 2(0)^2J_{ab}}{1 - (0)^4} = 2K_{ab} \tag{88}$$

When overlap is not zero, as in H_2, the picture is less clear; however, it is the case that as the internuclear separation increases, $\mathbf{K}_{ab}$ and $\mathbf{S}_{ab}$ decrease such that the ground state is always a singlet. Therefore, the key to understanding and designing high spin molecules is to minimize overlap while maximizing exchange.

High Spin Organic Molecules[9,10,13-15]

Consider 1,3-cyclobutanediyl, a localized organic biradical (Figure 4.3).

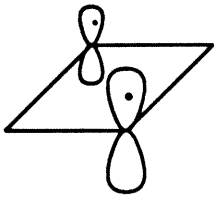

Figure 4.3: 1,3-Cyclobutanediyl

Ground State = ?

Generalized valence bond (GVB) wavefunctions for the both spin states can be constructed from the atomic (p) orbitals for the 1,3 carbons, a and b.

$$^1\Psi_{GVB} = \frac{1}{\sqrt{2 + 2S_{ab}}}[ab + ba] \times [\alpha\beta - \beta\alpha] \tag{89}$$

$$^3\Psi_{GVB} = \frac{1}{\sqrt{2 - 2S_{ab}}}[ab - ba] \times [\alpha\alpha,\ \alpha\beta + \beta\alpha, \text{ or } \beta\beta] \tag{90}$$

Notice that the normalization factor includes the GVB pair overlap $\mathbf{S}_{ab}$. If the overlap is zero, the wavefunctions are qualitatively identical (though from p instead of s orbitals) to those used for H_2. In any event, the normalization factors cancel when deriving the singlet-triplet energy gap, so the expression is identical to that for H_2.

$$^1\mathbf{E} - {}^3\mathbf{E} = \frac{4\mathbf{S}\mathbf{h}_{ab} + 2\mathbf{K}_{ab} - 2\mathbf{S}^2\mathbf{h}_{aa} - 2\mathbf{S}^2\mathbf{h}_{bb} - 2\mathbf{S}^2\mathbf{J}_{ab}}{1 - \mathbf{S}^4} \tag{91}$$

We can also consider 1,3-cyclobutanediyl using molecular orbital (MO) theory (Figure 4.4). The two radical atomic orbitals mix to provide two

formally nonbonding molecular orbitals (NBMOs). Due to through space interactions, one orbital (*A*) is antisymmetric, slightly antibonding and higher in energy than the other (*S*), which is symmetric and slightly bonding. The intervening methylenes provide a πCH_2 orbital that can interact with the *S* orbital but are prevented by symmetry from mixing with the *A* orbital. This interaction lowers the energy of the πCH_2 orbital and raises the energy of the *S* orbital. In the case of 1,3-cyclobutanediyl, the *S* orbital is raised so that it is degenerate, or nearly so, with the *A* orbital (although in other systems the *S* orbital could end up above or below *A*). Because the NBMOs are degenerate, a triplet ground state is at least possible, although MO theory at this level does not treat exchange or spin.

We can, however, adapt MO theory using GVB theory to incorporate spin and exchange. The *A* and *S* MOs can be constructed from the atomic orbitals *a* and *b*.

$$S = \tfrac{1}{2}(a + b)\sqrt{\frac{C_1 + C_2}{C_1}} \tag{92}$$

$$A = \tfrac{1}{2}(a - b)\sqrt{\frac{C_1 + C_2}{C_1}} \tag{93}$$

The values of the coefficients are determined by the MO energies. If the orbitals are degenerate, the coefficients are equal. The best singlet wavefunction (determined from MCSCF calculations) using these MOs is

$$^1\Psi_{MCSCF} = \frac{1}{\sqrt{C_1^2 + C_2^2}}[C_1 SS - C_2 AA] \times [\alpha\beta - \beta\alpha]. \tag{94}$$

The coefficients are also related to the GVB pair overlap.

$$S_{ab} = \frac{C_1 - C_2}{C_1 + C_2} \tag{95}$$

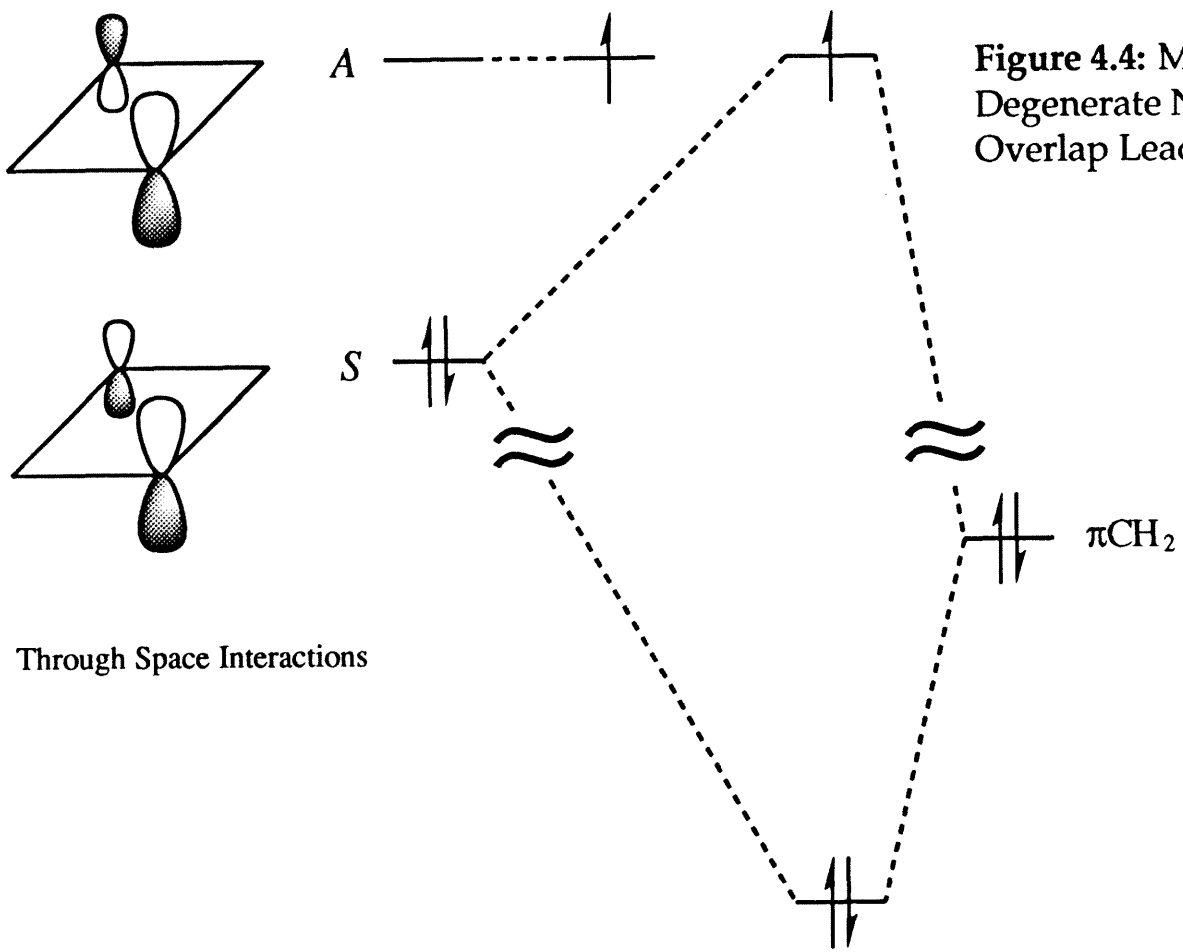

Through Space Interactions

Figure 4.4: MO Diagram of Cyclobutadiyl. Degenerate NBMOs are Equivalent to Zero Overlap Leading to a Triplet Ground State.

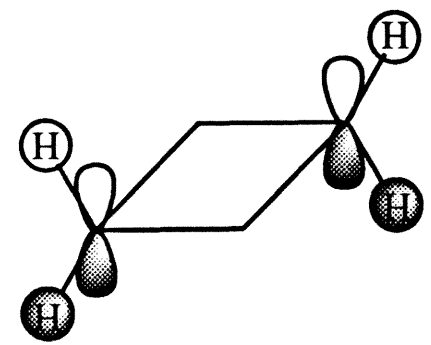

Through Bond Interactions

Although the GVB pair overlap is zero when $C_1 = C_2$, exchange interactions remain large. Therefore, *eliminating the S-A MO energy gap is the same as zeroing the GVB overlap.* So, although simple MO theory says nothing about spin or exchange, we *can* say that degenerate NBMOs coupled with significant exchange interactions will lead to a high spin ground state.

Spin Polarization[16,17]

Zero spin density is expected on the central carbon of trimethylenemethane because its NBMOs place the central carbon in a node. Experimental evidence shows, however, that there is *negative* spin density on the central carbon, and higher than expected positive spin density on the terminal carbons (Figure 4.5). Why is this? The nonbonding electrons

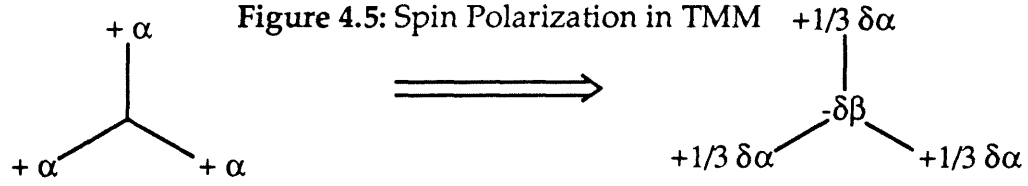

Figure 4.5: Spin Polarization in TMM

are correlated by exchange to remain far apart. We can consider each terminal carbon as if it possessed a nonbonding electron in a p orbital, like methyl radical. Due to Hund's rule (for atoms) the α electron in the σ_{CC} bond will tend to remain near the terminal carbon, leaving the β electron near the central carbon (Figure 4.6). This leads to greater than expected positive (α)

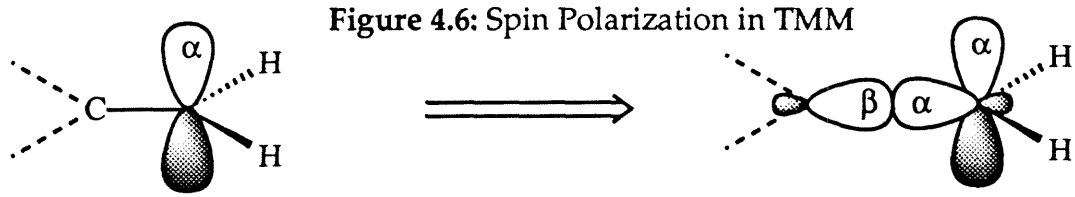

Figure 4.6: Spin Polarization in TMM

spin density on the terminal carbons, and negative (β) spin density on the central carbon. This effect is known as spin polarization and is due solely to exchange.

Topology Based Rules for Predicting Spin States[9,15,16,18]

In the last section, we showed that MO theory could be used to predict spin states (even though it does not treat spin explicitly) by relating it to GVB theory, which is less readily applied in many instances. In this section, we will develop a more facile model for designing high spin organic molecules by combining what we have learned so far with a few simple topology rules. To begin, consider (square) cyclobutadiene and trimethylenemethane, two molecules which have qualitatively similar Hückel molecular orbital (HMO) diagrams but different ground states (Figure 4.7). Both have degenerate NBMOs, but only one has a significant amount of exchange. In cyclobutadiene, one can make linear combinations of the NBMOs so that they

Figure 4.7: HMO Diagrams of Square Cyclobutadiene and TMM

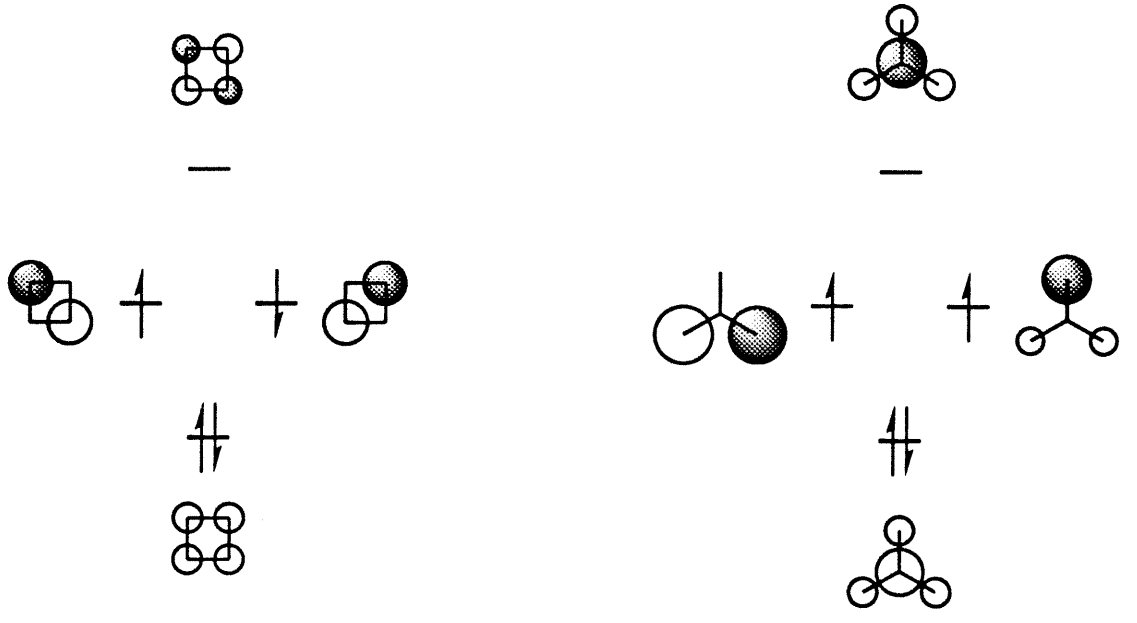

are *disjoint*, or span no common atoms. Because the π electrons never have to occupy the same atomic orbitals, the triplet does not experience diminished coulomb repulsions relative to the singlet and **K** is approximately zero. At this level of theory, the singlet and triplet states of square cyclobutadiene are predicted to be degenerate.

In trimethylenemethane, there exists no linear combination such that the two NBMOs are disjoint. Although the electrons can localize in different orbitals, they still must span some of the same atoms and thus **K** is large and positive. Therefore, a strong preference for a triplet ground state is predicted.

A simple mnemonic for determining whether NBMOs of alternate hydrocarbons which are degenerate at the Hückel level will lead to high or low spin is based on Ovchinnikov's star-nonstar system (Figure 4.8).[18] If the

Figure 4.8: The Star-Nonstar Rule Predicts Spin Ground States

2* = 2 non*
∴ G.S. = Singlet

3* > 1 non*
∴ G.S. = Triplet

5* > 3 non*
∴ G.S. = Triplet

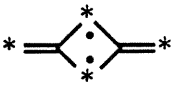

4* > 2 non*
∴ G.S. = Triplet

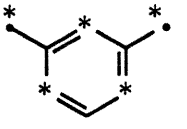

number of starred and nonstarred atoms is equivalent, the NBMOs will be disjoint, leading to a low spin state. Conversely, if there are more starred than nonstarred atoms, the orbitals will span common atoms leading to a high spin state. This simple strategy can be generalized for the design of high spin interactions in any organic, alternate π system.

Magnetic Characterization[2,15,16,19,20]

All matter responds to magnetic fields. The response of a sample to an externally applied field **H** is the magnetic induction (or density of lines of force) **B**, which is determined by the applied field and a contribution from the magnetization of the sample itself (**M**).

$$\mathbf{B} = \mathbf{H} + 4\pi\mathbf{M} \tag{96}$$

The observed magnetization M_{obs}, which can be described as the density of magnetic dipole moment, is in most materials a function of an observed suceptibility χ_{obs} times the applied field H.

$$M_{obs} = \chi_{obs} H \text{ or } \chi_{obs} = \frac{M}{H} \tag{97}$$

This suceptibility can be separated into diamagnetic, paramagnetic, and Pauli (temperature independent paramagnetic) components.

$$\chi_{obs} = \chi_{dia} + \chi_{para} + \chi_{pauli} \tag{98}$$

The χ_{pauli} component, which is a temperature independent paramagnetic suceptibility, is associated with conducting materials. As will be seen subsequently, χ_{para} for poorly conducting materials can be derived using Boltzmann statistics because the paramagnetic centers can be distinguished. In conductors, however, the paramagnetic electrons are indistinguishable particles and thus must be described using Fermi statistics. While Fermi statistics do depend on temperature, it is the case that paramagnetic suceptibilities derived therefrom are relatively insensitive to changes in temperature. An alternate intuitive explanation is provided by the following example. Consider the distribution of conduction electrons in a metal in an extremely weak magnetic field. The population of up spin, or α, electrons will be (nearly) the same as the population of down spin, or β electrons.

Immediately after the field is increased, the energy of the β fraction has increased by μB and the energy of the α fraction has decreased by $-\mu B$. Equilibrium will be achieved as some of the higher energy β electrons make the transition to the lower energy α state. At a substantial magnetic field, say 1.0 Tesla, the energy of μB is only about 10^{-4} eV, compared to a typical Fermi energy of 1.0 eV. Thus, there is only a slight excess of α electrons, leading to a small suceptibility; and, because $kT \gg \mu B$ for $T > 10$ K, the suceptibility should be relatively independent of reasonable temperature changes.

Diamagnetism is due to the repulsion of the magnetic field by closed shell electrons and is thus a property of all common matter. The diamagnetic suceptibility of most materials is small and negative, on the order of -1×10^{-6} emu/mol. For strongly paramagnetic materials, this is so small it is often neglected. In our weakly paramagnetic systems, however, χ_{dia} can be significant compared to χ_{para}.

Paramagnetism arises out of the interaction between randomly oriented, rapidly reorienting moments in a material with an external magnetic field, thus χ_{para} is a positive number. In a perfect paramagnet, there is no interaction between isolated moments. Because the tendency of moments to align with the field is opposed by thermal energy, χ_{para} is temperature dependent. Additionally, there is no spontaneous or permanent magnetic moment in a paramagnetic material.

Consider the behavior of a macroscopic magnetic dipole in an external, homogeneous magnetic field (Figure 4.9). The energy of the dipole is the negative product of the external field H with the component, μ_{Θ}, of the

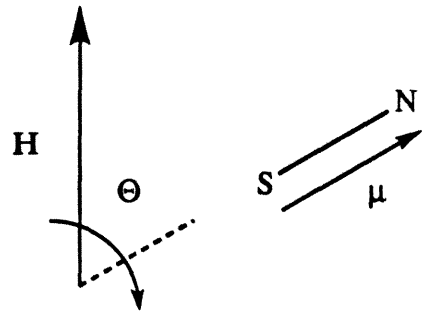

Figure 4.9: A Bar Magnet in an External Magnetic Field

dipole's magnetic moment μ in the direction of the field (Figure 4.10). Thus, the energy minimum exists when the dipole is parallel to the external field (Θ = 0°) and the energy maximum is reached when the dipole is antiparallel to

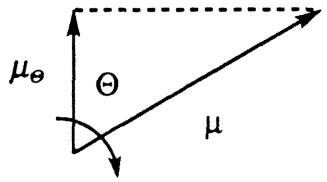

Figure 4.10: The energy of a magnetic dipole is scaled by cosΘ

$$E = -\mu\cos\Theta H = -\mu_\Theta H$$

the field (Θ = 180°). A classical dipole like a bar magnet is allowed to take on any angle Θ and thus any energy from $-\mu H$ to $+\mu H$. Electrons, however, as quantum dipoles, can adopt only one of two discrete orientations: Θ = 0°, corresponding to $m_s = {}^{+1}/_2$, α, or "up" spin, and Θ = 180°, corresponding to $m_s = {}^{-1}/_2$, β, or "down" spin. The magnetic dipole moment of the electron is

$$\mu_e = g_e \frac{q_e h}{4\pi m_e c} M_S = -g_e \beta m_S \,. \qquad (99)$$

The quantity β (not to be confused with β spin) converts angular momentum into magnetic moment and is called the Bohr magneton (β = 9.2741 x 10^{-21} erg $gauss^{-1}$). The electron spectroscopic splitting factor g accounts for spin angular momentum. For a free electron, $g = g_e = 2.00232$, and for most organic radicals $g \approx 2$, although some transition metals deviate substantially from this value. The negative sign comes from the electron charge q_e.

The moments in an organic paramagnetic material are derived from the spin angular momentum of unpaired electrons in the material. Orbital angular momentum, which is an important contribution to the paramagnetism in transition metal compounds, and nuclear magnetic dipole moments, which are three orders of magnitude smaller than electron spin moments, are unimportant here. Application of an external magnetic field will tend to align these moments with the direction of the field. The interaction energy of the individual moments with the field are given by

$$E = g\beta m_s H \quad . \tag{100}$$

For a system of noninteracting monoradicals, the two m_s states are degenerate. Application of an external field splits these states into two discrete energy levels. This effect is known as Zeeman splitting (Figure 4.11).

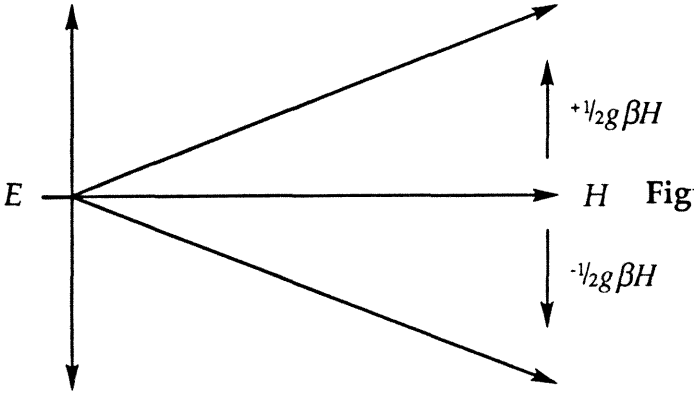

Figure 4.11: Zeeman Splitting

Thus, for a simple system where $m_s = \pm \frac{1}{2}$, the energies of the two states are $\pm \frac{1}{2} g\beta H$ and their separation is $g\beta H$. As noted before, the suceptibility is temperature dependent, and is determined by the opposition between thermal energy and the magnetic interaction energy. Experimentally, Curie found that for small fields and temperatures above 50 K, χ_{para} decreased with increasing temperature.

$$\chi_{para} = \frac{C}{T} \tag{101}$$

$$\chi_{obs} = \chi_{para} + \chi_{dia} = \frac{C}{T} + \chi_{dia} \tag{102}$$

Therefore, in a plot of χ_{obs} vs 1/T between 50 to 100 K, the y intercept at extrapolation to infinite temperature is the temperature independent suceptibility (χ_{dia} for our systems) and the slope is C, the Curie constant, which is characteristic of the material. A further adaptation of the Curie law is the Curie-Weiss law.

$$\chi_{para} = \frac{C}{T - \Theta} \tag{103}$$

This is usually plotted as its inverse.

$$\frac{1}{\chi_{para}} = \frac{T}{C} - \frac{\Theta}{C} \tag{104}$$

The Curie-Weiss constant Θ, in units of degrees Kelvin, is diagnostic of short-range ferromagnetic or antiferromagnetic interactions at low temperature. A positive value indicates ferromagnetic interactions, and a negative value denotes antiferromagnetic interactions. A Θ of zero indicates a perfect paramagnet. For our weakly paramagnetic samples, Θ's within a few degrees Kelvin of zero are considered to indicate a perfect paramagnet.

Idealized Curie-Weiss plots are shown in Figure 4.12. The onset of deviation of the data from a straight line is the critical temperature for the ferromagnetic or antiferromagnetic interactions. A more sensitive means of observing the relative balance of ferromagnetic and antiferromagnetic interactions is to plot $\chi_{para} \bullet T$ versus T (Figure 4.13); since $\chi_{para} \bullet T$ is proportional to the effective moment, this plot is known as a relative effective moment plot. For a perfect paramagnet, where there is no magnetic interaction between isolated moments, this plot is a horizontal line; a positive deviation indicates increasing ferromagnetic interactions and a

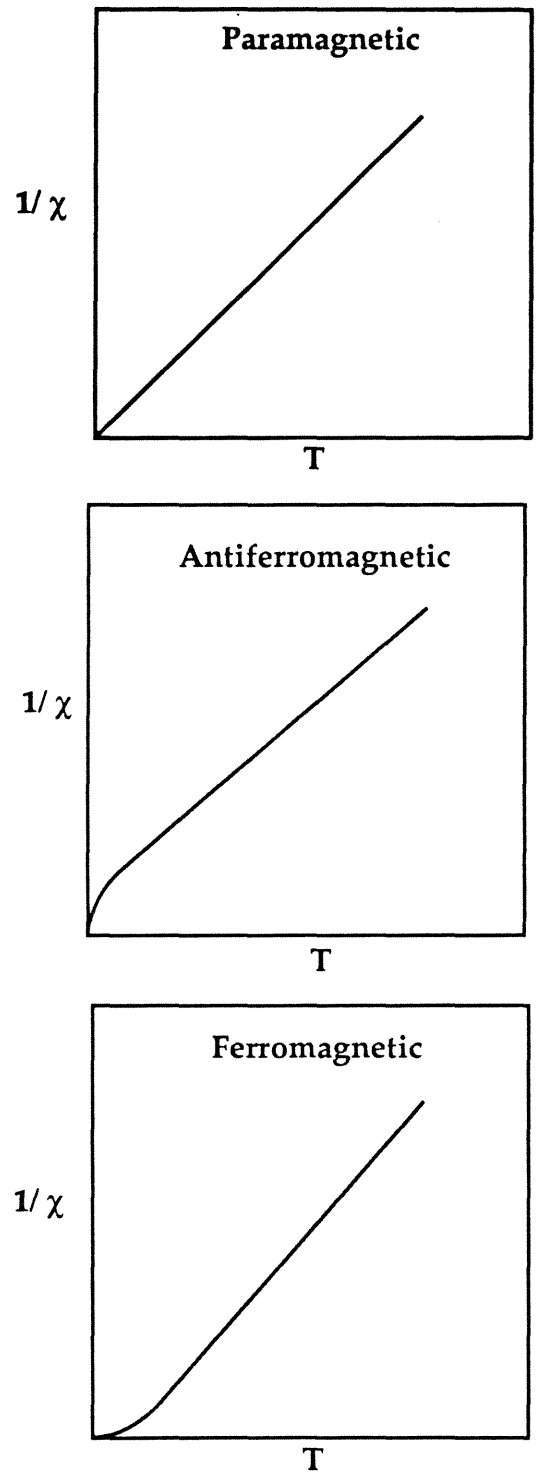

Figure 4.12: Idealized Curie-Weiss Plots for Paramagnetic (top), Antiferromagnetic (middle), and Ferromagnetic Material (bottom).

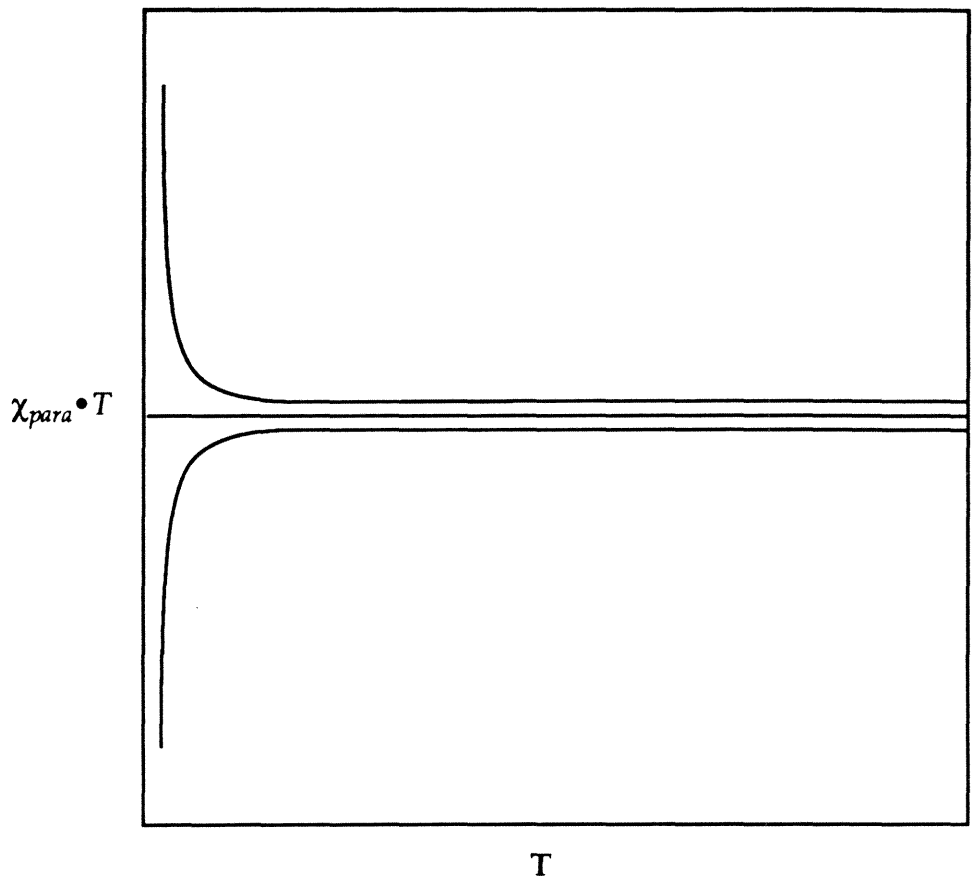

Figure 4.13 Idealized Relative Effective Moment Plot. The middle line extending to T = 0 indicates a perfect paramagnet. The top line, curving upwards, indicates increasing, net ferromagnetic coupling; the bottom line, curving downward, indicates increasing, net antiferromagnetic coupling.

negative deviation indicates antiferromagnetic interactions.

The paramagnetic suceptibility can be derived explicitly. Here, we consider a simple system where $m_s = \pm 1/2$, no contributions from orbital angular momentum, and no interaction between paramagnetic centers. The energies of the two possible alignments of an electron's spin with the magnetic field are:

$$E_{-1/2} = -1/2 g\beta H \tag{105}$$

$$E_{+1/2} = +1/2 g\beta H \tag{106}$$

If these moments are noninteracting (i.e., distinguishable), and able to reorient freely (i.e., isotropic), Boltzmann statistics can be used to give the populations of both energy states. Let N be the volume density of moments and N_i be the volume density of moments in the ith state. Then,

$$N = N_{+1/2} + N_{-1/2}. \tag{107}$$

From the Boltzmann distribution the population of each state is a function of temperature.

$$N_{-1/2} = cNe^{-g\beta H/2kT} \tag{108}$$

$$N_{+1/2} = cNe^{g\beta H/2kT} \tag{109}$$

Here c is a constant.

The total magnetization results from the differential population of the two states. Because the parallel alignment of a spin with the magnetic field is lower in energy, the magnetization is due to excess parallel spin.

$$M = 1/2 g\beta \left(N_{-1/2} - N_{+1/2}\right)$$

$$= 1/2 g\beta cN \left(e^{g\beta H/2kT} - e^{-g\beta H/2kT}\right) \tag{110}$$

The constant c and the total volume density of moments N can be removed. Dividing through by N gives the average net moment.

$$\langle \mu \rangle = \frac{M}{N} = \frac{{}^1\!/_2 g\beta c N\left(e^{g\beta H/2kT} - e^{-g\beta H/2kT}\right)}{N_{+1/2} + N_{-1/2}}$$

$$= \frac{{}^1\!/_2 g\beta c N\left(e^{g\beta H/2kT} - e^{-g\beta H/2kT}\right)}{cN\left(e^{g\beta H/2kT} + e^{-g\beta H/2kT}\right)}$$

$$= \frac{g\beta\left(e^{g\beta H/2kT} - e^{-g\beta H/2kT}\right)}{2\left(e^{g\beta H/2kT} + e^{-g\beta H/2kT}\right)} \tag{111}$$

At low fields and high temperatures, i.e., small values of $|m_s g\beta H/kT|$, the exponents can be expanded.

$$\langle \mu \rangle \approx \frac{g\beta\left(\left(1 + \frac{g\beta H}{2kT}\right) - \left(1 - \frac{g\beta H}{2kT}\right)\right)}{2\left(\left(1 + \frac{g\beta H}{2kT}\right) + \left(1 - \frac{g\beta H}{2kT}\right)\right)} \tag{112}$$

$$\langle \mu \rangle \approx \frac{g^2\beta^2 H}{2kT} \tag{113}$$

This is equivalent to using the hyperbolic tangent relation for y « 1.

$$\frac{e^x - e^{-x}}{e^x + e^{-x}} = \tanh x \approx x \tag{114}$$

The exponetial expression for the average net moment is easily generalized for any value of m_s.

$$\langle \mu_z \rangle = \frac{\sum_{m_S=-S}^{+S} g\beta m_S e^{-m_S g\beta H_z/kT}}{\sum_{m_S=-S}^{+S} e^{-m_S g\beta H_z/kT}} \tag{115}$$

This is also related to the magnetic partition function W.

$$\langle \mu_z \rangle = \frac{kT}{W} \frac{\partial W}{\partial H_z} = kT \frac{\partial \ln W}{\partial H_z} \tag{116}$$

We can define a quantity $\eta_z = g\beta H_z / kT$ which represents the conflict between the magnetization energy and the thermal energy. As we have seen in the Curie example, for small η, the population of magnetic substates is independent of field because the thermal energy dominates the magnetization energy. For large η, the field can significantly affect the population of magnetic substates, eventually leading to saturation, where only the lowest energy states are populated, i.e., all the spins are aligned parallel to the field.

Substituting η, the magnetic partition function W may be rewritten.

$$W = \sum_{m_S=-S}^{+S} e^{-\eta_z m_S}$$

$$= \frac{e^{-\eta_z S} - e^{\eta_z (S+1)}}{1 - e^{\eta_z}}$$

$$= \frac{e^{-\eta_z (S+1/2)} - e^{\eta_z (S+1/2)}}{e^{-\eta_z/2} - e^{\eta_z/2}} \tag{117}$$

Using the hyperbolic sine relation

$$\sinh x = e^{-x} - e^{x}, \tag{118}$$

we can write

$$W = \frac{\sinh (S + 1/2)\eta_z}{\sinh \eta_z/2}. \tag{119}$$

The average net moment can be reexpressed.

$$\langle m_z \rangle = kT \frac{\partial \ln W}{\partial H_z} = kT \frac{\partial \ln W}{\partial \eta_z} \frac{\partial \eta_z}{\partial H_z} \tag{120}$$

Because

$$\eta = \frac{g\beta H_z}{kT}, \quad \frac{\partial \eta_z}{\partial H_z} = \frac{g\beta}{kT} \tag{121}$$

and

$$\langle \mu_z \rangle = kT \frac{\partial \ln W}{\partial \eta} \frac{g\beta}{kT} \tag{122}$$

$$\langle \mu_z \rangle = g\beta \frac{\partial \ln W}{\partial \eta} \tag{123}$$

$$\langle \mu_z \rangle = \frac{g\beta}{W} \frac{\partial W}{\partial \eta}. \tag{124}$$

Plugging in for W,

$$\langle \mu_z \rangle = \frac{g\beta}{\dfrac{\sinh (S + 1/2)\eta_z}{\sinh \eta_z/2}} \frac{\partial \left(\dfrac{\sinh (S + 1/2)\eta_z}{\sinh \eta_z/2} \right)}{\partial \eta} \tag{125}$$

$$\langle \mu_z \rangle = \frac{g\beta}{\dfrac{\sinh (S + 1/2)\eta_z}{\sinh \eta_z/2}} \left[\frac{S + 1/2 \cosh (S + 1/2)\eta_z}{\sinh \eta_z/2} - \frac{1}{2} \frac{\sinh (S + 1/2)\eta_z}{\sinh \eta_z^2/2} \cosh \eta_z/2 \right] \tag{126}$$

where use has been made of the relation

$$\frac{d}{dx} \sinh x = \cosh x. \tag{127}$$

Simplifying,

$$\langle \mu_z \rangle = g\beta [(S + 1/2) \cosh (S + 1/2)\eta_z - 1/2 \coth \eta_z/2]. \tag{128}$$

The Brillouin function in terms of S and η is

$$B_S(\eta) = \frac{1}{S} [(S + 1/2) \cosh (S + 1/2)\eta - 1/2 \coth \eta/2]. \tag{129}$$

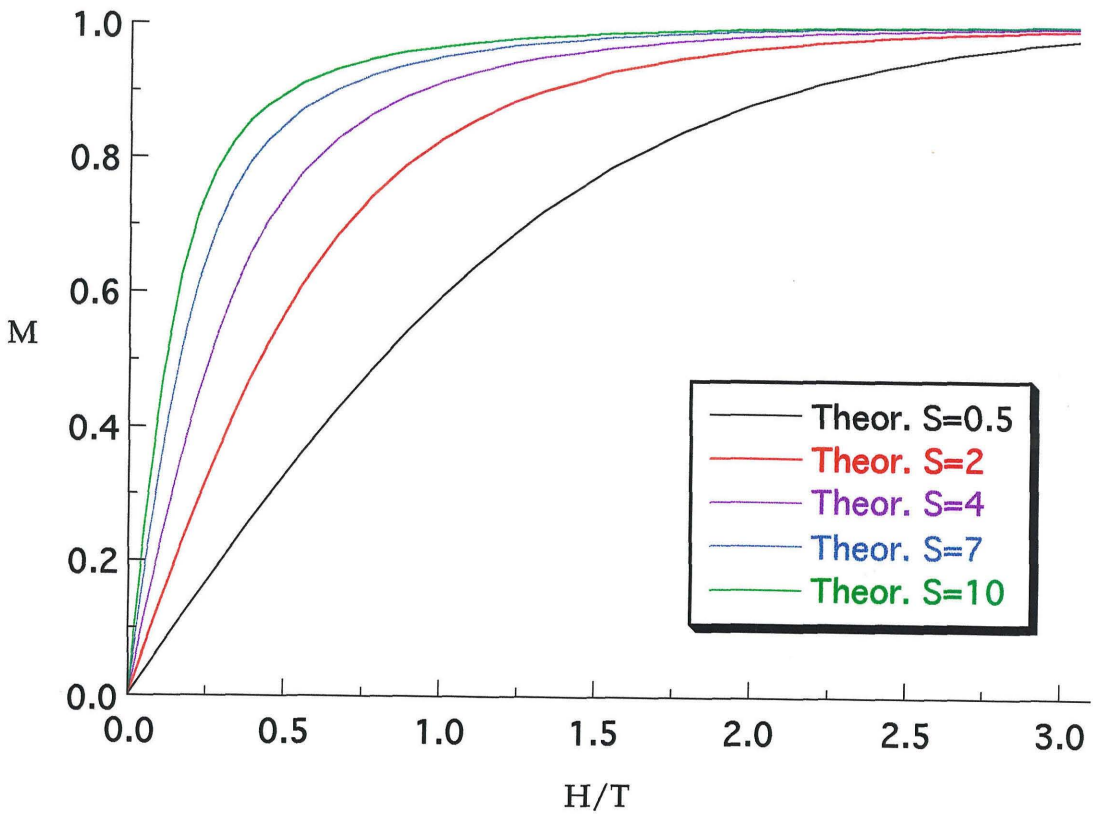

Figure 4.14: Theoretical Saturation Plots for Various S Values.

The average net moment, represented in terms of the Brillouin function, is

$$\langle \mu_z \rangle = g\beta S B_S(\eta). \tag{130}$$

Because the macroscopic magnetization is just the total of the individual moments,

$$M = N\langle \mu_z \rangle = Ng\beta S B_S(\eta). \tag{131}$$

The previously discussed saturation magnetization M_{sat} is defined by $Ng\beta S$. Thus, by measuring the resultant moment as a function of H/T and fitting the data using the Brillouin function, the value of S may be determined.

The observed moment M_{obs} also has a diamagnetic component.

$$M_{obs} = M_{dia} + M_{para} = X_{dia}H + Ng\beta S B_S(\eta) = \chi_{dia}H + M_{sat}B_S(\eta) \tag{132}$$

Thus, by measuring magnetization as a function of H/T and fitting to the Brillouin function, the values S, M_{sat}, and χ_{dia} can be obtained. Alternatively, the diamagnetic suceptibility may be measured from a Curie plot and the M_{dia} contribution subtracted before fitting to the Brillouin function. Implementations of each fit (for the program Kaleidegraph), which operate on the raw data to give S, M_{sat} and X_{dia}, are given in Appendix D.

What is the meaning of this S value? In a pure sample of a single paramagnetic species, the spin state of the species is $2S + 1$, e.g., $S = 0.5$ for a doublet, $S = 1$ for a triplet, etc. In our doped polymer systems, there undoubtably exist distributions of various doped lengths. The observed moment is then due to a distribution of paramagnetic moments. It has been shown that to first order, S in these systems may be regarded as an average of all the individual moments in the sample. The fit to the Brillouin function,

as implemented, introduces a slight bias (≤ 10%) towards a higher *S* value when fitting simulated data from a binary mixture of paramagnetic moments. This bias is small enough compared to the disparity expected between significantly different samples so that no meaningful change in the interpretation of our data is indicated.

Chapter 4 References

1. Mattis, D. C. *The Theory of Magnetism I;* 2nd ed.; Springer-Verlag: New York, 1988; Vol. 17, pp 295.

2. Carlin, R. L. *Magnetochemistry;* Springer-Verlag: New York, 1986, pp 1-328.

3. Hurd, C. M. *Contemp. Phys.* **1982**, *23*, 469-493.

4. Dirac, P. A. M. *The Principles of Quantum Mechanics;* Oxford: Clarendon, 1930.

5. McQuarrie, D. A. *Quantum Chemistry;* University Science Books: Mill Valley, California, 1983.

6. Eisberg, R.; Resnick, R. *Quantum Physics;* 2nd ed., John Wiley and Sons: New York, 1985.

7. Beveridge, D. L.; Pople, J. A. *Approximate Molecular Orbital Theory;* McGraw-Hill: New York, 1970; pp 1-56.

8. Feenberg, E.; Pake, G. E. *Notes on the Quantum Theory of Angular Momentum;* Stanford University: Palo Alto, 1963; pp 1-28.

9. Dougherty, D. A. *Acc. Chem. Res.* **1991**, *24*, 88-94.

10. Dougherty, D. A.; Goldberg, A. H. *J. Am. Chem. Soc.* **1983**, *105*, 284-290.

11. Lowe, J. P. *Quantum Chemistry;* Academic: New York, 1978; pp 107-134.

12. Rowland, C.; Salem, L. *Angew. Chem. I.E.E.* **1972**, *11*, 92-11.

13. Coms, F. D.; Dougherty, D. A.; Jain, R.; Sponsler, M. B. *J. Am. Chem. Soc.* **1988**, *110*, 1356-1366.

14. Coms, F. D.; Dougherty, D. A.; Jain, R.; Sponsler, M. B. *J. Am. Chem. Soc.* **1989,** *111,* 2240-2252.

15. Dougherty, D. A. In *Kinetics and Spectroscopy of Carbenes and Biradicals;* Platz, M. S., Ed.; Plenum: New York, 1990; pp 117-142.

16. Borden, W. T.; Davidson, E. R. *J. Am. Chem. Soc.* **1977,** *99,* 4587-4594.

17. Bolton, J. R.; Wertz, J. E. *Electron Spin Resonance;* Chapman and Hall: London, 1986.

18. Ovchinnikov, A. A. *Theoret. Chim. Acta (Berl.)* **1978,** *47,* 297-304.

19. Kaisaki, D. A. Ph.D. Thesis, California Institute of Technology, 1990.

20. Jacobs, S. J. Ph.D. Thesis, California Institute of Technology, 1994.

Appendix A. Additional Polymer Models for One-Dimensional Polaronic Ferromagnetism

A number of other systems were designed to demonstrate the one-dimensional polaronic ferromagnet (Figure A.1).[1] Acronyms of individual polymers are used; e.g., poly-*meta*-phenylene-*para*-phenylene is **PMP1P**, poly-*meta*-phenylene-(naphthalene) is **PMPN**, etc. Of the precursors, *para*-dibromobenzene and *para*-dibromobiphenyl were commercially available, while *para*-diiodoterphenyl,[2] 2,6-di(trifluoromethanesulfonyl)napthalene,[3] and 2,6-di(trifluoromethanesulfonyl)anthracene[3] were synthesized in one step from terphenyl, 2,6-dihydroxynaphthalene, and 2,6-dihydroxyanthracene. Synthesis of **PMP1P**, **PMP2P**, **PMP3P**, and **PMPN** was accomplished by coupling with 5-tetradecylbenzene-1,3-bis-(1,3,2-benzodioxaborole) under Suzuki conditions.[1] These polymers formed soluble, off-white to brown, flexible films. Doping was accomplished for **PMP1P** and **PMP2P** by exposure of a thin film to gaseous arsenic pentafluoride, and for **PMPN** and **PMP2P** (again) by stirring in THF with sodium metal. After removing excess dopant/solvent under vacuum, the doped samples were submitted for magnetic analysis. Results were unexceptional; samples which gave a strong signal had spin concentrations between 0.77 to 3.7 and *S* values from 0.6 to 0.9 (Table A.1). Representative saturation and effective moment plots are shown in Figure A.2.

Table A.1: *S* values & Spin Concentrations (Parentheses); Measured at 1.8 K.

Polymer	AsF5	Sodium(excess)
PMP1P	12[a] (0.03)	—b—
PMP2P	0.67(0.77)[c]	0.66(1.3)
	0.63(2.9)[d]	0.90(1.4)
PMPN	—b—	0.63(3.7)

a. ±6; fit is extremely poor b. Not performed c. Light doping d. Heavy doping

Scheme A.1: Models for Polaronic Ferromagnetism

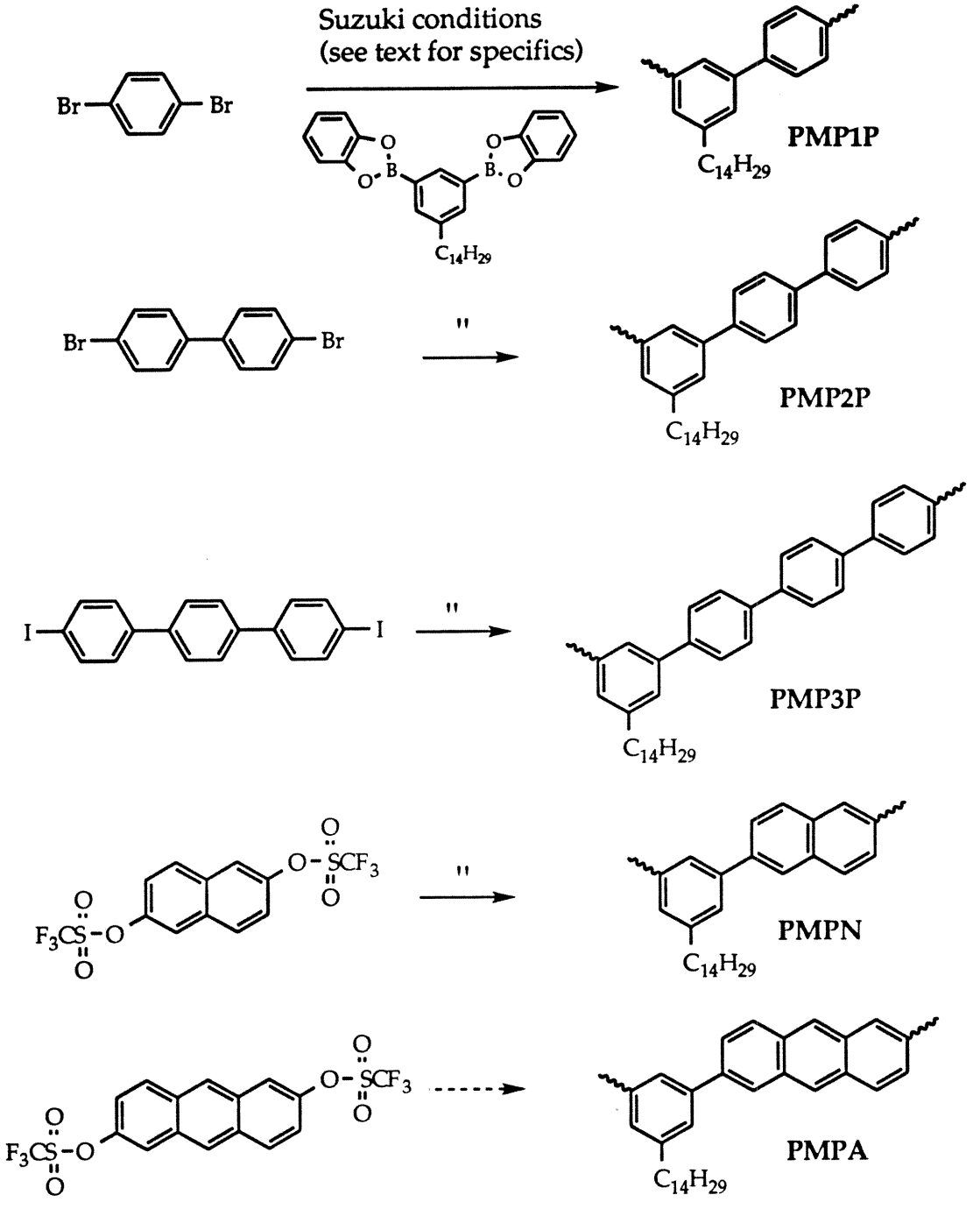

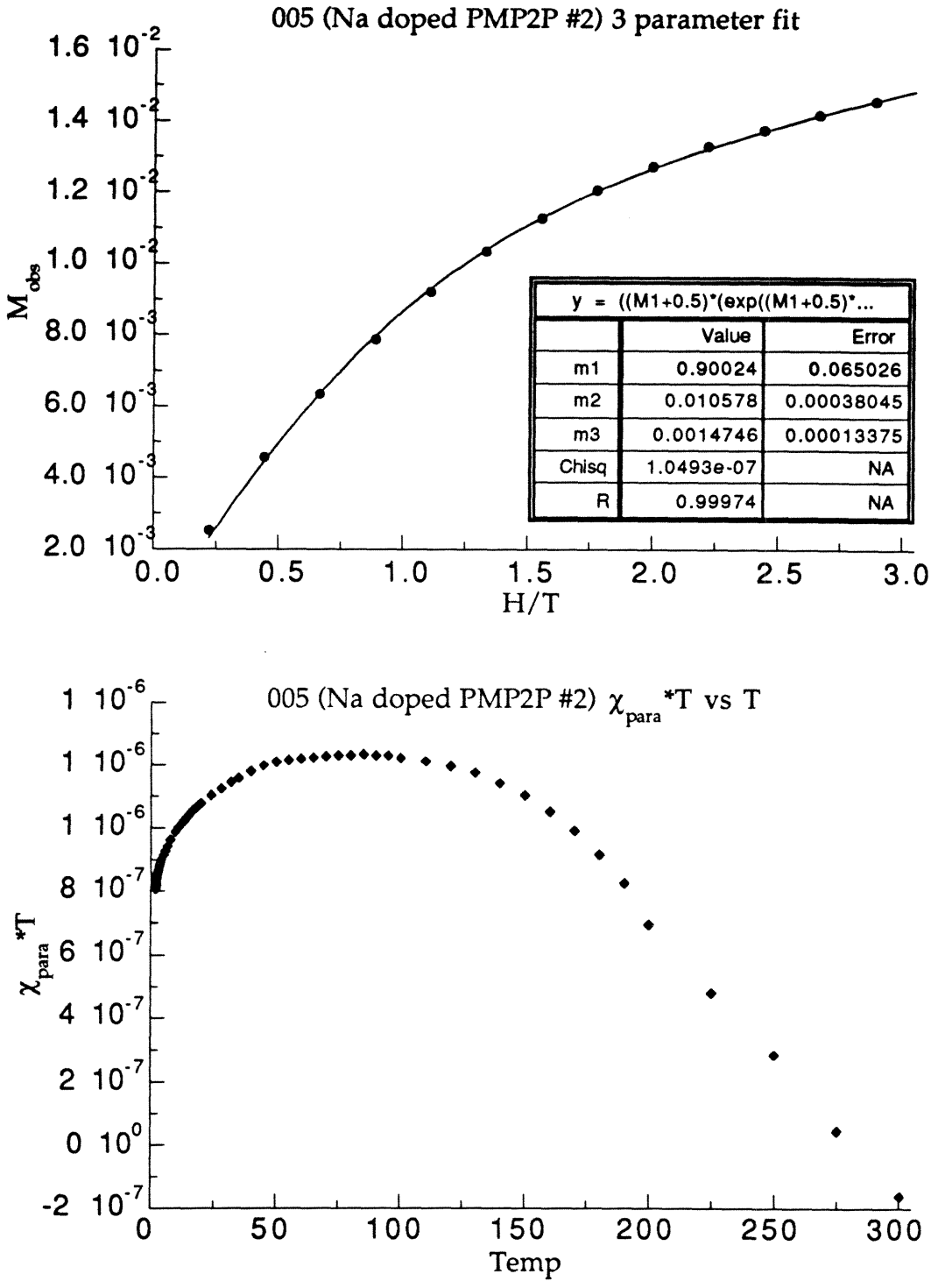

Figure A.1: Representative Plots. Top: **PMP2P**, XS Na, Saturation Plot. Bottom: **PMP2P**, XS Na, Relative Effective Moment Plot.

Poly-*meta*-phenylene-*para*-phenylene (PMP1P)[1] 1,4-Dibromobenzene (0.107 g, 0.000455 mol), 5-tetradecylbenzene-1,3-bis-(1,3,2-benzodioxaborole) (0.217 g, 0.000424 mol), tetrakis(triphenylphosphine) palladium(0) (0.0175 g, 0.0000151 mol) and Na_2CO_3 soln (2 M, 1 mL, 0.002 mol) were added to toluene (50 mL). The mixture was carefully purged with argon, protected from light, refluxed for 7 d, then cooled to room temperature and poured into half-saturated NaCl soln. The mixture was shaken vigorously, separated, and the organic layer reduced to a solid using a rotary evaporator. The sticky black residue was Soxlet-extracted for 24 h with 95% ethanol followed by 24 h with toluene. The toluene fraction was reduced by rotary evaporation followed by 24 h of a 0.1 Torr vacuum to give 0.0624 g (42%) of a soft, brown solid. MW by GPC, in CH_2Cl_2 vs. polystyrene standard, PDI = 1.27, M_n = 5300, M_w = 6730, corresponding to a degree of polymerization of 15-19. 300 MHz ^1H NMR, $CDCl_3$ δ = 0.87, m, 3H; 1.23, s, 22H; 1.7 broad s, 2H; 2.75, broad s, 2H; 7.44, broad s, 3H; 7.75, s, 4H. 300 MHz ^{13}C NMR, $CDCl_3$, δ = 14.7, 23.3, 30.0 (broad), 32.2, 32.5, 36.8, 124.0, 127.0, 127.9, 128.2, 128.5, 129.4, 141.0, 142.0 ppm. FTIR, 2916, 2850, 1590, 1459, 1454, 1383, 1259, 1112, 1009, 824 cm^{-1}. UV/Vis, λ_{max} = 285 nm. Elemental analysis: calculated for $C_{26}H_{36}$, C, 89.59; H, 10.41. Found: C, 79.65; H, 9.65.

Poly-*meta*-phenylene-*para*-biphenylene (PMP2P)[1] 4,4'-Dibromobiphenyl (0.632 g, 0.00203 mol), 5-tetradecylbenzene-1,3-bis-(1,3,2-benzodioxaborole) (1.02 g, 0.00201 mol), tetrakis(triphenylphosphine) palladium(0) (0.0232 g, 0.0000201 mol) and Na_2CO_3 soln (2 M, 5 mL, 0.01 mol) were added to toluene (50 mL). The mixture was carefully purged with argon, protected from light, refluxed for 7 d, then cooled to room temperature and poured into half-saturated NaCl soln. The mixture was shaken vigorously, separated, and the

organic layer reduced to a solid using a rotary evaporator. The sticky black-green residue was Soxlet-extracted for 24 h with 95% ethanol followed by 24 h with THF. The THF fraction was reduced by rotary evaporation followed by 24 h of a 0.1 Torr vacuum to give 0.705 g (83%) of a transparent tan film. MW by GPC, in CH_2Cl_2 vs. polystyrene standard, PDI = 1.3, M_n = 7500, M_w = 9770, corresponding to a degree of polymerization of 18-23. 300 MHz ^1H NMR, $CDCl_3$ δ = 0.86, broad s, 3H; 1.23, s, 22H; 1.73 broad s, 2H; 2.76, broad s, 2H; 7.44, broad s, 3H; 7.71, broad s, 8H. 300 MHz ^{13}C NMR, $CDCl_3$, δ = 14.7, 23.3, 30.0 (broad), 30.9, 32.3, 32.5, 36.8, 124.0, 127.0, 128.0, 128.3, 128.5, 129.4, 132.5, 133.4, 140.2, 141.0, 141.9, 144.7 ppm. FTIR, 2924, 2852, 1596, 1500, 1465, 1388, 1259, 1120, 1003, 817 cm^{-1}. UV/Vis, λ_{max} = 305 nm. Elemental analysis: calculated for $C_{32}H_{40}$, C, 90.51; H, 9.49. Found: C, 85.45; H, 8.95.

***para*-Diiodoterphenyl**[2] *para*-Terphenyl (2.30 g, 0.0100 mol) and iodine (2.54 g, 0.0100 mol) were stirred in carbon tetrachloride. Next, [bis(trifluoroacetoxy)iodo]benzene (4.52 g, 0.0105 mol) was added and the purple mixture was stirred for 1 h. The resultant white precipitate was collected by vacuum filtration and washed with chloroform (100 mL) and diethyl ether (100 mL). The white residue was recrystallized from toluene/carbon tetrachloride to give 3.16 g (66%) of white flakes. MP = 316-317 (lit.[2] 312) °C. Elemental analysis: calculated for $C_{18}H_{12}I_2$, C, 44.84; H, 2.51; I, 52.65. Found: C, 44.55; H, 2.64; I, 52.63.

Poly-*meta*-phenylene-*para*-terphenylene (PMP3P)[1] 4,4''-Diiodoterphenyl (0.239 g, 0.000496 mol), 5-tetradecylbenzene-1,3-bis-(1,3,2-benzodioxaborole) (0.251 g, 0.000491 mol), tetrakis(triphenylphosphine) palladium(0) (0.0032 g, 0.0000028 mol) and Na_2CO_3 soln (2 M, 5 mL, 0.01 mol) were added to toluene (50 mL). The mixture was carefully purged with argon, protected from light,

refluxed for 7 d, then cooled to room temperature and poured into saturated NaCl soln (100 mL) and hydrochloric acid (0.5 M, 100 mL). The mixture was shaken vigorously, separated, and the organic layer reduced to a solid using a rotary evaporator. The tan residue was purified by precipitating three times from chloroform by adding 95% ethanol. The off-white residue was redissolved in chloroform and reduced by rotary evaporation followed by 24 h of a 0.1 Torr vacuum to give 0.178 g (72%) of a translucent white film. MW by GPC, in CH_2Cl_2 vs. polystyrene standard, PDI = 1.71, M_n = 2550, M_w = 4360, corresponding to a degree of polymerization of 5-9. 300 MHz ^1H NMR, $CDCl_3$ δ = 0.96, m, 3H; 1.36, s, 22H; 1.78 broad s, 2H; 2.81, broad s, 2H; 7.53, broad s, 3H; 7.79, broad s, 12H. 300 MHz ^{13}C NMR, $CDCl_3$, δ = 14.3, 22.9, 29.8 (broad), 31.8, 36.4, 123.4, 126.5, 127.4, 127.7, 128.9, 138.0, 139.5, 140.4, 141.3, 144.2 ppm. FTIR, 2923, 2852, 1596, 1500, 1455, 1388, 1261, 1120, 820 cm^{-1}. UV/Vis, λ_{max} = 316 nm. El. analysis: calculated for $C_{38}H_{44}$, C, 91.14; H, 8.86. Found: C, 88.37; H, 8.78.

2,6-Di(trifluoromethanesulfonyl)napthalene[3] 2,6-Dihydroxynapthalene (3.81 g, 0.0238 mol) was stirred in CH_2Cl_2 (150 mL) and cooled to 0 °C. To this was added trifluromethanesulfonic anhydride (10.0 mL, 0.0594 mol) followed by triethylamine (9.9 mL, 0.071 mol). The resultant brown mixture was stirred overnight and then poured into 100 mL of pH 7 buffer (1.20 mol potassium dihydrogen phosphate and 1.60 mol potassium hydrogen phosphate dissolved in 1L of water), and separated. The organic layer was dried over $MgSO_4$, filtered, reduced using a rotary evaporator, and the resulting solid recrystallized three times from toluene/hexanes to give 6.37 g (63%) of white crystals. 300 MHz ^1H NMR, $CDCl_3$, δ = 7.39 ppm, dd, J = 2, 8 Hz, 2H; 7.73, d, J = 2 Hz, 2H; 7.88, d, J = 9 Hz, 2H. 300 MHz ^{13}C NMR, $CDCl_3$, δ = 116.6, 119.4, 121.5, 130.8, 132.3, 147.8 ppm. FTIR, NaCl, ν = 1593, 1508, 1417, 1367, 1246, 1206, 1136,

1100, 935, 884, 849, 799, 764 cm^{-1}. MP = 83-84 °C. Elemental analysis: calculated for $C_{12}H_6F_6O_6S_2$, C, 33.97; H, 1.43; F, 26.87; O, 22.62; S, 15.11. Found: C, 34.09; H, 1.56; F, 26.34; S, 15.58; O unavailible in presence of F, but remainder 25.43.

Poly-*meta*-phenylenenaphthalene (PMPN)[1] Triphenylphosphine (0.0069 g, 0.000026 mol), 2,6-di(trifluoromethanesulfonyl)napthalene (0.465 g, 0.00110 mol), 5-tetradecylbenzene-1,3-bis-(1,3,2-benzodioxaborole) (0.556 g, 0.00109 mol), tris(dibenzylideneacetone) dipalladium(0) (0.0030 g, 0.0000033 mol) and Na_2CO_3 soln (2 M, 3 mL, 0.007 mol) were added to toluene (50 mL). The mixture was carefully purged with argon, protected from light, refluxed for 10 d, then cooled to room temperature and poured into saturated NaCl soln (100 mL) and hydrochloric acid (4 M, 100 mL). The mixture was shaken vigorously, separated, washed with saturated $NaHCO_3$ soln, and the organic layer reduced to a solid using a rotary evaporator. The grey residue was purified by precipitating three times from chloroform by adding 95% ethanol. The grey residue was redissolved in chloroform and reduced by rotary evaporation followed by 24 h of a 0.1 Torr vacuum to give 0.433 g (quantitative) of a translucent grey film. MW by GPC, in CH_2Cl_2 vs. polystyrene standard, PDI = 1.28, M_n = 3560, M_w = 4670, corresponding to a degree of polymerization of 9-12. 300 MHz ^1H NMR, $CDCl_3$ δ = 0.87, m, 3H; 1.26, s, 22H; 1.77 broad s, 2H; 2.81, broad s, 2H; 7.2-7.8, m, 9H. 300 MHz ^{13}C NMR, $CDCl_3$, δ = 14.3, 22.9, 29.8, 31.9, 32.1, 36.5, 124.1, 125.8, 126.3, 126.8, 128.9, 133.1, 138.9, 141.8, 144.4 ppm. FTIR, 3056, 3026, 2915, 2845, 1588, 1457, 1422, 1211, 1141, 869, 809 cm^{-1}. UV/Vis, λ_{max} = 270, 318 nm. Elemental analysis: calculated for $C_{30}H_{38}$, C, 90.39; H, 9.61. Found: C, 86.65; H, 8.93.

2,6-Di(trifluoromethanesulfonyl)anthracene[3] 2,6-Dihydroxyanthracene (3.80 g, 0.0181 mol) was stirred in CH_2Cl_2 (200 mL) and cooled to -78 °C. To this was added trifluromethanesulfonic anhydride (9.6 mL, 0.057 mol) followed by triethylamine (12 mL, 0.090 mol). The resultant light brown mixture was allowed to warm to room temperature, stirred overnight and then poured into 200 mL of aqueous pH 7 buffer (1.20 mol potassium dihydrogen phosphate and 1.60 mol potassium hydrogen phosphate dissolved in 1L of water), and separated. The organic layer was dried over $MgSO_4$, filtered, reduced using a rotary evaporator, and the resulting solid recrystallized five times from toluene/hexanes to give 1.40 g (63%) of white crystals. 300 MHz ^1H NMR, $CDCl_3$, δ = 7.16 ppm, s, 2H; 7.64 ppm, dd, J = 3, 9 Hz, 2H; 8.12, d, J = 2 Hz, 2H; 8.38, d, J = 9 Hz, 2H. FTIR, NaCl, ν = 1668, 1588, 1422, 1317, 1296, 1246, 1206, 1131, 985, 924, 894, 859, 829, 743, 708 cm^{-1}. MP = 216 °C. Elemental analysis: calculated for $C_{16}H_8F_6O_6S_2$, C, 40.51; H, 1.70; F, 24.03; O, 22.24; S, 13.52. Found: C, 38.21; H, 1.17; F, 23.92; S, 13.44; O unavailible in presence of F, but remainder 23.26.

Appendix A References

1. See chapter 2 in this thesis and references therin.

2. Merkushev, E. B.; Yudina, N. D. *Zh. Org. Khim.* **1981**, *17*, 2598-2601.

3. Imhoff, M. A.; Summerville, R. H.; Schleyer, Paul v. R.; Martinez, A. G.; Hanack, M.; Dueber, T. E.; Stang, P. J. *J. Amer. Chem. Soc.* **1970**, *92*, 3802-3804.

Appendix B. Crystal Structure Data for Bisgalvinol V

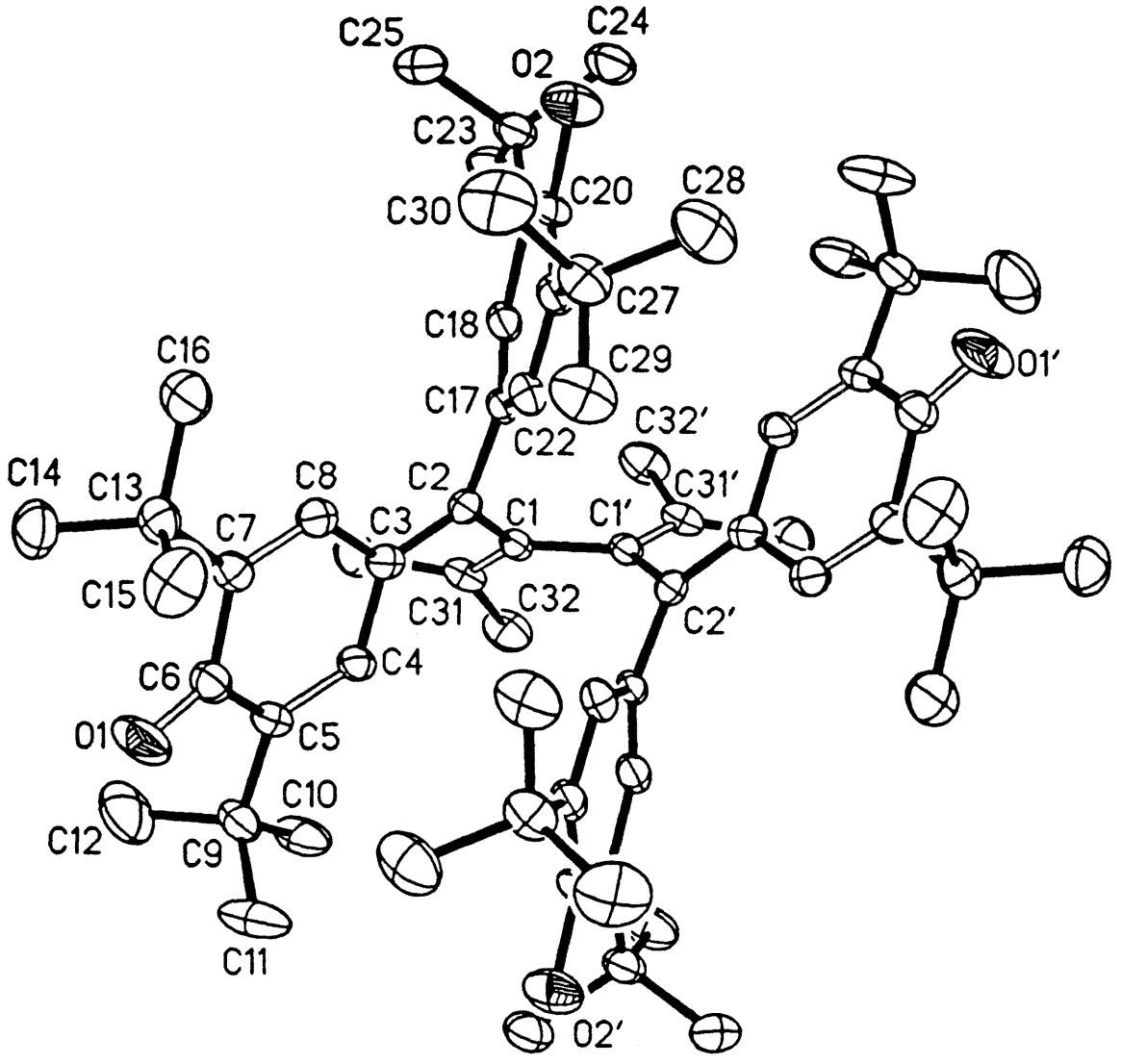

Figure B.1: ORTEP Plot of Bisgalvinol **V**

X-ray Diffraction Study of Bisgalvinol V

Crystals of bisgalvinol V (Chapter 3) were grown from a saturated methanol solution. The grown crystals were submitted to the X-ray Diffraction Center at the Department of Chemistry, University of California-Irvine, run by Dr. Joseph Ziller. Experimental details and data follow.

Collection of X-ray Diffraction Data

An orange crystal of approximate dimensions 0.27 X 0.33 X 0.40 mm was oil-mounted on a glass fiber and transferred to the Siemens P3 diffractometer (which is equipped with a modified LT-2 low temperature system). Determination of Laue symmetry, crystal class, unit cell parameters and the crystal's orientation matrix were carried out by previously described techniques similar to those of Churchill.[1] Low temperature (158 K) intensity data were collected via a θ–2θ scan technique with MoKα radiation under the conditions given in Table B.1.

All 4280 data were corrected for Lorentz and polarization effects and placed on an approximately absolute scale. Any reflection with I(net) < O was assigned the value $|F_o| = 0$. The systematic extinctions observed were *hkl* for $h+k = 2n+1$ and *h0l* for $l = 2n+1$; the diffraction symmetry was 2/m. The two possible monoclinic space groups are Cc [C^4_s ; No. 9] or C2/c [C^6_{2h}; No. 15]. The centrosymmetric space group C2/c was later determined to be the correct choice.

Solution and Refinement of the Crystal Structure

All crystallographic calculations were carried out using either the UCI modified version of the UCLA Crystallographic Computing Package[2] or the SHELXTL PLUS program set.[3] The analytical scattering factors for neutral atoms were used throughout the analysis;[4a] both the real ($\Delta f'$) and imaginary ($i\Delta f''$) components of anomalous dispersion were included. The quantity

minimized during least-squares analysis was $Sw(|F_o|-|F_c|)^2$ where $w^{-1} = \sigma^2(|F_o|) + 0.0007(|F_o|)^2$.

The structure was solved by direct methods (SHELXTL PLUS), and refined by full-matrix least-squares techniques. The molecule is located about a two-fold rotation axis (0, y, 1/4). Hydrogen atoms were included using a riding model with d(C-H) = 0.96 Å, d(O-H) 0.85 Å and U(iso) = 0.08 $Å^2$. Refinement of positional and anisotropic thermal parameters led to convergence with R_F = 7.1%, R_{wF} = 7.2% and GOF = 1.50 for 317 variables refined against the 2773 data with $|F_o| > 3.0\sigma(|F_o|)$. A final difference-Fourier map was "clean," ρ(max) = 0.28 $eÅ^{-3}$.

Appendix B References

1. Churchill, M. R.; Lashewycz, R. A.; Rotella, F. *J. Inorg. Chem.* **1977**, *16*, 265.

2. UCLA Crystallographic Computing Package, University of California Los Angeles, 1981, C. Strouse; personal communication.

3. Siemens Analytical X-Ray Instruments, Inc.,; Madison, WI 1990.

4. *International Tables for X-Ray Crystallography*; Kynoch Press: Birmingham, England, 1974; (a) pp 99-101; (b) pp 149-150.

* The ORTEP plot is shown at the 50~ probability level.

Acknowledgement. Funds for the purchase of the Siemens R3m/V diffractometer system were made available to UCI from the National Science Foundation under Grant CHE-85-14495.

Table B.1: Experimental Data for the X-ray Diffraction Study

Formula: $C_{66}H_{94}O_4$

Fw: 951.4

Temperature (K): 158

Crystal System: Monoclinic

Space Group: C2/c

$\underline{a}$ = 17.650(4) Å

$\underline{b}$ = 18.434(5) Å

$\underline{c}$ = 19.199(4) Å

β = 104.88(2)°

$\underline{V}$ = 6037(2) A3

Z = 4

D_{calcd} Mg/m^3 = 1.05

Diffractometer: Siemens P3 (R3m/V System)

Radiation: MoKα (λ = 0.710730 Å)

Monochromator: Highly oriented graphite

Data Collected: $+h, +k, +l$

Scan Type: θ-2θ

Scan Range: 1.20° plus Kα-separation

Scan Speed: 3.0 deg min^{-1} (in ω)

2θ Range: 4.0 to 45.0°

μ(MoKα), mm^{-1} = 0.059

Reflections Collected: 4280

Reflections with $|F_o| > 3.0\sigma(|F_o|$: 2773

No. of Variables: 317

R_F = 7.11%, R_{wF} = 7.2%

Goodness of Fit: 1.50

Table B.2: Atomic Coordinates ($X10^4$) and Equivalent Isotropic Displacement Coefficients ($Å^2$ $X10^4$)

	x	y	z	U(eq)
C(1)	-393(2)	6051(2)	2234(2)	216(13)
C(2)	-600(2)	6739(2)	1818(2)	221(14)
C(3)	-1288(2)	7109(2)	1798(2)	231(14)
C(4)	-1813(2)	6882(2)	2227(2)	244(14)
C(5)	-2520(2)	7198(2)	2183(2)	272(15)
C(6)	-2726(2)	7863(2)	1748(2)	308(16)
C(7)	-2223(2)	8087(2)	1273(2)	258(14)
C(8)	-1551(2)	7713(2)	1311(2)	253(14)
C(9)	-3101(2)	6894(2)	2586(2)	333(16)
C(10)	-2819(3)	6163(2)	2942(2)	468(19)
C(11)	-3200(3)	7411(3)	3181(3)	555(21)
C(12)	-3896(3)	6755(3)	2038(3)	664(23)
C(1)	-2470(2)	8731(2)	760(2)	296(15)
C(14)	-3309(3)	8622(3)	290(2)	467(18)
C(15)	-2434(3)	9431(2)	1201(3)	533(20)
C(16)	-1937(3)	8822(2)	250(2)	440(18)
C(17)	-25(2)	7041(2)	1443(2)	203(13)
C(18)	241(2)	6620(2)	949(2)	266(14)
C(19)	701(2)	6914(2)	521(2)	266(14)
C(20)	910(2)	7655(2)	636(2)	277(15)
C(21)	691(2)	8086(2)	1146(2)	257(14)
C(22)	208(2)	7766(2)	1533(2)	256(15)
C(23)	906(2)	6462(2)	-83(2)	313(15)
C(24)	1799(2)	6442(2)	-25(2)	411(17)
C(25)	456(3)	6774(3)	-822(2)	439(18)
C(26)	637(3)	5675(2)	-67(2)	407(18)
C(27)	924(2)	8892(2)	1261(2)	352(17)
C(28)	1814(3)	8978(3)	1502(3)	535(20)
C(29)	596(3)	9238(2)	1850(3)	475(19)
C(30)	586(3)	9327(2)	566(3)	592(22)
C(31)	-897(2)	5482(2)	2157(2)	273(15)
C(32)	-801(3)	4851(2)	2673(2)	396(17)
C(33)	-1626(2)	5421(2)	1540(2)	363(16)
O(1)	-3297(2)	8236(2)	1784(2)	530(13)
O(2)	1353(2)	7960(2)	212(2)	441(12)

* Equivalent isotropic U defined as one third of the trace of the orthogonalized U_{ij} tensor

Table B.3: Interatomic Distances (A) with Esd's

C(1)-C(2)	1.493(5)	C(1)-C(31)	1.359(5)
C(1)-C(1')	1.498(6)	C(2)-C(3)	1.386(5)
C(2)-C(17)	1.495(6)	C(3)-C(4)	1.449(6)
C(3)-C(8)	1.451(5)	C(4)-C(S)	1.361(6)
C(S)-C(6)	1.476(5)	C(5)-C(9)	1.540(6)
C(6)-C(7)	1.485(6)	C(6)-O(1)	1.236(5)
C(7)-C(8)	1.359(6)	C(7)-C(13)	1.532(5)
C(9)-C(10)	1.534(6)	C(9)-C(11)	1.532(7)
C(9)-C(12)	1.544(6)	C(13)-C(14)	1.538(5)
C(13)-C(15)	1.535(6)	C(13)-C(16)	1.530(7)
C(17)-C(18)	1.396(6)	C(17)-C(22)	1.395(5)
C(18)-C(19)	1.403(6)	C(19)-C(20)	1.418(6)
C(19)-C(23)	1.545(6)	C(20)-C(21)	1.389(6)
C(20)-O(2)	1.384(5)	C(21)-C(22)	1.397(6)
C(21)-C(27)	1.542(5)	C(23)-C(24)	1.552(6)
C(23)-C(25)	1.549(5)	C(23)-C(26)	1.529(6)
C(27)-C(28)	1.527(6)	C(27)-C(29)	1.536(7)
C(27)-C(30)	1.539(6)	C(31)-C(32)	1.508(6)
C(31)-C(33)	1.513(5)		

Table B.4: Interatomic Angles (Deg.) with Esd's.

C(2)-C(1)-C(31)	122.3(3)	C(2)-C(1)-C(1')	114.9(2)
C(31)-C(1)-C(1')	122.7(3)	C(1)-C(2)-C(3)	121.7(4)
C(1)-C(2)-C(17)	118.2(3)	C(3)-C(2)-C(17)	120.1(3)
C(2)-C(3)-C(4)	121.7(3)	C(2)-C(3)-C(8)	121.9(4)
C(4)-C(3)-C(8)	116.3(3)	C(3)-C(4)-C(5)	123.4(3)
C(4)-C(5)-C(6)	118.7(4)	C(4)-C(5)-C(9)	122.1(3)
C(6)-C(S)-C(9)	119.2(3)	C(S)-C(6)-C(7)	118.6(4)
C(S)-C(6)-O(1)	121.1(4)	C(7)-C(6)-O(1)	120.3(4)
C(6)-C(7)-C(8)	118.6(3)	C(6)-C(7)-C(13)	119.6(3)
C(8)-C(7)-C(13)	121.8(4)	C(3)-C(8)-C(7)	123.6(4)
C(S)-C(9)-C(10)	111.2(3)	C(S)-C(9)-C(11)	111.5(3)
C(10)-C(9)-C(11)	107.5(4)	C(S)-C(9)-C(12)	108.9(4)
C(10)-C(9)-C(12)	107.0(4)	C(11)-C(9)-C(12)	110.7(4)
C(7)-C(13)-C(14)	110.3(3)	C(7)-C(13)-C(15)	109.4(3)
C(14)-C(13)-C(15)	109.3(3)	C(7)-C(13)-C(16)	112.1(3)
C(14)-C(13)-C(16)	107.2(3)	C(1S)-C(13)-C(16)	108.4(3)
C(2)-C(17)-C(18)	120.5(3)	C(2)-C(17)-C(22)	120.8(3)
C(18)-C(17)-C(22)	118.5(4)	C(17)-C(18)-C(19)	121.9(4)
C(18)-C(19)-C(20)	116.6(4)	C(18)-C(19)-C(23)	120.9(3)
C(20)-C(19)-C(23)	122.4(4)	C(19)-C(20)-C(21)	123.5(4)
C(19)-C(20)-O(2)	117.6(4)	C(21)-C(20)-O(2)	118.9(3)
C(20)-C(21)-C(22)	116.8(3)	C(20)-C(21)-C(27)	122.6(4)
C(22)-C(21)-C(27)	120.5(4)	C(17)-C(22)-C(21)	122.6(4)
C(19)-C(23)-C(24)	112.9(3)	C(19)-C(23)-C(25)	108.9(3)
C(24)-C(23)-C(25)	110.3(4)	C(19)-C(23)-C(26)	111.3(4)
C(24)-C(23)-C(26)	106.9(3)	C(25)-C(23)-C(26)	106.4(3)
C(21)-C(27)-C(28)	111.0(3)	C(21)-C(27)-C(29)	111.6(4)
C(28)-C(27)-C(29)	106.6(3)	C(21)-C(27)-C(30)	110.4(3)
C(28)-C(27)-C(30)	110.4(4)	C(29)-C(27)-C(30)	106.6(4)
C(1)-C(31)-C(32)	124.3(3)	C(1)-C(31)-C(33)	122.9(3)
C(32)-C(31)-C(33)	112.8(3)		

Table B.5: Anisotropic Displacement Coefficients ($Å^2$ X10^4)

	U_{11}	U_{22}	U_{33}	U_{12}	U_{13}	U_{23}
C(1)	183(20)	240(21)	242(22)	-5(18)	84(17)	-35(18)
C(2)	213(22)	251(22)	191(21)	-23(18)	38(18)	-45(18)
C(3)	242(23)	232(22)	226(22)	-51(19)	73(19)	-41(19)
C(4)	222(23)	276(22)	243(22)	-53(19)	76(19)	-42(18)
C(5)	255(24)	319(25)	273(24)	10(19)	125(20)	-1(20)
C(6)	264(25)	343(26)	323(25)	15(21)	90(21)	-44(21)
C(7)	256(23)	233(22)	293(23)	7(19)	86(20)	-33(19)
C(8)	253(23)	253(22)	251(23)	-50(19)	65(19)	-25(19)
C(9)	250(24)	372(26)	416(26)	44(21)	153(21)	81(22)
C(10)	467(30)	524(31)	527(31)	-10(25)	333(26)	91(26)
C(11)	722(37)	500(31)	640(34)	116(28)	531(31)	92(27)
C(12)	352(31)	841(42)	830(40)	-82(29)	209(30)	216(33)
C(13)	277(24)	253(23)	350(25)	56(19)	66(21)	38(20)
C(14)	373(28)	520(30)	461(29)	79(24)	19(24)	113(24)
C(15)	670(36)	333(27)	548(33)	78(25)	65(28)	28(25)
C(16)	406(28)	425(28)	499(30)	119(23)	136(24)	213(24)
C(17)	139(21)	238(23)	231(22)	12(18)	49(18)	27(18)
C(18)	188(22)	296(23)	308(24)	-9(19)	54(19)	44(20)
C(19)	215(22)	330(25)	261(23)	-15(19)	77(19)	15(19)
C(20)	218(23)	324(24)	323(24)	-73(20)	130(20)	66(21)
C(21)	189(22)	287(23)	293(23)	0(19)	61(20)	25(20)
C(22)	200(22)	244(23)	315(24)	14(18)	52(20)	19(19)
C(23)	274(24)	386(25)	318(25)	-38(20)	147(21)	-44(21)
C(24)	361(26)	512(29)	422(27)	-1(24)	211(22)	-53(24)
C(25)	431(28)	602(32)	323(27)	-68(25)	167(23)	38(24)
C(26)	427(28)	374(27)	485(30)	-60(22)	237(24)	-112(23)
C(27)	376(27)	230(23)	478(29)	-72(20)	158(24)	45(21)
C(28)	465(32)	434(29)	752(37)	-172(25)	237(28)	-145(27)
C(29)	543(32)	279(25)	662(34)	-127(23)	263(28)	-79(24)
C(30)	799(40)	304(27)	735(38)	-7(27)	307(32)	166(26)
C(31)	259(24)	255(23)	354(25)	12(19)	171(21)	2(19)
C(32)	406(28)	325(25)	512(29)	-54(21)	219(24)	88(23)
C(33)	304(26)	374(26)	409(27)	-110(21)	88(22)	-124(22)
O(1)	444(20)	589(22)	662(23)	280(17)	333(18)	211(18)
O(2)	504(20)	365(18)	532(20)	-153(15)	272(17)	37(15)

The anisotropic displacement exponent takes the form:

$-2\pi^2 (h^2a^{*2}U_{11} + ... + 2hka^*b^*U_{12})$

Table B.6: H-Atom Coordinates ($X10^4$) and Isotropic Displacement Coefficients ($Å^2$ $X10^4$).

	x	y	z	U
H(4A)	-1653	6489	2561	800
H(8A)	-1231	7855	998	800
H(10A)	-2755	5826	2579	800
H(10B)	-2325	6227	3293	800
H(10C)	-3199	5978	3175	800
H(11A)	-2698	7489	3515	800
H(11B)	-3406	7865	2969	800
H(11C)	-3554	7205	3432	800
H(12A)	-3819	6428	1673	800
H(12B)	-4256	6544	2281	800
H(12C)	-4107	7204	1818	800
H(14A)	-3339	8184	13	800
H(14B)	-3667	8591	591	800
H(14C)	-3447	9028	-31	800
H(1SA)	-1909	9493	1498	800
H(1SB)	-2572	9837	880	800
H(1SC)	-2792	9400	1502	800
H(16A)	-1952	8392	-35	800
H(16B)	-2115	9228	-62	800
H(16C)	-1409	8907	530	800
H(18A)	109	6114	905	800
H(22A)	36	8054	1880	800
H(24A)	1990	6928	-36	800
H(24B)	2064	6215	422	800
H(24C)	1897	6171	-421	800
H(25A)	-97	6782	-856	800
H(25B)	635	7258	-872	800
H(25C)	553	6475	-1200	800
H(26A)	83	5657	-107	800
H(26B)	749	5414	-462	800
H(26C)	916	5458	381	800
H(28A)	1951	9482	1571	800
H(28B)	2009	8722	1949	800
H(28C)	2042	8778	1141	800
H(29A)	746	9740	1908	800
H(29B)	33	9202	1717	800
H(29C)	804	8986	2296	800
H(30A)	734	9827	648	800
H(30B)	791	9137	186	800
H(30C)	24	9288	431	800
H(32A)	-331	4915	3055	800

H(32B)	-1246	4829	2874	800
H(32C)	-765	4409	2419	800
H(33A)	-1659	5833	1228	800
H(33B)	-1600	4986	1272	800
H(33C)	-2081	5405	1727	800
H(2A)	1434	8402	336	800

Table B.7: Fractional Coordinates for All Atoms (Including Symmetry Equivalents)

ATOM	X	Y	Z
C1	-0.03931	0.60512	0.22335
C2	-0.05997	0.67388	0.18176
C3	-0.12883	0.71093	0.17981
C4	-0.18127	0.68819	0.22266
C5	-0.25202	0.71982	0.21828
C6	-0.27265	0.78633	0.17478
C7	-0.22233	0.80871	0.12733
C8	-0.15506	0.77130	0.13113
C9	-0.31007	0.68939	0.25861
C10	-0.28186	0.61631	0.29418
C11	-0.31998	0.74109	0.31813
C12	-0.38959	0.67549	0.20382
C13	-0.24696	0.87309	0.07604
C14	-0.33093	0.86216	0.02901
C15	-0.24337	0.94308	0.12009
C16	-0.19373	0.88215	0.02504
C17	0.00249	0.70414	0.14426
C18	0.02412	0.66199	0.09493
C19	0.07006	0.69140	0.05211
C20	0.09098	0.76553	0.06362
C21	0.06913	0.80860	0.11459
C22	0.02082	0.77659	0.15326
C23	0.09058	0.64616	-0.00827
C24	0.17987	0.64418	-0.00250
C25	0.04558	0.67742	-0.08224
C26	0.06366	0.56749	-0.00672
C27	0.09238	0.88920	0.12606
C28	0.18135	0.89781	0.15020
C29	0.05956	0.92384	0.18498
C30	0.05857	0.93268	0.05663
C31	-0.08973	0.54822	0.21573
C32	-0.08008	0.48515	0.26730
C33	-0.16256	0.54208	0.15399
O1	-0.32972	0.82363	0.17844

O2	0.13532	0.79600	0.02125
C1A	0.03930	0.60512	0.27665
C2A	0.05996	0.67388	0.31824
C3A	0.12883	0.71093	0.32019
C4A	0.18126	0.68819	0.27734
C5A	0.25202	0.71982	0.28172
C6A	0.27265	0.78633	0.32522
C7A	0.22232	0.80871	0.37267
C8A	0.15506	0.77130	0.36887
C9A	0.31007	0.68939	0.24139
C10A	0.28186	0.61631	0.20582
C11A	0.31997	0.74109	0.18187
C12A	0.38958	0.67549	0.29618
C13A	0.24696	0.87310	0.42396
C14A	0.33093	0.86216	0.47099
C1SA	0.24337	0.94308	0.37991
C16A	0.19373	0.88215	0.47496
C17A	0.00248	0.70414	0.35574
C18A	-0.02412	0.66199	0.40507
C19A	-0.07006	0.69140	0.44789
C20A	-0.09098	0.76554	0.43638
C21A	-0.06913	0.80860	0.38541
C22A	-0.02082	0.77659	0.34674
C23A	-0.09058	0.64617	0.50827
C24A	-0.17987	0.64418	0.50250
C25A	-0.04558	0.67742	0.58224
C26A	-0.06366	0.56749	0.50672
C27A	-0.09238	0.88920	0.37394
C28A	-0.18135	0.89781	0.34980
C29A	-0.05957	0.92385	0.31502
C30A	-0.05857	0.93268	0.44337
C31A	0.08973	0.54822	0.28427
C32A	0.08007	0.48516	0.23270
C33A	0.16256	0.54209	0.34601
O1A	0.32972	0.82363	0.32156
O2A	-0.13533	0.79600	0.47875
H4A	-0.16527	0.64888	0.25606
H8B	-0.12310	0.78548	0.09977
H10A	-0.27553	0.58261	0.25791
H10B	-0.23250	0.62273	0.32930
H10C	-0.31992	0.59783	0.31754
H11A	-0.26978	0.74894	0.35154
H11B	-0.34057	0.78649	0.29695
H11C	-0.35543	0.72046	0.34322
H12A	-0.38186	0.64279	0.16728
H12B	-0.42556	0.65436	0.22805

H12C	-0.41070	0.72039	0.18178
H14A	-0.33392	0.81842	0.00127
H14B	-0.36668	0.85913	0.05914
H14C	-0.34471	0.90281	-0.00306
H15A	-0.19090	0.94935	0.14983
H15B	-0.25722	0.98367	0.08795
H15C	-0.27919	0.93999	0.15016
H16A	-0.19522	0.83915	-0.00351
H16B	-0.21149	0.92279	-0.00621
H16C	-0.14091	0.89068	0.05301
H18A	0.01090	0.61141	0.09054
H22A	0.00358	0.80542	0.18797
H24A	0.19896	0.69281	-0.00355
H24B	0.20639	0.62149	0.04224
H24C	0.18967	0.61713	-0.04209
H25A	-0.00969	0.67822	-0.08562
H25B	0.06351	0.72583	-0.08718
H25C	0.05528	0.64749	-0.12002
H26A	0.00829	0.56569	-0.01067
H26B	0.07491	0.54142	-0.04625
H26C	0.09163	0.54578	0.03808
H28A	0.19505	0.94816	0.15706
H28B	0.20089	0.87224	0.19488
H28C	0.20418	0.87779	0.11406
H29A	0.07456	0.97396	0.19080
H29B	0.00334	0.92017	0.17167
H29C	0.08037	0.89858	0.22964
H30A	0.07336	0.98268	0.06475
H30B	0.07914	0.91369	0.01859
H30C	0.00237	0.92882	0.04307
H32A	-0.03311	0.49154	0.30546
H32B	-0.12457	0.48287	0.28741
H32C	-0.07650	0.44092	0.24193
H33A	-0.16590	0.58334	0.12279
H33B	-0.16001	0.49858	0.12719
H33C	-0.20808	0.54053	0.17269
H32D	0.03311	0.49154	0.19454
H32E	0.12457	0.48287	0.21259
H32F	0.07650	0.44092	0.25807
H33D	0.16590	0.58335	0.37721
H33E	0.16001	0.49858	0.37281
H33F	0.20807	0.54053	0.32731
H4AA	0.16526	0.64888	0.24394
H8AA	0.12310	0.78548	0.40023
H18B	-0.01091	0.61141	0.40946
H22B	-0.00358	0.80542	0.31203

H10D	0.27552	0.58261	0.24209
H10E	0.23249	0.62274	0.17070
H10F	0.31992	0.59783	0.18246
H11D	0.26978	0.74894	0.14846
H11E	0.34057	0.78649	0.20305
H11F	0.35543	0.72046	0.15678
H12D	0.38186	0.64279	0.33272
H12E	0.42556	0.65436	0.27195
H12F	0.41069	0.72039	0.31822
H14D	0.33392	0.81842	0.49873
H14E	0.36668	0.85913	0.44086
H14F	0.34471	0.90281	0.50306
H15D	0.19090	0.94935	0.35017
H15E	0.25721	0.98368	0.41205
H15F	0.27919	0.93999	0.34984
H16D	0.19522	0.83915	0.50351
H16E	0.21148	0.92279	0.50621
H16F	0.14090	0.89068	0.44699
H24D	-0.19896	0.69281	0.50355
H24E	-0.20639	0.62149	0.45776
H24F	-0.18967	0.61713	0.54209
H25D	0.00969	0.67823	0.58562
H25E	-0.06351	0.72583	0.58718
H25F	-0.05529	0.64749	0.62002
H26D	-0.00830	0.56569	0.51067
H26E	-0.07492	0.54142	0.54625
H26F	-0.09163	0.54579	0.46192
H28D	-0.19506	0.94816	0.34294
H28E	-0.20089	0.87224	0.30512
H28F	-0.20418	0.87779	0.38594
H29D	-0.07457	0.97396	0.30920
H29E	-0.00335	0.92018	0.32833
H29F	-0.08037	0.89858	0.27036
H30D	-0.07336	0.98268	0.43525
H30E	-0.07914	0.91369	0.48141
H30F	-0.00238	0.92882	0.45693
H2A	0.14345	0.84016	0.03363
H2AA	-0.14345	0.84016	0.46637

STRUCTURE DETERMINATION SUMMARY

Table B.8: Crystal Data.

Empirical Formula	$C_{66}H_{94}O_4$	
Color; Habit	Orange prism	
Crystal Size (mm)	0.27 X 0.33 X 0.40	
Crystal System	Monoclinic	
Space Group	C2/c	
Unit Cell Dimensiona		a = 17.650(4) A
		b = 18.434(5) A
		c = 19.199(4) A
		β = 104.88(2)°
Volume		6037(2) Å^3
Z		4
Formula weight		951.4
Density(calc.)		1.047 Mg/m^3
Absorption Coefficient		0.059 mm^{-1}
F(000)	2088	

Table B.9: Data Collection.

Diffractometer System	Siemens R3m/V
Radiation	MoKα (λ = 0.71073 Å)
Temperature (K)	158
Monochromator	Highly oriented graphite crystal
2θ Range	4.0 to 45.0°
Scan Type	9-2
Scan Speed	Fixed; 3.00° /min. in ω
Scan Range (ω)	1.20° plus Kα-separation
Background Measurement	Estimated from 96 step profile
Standard Reflections	2 measured every 98 reflections
Index Ranges	$0 \leq h \leq 19$, $0 \leq k \leq 19$
	$-20 \leq l \leq 20$
Reflections Collected	4280
Independent Reflections	3492 (R_{int} = 1.3%); ($\|F_o\| > 0$)
Observed Reflections	2773 ($\|F_o\| > 3.0\sigma(\|F_o\|)$)

Table B.10: Solution and Refinement

System Used (MicroVAX II)	Siemens SHELXTL PLUS
Solution	Direct Methods
Refinement Method	Full-Matrix Least-Squares
Quantity Minimized	$\Sigma w(\|F_o\| - \|F_c\|)^2$
Extinction Correction	$\chi = 0.00009(4)$, where $F^* = F [1 + 0.002\chi F^2/\sin(2\theta)]^{-1/4}$
Hydrogen Atoms	Riding model, fixed isotropic U
Weighting Scheme	$w^{-1} = \sigma^2(\|F_o\|) + 0.0007(\|F_o\|)^2$
Final R Indices (obs. data)	$R_F = 7.1\%$, $R_{wF} = 7.2$
Goodness-of-Fit	1.50
Number of Variables	317
Data-to-Parameter Ratio	8.7:1
Largest and Mean Δ/σ	0.001, < 0.001
Largest Difference Peak	0.28 eÅ^{-3}
Largest Difference Hole	-0.31 eÅ^{-3}

Appendix C. Additional Synthetic Procedures

Tetraphenol Analogs

I wanted to make a number of analogs of tetraphenol **I** (Chapter 3) where two of the phenols, one from each side of the central cyclobutane, were replaced with less bulky substituents such as phenyl, methyl, hydrogen, and *tert*-butyl (actually, the latter turns out to be more hindered) (Figure C.1).

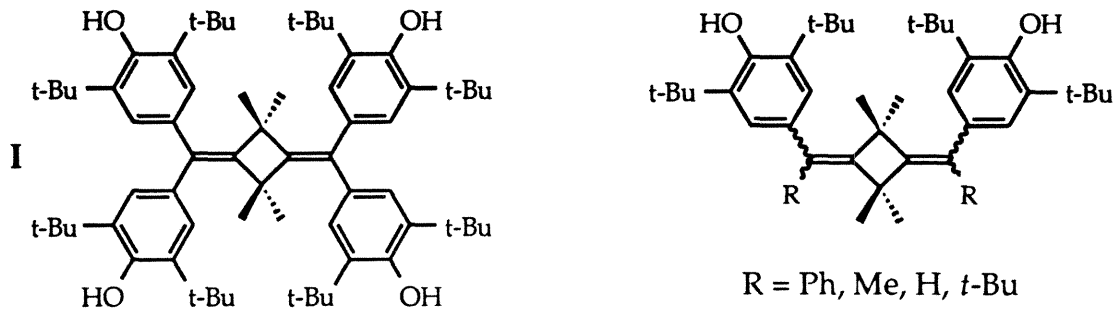

Figure C.1: Desired analogs of tetraphenol **I**

The synthetic approaches are straightforward (Scheme C.1). For Ph, Me or H-substituted compounds, 4-bromo-2,6-di-*tert*-butylanisole was reacted with two equivalents of *tert*-butyllithium.[1] Adding a substituted dialkylamide, followed by mild acidic workup, gave the desired carbonyl compounds in high yield.[2] For the *tert*-butyl substituted compound, the aryllithium solution was reacted with trimethylacetonitrile instead; acidic workup furnished the desired compound in high yield. These were then refluxed with anhydrous hydrazine to give the corresponding hydrazones.[3] Unfortunately, despite trying a wide variety of oxidants, and at low temperatures, only the *tert*-butyl substituted diazo compound could be made and sustained in sufficient yield for subsequent Barton-Kellogg coupling with 2,,2,4,4-tetramethylcyclobutane-1,3-dithione.[4,5] The resulting bisepisulfide could not be desulfurized by triphenylphosphine,[6] presumably due to steric hinderance.

Scheme C.1: Attempted Synthesis of **I** Analogs

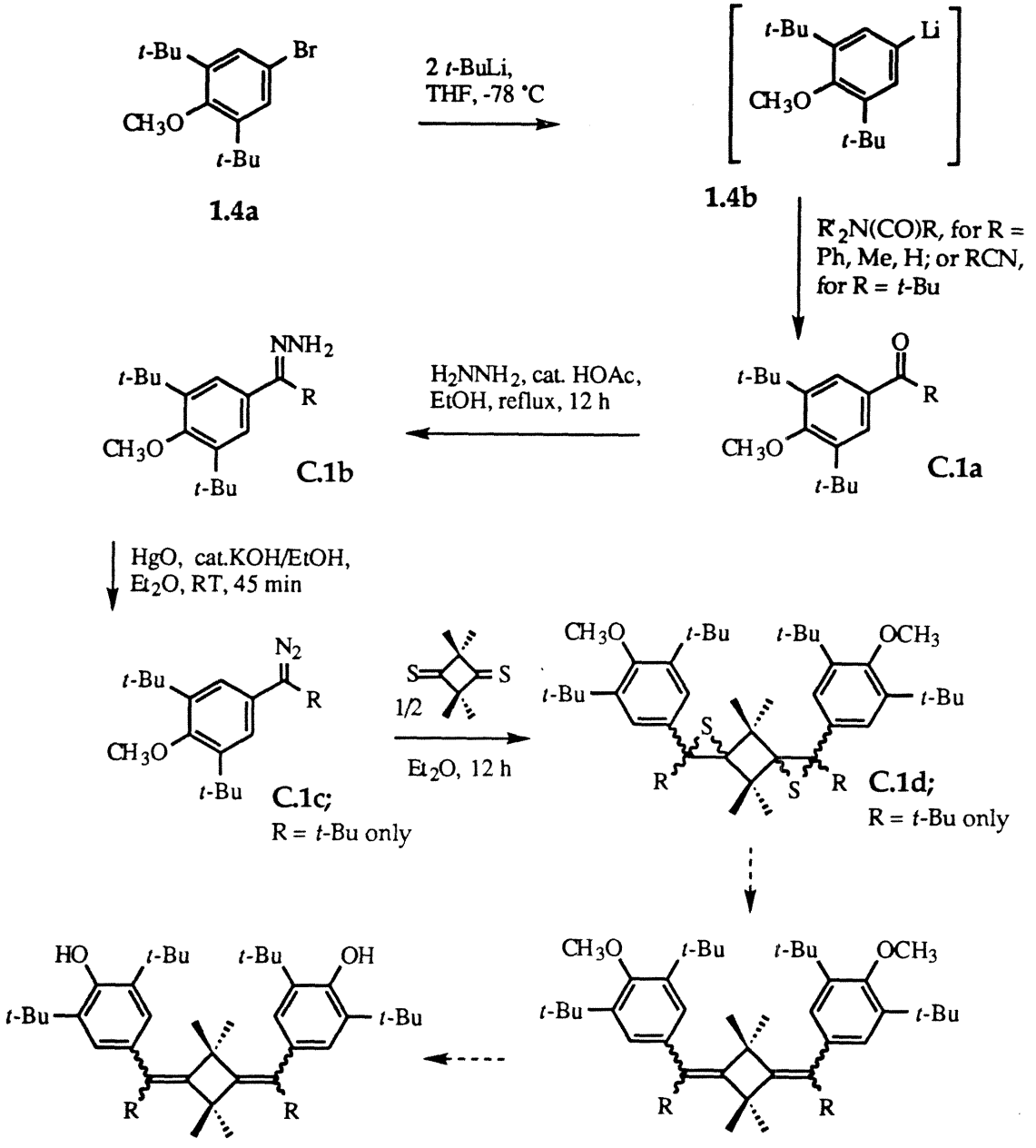

(3,5-di-*tert*-butyl-4-hydroxyphenyl)(phenyl)methanone (C.1a, R=Ph)[1,2] **4-Bromo-2,6-di-*tert*-butylanisole (3.4b,** 12.3 g, 0.0411 mol) was added to THF (200 mL) and cooled to -78 °C with a dry ice/acetone bath. A solution of *tert*.-butyllithium in hexanes (1.7 M, 48.3 mL, 0.0822 mol) was added over 10 min using a syringe. After stirring the resulting pale yellow solution for 1 h, N,N-dimethylbenzamide (6.13 g, 0.0411 mol) was added in one portion, causing a slight rise in temperature. After 10 min, the cooling bath was removed and the reaction was allowed to warm to room temperature. The reaction was quenched by carefully adding water (10 mL), then pouring into saturated NH_4Cl soln (250 mL) and extracted with 3 X 200 mL of Et_2O. The combined extracts were dried over $MgSO_4$, filtered, and the solvent was removed using a rotary evaporator. The residue was dissolved in benzene, passed through a short silica gel column, put on a rotary evaporator to remove solvent, and the resulting residue recrystallized from 95% ethanol to give 7.87 g (59%) of pale yellow crystals. TLC, yellow spot at RF 0.4, molybdate stain, 5% ethyl acetate/petroleum ether. GC/MS, 50-250°C, 10°C/min, m/z 324 (M^+) @ 21.7 min. 300 MHz ^1H NMR, $CDCl_3$, δ = 1.42 ppm, s, 18H; 3.75, s, 3H; 7.3-7.8, m, 7H. FTIR, NaCl, ν = 2955, 1655, 1583, 1442, 1414, 1392, 1357, 1333, 1250, 1220, 1115, 1009, 885, 774, 694 cm^{-1}.

(3,5-di-*tert*-butyl-4-hydroxyphenyl)(*tert*-butyl)methanone (C.1a, R=*t*-Bu)[1,2] **4-Bromo-2,6-di-*tert*-butylanisole (3.4b,** 25.4 g, 0.0850 mol) was added to THF (300 mL) and cooled to -78 °C with a dry ice/acetone bath. A solution of *tert*.-butyllithium in hexanes (1.7 M, 100 mL, 0.17 mol) was added via cannula over 10 min. After stirring the resulting pale yellow solution for an additional 20 min, trimethylacetonitrile (9.4 mL, 0.085 mol) was added using a syringe. The cooling bath was removed and the reaction was allowed to

warm to room temperature overnight. The reaction was quenched by carefully adding water (20 mL), then 3 M hydrochloric acid, and stirred for 3 h. This was extracted with 3 X 250 mL of Et_2O. The combined extracts were washed with saturated $NaHCO_3$ soln, dried over $MgSO_4$, filtered, and the solvent was removed using a rotary evaporator. The residue was recrystallized from 95% ethanol to give 20.2 g (78%) of colorless crystals. TLC, UV spot at RF 0.4, no stain, 5% ethyl acetate/petroleum ether. GC/MS, 50-250°C, 10°C/min, m/z 304 (M^+) @ 16.9 min. 300 MHz ^1H NMR, $CDCl_3$, δ = 1.20 ppm, s, 9 H; 1.45, s, 18H; 3.75, s, 3H; 7.01, s, 2H. FTIR, NaCl, ν = 2955, 1663, 1588, 1472, 1387, 1362, 1291, 1251, 1221, 1176, 1110, 1050, 995, 884, 864, 759 cm^{-1}. MP = 75-76 °C.

(3,5-di-*tert*-butyl-4-hydroxyphenyl)(methyl)methanone (C.1a, R=Me)[1,2] 4-Bromo-2,6-di-*tert*-butylanisole (**3.4b**, 12.1 g, 0.0406 mol) was added to THF (200 mL) and cooled to -78 °C with a dry ice/acetone bath. A solution of *tert.*-butyllithium in hexanes (1.7 M, 47.8 mL, 0.0812 mol) was added via syringe over 5 min. After stirring the resulting pale yellow solution for 1 h, N,N-dimethylacetamide (3.76 mL, 0.0404 mol) was added using a syringe. The cooling bath was removed and the reaction was allowed to warm to room temperature. The reaction was quenched by carefully adding water (10 mL), then pouring into saturated NH_4Cl soln (250 mL). This was extracted with 3 X 250 mL of Et_2O. The combined extracts were washed with saturated $NaHCO_3$ soln, dried over $MgSO_4$, filtered, and the solvent was removed using a rotary evaporator. The residue was purified by flash chromatography using 1:1 benzene: hexanes, followed by rotary evaporation to give 5.83 g (55%) of yellow powder. TLC, UV spot at RF 0.3, no stain, 5% ethyl acetate/petroleum ether. GC/MS, 50-250°C, 10°C/min, m/z 262 (M^+) @ 16.6 min.

(3,5-di-*tert*-butyl-4-hydroxyphenyl)methanone (C.1a, R=H)[1,2] 4-Bromo-2,6-di-*tert*-butylanisole (**3.4b**, 12.1 g, 0.0406 mol) was added to THF (200 mL) and cooled to -78 °C with a dry ice/acetone bath. A solution of *tert*.-butyllithium in hexanes (1.7 M, 47.8 mL, 0.0812 mol) was added via syringe over 5 min. After stirring the resulting pale yellow solution for 1 h, 1-formylpiperidine (4.7 mL, 0.0609 mol) was added using a syringe. The cooling bath was removed and the reaction was allowed to warm to room temperature. The reaction was quenched by carefully adding water (10 mL), then pouring into saturated NH_4Cl soln (250 mL). This was extracted with 3 X 250 mL of Et_2O. The combined extracts were washed with saturated $NaHCO_3$ soln, dried over $MgSO_4$, filtered, and the solvent was removed using a rotary evaporator. The residue was recrystallized from 95% ethanol to give 9.38 g (93%) of yellow powder. TLC, UV spot at RF 0.3, no stain, 5% ethyl acetate/petroleum ether. GC/MS, 50-250°C, 10°C/min, m/z 248 (M^+) @ 16.2 min.

(3,5-di-*tert*-butyl-4-hydroxyphenyl)(phenyl)methylhydrazone (C.1b, R=Ph)[3]

Anhydrous hydrazine (7.7 mL, 0..24 mol), benzophenone **C.1a(R=Ph)** (7.87 g, 0.0243 mol), and a few drops of glacial acetic acid were added to absolute ethanol (200 mL). After refluxing for 12 h, the mixture was cooled to room temperature, poured into water (250 mL) and extracted with 3 X 250 mL of Et_2O. After removal of the solvent using a rotary evaporator, the residue was partially purified on a silica gel column using graded elution of 5-30% Et_2O in petroleum ether. The partially pure fractions were combined and the solvent removed on a rotary evaporator. Recrystallization from heptane gave the hydrazone (6.98 g) in 85% yield as sticky tan crystals. TLC, grey-blue spot at RF 0.25, molybdate stain, 33% Et_2O/petroleum ether. GC/MS, 50-250°C, 10°C/min, m/z 339 (MH^+) @ 21.4 min. 300 MHz ^1H NMR, $CDCl_3$, δ =

1.37 ppm, s, 9H; 1.45, s, 9H; 3.70, s, and 3.79, s, total 3H; 5.34, broad s, 1H; 5.47, broad s, 1H; 7.29-7.15, 7H. FTIR, NaCl, ν = 3398 (broad), 3287, 3197, 2955, 1653, 1583, 1538, 1442, 1412, 1392, 1357, 1332, 1251, 1221, 1171, 1115, 1065, 1005, 884, 854, 774, 753, 693 cm^{-1}.

(3,5-di-*tert*-butyl-4-hydroxyphenyl)(*tert*-butyl)methylhydrazone (C.1b, R=*t*-Bu)[3] Anhydrous hydrazine (4.2 mL, 0.13 mol), ketone **C.1a(R=*t*-Bu)** (4.00 g, 0.0131 mol), and 10 drops of glacial acetic acid were added to absolute ethanol (150 mL). After refluxing for 15 h, the mixture was cooled to room temperature, poured into water (200 mL) and extracted with 3 X 100 mL of Et_2O. After removal of the solvent using a rotary evaporator, the residue was recrystallized from 95% ethanol to give the hydrazone (4.17 g) in quantitative yield as large yellow crystals. TLC, blue spot at RF 0.3, molybdate stain, 33% Et_2O/petroleum ether. GC/MS, 50-250°C, 10°C/min, m/z 318 (M^+) @ 18.5 min. 300 MHz ^1H NMR, $CDCl_3$, δ = 1.19 ppm, s, 9h; 1.43, s, 18H; 3.72, s, 3H; 4.4, broad s, 2H; 6.95, s, 2H. FTIR, NaCl, ν = 2955, 2865, 1632, 1585, 1457, 1390, 1387, 1362, 1251, 1221, 1176, 1110, 1050, 999, 884, 854 cm^{-1}.

(3,5-di-*tert*-butyl-4-hydroxyphenyl)(methyl)methylhydrazone (C.1b, R = Me)[3] Anhydrous hydrazine (7.0 mL, 0.22 mol), ketone **C.1a(R=Me)** (5.83 g, 0.0222 mol), and 10 drops of glacial acetic acid were added to absolute ethanol (100 mL). After refluxing overnight, the mixture was cooled to room temperature, poured into water (300 mL) and extracted with 3 X 100 mL of Et_2O. After removal of the solvent using a rotary evaporator, the residue was recrystallized from methanol/toluene to give the hydrazone (5.54 g) in 90% yield as a yellow powder. TLC, blue spot at RF 0.1, molybdate stain, 5% ethyl acetate/petroleum ether. GC/MS, 50-250°C, 10°C/min, m/z 246 (M^+ minus NNH_2) @ 14.8 min. 300 MHz ^1H NMR, $CDCl_3$, δ = 1.42 ppm, s, 18H; 2.13, s,

3H; 3.67, s, 3H; 5.25, s, 2H; 7.51, s, 2H. FTIR, NaCl, ν = 2955, 2865, 1603, 1538, 1447 (broad), 1392, 1357, 1312, 1241, 1221, 1110, 1005, 884, 754 cm^{-1}.

(3,5-di-*tert*-butyl-4-hydroxyphenyl)methylhydrazone (C.1b, R=Me)[3] Anhydrous hydrazine (14.4 mL, 0.453 mol), ketone **C.1a(R=H)** (9.38 g, 0.0378 mol), and 10 drops of glacial acetic acid were added to absolute ethanol (150 mL). After refluxing overnight, the mixture was cooled to room temperature, poured into water (250 mL) and extracted with 3 X 150 mL of Et_2O. After removal of the solvent using a rotary evaporator, the residue was recrystallized from 95% ethanol to give the hydrazone (2.81 g) in 28% yield as a yellow powder. A significant byproduct was the bishydrazone (3.8 g, 38%); this could probably be avoided by using a 25-fold or greater excess of hydrazine. TLC, blue spot at RF 0.2, molybdate stain, 33% Et_2O/petroleum ether. 300 MHz ^1H NMR, $CDCl_3$, δ = 1.44 ppm, s, 18H; 3.72, s, 3H; 5.42, s, 2H; 7.74, s, 1H. FTIR, NaCl, ν = 2955, 2865, 1623, 1563, 1457, 1442, 1402, 1387, 1357, 1322, 1251, 1216, 1110, 1005, 955, 885, 819, 799, 754 cm^{-1}.

Research Towards a Stable Analog of Non-Kekulé Benzene

Previous work in this group has demonstrated the existence of the ground state triplet 2,4-dimethylene-1,3-cyclobutanediyl, and its ability to be interconverted with its closed shell, singlet isomer, 2,4-dimethylene bicyclobutane, by photolysis (Figure C.2). This system, however, is only stable

Figure C.2: Magnetooptical Switching in 2,4-Dimethylene-1,3-cyclobutanediyl

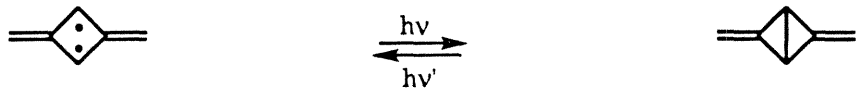

at low temperature in a solid matrix. Because its decay paths apparently do not involve unimolecular decomposition, I wondered whether replacing the six hydrogens in 2,4-dimethylene-1,3-cyclobutanediyl with bulky phenyl groups might create a significantly stabilized analog. To this end, the dihydro precursor to hexaphenyl non-Kekulé benzene was synthesized, using conventional chemistry (Scheme C.2).[7,8] Crystals of *trans*-cinnamic acid were suspended in distilled water and photolyzed with a Pyrex filtered lamp to give α-truxillic acid (**C.2a**). Refluxing in acidic methanol gave α-dimethyltruxillate (**C.2b**). Reaction of this with a little more than four equivalents of phenyllithium[2] gave 2,4-bis-(diphenylhydroxymethane)-1,3-diphenylcyclobutane (**C.2c**); attempts using phenylmagnesium bromide were unsuccessful. Dehydration of diol **C.2c** was performed using thionyl chloride in pyridine,[9-11] although the yield was low and purification was extremely difficult. At least thirty alternate dehydrations were tried, most of which failed to work or chewed up the starting material, and none of which surpassed the thionyl chloride procedure. Several attempts were made to abstract the hydrogens from (using nickel peroxide, silver(II)oxide, etc.) or

Scheme C2: Synthesis towards hexaphenyl-non-Kekulé benzene

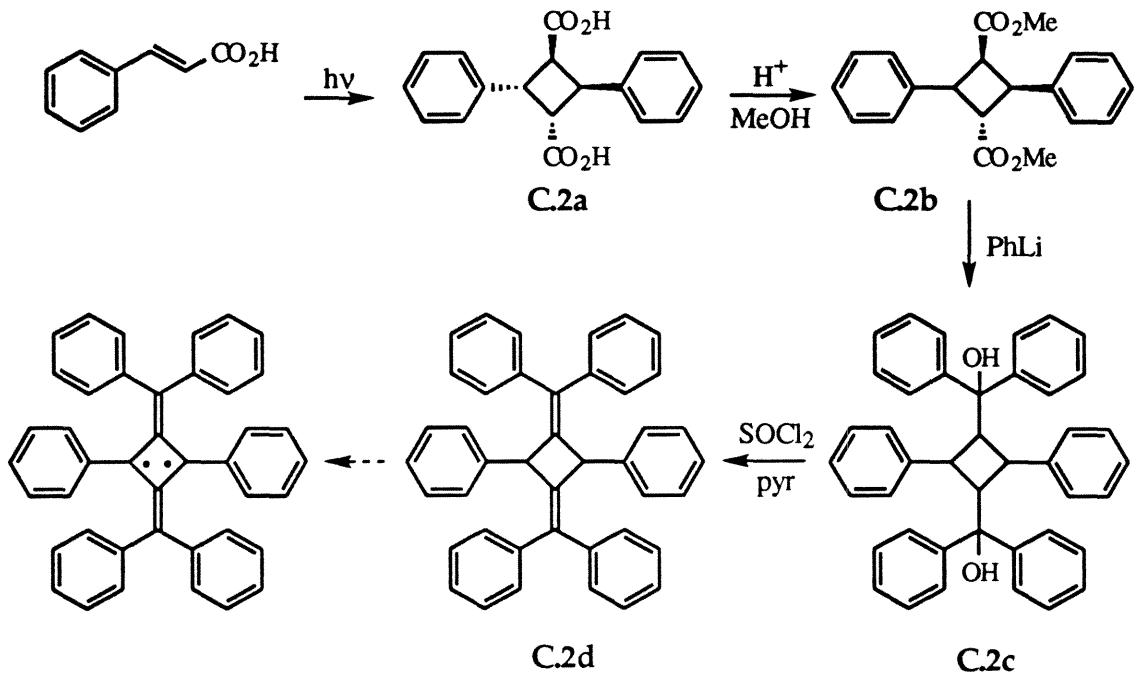

deprotonate (using alkyllithium) the dihydro precursor, 2,4-bis-(diphenylmethylene)-1,3-diphenylcyclobutane **C.2d**, but only resulted in decomposition. It may be that electron density delocalizes to the *para* position on the phenyl rings, allowing decomposition reactions. One possible solution would be to place *tert*-butyl groups in those positions by a Friedel-Crafts *tert*-butylation of α-dimethyltruxillate (**C.2b**) and reaction of that product with *para-tert*-butylphenyllithium as before.

α-truxillic acid (C.2a)[7] *trans*-Cinnamic acid (106 g, 0.716 mol) was stirred in 3 L of water and exposed to a Pyrex-filtered 450 W Hanovia immersion lamp for 72 h. The suspension was then vacuum filtered to dryness. The recovered solid was boiled in benzene (500 mL) for 5 min, vacuum filtered, and washed with an additional 2 X 250 mL of boiling benzene. The benzene fractions were concentrated, reheated, cooled, and vacuum filtered to give 67 g of crystalline

trans-cinnamic acid. The benzene-insoluble solid was recrystallized from methanol/THF to give 39 g (37%, quantitative including recycled starting material) of α-truxillic acid as white crystals. 300 MHz ^{1}H NMR, d_6-DMSO, δ = 3.75 ppm, dd, 2H; 4.25 ppm, dd, 2H; 7.1-7.3 ppm, m, 10H.

α-dimethyltruxillate (C.2b)[8] α-truxillic acid (**C.2a**) (26.0 g, 0.0877 mol) and 1 mL of concentrated sulfuric acid were added to 400 mL of methanol (both the starting material and the product are insoluble in methanol). The mixture was stirred and refluxed for 48 h, then cooled to 0 °C, vacuum filtered, and washed with an additional 2 X 200 mL of cold methanol. The solid was recrystallized from methanol/benzene to give 28.25 g (quantitative) of white crystals. GC/MS, 50-250°C, 10°C/min, m/z 324 (M^+) @ 20.2 min. 300 MHz ^{1}H NMR, $CDCl_3$, δ = 3.37 ppm, s, 6H; 4.1 ppm, m, 2H; 4.5 ppm, m, 2H; 7.2-7.5 ppm, m, 10H. 300 MHz ^{13}C NMR, $CDCl_3$, δ = 41.5, 46.7, 51.5, 127.2, 127.5, 128.5, 138.7, 172.4 ppm. FTIR, NaCl, ν = 3060, 1725, 1449, 1372, 1255, 1232, 1196, 1166, 1120, 1073, 814, 767, 744, 697 cm^{-1}. MP = 171-172 °C.

2,4-Bis-(diphenylhydroxymethyl)-1,3-diphenylcyclobutane (C.2c)[8] α-Dimethyltruxillate (**C.2b**) (7.50 g, 0.0231 mol) was dried at 0.1 Torr over phosphorus pentoxide for 24 h, and subsequently dissolved in THF (200 mL). The solution was cooled to -78 °C with a dry ice/acetone bath. Phenyllithium (70.0 mL, 0.14 mol, 2.0 M) in hexanes was added over 10 min. The cooling bath was removed and the reaction was allowed to stir and warm to room temperature over 12 h. The resulting purple mixture was then cooled to 0 °C and saturated NH_4Cl soln (10 mL) was carefully added. The mixture, which had turned yellow, was poured into saturated NH_4Cl soln (250 mL). The organic layer was separated, dried over $MgSO_4$, passed through a silica gel plug, and put on a rotary evaporator to remove the solvent. The residue was

recrystallized from CH_3CN/toluene to give 10.6 g (80.2%, 94.6% per phenyl) of white crystals. 300 MHz ^1H NMR, $CDCl_3$, δ = 2.46 ppm, s, 2H; 4.55, m, 2H; 4.66, m, 2H; 6.88-7.41, m, 30H. 300 MHz ^{13}C NMR, $CDCl_3$, δ = 42.2, 49.1, 80.5, 126.0, 126.1, 126.3, 126.8, 128.2, 128.5, 128.6, 128.9, 129.2, 139.9, 146.2, 147.1 ppm. FTIR, KBr, ν = 3516, sharp, 3084, 3060, 3013, 2966 cm^{-1}. MP = 267 °C.

2,4-Bis-(diphenylmethylene)-1,3-diphenylcyclobutane (C.2d)[8] Diol **C.2c** (0.500 g, 0.000873 mol) was added to pyridine (distilled and stored over molecular sieves, 25 mL) and cooled to -30 °C. Thionyl chloride (1.0 mL, 0.013 mol) was added via syringe in one portion. The resulting yellow solution was stirred and allowed to warm to room temperature, then poured into half-saturated NaCl soln. This was extracted with 3 X 75 mL of Et_2O and the solvent was removed on a rotary evaporator. The crude residue was purified by graded elution (0-20% Et_2O in petroleum ether) on a Chromatatron (Harrison Research). TLC, blue spot at RF 0.7, molybdate stain, 5% ethyl acetate/petroleum ether. HRMS, DEI-PFK, found MW = 536.250500, calculated MW = 536.250401, for M^+ = $C_{42}H_{32}$. 300 MHz ^1H NMR, $CDCl_3$, δ = 5.53 ppm, s, 2H; 6.85, m, 6.91, m, 7.04, m, 7.10, m, total 30H. 300 MHz ^{13}C NMR, $CDCl_3$, δ = 57.2, 125.7, 126.6, 127.5, 127.7, 127.8, 129.1, 139.9, 140.3, 143.1 ppm. FTIR, NaCl, ν = 3076, 3056, 3016, 2923, 1593, 1487, 1437, 1070, 1025, 914, 859, 769, 754 cm^{-1}. UV/Vis, λ_{max} = 254 nm. Elemental analysis: calculated for $C_{42}H_{32}$; C, 93.99; H, 6.01. Found: C, 93.96; H, 6.01.

Research Towards a TMM-Analog Ferromagnetic Coupling Unit

We desired to make a model for polaronic ferromagnetism using trimethylenemethane (technically 1,1 ethylene) as a ferromagnetic coupling unit. To this end, hindered alkene monomer **C.3f** (Scheme C.3) was designed. Refluxing 2,2,5,5-tetramethycyclopentanone with hydrazine hydrate in diethylene glycol gave hydrazone **C.3a**.[3] *para*-Dibromobenzophenone hydrazone (**C.3c**) was synthesized similarly.[3] Reaction of **C.3a** with sulfuryl monochloride and triethylamine gave thione **C.3b**,[12] which was added directly to a solution containing bis(*para*-bromophenyl)diazomethane **C.3c**,[3] resulting in episulfide **C.3e**. Desulfurization with triphenylphosphine gave alkene **C.3d**.[6] Unfortunately, Suzuki coupling[13] of this with *para*-phenylbisboric acid gave only a monocoupled product.

Scheme C.3: Synthesis of a Hindered Alkene

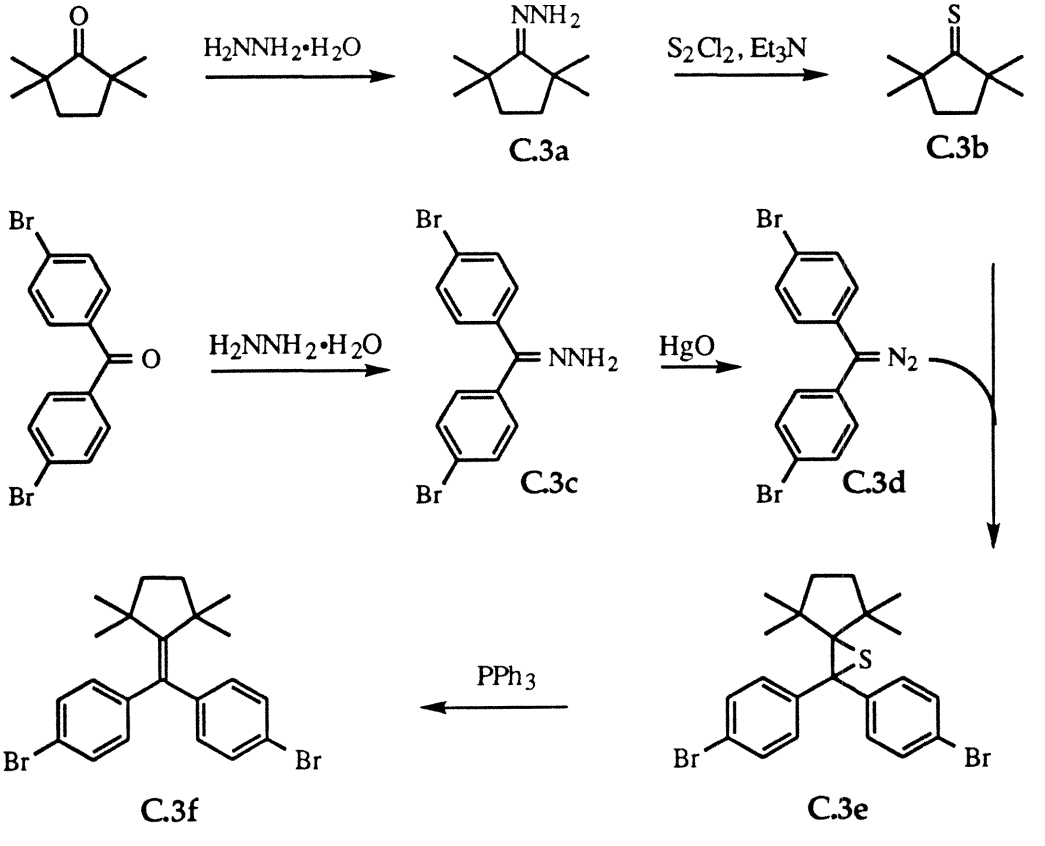

2,2,5,5-tetramethylcyclopentanonehydrazone (C.3a): 2,2,5,5-tetramethylcyclopentanone (5.96 g, 0.0425 mol), 55% aq hydrazine (24.0 ml, 0.425 mol) and 250 mL of di(ethylene glycol) were put into a flask equipped with a condenser and purged with argon. The mixture was stirred at reflux until no starting material could be observe by GC/MS, about 5 days. The mixture was cooled to room temperature, poured into 250 mL of water, and extracted with 3 X 125 mL of Et_2O. The combined organic fractions were dried over $MgSO_4$, filtered, and put on a rotary evaporator to remove solvent. The residue was sublimed at 0.1 Torr, 45-50 °C, to give 5.00 g (76.0%) of white crystals. GC/MS, 50-250°C, 10°C/min, m/z 154 (M^+) @ 6.8 min. 300 MHz ^1H NMR, $CDCl_3$, δ = 1.11 ppm, s, 6H; 1.45, s, 6H; 1.60, m, 2H; 1.75, m, 2H; 5.1, broad s, 2H. FTIR, NaCl, ν = 3357, 3217 (broad), 2935, 2855, 1613, 1452, 1362, 1221, 1080, 1070, 1040, 995, 844, 767 cm^{-1}.

2,2,5,5-Tetramethylcyclopentanethione (C.3b): Hydrazone **C.3a** (2.23 g, 0.0144 mol) and sulfuryl monochloride (1.21 mL, 0.0152 mol) were each dissolved separately in benzene (25 mL). The two solutions were added dropwise over 15 min to a stirred solution of triethylamine (4.0 mL, 0.029 mol) in benzene (25 mL) which was cooled with an ice water bath. After the addition was complete, the reaction was stirred for 1 h at 5 °C, at which point the hydrazone could no longer be observed by GC/MS. The orange-pink reaction mixture was then washed with 3 X 100 mL of half-saturated NaCl soln, dried over $MgSO_4$, passed through a short silica gel plug and used in the next step without isolation. GC/MS, 36 °C for 10 min, then 36-250°C, 10°C/min, m/z 156 (M^+) @ 13.7 min.

4,4'-Dibromobenzophenone (C.3c): Aqueous hydrazine (55%, 65 mL, 1.2 mol) and 4,4'-dibromobenzophenone (26.0 g, 0.0765 mol) were added to 95%

ethanol (250 mL). After refluxing overnight, the reaction was light yellow and all solid had dissolved. After 4 d, the mixture was cooled to room temperature, poured into water (500 mL) and extracted with 3 X 250 mL of Et_2O. After drying the combined extracts over $MgSO_4$, passing through a short plug of silica gel, and removal of the solvent using a rotary evaporator, the residue was recrystallized from 95% ethanol to give the hydrazone (26.3 g) in 97% yield as white crystals. TLC, blue spot at RF 0.3, molybdate stain, 33% Et_2O/petroleum ether. GC/MS, 50-250°C, 10°C/min, m/z 354 (M^+) @ 21.4 min. FTIR, NaCl, ν = 3398 (broad), 3277 (broad), 3197 (broad), 3056, 1588, 1482, 1387, 1327, 1261, 1166, 1065, 1005, 950, 935, 824, 749 cm^{-1}.

Episulfide C.3e: Hydrazone **C.3c** (5.07 g, 0.0143 mol), $MgSO_4$ (1.7 g, 0.014 mol), and 3 drops of saturated KOH/absolute ethanol soln were added to Et_2O. Precautions were taken to protect the reaction from light. Addition of freshly activated mercuric oxide (17.8 g, .0822 mol) caused a red-purple color to appear, which was presumably **bis(4-bromophenyl)diazomethane (C.3d)**. After 1 h, when hydrazone was no longer visible on TLC, the reaction was filtered through a fine glass frit and mixed with the solution of thione **C.3b**. This mixtue was stirred for 15 h, at which point the reaction was nearly colorless. The crude residue obtained by removing the solvent on a rotary evaporator (6.9 g, quantitative) was used in the next step without further purification. GC/MS, 50-250°C, 10°C/min, m/z 480 (M^+) @ 27.9 min.

Alkene C.3f: Episulfide **C.3e** (22.3 g, 0.0568 mol) and triphenylphosphine (29.8 g, 0.114 mol) were added to benzene (250 mL) and refluxed with stirring for 24 h. The solid residue collected after removing the benzene on a rotary evaporator was boiled for 10 min in 50 mL of a 1:1 solution of carbon tetrachloride and 95% ethanol. After removing the solvent on a rotary

evaporator, the solid residue was dissolved in Et_2O/THF and washed with 5 X 250 mL of saturated NaCl and then 5 X 250 mL of water. The organic layer was dried over $MgSO_4$, filtered, passed through a short plug of silica gel, and put on a rotary evaporator to remove the solvent. The residue was recrystallized from 95% ethanol and benzene to give 23.2 g (91%) of white crystals. TLC, dark blue spot at RF 0.7, molybdate stain, 5% ethyl acetate/petroleum ether. GC/MS, 50-250°C, 10°C/min, m/z 448 (M^+) @ 23.1 min. 300 MHz ^1H NMR, $CDCl_3$, δ = 0.96 ppm, s, 12H; 1.56, s, 4H; 7.07, s, 2H; 7.10, s, 2H; 7.36, s, 2H; 7.39, s, 2H. 300 MHz ^{13}C NMR, $CDCl_3$, δ = 30.7, 41.9, 45.9, 120.7, 131.5, 134.9, 143.4, 157.8 ppm. MP = 178-179 °C. Elemental analysis: calculated for $C_{22}H_{24}Br_2$, C, 58.95; H, 5.40; Br, 35.65. Found: C, 58.98; H, 5.65; Br, 36.22.

Appendix C References

1. Hoye, T. R.; Martin, S. J.; Peck, D. R. *J. Org. Chem.* **1982**, *47*, 331-337.

2. Carey, F. A.; Sundberg, R. J. *Advanced Organic Chemistry*; Plenum: New York, 1990, Part A, p 454.

3. (a) Howard, K. L.; Smith, L. I. *Org. Syn.* coll. vol. III, 351-352. (b) Miller, J. B. *J. Org. Chem.* **1959**, *24*, 560-561.

4. Freund, F.; Hünig, S. *J. Org. Chem.* **1987**, *52*, 2154-2161.

5. Abeguz, B.; Krapcho, A. P.; Rao, D. R.; Silvon, M. P. *J. Org. Chem.* **1971**, *36*, 3885-3890.

6. Dali, B. B.; Kelly, T. R.; Tsang, W. G. *Tetrahedron Lett.* **1977**, 3859-3862.

7. Farnum, D. G.; Mostashari, A. J. *Org. Syn.* coll. vol. I, 103-104.

8. Dehmlow, Eckehard V.; Ezimora, Gordian C. *Tetrahedron Lett.* **1972**, *13*, 1265-1270.

9. Schwartz, A.; Madan, P. *J. Org. Chem.* **1986**, *51*, 5463-5465.

10. Gaston, J. L.; Grundon, M. F.; James, K. J. *J. Chem. Soc., Perkin Trans. 1* **1979**, 1136-1138.

11. Allen, W. S.; Bernstein, S. *J. Am. Chem. Soc.* **1955**, *77*, 1028-1032.

12. Okasaki, R.; Inoue, K.; Inamoto, N. *Bull. Chem. Soc. Jpn.* **1981**, *54*, 3541-3545.

13. (a) Wallow, T. I.; Novak, B. M. *J. Am. Chem. Soc.* **1991**, *113*, 7411-7412. (b) Wallow, T. I.; Novak, B. M. *J. Org. Chem.* **1994**, *59*, 5034-5037.

Appendix D. Brillouin Function Fitting Implementation for KaleidaGraph

3 parameter fit

((m1+0.5)*(exp((M1+0.5)*1.3405*m0)+exp(-(m1+0.5)*1.3405*m0))/
(exp((m1+0.5)*1.3405*m0)-exp(-(m1+0.5)*1.3405*m0)) -
0.5*(exp(0.67025*m0)+exp(-0.67025*m0))/(exp(0.67025*m0) - exp(-
0.67025*m0)))*m2/m1 + m3*m0; m1=x; m2=x; m3 = x

2 parameter fit

((m1+0.5)*(exp((M1+0.5)*1.3405*m0)+exp(-(m1+0.5)*1.3405*m0))/
(exp((m1+0.5)*1.3405*m0)-exp(-(m1+0.5)*1.3405*m0)) -
0.5*(exp(0.67025*m0)+exp(-0.67025*m0))/(exp(0.67025*m0) - exp(-
0.67025*m0)))*m2/M1; m1= x ; m2= x

Key:

m0 is experimental H/T data, in Tesla/K

m1 is S

m2 is M_{sat} in emu•Gauss

m3 is χ_{dia}*10000*T

x represents the initial guess

Appendix D References

Carlin, R. L. *Magnetochemistry*; Springer-Verlag: New York, 1986.

Jacobs, S. J. Ph.D. Thesis, California Institute of Technology, 1994.